Dynamic covalent macrocycles and macrobicyclic cages : self-sorting, kinetics and thermodynamics

Zhaozheng Yang

UNIVERSITÉ DE STRASBOURG

ÉCOLE DOCTORALE 222

Laboratoire de Chimie Supramoléculaire
Institut de Science et d'Ingénierie Supramoléculaires (ISIS)

THÈSE de DOCTORAT

Présentée par :

Zhaozheng YANG

Soutenue le : **01 Décembre 2022**

Pour obtenir le grade de : **Docteur de l'université de Strasbourg**

Discipline/ Spécialité : Chimie

Dynamic Covalent Macrocycles and Macrobicyclic Cages: Self-Sorting, Kinetics and Thermodynamics

THÈSE dirigée par :

Prof. Jean-Marie LEHN	Directeur de thèse, Université de Strasbourg

RAPPORTEURS :

Prof. Mihail BARBOIU	Rapporteur, Université de Montpellier
Prof. Daniel MEYER	Rapporteur, Institut de Chimie Séparative de Marcoule

AUTRES MEMBRES DU JURY :

Prof. Sylvie FERLAY	Examinateur, Université de Strasbourg

Zhaozheng YANG

Dynamic Covalent Macrocycles and Macrobicyclic Cages: Self-Sorting, Kinetics and Thermodynamics

Résumé

L'étude des systèmes d'auto-triage, notamment leur comportement sous contrôle cinétique, pourrait ouvrir la voie à une meilleure compréhension des propriétés intrinsèques et de l'intrication de la matière. Cette thèse est centrée autour de l'étude des caractéristiques cinétiques et thermodynamiques dans les systèmes d'auto-triage de macrocycles de polyimines et de cages macrobicycliques. Les forces motrices de chaque distribution, obtenues à la fois à des temps de réaction courts et après avoir atteint l'équilibre, ont été étudiées dans un premier temps. Ces résultats mettent en évidence le rôle essentiel du choix judicieux des composants initiaux, qui permet l'évolution des DCLs (initialement composées des produits cinétiques hors équilibre) vers des états thermodynamiquement favorisés. Dans le dernier chapitre, les interconnexions isomériques entre les constituants ont été évaluées afin d'explorer une nouvelle approche pour le développement de DCLs d'une plus grande complexité.

Mots cles : chimie covalente dynamique, bibliothèque covalente dynamique, triage automatique dynamique, macrocycles, cages moléculaires, systèmes hors équilibre, commutation cinétique

Abstract

The study of self-sorting systems, especially their behaviour under kinetic control, may pave the way to understand the intrinsic properties and intricacy of matter. This thesis focuses on the study of kinetic and thermodynamic features in self-sorting systems of polyimine macrocycles and macrobicyclic cages. The driving forces for each distribution obtained at both short reaction times and after reaching the equilibrium were firstly investigated. The results highlight the essential role of an appropriate design of initial components, which allows the evolution of DCLs from out-of-equilibrium kinetic products to thermodynamically favoured states. In the last chapter, isomeric interconnections between constituents were evaluated in order to provide a new aspect for developing DCLs of higher complexity.

Key words: dynamic covalent chemistry, dynamic covalent library, dynamic self-sorting, macrocycles, molecular cages, out-of-equilibrium systems, kinetic switching

TABLE OF CONTENTS

Acknowledgements

It is my fortune to be able to pursue my Ph.D. at institut de science et d'ingénierie supramoléculaires (I.S.I.S), one of the world's leading institutes. First of all, I would like to sincerely thank Prof. Jean-Marie Lehn for giving me the opportunity to work in his lab. I truly appreciate that he is always there for discussions and suggestions. His guidance enhanced my enthusiasm and confidence in research which allowed me to face failures and adapt to challenges. His profound knowledge, scientific rigor and innovative spirit will benefit me for my entire life.

I would like to deeply indebted to Prof. Jack Harrowfield for his instructive suggestions on my project and for his careful and patient help in correcting my thesis. I would also like to extend my gratitude to our former senior colleagues Dr. Artem Osypenko and Dr. Jean-François Ayme, for their selflessness supports both in science and in personal life.

I would also like to thank Dr. Jean-Louis Schmitt, Cyril Antheaume, Hava Aksoy and Wahnyalo Kazöne for helping me with NMR and MS analysis. As well as to Dr. Lydia Karmazin and Corinne Bailly for the X-Ray analysis and interpretation of my crystals.

I also want to thank our secretary Jacqueline Claudon and Annia Bertrand, who helped me with administrative procedures and my personal life. Merci Jacqueline! Muchas gracias, querida Annia!

I also want to express my gratitude to the following people in I.S.I.S., who helped me revise my PhD thesis: Dr. Youssef Atoini, Dr. Jean-Louis Schmitt, Dr. Ferran Esteve, Maria Jesus Aguilera Roldan, Tanguy Rieu, Bohdan Kozibroda and Dr. Jing Yi.

I would like to thank Dr. Meixia He and her husband Dr. Shaofei Zhang for greeting me on my first day in Strasbourg. I would also like to thank all the members in this group, especially Dr. Antonio Santoro, Dr. Youssef Atoini as well as Dr. Meixia He, who provided me great help when I first came and settled down in Strasbourg and in I.S.I.S.. And I want to say big congrats to Youssef on becoming a new dad! Many thanks to Dr. Guangwen Men, Dr. Ruirui Gu, Dr. Martin Herder, Dr. Sirinan Kulchat, Dr. Aline Chevalier, Yufei Wang, Dr. Chengyi Zhu, Dr. Paulo Fernando Do Amaral Costa, Dr. Sapna Gahlot, Stanislav Osypenko, Fidan Rahmatova for their kind support and companionship during these years.

Words cannot express my gratitude to my parents for their constant encouragement and to my girlfriend Dr. Jing Yi for being my long-term personal French spokesman and for her companion.

I would like to acknowledge the “China Scholarship Council” and “Lehn Institute of Functional Materials, Sun Yat-Sen university” for their financial support on my PhD study.

Last but not least, thanks should also go to Prof. Mihail Barboiu from Université de Montpellier, Prof. Daniel Meyer from Institut de Chimie Séparative de Marcoule and Prof. Sylvie Ferlay from Université de Strasbourg for their patient examination of my work.

List of Abbreviation

CDC	Constitutional Dynamic Chemistry
CDL	Constitutional Dynamic Library
DCL	Dynamic Combinatorial Library
CDN	Constitutional Dynamic Network
DNCC	Dynamic Non-Covalent Chemistry
DCC or DCvC	Dynamic Covalent Chemistry
NMR	Nuclear magnetic Resonance
HRMS	High Resolution Mass Spectroscopy
ESI	Electro Spray Ionization
Equiv.	Equivalent
min	Minute
h	hour
mM	Millimolar per Liter
OTf	Trifluoromethanesulfonate

RESUME DE LA THESE DE DOCTORAT

1) Introduction

Le développement actif de la chimie covalente dynamique (DCC pour *dynamic covalent* chemistry) offre un outil puissant aux chimistes pour générer des architectures organiques discrètes à partir d'un mélange de composants, liées par des liaisons covalentes réversibles. En particulier, de nouvelles architectures dynamiques macrocycliques et macrobicycliques—assemblées par la formation de multiples liaisons imines réversibles (entre des amines et des composés carbonylés) —ont été développées. Des structures telles que les tétraimino-macrocycles et les cages moléculaires de type cryptand macrobicyclique hexaimino en sont de parfaites illustrations. Comme c'est le cas pour leurs analogues non dynamiques, la cavité intramoléculaire de ces structures bien définies peut conduire à des applications telles que la détection[3] et la catalyse.

Du point de vue de leur méthodologie synthétique, les structures assemblées dynamiquement permettent d'accéder à de nouveaux comportements comme l'auto-triage et l'adaptabilité. Les systèmes d'auto-sélection (que l'on peut aussi appeler auto-triage) basés sur des bibliothèques covalentes dynamiques (DCL pour dynamic covalent libraries) générées par la DCC fonctionnent par incorporation, décorporation et échange de composants, suivant les relations agonistes et antagonistes entre les constituants. La formation sélective d'architectures résultantes de combinaisons spécifiques parmi les différentes possibilités dans la DCL via l'auto-triage est particulièrement intéressante. La génération d'architectures bien définies par l'auto-triage des composants à partir de DCL multi-composants implique une compétition entre la formation: i) d'entités auto-triées homoleptiques discrètes (homo-auto-tri); ii) d'entités auto-triées hétéroleptiques d'assemblages mixtes (hétéro-auto-tri) possédant différents blocs de construction; iii) de mélanges statistiques de résultats désordonnés. L'enjeu est de contrôler rationnellement le système de manière à ce que l'augmentation de la complexité moléculaire (augmentation du nombre de composants et de groupes réactifs sur un seul composant) n'entraîne pas des connexions aléatoires résultant de condensations indésirables ou de formation de polymères dues à la similitude des énergies de liaisons. Pour relever ce défi, il est crucial de décrypter le mécanisme d'auto-triage et d'en tirer profit.

Cependant, assez peu d'études ont traité du mécanisme des processus d'auto-assemblage et d'auto-triage basés sur la chimie covalente dynamique. Cela est dû en grande partie à la difficulté d'analyser la formation de combinaisons potentielles de produits intermédiaires générés de manière transitoire au sein d'une même DCL. Le suivi de formation des produits et la compréhension de la conversion des intermédiaires présentent un intérêt particulier et seront utiles pour la prédiction des résultats d'auto-triage.

2) Résultats et discussions

2.1. Les processus d'auto-sélection des macrocycles [2+2] et des cages macrobicycliques [3+2]

Dans ce chapitre, nous nous sommes concentrés sur les multiples processus de condensation d'imines et les mécanismes d'auto-sélection entre les composants qui se déroulent dans ces macrocycles et cages macrobicycliques. D'après les investigations cinétiques réalisées, un mécanisme plausible d'assemblage à trois voies vers la formation de macrocycles organiques covalents [2+2] a été suggéré (**Schéma 1**). Le processus de formation des cages macrobicycliques est plus compliqué que celui des macrocycles. Lorsque les cages macrobicycliques sont mises en œuvre dans un système d'auto-sélection à trois composants, au moins quarante-trois espèces et de nombreuses réactions internes peuvent être générées. Une caractéristique importante de ces processus réside dans le comportement d'auto-correction qui se produit sur la base de condensations d'imines réversibles. Les résultats ont indiqué que les intermédiaires hétéroleptiques générés aléatoirement au cours de ce processus peuvent être corrigés par dissociation et recombinaison, à savoir le processus d'auto-correction, conduisant à la génération parallèle d'espèces homoleptiques. En outre, les différences entre la longueur de la chaîne des éléments constitutifs et le rapport stœchiométrique des substrats sont confirmés comme étant les deux facteurs clés pour la mise en œuvre d'un auto-triage de haute-fidélité.

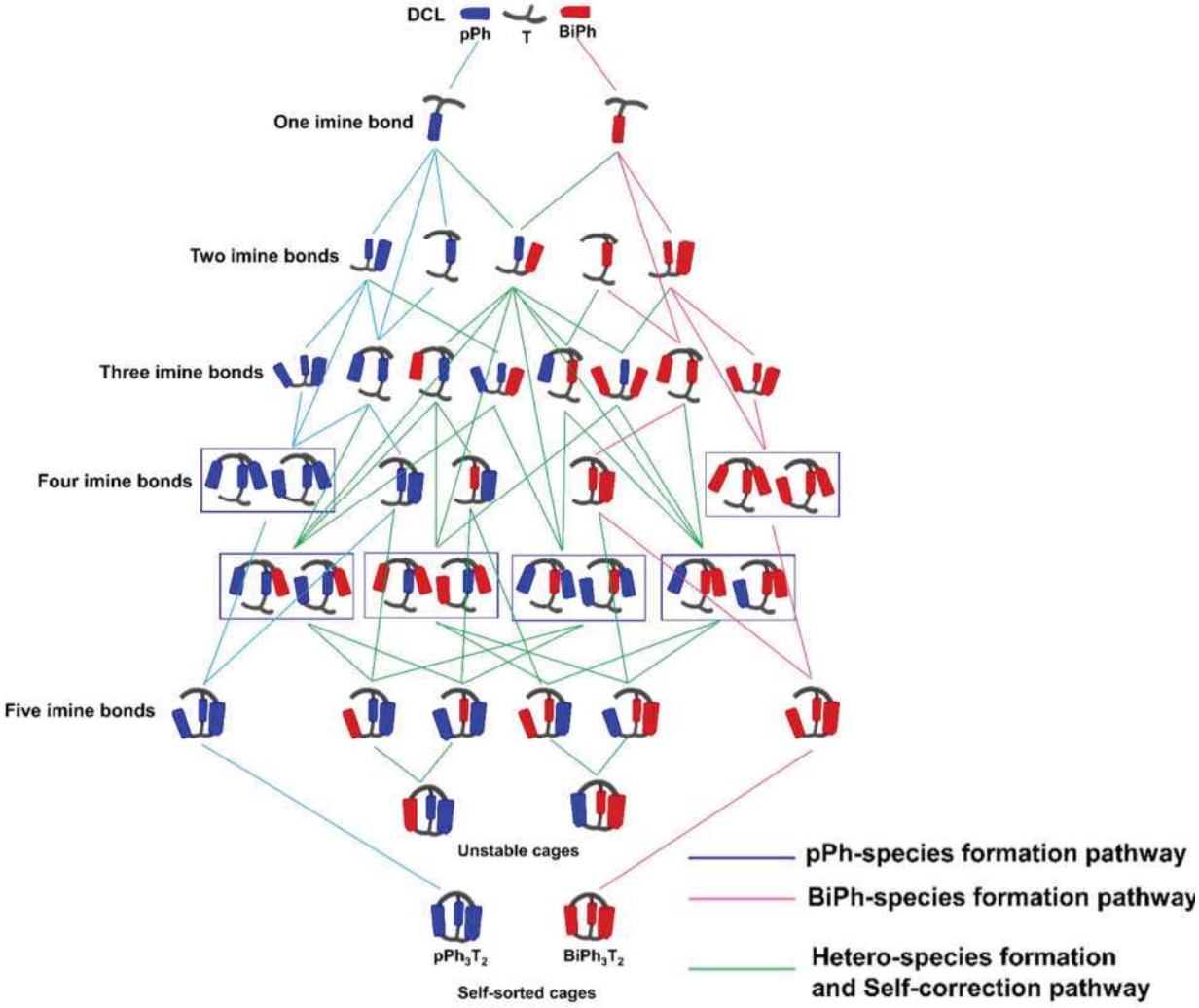

Schéma 1. Présentation schématique des possibles voies d'auto-triage des cages macrobicycliques dynamiques covalentes à base d'imines.

2.2 Auto-sélection et commutation cinétique dans deux ordres cycliques : macrocycles et cages

La construction de systèmes d'auto-triage covalents dynamiques organiques purs contenant des structures multi-topologiques est une méthode judicieuse pour augmenter la multiplicité et la diversité des systèmes chimiques. Des réseaux dynamiques constitutionnels [2 × 2] (CDN pour constitutional dynamic networks) ont été obtenus soit à partir de DCLs à quatre composants dont une diamine, une triamine et deux dialdéhydes, soit à partir de

mélanges préformés de macrocycles et de cages (**Schéma 2**). En opérant à la fois par des propriétés cinétiques et thermodynamiques, les systèmes d'auto-triage révèlent l'apparition d'une commutation cinétique via l'échange de composants au cours de la formation de macrocycles et de cages macrobicycliques. Ce comportement confère une amplification dépendante du temps et une commutation orthogonale entre les constituants dans la diagonale de leur CDN [2 × 2] associée. Ce chapitre a révélé l'apparition de commutations cinétiques par échange de composants au cours de la formation de macrocycles et de cages macrobicycliques par auto-triage.

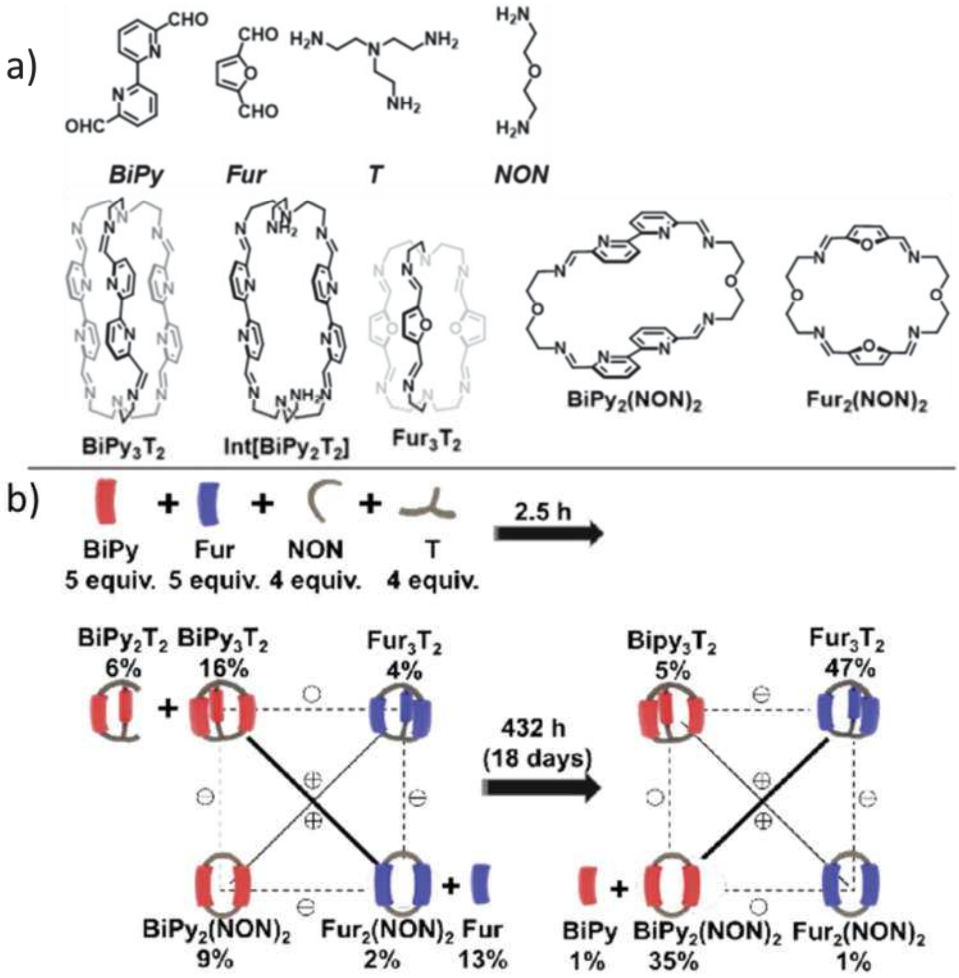

Schéma 2. (a) La structure des composants et des constituants au sein de la CDN. (b) La commutation orthogonale des constituants et une distribution cinétique à une distribution thermodynamique, sur une période de 18 jours

2.3 Transformation cinétique du tri aux macrocycles non triés

Nous avons exploité le comportement d'auto-triage en mélangeant la 2,6-pyridinedicarboxaldehyde (**Py**) avec deux diamines de longueur similaire, **NON** et **NNN** dans un rapport 2: 2: 2. Lors du mélange des composants, le macrocycle homoleptique **$Py_2(NNN)_2$** a culminé à 61 % de rendement au début du processus. Au fil du temps, une quantité partielle de **$Py_2(NNN)_2$** a progressivement été décomposée et les deux autres macrocycles **$Py_2(NON)_2$**, **Py_2(NON-NNN)** se sont formés en continu. Enfin, l'équilibre de la réaction a été atteint en 780 min, résultant en un mélange presque statistique avec 25% de **$Py_2(NNN)_2$**, 23% de **$Py_2(NON)_2$**, 43% de **Py_2(NON-NNN)**, accompagné de 7% de mélanges intermédiaires.

L'évolution en fonction du temps pourrait être affectée par la variation de température, la présence des ions métalliques et le type de solvants. De plus, cet auto-triage transitoire contrôlé cinétiquement peut être réalisé dans des DCL contenant trois diamines structurellement similaires. Dans l'ensemble, en raison d'une différente réactivité, ainsi que d'une structure similaire des composants, une évolution unique se déroule et passe d'un état auto-trié cinétiquement piégé à des mélanges presque statistiques non triés.

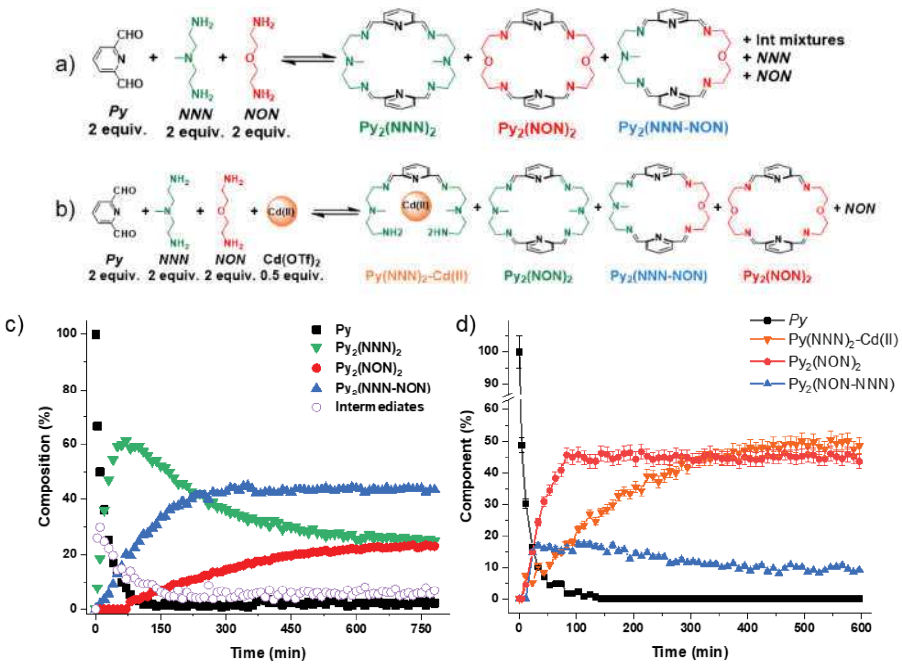

Schéma 3. Evolution cinétique des produits générés à partir de (a, c) **Py + NNN + NON** et (b, d) **Py + NNN + NON + Cd(II)** en fonction du temps.

2.4 Perturbation des DCLs via un processus d'auto-triage

Nous avons synthétisé des cages organiques avec des ligands pontants asymétriques pour réaliser le phénomène d'auto-triage. Après mélange des réactifs de départ, deux diastéréoisomères, **Cage bbb** et **Cage bbp** ont été obtenus. Exploitant les propriétés de réversibilité dynamique et de coordination en présence de Zn(II), la cage **bbp** se transforme progressivement en **Cage bbb-Zn**, le Zn(II) préférant former une géométrie de coordination octaédrique. Cette étude nous a permis de déterminer les facteurs qui influencent la fiabilité des processus d'auto-triage, parmi lesquels les propriétés électroniques des composants organiques ainsi que la nature des cations métalliques. Dans des conditions appropriées, les deux cages organiques peuvent être séparées. De plus, l'unité structurelle asymétrique fournit deux environnements chimiques différents à l'intérieur des cages organiques. Ces environnements peuvent être utilisés pour la coordination avec des différents métaux afin d'obtenir des cages organiques qui contiennent du centre bimétalliques hétéronucléaires.

L'utilisation de ligands dissymétriques pour la synthèse de nouvelles cages organiques grâce à la stratégie de simplification auto-triée a fourni de nouvelles idées pour la conception et la synthèse de nouveaux types de cages covalentes organiques.

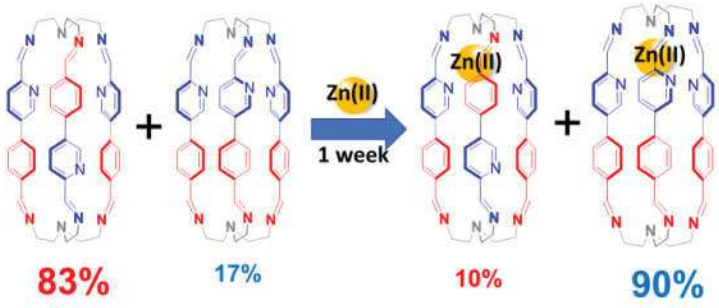

Schéma 4. Génération de deux cages isomères à partir du ligand **Py-Ph** et **T**, ainsi que leur conversion dynamique en présence de triflate de Zn(II).

3) Conclusion générale

En conclusion, la présente thèse illustre l'utilisation de liaisons covalentes dynamiques de type imine comme outils utiles dans la construction de systèmes d'auto-sélection/triage. Les propriétés d'auto-triage ont été démontrées en utilisant des macrocycles et des cages

macrobicycliques comme modèles sous plusieurs aspects : mécanistique, du comportement de commutation cinétique, ainsi que les états hors équilibre. Comprendre le principe du triage est utile pour concevoir et mettre en œuvre des bibliothèques dynamiques constitutionnelles impliquant une grande diversité de composition et un ordre de complexité plus élevé.

Il est d'une grande importance de comprendre les facteurs qui conduisent à l'auto-triage ainsi que les propriétés cinétiques et thermodynamiques des constituants et des DCLs. Les systèmes dynamiques constitutionnels qui passent en fonction du temps d'un état hors-équilibre vers son état d'équilibre, jouent un rôle fondamental dans la compréhension de la complexification de la matière.

Chapter I. General Introduction

1. Constitutional Dynamic Chemistry

1.1. Background

Supramolecular chemistry focusing on the study of weak, reversible non-covalent intermolecular forces has been rapidly developed over the past decades.[1–4] Emanating from basic research on molecular recognition, supramolecular chemistry has been defined as "chemistry beyond the molecule",[1] where molecules interact with each other by means other than covalent bonds. The development by Emil Fischer of the "lock and key model" for complementary enzyme-substrate interactions was a forerunner of this realm.[5] As biological behaviours such as enzyme binding, DNA replication, and protein folding, can often be interpreted in terms of supramolecular interactions, supramolecular chemistry can be seen as a powerful toolkit for the generation of highly complex, self-organized and functional chemical systems.

Labile intermolecular interactions such as van der Waals (dispersion) forces, π–π stacking, hydrogen bonding, and acceptor–donor interactions have been widely exploited in attempts to mimic self-organization in Nature, and one of the most successful approaches has been based on metal-ion-ligand binding (coordination template effect). Fascinating examples of the chemistry generated through this approach can be found in the self-assembly of metallosupramolecular circular helicates,[6,7] grids,[8,9] catenanes and rotaxanes,[10,11] Borromean rings,[12] and cages[13–15].

The key feature of most supramolecular architectures is their intrinsically dynamic (or adaptive) nature, which enables them to adapt and rearrange their structures or constitutions in response to external stimuli.[16] For example, the reversible adaptation of a coiled ligand to uncoiled form could be controlled by metal ions.[9,17] In the absence of Pb(II), a (hydrazone-pyrimidine)$_{10}$ ligand **H$_{10}$** exhibited a helical conformation. Instead, the addition of 10 equiv. of Pb(II) to the system resulted in the formation of a linear complex **LPb$_{10}$**. Subsequent removal of Pb(II) allowed to liberate the ligand **H$_{10}$** and brought back the ligand to its helical conformation. Based on the adaptive feature of responding to external stimuli, supramolecular chemistry is also known as Dynamic Non-Covalent Chemistry (DNCC).

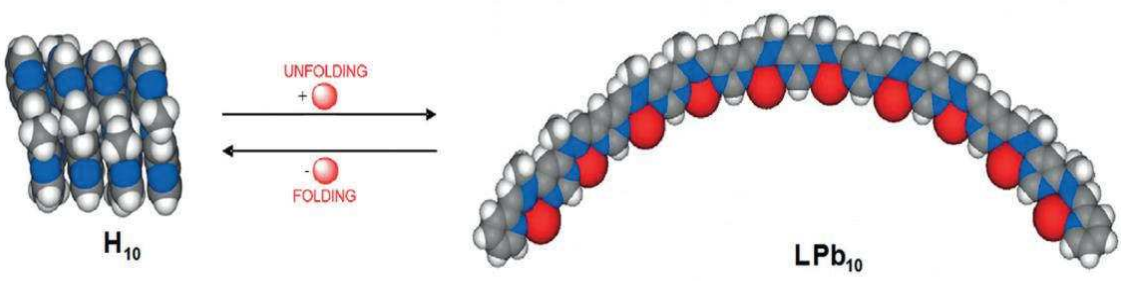

Figure I-1. A representation of reversible extension/contraction motion of a coiled hyz-pym ligand **H_{10}** into uncoiled complex in response to Pb(II) (Figure reproduced from reference[17]).

A widening understanding of supramolecular chemistry has driven chemists to incorporate dynamic features into molecular chemistry, even though covalent bonding is considered to be stronger than supramolecular interactions. The development of molecular assemblies with the ability to adapt in response to external effectors requires the use of dynamic covalent reactions. In line with supramolecular interactions, dynamic covalent reactions allow the formation and breakdown of covalent bonds under thermodynamic control. Within this context, the concept of Dynamic Covalent Chemistry (DCC or DCvC) was born.[18–20]

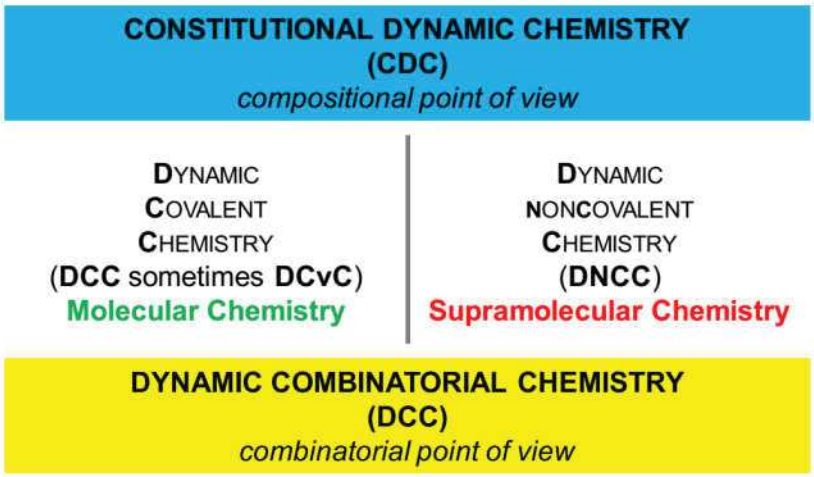

Figure I-2. Conceptual representation of Dynamic Combinatorial Chemistry (DCC) and Constitutional Dynamic Chemistry (CDC) (Figure reproduced from reference[21]).

The selective regulation of constituents by means of recombination of components at both the molecular and supramolecular levels defines the domain of *Dynamic Combinatorial Chemistry* (DCC).[22,23] On the other hand, the resulting constitutional variations also implicate

the realm of *Constitutional Dynamic Chemistry* (CDC).[24,25] The former emphasizes the dynamic interconnection of different chemical entities from the combinatorial point of view. In contrast, the latter is rather focused on the essential characteristics of chemical entities from the compositional point of view. The full collection of all possible constituents really or virtually generated *via* reversible connection defines a dynamic combinatorial library (DCL) or *constitutional dynamic library* (CDL).[26,27] When a DCL is subjected to external stimuli, these constituents engage in appropriate (positive and negative) feedbacks in response to the external factors to up- or down-regulate the composition of constituents. In full, a DCL features the following characteristics:[28]

- ✓ **Conversion**, the overall number of constituents regarding their initial components;
- ✓ **Composition**, the distribution or relative abundance of different constituents, as well as the selectivity of the system;
- ✓ **Expression**, the defined constituent which originates from conversion and selectivity.

The principle of regulating the composition of a DCL relies on various thermodynamic or kinetic properties of each constituent.[29,30] Examples of molecular recognition driven selection and amplification of the thermodynamically favoured constituents can be found in the "lock and key model".[22,27] A mixture of fragments(components) can generate a DCL containing a set of all the possible potential keys (constituents) under thermodynamic control. When this DCL is treated with a lock (an external effector), one (or more) key that fits best with the lock will be bound preferentially. This selection could either be thermodynamically controlled, through which the key that exhibits the strongest interaction with the lock will be produced, or be kinetically controlled, through which the key that forms fastest within the lock will be produced. This idea of fast screening the most complementary compounds in the presence of targets (receptors) has been specially developed in the field of drug discovery.[31–33]

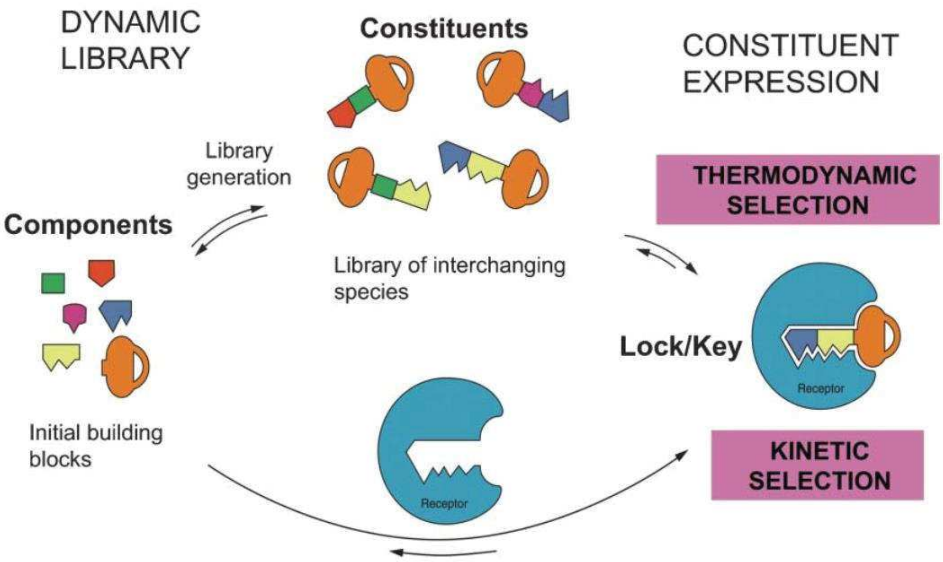

Figure I-3. Schematic representation of the concepts behind dynamic combinatorial chemistry and virtual combinatorial libraries. (Figure reproduced from reference[28])

1.2. Constitutional dynamic networks

In 2006, the interconnectivity of constituents was first represented in a square graph, termed a constitutional dynamic network (CDN) by Giuseppone and Lehn.[34] Basically, a DCL of four constituents **AB**, **AB′**, **A′B**, and **A′B′**, can be generated by dynamic reversible connections of components **A**, **A′**, **B**, and **B′**. The interconnections of the four constituents can be represented by a [2 × 2] square graph. The constituents that share one component and are therefore involved in antagonistic interactions (*e.g.*, **AB** and **AB′** or **A′B** and **A′B′**) are placed on the edges of the square, whereas constituents having no common component and exhibiting agonistic correlations (*e.g.*, **AB** and **A′B′** or **A′B** and **AB′**) are connected by the diagonals.

If the thermodynamic stabilities of four constituents **AB**, **A′B**, **AB′** and **A′B′** are similar, the concentration of each constituent in an equilibrated DCL should be similar as well. Such a distribution is defined as a statistical distribution (**Figure I-4** left). This equilibrated DCL is able to regulate its constitutional distribution in response to external effectors (**E**) through component recombination, therefore increasing one pair of the agonistic constituents and giving rise to a biased distribution (or enforced distribution, **Figure I-4** right). The external stimuli could be physical factors (*e.g.*, light,[35–38]temperature,[37] electric field,[39,40] or mechanical pressure[41]) or chemical factors *(e.g.*, metal ions,[29,42–44] pH[45–47]). Overall, the

stimuli induced DCL re-equilibrium not only underlines the selection of the fittest constituent, but also the up-regulation of the least fit agonistic constituent. Several specific examples of DCLs adapted to different effectors are described below in detail.

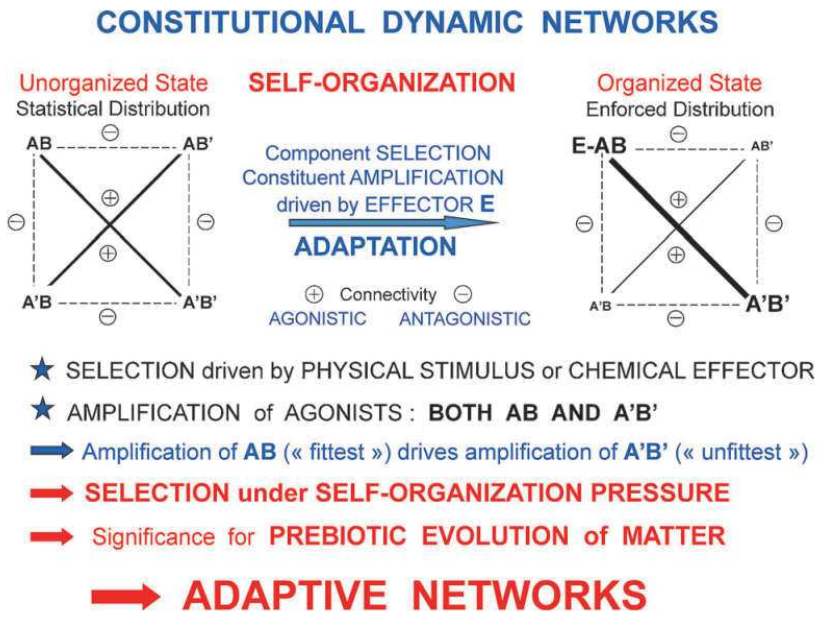

Figure I-4. Schematic representation of interconnectivities of constituents and their adaptation behaviour in response to effector **E** in a [2 × 2] CDN. (Figure reproduced from reference[48])

1.2.1. Adaptation to metal ions

In general chemical synthesis, metal ions have many uses, most importantly through selective coordination of one product within a mixture and through catalysis of product formation.[49] Both roles are particularly important in the chemistry of imines and related species such as hydrazones.[50] In the metallosupramolecular chemistry of C=N donor ligands, rational use of metal ions has led to specific adaptation behaviour of DCLs involving amplification of a responsive constituent and its agonist, with the concomitant reduction of the concentrations of their antagonists[42,51].

An elegant illustration of the regulation of distributions of DCLs by metallo-selection was achieved by Men and Lehn (**Figure I-5**).[52] A DCL of nine constituents was generated from three aldehydes (**A_4**, **A_6** and **A_7**) and three different amines (**D_3**, **D_4** and **C_1**), for which the interconnections can be represented by a [3 × 3] CDN (Figure 5). Upon addition of two metal cations (Fe(II) and Cu(I)) simultaneously or sequentially (Fe(II) then Cu(I)) to the pre-

equilibrated incomplete CDN ***NE***, the [3 × 3] CDN underwent a coordination controlled perturbation. The addition of Fe(II) resulted in the amplification of a single Fe(II) complex associated with its agonistic [2 × 2] sub-network. Subsequent addition of Cu(I) re-equilibrated the [2 × 2] sub-network, leading to the selective formation of a Cu(I) complex and its agonist. It is interesting to note that the DCL was destroyed by the first addition of Cu(I) because component D_4 caused the oxidation of Cu(I) to Cu(II). This work demonstrated that system complexity can be heightened by introducing additional effectors to a DCL but that this may result in a high level of selection and simpler outputs through the recombination of constituents.

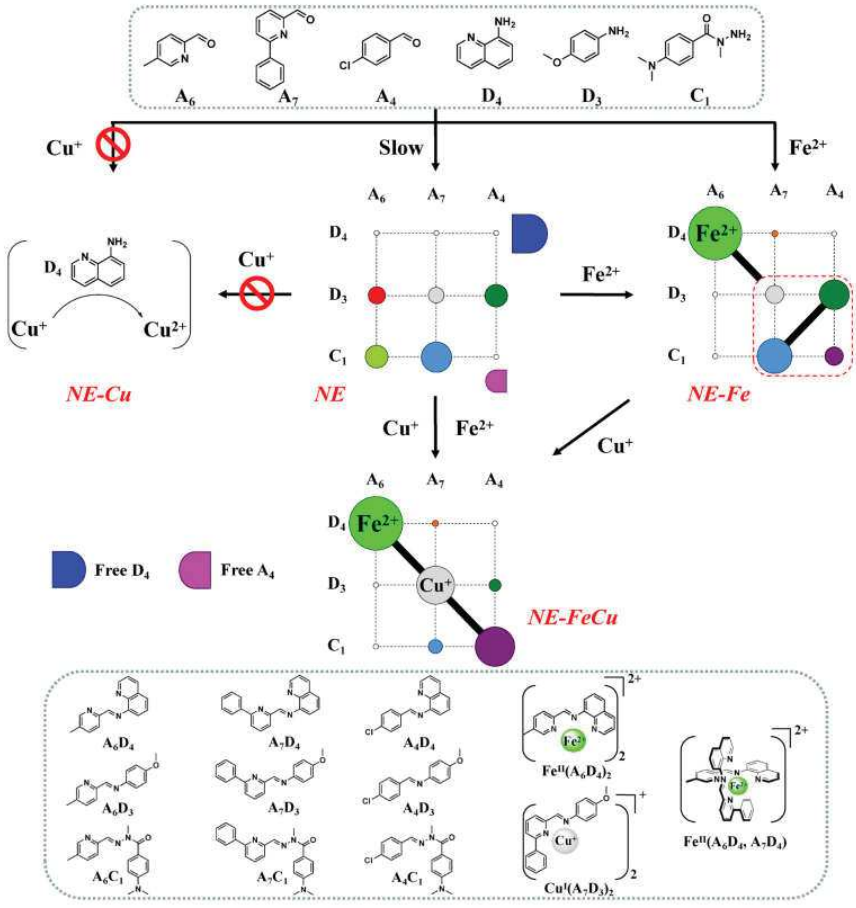

Figure I-5. Adaptation of the [3 × 3] CDN of a DCL of nine constituents formed from a mixture of six components (Figure reproduced from reference[52]).

Recently, adaptation to metal ions was analysed in terms of a "*dynamic fingerprint*" by Osypenko and Lehn for a biphasic system of immiscible solvents (**Figure I-6**).[21] DCLs containing imine constituents were pre-constructed as receptor library for metal cations in a

solvent mixture of chloroform and water. The key aspect of this "*dynamic fingerprint*" system is that adding metal cations into the water phase (information writing) resulted in distribution changes of constituents in the organic phase (information reading) via components reconstruction across the interface between two solvents. Chemical information written in one space domain affected the constitution of the chemical entities in the other domain, revealing a manner to deliver messages without a messenger.

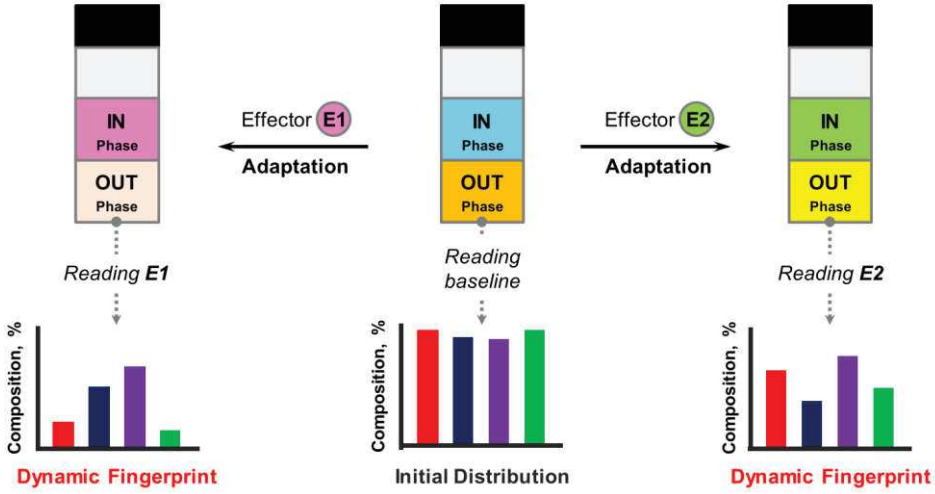

Figure I-6. Schematic representation of the generation of "*dynamic fingerprint*": addition of a particular effector **E1** or **E2** into the aqueous IN-phase, leads to the compositional variation of the organic OUT-phase. (Figure reproduced from reference[21]).

1.2.2. Adaptation to light

Compounds with C=N double bond, for example, imines, oximes or hydrazones, are a class presenting tunable photo/thermo-switches which display photo/thermo- responsive *E/Z* configurational isomerization via rotation about the C=N double bonds.[53] This switching between E/Z isomers can also be induced by metal cations. Supramolecular assemblies made through interactions with C=N double bonds can show reversible photo- and coordination-controlled ion release, phase separation[36], morphological change[54] and sol-gel transitions[55].

In 2014, Vantomme and Lehn investigated photo-induced isomerization and constituents redistribution of a DCL composed of acylhydrazone constituents ***E*-^{1}A^{1}C**, ^{1}A^{3}C, ^{2}A^{1}C, and ^{2}A^{3}C (**Figure I-7**).[44] Irradiation resulted in photoisomerization of constituent ***E*-^{1}A^{1}C** from its *E* conformation to the *Z* conformation (***Z*-^{1}A^{1}C**). Since intramolecular hydrogen bonding can

further stabilize the *Z* configuration, more ***Z*-^{1}A^{1}C** as well as its agonist **^{2}A^{3}C** were generated. Subsequently, an informational double entry CDN matrix based on four DCLs that are adaptive to both physical (light) and chemical (metal ions) dual stimuli was reported.[56] These studies illustrated the potential uses of DCLs as devices for information storage by means of distribution changes.

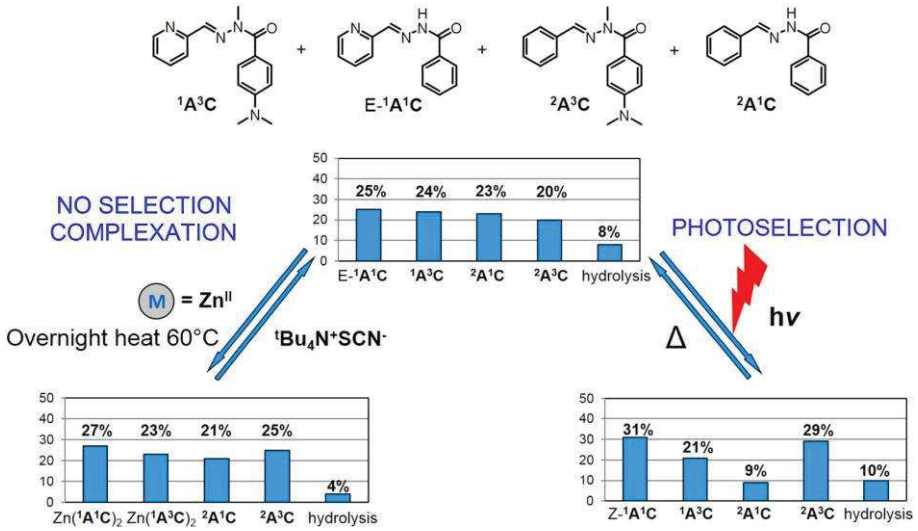

Figure I-7. Adaptation of a [2 × 2] DCL of four pyridylacylhydrazone constituents under metalloselection on addition of Zn(II) and photoselection by photoisomerization of E-^{1}A^{1}C into Z-^{1}A^{1}C on light irradiation (Figure reproduced from reference[44])

1.2.3. Adaptation to morphological change

Integrating stimulus induced isomerization into dynamic materials can result in morphological changes. For example, Ulrich and Lehn studied metal cation-induced reversible switching from linear polymeric to macrocyclic forms of diimines derived from a dialdehyde functionalized to provide metal ion chelation sites (**Figure I-8a**).[54] In the absence of metal ions, the core dialdehyde adopted a W shape with the aldehyde groups in a divergent array and formed linear oligomers or polymers by condensation with diamines. The addition of metal ions led to their binding to the tridentate (NNN donors) core of the dialdehyde and a conformational change placing the two aldehyde substituents in a close (near parallel) array suited to bridging by diimine formation with diamines of appropriate length and the formation of mononuclear macrocyclic ligand complexes. A similar methodology of metal

ion-controlled isomerization has been applied to achieve self-sorting and component selection in a competitive dynamic system containing two different amines.[57]

In combining both the metallo-selection and photo-selection behaviour of the same acylhydrazone as that of the Ulrich-Lehn study, dynamic systems featuring dual responses to both light and metal ions were reported by Vantomme and Lehn in 2014 (**Figure I-8b**).[35] This system demonstrated adaptive behaviour in three states: a non-selective oligomeric state, a metallo-selective macrocyclic state and a photo-selective macrocyclic state.

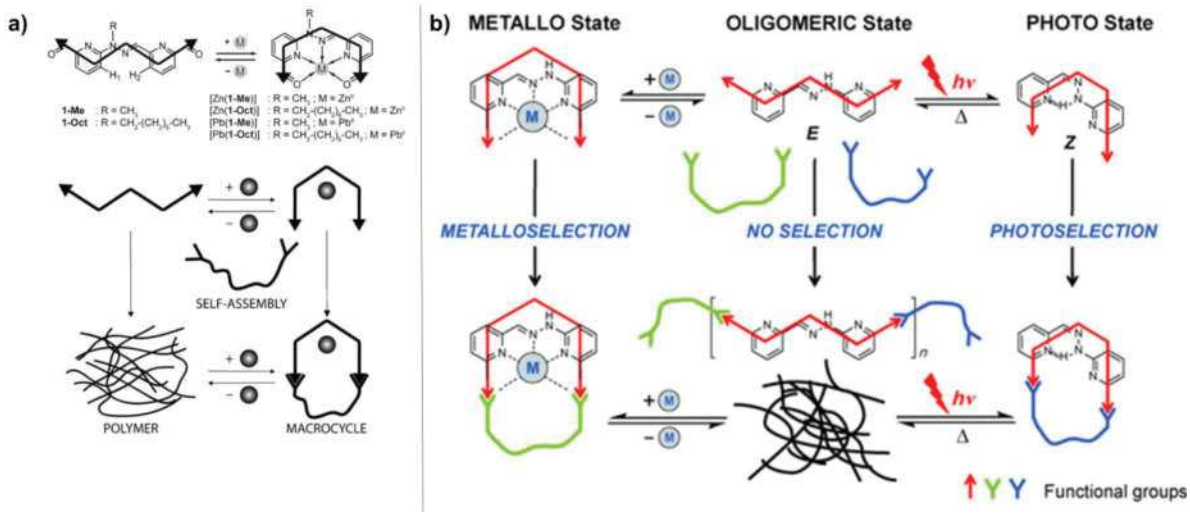

Figure I-8. Reversible switching from linear polymeric to macrocyclic states through component allosteric switching from W shape to U shape under (a) metallo-selection or (b) metallo-selection and photo-selection ((a) Figure reproduced from reference[54], (b) Figure reproduced from reference[35])

1.2.4. Adaptation to self-assembly and temperature

DCLs can be obtained by using well-known readily reversible reactions such as amine/carbonyl condensation, disulfide exchange, peptide exchange, olefin metathesis, and Diels−Alder condensation. Another reversible reaction of interest is the C=C/C=N organo-metathesis reported by Kulchat and Lehn.[58] The component recombination here took place between Knoevenagel (**Kn**) compounds derived from 1,3-dimethylbarbituric acid and imines through the formation of a four-membered azetidine intermediate.[59]

Temperature and self-assembly controlled triply dynamic DCLs were characterized by Gu and Lehn, on the basis of C=C/C=N organo-metathesis **Kn** double-step assemblies (**Figure I-9**).[60] **Kn** compounds can readily form supramolecular polymeric stacks in two

steps of a self-assembly pathway, i.e., self-assembly of **Kn** compounds into macrocyclic hexameric rosette by hydrogen bonding and self-assembly of the rosettes into supramolecular polymers by stacking. They designed DCLs with components containing adamantane groups to inhibit the polymeric stacking of rosettes. For example，a DCL was constructed by mixing equimolar concentrations of agonistic constituents, **Kn1** and imine **A3**. Upon heating, the DCL underwent C=C/C=N exchange and resulted in a statistical distribution of four constituents (**Kn1**, **Kn3**, **A1**, **A3**). Although both **Kn1** and **Kn3** can assemble into macrocyclic hexameric rosettes by hydrogen bonding, the adamantane group of **Kn1** inhibits its stacking, leading to its forming less stable supramolecular polymeric stacks. Hence, cooling of the DCL induced the generation of supramolecular polymeric stacks (**SP**) by **Kn3** and led to the selective amplification of **Kn3** and **A1** through C=C/C=N organo-metathesis.

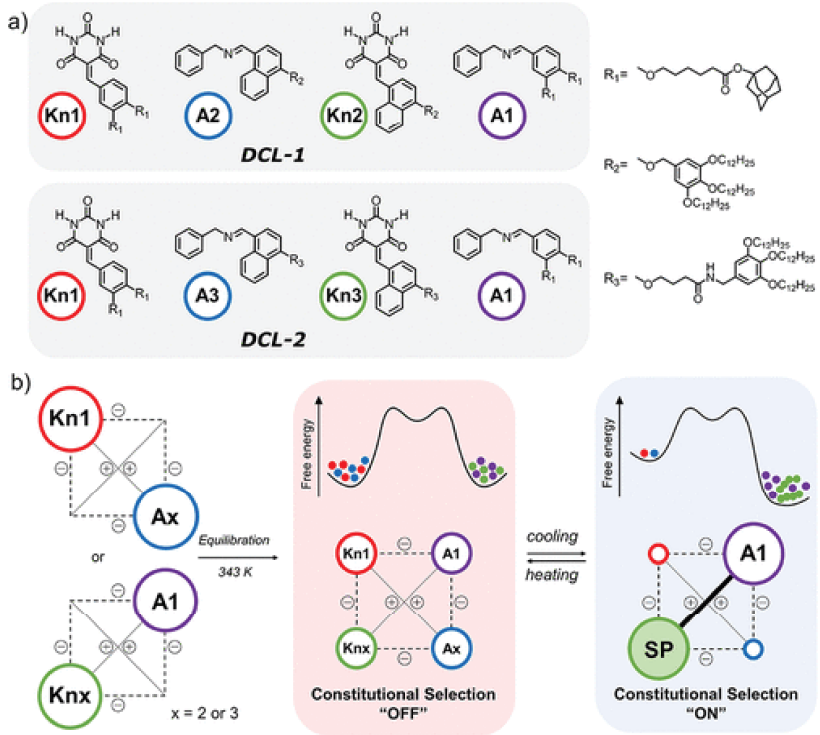

Figure I-9. Reversible adaptation of DCLs generated by Knoevenagel constituents and imines through C=C/C=N organo-metathesis (Figure reproduced from reference[60]).

1.2.5. Modulated adaptation to enzyme human carbonic anhydrase II (CA II)

In biology, carbonic anhydrases (CAs) are essentially Zn-based metalloenzymes that are engaged in the reversible hydration reaction between CO_2 and bicarbonate. Recently, studies

in the drug design area have targeted these CAs as they are involved in multiple physiological processes in cells such as the generation and regulation of proton gradients and ion exchanges.[61] While DCLs have gained prominence in tuning the catalytic functionality of various metalloenzymes, this is especially the case for CAs.[26,62,63]

On this behalf, Casciuc and Lehn evaluated predicting and modelling the distributional variations of imine-based DCLs adapted to carbonic anhydrase II (CA II) using a cheminformatics model.[64] Employing the constants of formation and affinities to CA II of nearly 60 000 imines, the perturbation of CA II by DCLs consisting of *n* aldehydes × *m* amines was predicted. Although the ideal selection and adaptation behaviours were not achieved in the current DCLs, the prediction model is still considered to evaluate and optimize promising agents in early drug discovery stages.

2. Dynamic Covalent Macrocycles and Cages

Many biological reactions are carried out in a confined region, such as the replication and transcription of DNA in the nucleus of the nucleoskeleton. The spatially restricted effect provides a special chemical environment that allows effective control of biochemical reactions. To mimic this phenomenon in nature, chemists have designed and synthesized various kinds of covalent organic macrocycles and cages with defined cavities. Such macrocycles and cages have shown promising applications in gas storage and separation,[65,66] catalysis,[67,68] sensing,[69,70] and biomedicine.[71]

The study of covalent macrocyclic and particularly macrobicyclic (cage-like) structures began to flourish in the 1960s following the seminal work of C. J. Pedersen,[72,73] D. J. Cram,[74] and J.-M. Lehn[1,75] on polyether systems and a landmark in the field was that Cram, Lehn and Pedersen were awarded jointly the Nobel Prize in Chemistry in 1987, due to “their development and use of molecules with structure-specific interactions of high selectivity”. The structure of macrocycles and cages made by covalent bonds are robust, however, and do not respond substantially to external environmental changes. An efficient way of endowing such covalent macrocycles and cages with dynamic and adaptive features is to link building blocks through reversible dynamic covalent connections. During the past decades, dynamic covalent reactions, such as imine formation, alkyne metathesis, disulfide exchange, and boronic acid condensation, have been widely used in the synthesis of dynamic macrocycles

and cages.[18] Here, this section is mainly focused on dynamic covalent macrocycles and cages generated by imine condensation. Many biological reactions are carried out in a confined region, as for instance the replication and transcription of DNA in the nucleus of the nucleoskeleton. The spatially restricted effect provides a special chemical environment that allows effective control of biochemical reactions. To mimic this phenomenon in nature, chemists have designed and synthesized various kinds of covalent organic macrocycles and cages with defined cavities. Such macrocycles and cages have shown promising applications in gas storage and separation,[65,66] catalysis,[67,68] sensing,[69,70] and biomedicine.[71]

The study of covalent macrocyclic and macrobicyclic (cage-like) structures began to flourish in the 1960s following the seminal work of C. J. Pedersen,[72,73] D. J. Cram,[74] and J.-M. Lehn on polyether systems.[1,75] A landmark in the field was that Cram, Lehn and Pedersen were jointly awarded the Nobel Prize in Chemistry in 1987, due to "their development and use of molecules with structure-specific interactions of high selectivity". The structures of macrocycles and cages made by covalent bonds are quite robust and do not substantially respond to external environmental changes. An efficient way of endowing such covalent macrocycles and cages with dynamic and adaptive features is to link building blocks through reversible dynamic covalent connections. During the past decades, dynamic covalent reactions, such as imine formation, alkyne metathesis, disulfide exchange, and boronic acid condensation, have been widely used in the synthesis of dynamic macrocycles and cages.[18] This section below is mainly focused on dynamic covalent macrocycles and cages generated by imine condensation.

2.1. Dynamic covalent polyimine macrocycles

A large number of imine macrocyclic compounds, which were mainly obtained by [1+1], [2+2], [3+3] or even [4+4] imine condensations (**Figures I-10**),[76–79] has been reported. The condensation reaction involves only two reactants, one dicarbonyl compound and one diamine. As a benefit due to the dynamic nature of a DCvC, external templates can efficiently help to select the size and improve the yield of a certain macrocycle from the DCLs.

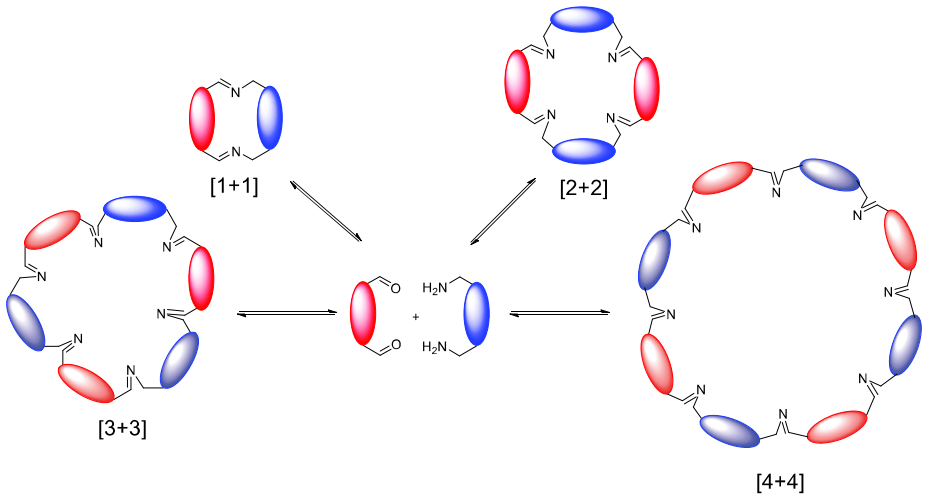

Figure I-10. Schematic representation of dynamic covalent macrocycles obtained by imine condensation

The use of metal ions as templates for synthesizing macrocycles has been intensively studied.[49] One of the pioneering studies was reported in the 1960s on the synthesis of polyamine-imine macrocycles. Curtis found that by reaction with appropriate diamine complexes and carbonyl compounds coordinated macrocyclic complexes could be obtained (**Figure I-11**).[80]

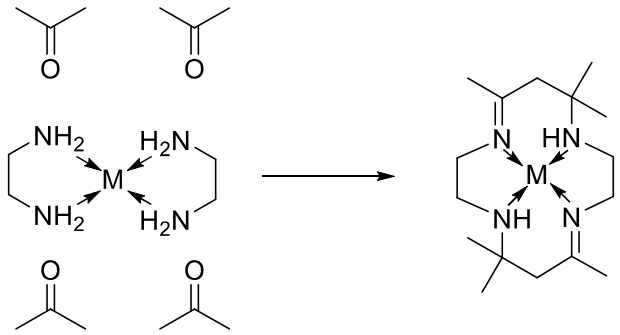

Figure I-11. The synthesis of hexamethyl tetra-azacyclotetradecadiene complex.

Lisowski *et al.* demonstrated that the size of the obtained macrocycles could be affected by the stoichiometry of the reaction mixture.[81] Without metal ions or in the presence of 0.5 equivalents of Zn^{2+}, the reaction of 4-tert-butyl-2,6-diformylphenol with (1R,2R)- or (1S,2S)-1,2-diaminocyclohexane produced mainly the [3+3] macrocycle. When 1 equivalent of Zn^{2+} was present in the system, the main product shifted to [2+2] macrocycle zinc complex.

In addition to metal ions, organic cations can also be used as templates. Jiang and co-workers reported the compositional and configurational modulation of syn/anti macrocycles

by quaternary ammonium cations (**Figures I-10**).[82] After mixing a bis-naphthalene dialdehyde and its analogous diamine, a DCL containing numerous constituents including [2+2] condensed isomers of ***syn*** and ***anti***-forms resulted. With the addition of quaternary ammonium cations, only one specific [2+2] condensed macrocycle, either ***syn*** or ***anti*** isomer, was selectively produced. An adaptive *anti-syn-anti* structural reconfiguration was also performed by the sequential addition of three different quaternary ammonium cations.

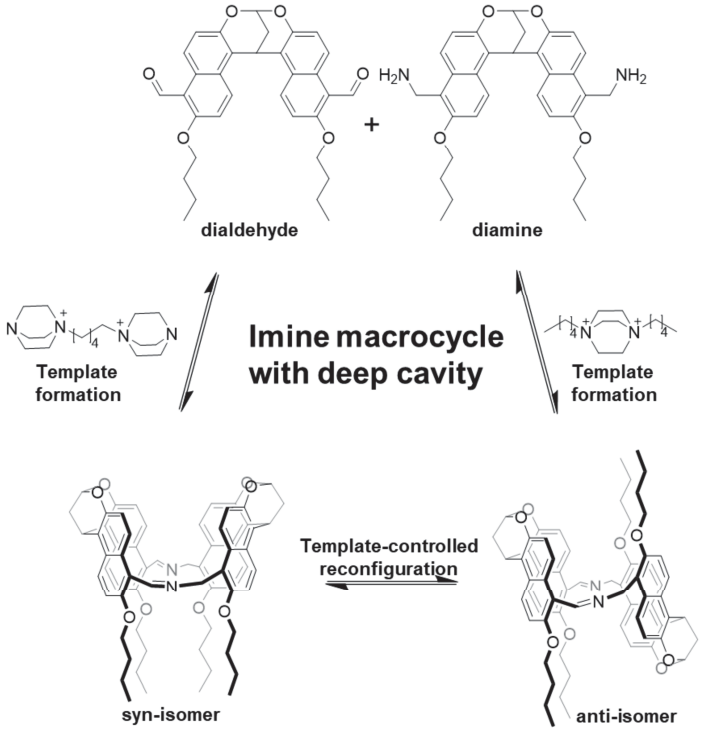

Figure I-12. Guest-controlled reconfiguration of macrocyclic syn/anti isomers

2.2. Dynamic covalent polyimine cages

In 1987, Jazwinski and Lehn *et al*,[83] reported a class of polyaza macrobicycles obtained from dialdehydes and a triamine (tren) via [3+2] condensation reactions (**Figures I-13**) without the use of a template. A year later, using an approach of this type MacDowell and Nelson extended the family members of such macrobicyclic cages.[84] Their pioneering research laid a robust foundation for the rapid development of polyimine covalent cages. As in the case of macrocycles, the reversible nature of the imine bonds also conferred the imine cages with unique stimulus responsive behaviours. Various cages with interesting topologies and functions can be obtained using different polyaldehyde and polyamine compounds.[85–88]

As for their macromonocyclic relatives, these cages are dynamic and are able to adapt in response to environmental changes.[89]

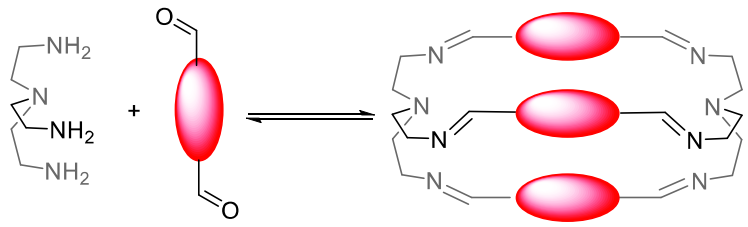

Figure I-13. Synthesis strategy of [3+2] imine macrobicyclic cages

2.2.1 Transformation from Monomeric Cages to Interlocked Cages

As indicated in a paper published in 2006 by Liu and Warmuth, the cage structures obtained from imine condensations are subject to solvent effects.[90] They found that for the condensation reaction of a tetraformylcavitand with ethylenediamine, a [4+8] organic cage was obtained in THF in 35% yield, a [6+12] organic cage (82% yield) in chloroform while the largest cage was formed in DCM as an [8+16] species (65% yield).

Cooper and co-workers reported the synthesis of three [4+6] tetrahedral porous organic cages produced through imine condensation of 1,3,5-triformylbenzene with a series of 1,2-ethylenediamine derivatives in 2009.[91] The solid [4+6] cage is stable for many months, but in appropriate solvents could be converted into triply interlocked catenanes even in the absence of acid.[27] Thus, after 50 days in a dichloromethane/p-xylene mixture, a dimeric triply interlocked catenane crystallised out. Crystallographic analyses indicated that the π-π stacking interaction between two encapsulated arenes may have helped to stabilize the interlocked cage. The low solubility of the catenane may also have been a factor determining its isolation.

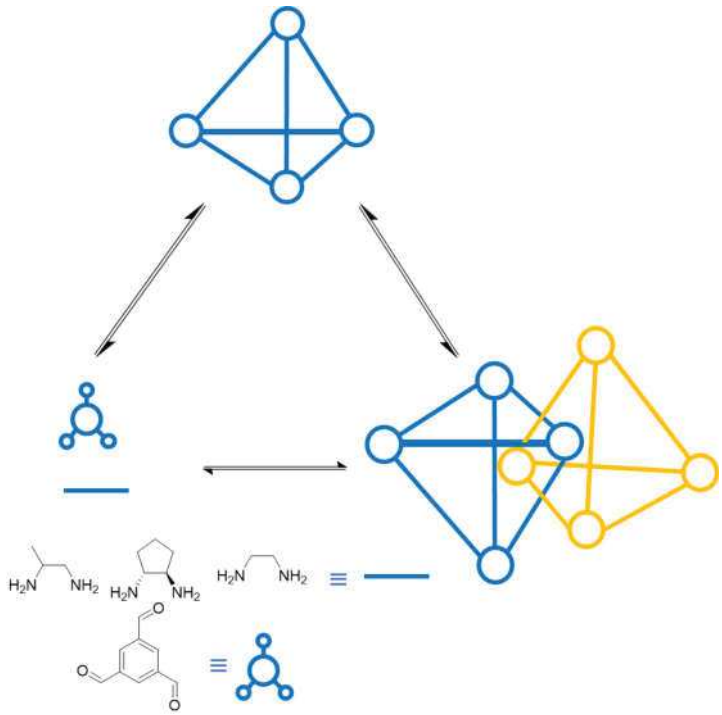

Figure I-14. Formation of [4+6] monomeric cages and dimerization into triply interlocked catenanes.

In 2018, the same group subsequently characterized 33 pure discrete [4+6] cages obtained from 78 independent reaction mixtures involving the permutation of 3 candidate triamines and 26 candidate dialdehydes or trialdehydes (**Figures I-15**).[92] More importantly, the recrystallisation of [4+6] cages led to the generation of a new topology of doubly bridged triply interlocked [8+12] cage catenanes. DFT calculations confirmed the lower formation energy of interlocked [8+12] cage catenanes than that of the [4+6] cages.

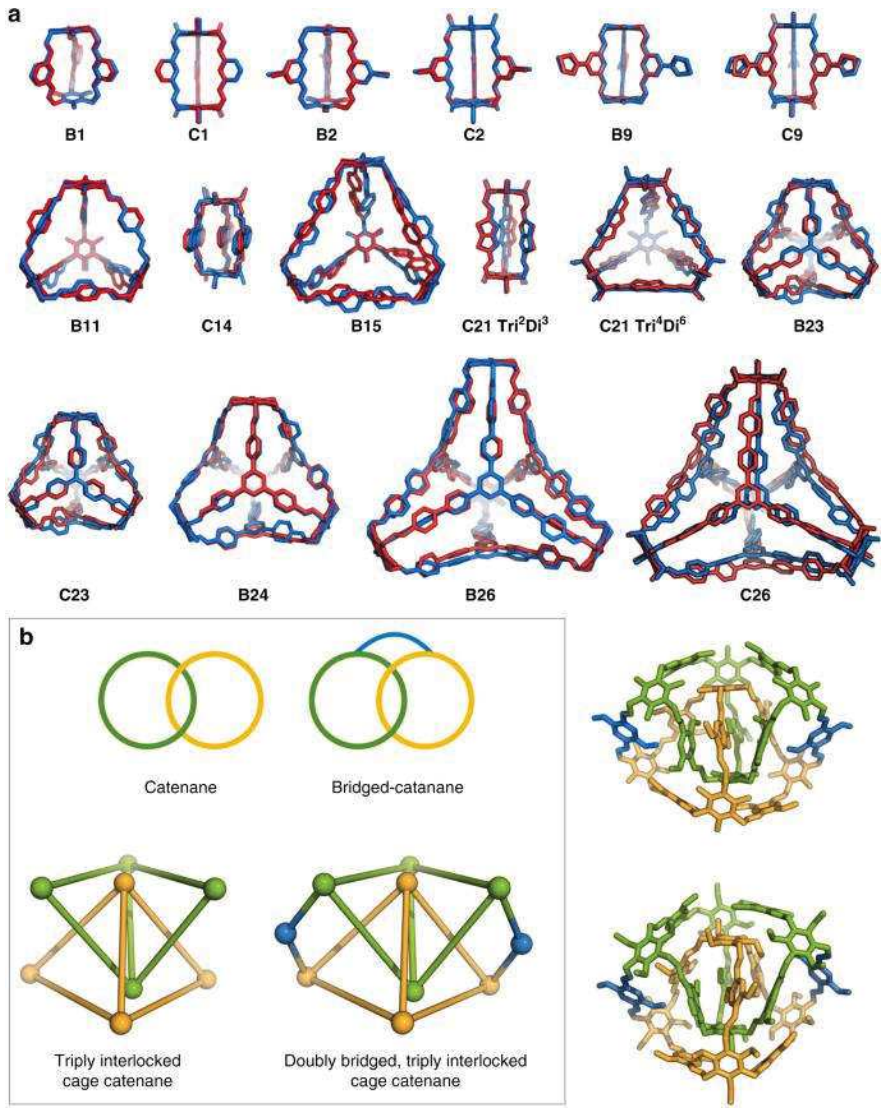

Figure I-15. Crystal structures of [4 + 6] cages and [8 + 12] covalently bridged, triply interlocked cage catenanes.[92] (Figure reproduced from reference[92])

2.2.1. Guest-induced assembly and disassembly

A guest may have an influence on both the formation and decomposition of a cage. In 2017, Zonta *et al.* reported the assembly and disassembly study of an imine cage which was synthesized *via* [2+3] imine condensation of a **(TPMA)Zn(II)** complex with ethylenediamine (**Figures I-16**).[93] In the presence of a single alkyl chain dicarboxylic acid of the C4-C14 series, the trialdehyde complex bound to the diacid and accelerated the formation rate of the imine cage as a template. Without the addition of the diacid, the imine cage formed slowly. Of all the diacids used, the C8 diacid exhibited the best binding ability with the imine cage.

The authors also studied the hydrolysis kinetics of this imine cage and concluded that the rate of hydrolysis was correlated with the size/length of the diacid rather than the binding constants of the cage with diacid guests. This was explained by postulating that the diacids bridged the two Zn(II) sites within the cage, with the short-chain diacids (C4-C6) drawing the Zn(II) centres together and retarding hydrolysis, while the long-chain diacids (C10-C14) would have to twist and fold to form the internal bridge, thus creating compression which would be relieved by the hydrolysis. Therefore, the hydrolysis experiments indicated that the disassembly rate of an imine cage could be influenced the by strain release of a guest.

In a further study, the same authors described a DCL of imine cages produced by reaction of the **(TPMA)Zn(II)** complex with a mixture of diamine blocks of different sizes for efficiently sensing dicarboxylate anions of C5-C14 chain length.[94] The DCL of imine cages behaved differently as a function of the different lengths of the C5-C14 diacids. Briefly, the composition of the principal constituents in the DCL responds similarly to longer dicarboxylates.

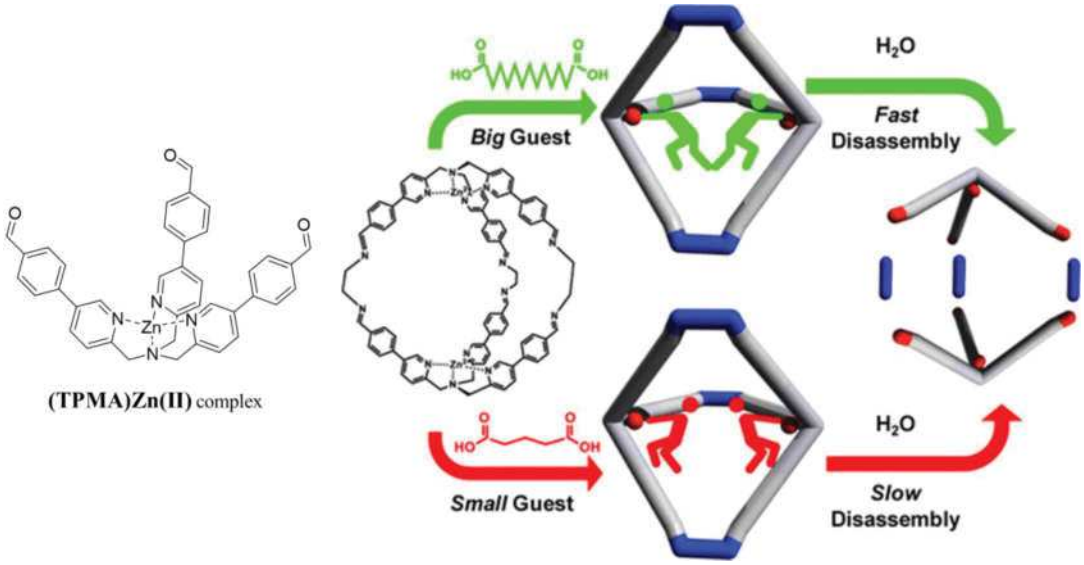

Figure I-16. Assembly and disassembly of an imine cage generated by condensation of **(TPMA)Zn(II)** complex with diamine in the presence of long-chain diacids C4–C14 (Figure reproduced from reference[93]).

2.2.2. Exchange of building blocks

Due to the coordination ability of nitrogen atoms in imine bonds, aldimines can be used

in the synthesis of metal organic cages. This sort of cage-like architecture containing both non-covalent and dynamic covalent connections possesses good dynamic features.

Nitschke *et al.* studied the imine exchange behaviour at the vertices of $Fe(II)_4L_6$ imine based tetrahedral metal organic cages (**Figures I-17**).[95] In the presence of Fe(II) ions, metal-organic cage **2** arose by condensation of *p*-chloroaniline with 3,3'-bipyridine-6,6'-dicarbaldehyde. Subsequently, due to the large difference in electronic properties of the two electron-rich substituents *p*-methylaniline (σ = -0.17) and *p*-methoxyaniline (σ = -0.27) compared to the electron-deficient *p*-chloroaniline (σ = +0.23), cages **3** and **4** were obtained by quantitative exchange of *p*-chloroaniline units with *p*-methylaniline and *p*-methoxyaniline, respectively. The electronic properties of *p*-methylaniline (σ = -0.17), and *p*-methoxyaniline (σ = -0.27) are less different, so the conversion from cage **3** to **4** was achieved in only 79% yield. ESI-MS demonstrated that when p-chloroaniline, *p*-bromoaniline, and *p*-iodoaniline (4 equivalents each) were mixed with 3,3'-bipyridine-6,6'-dicarbaldehyde (6 equivalents) in the presence of Fe(II) ions, a DCL containing 91 constituents can be generated. Upon adding 12 equivalents of the more electron-rich *p*-methoxyaniline, all of these 91 constituents were converted to the homonuclear cage **4**.

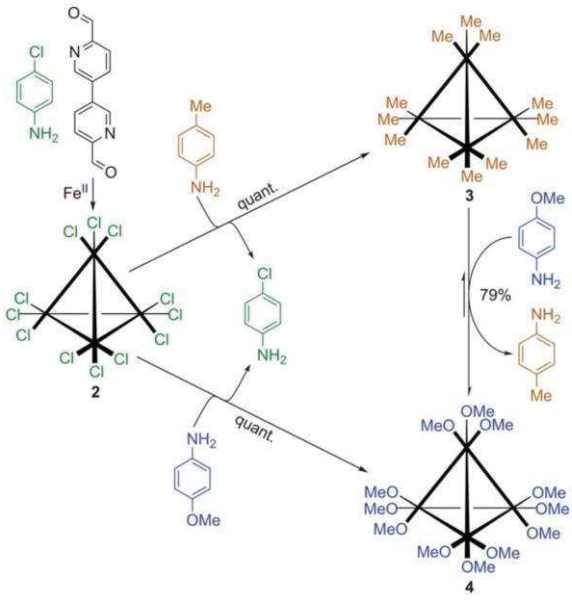

Figure I-17. Component exchange in the tetrahedral Fe(II) cages driven by electronic-rich anilines. (Figure reproduced from reference[95]).

2.2.3. Dissipative transimination

In nature, chemical fuels, such as ATP, are continuously converted into high-energy species to allow the operation of dissipative self-assembly behaviour. Artificial dissipative systems mimicking these natural phenomena have attracted increasing attention in recent years.[96,97]

The concept of dissipative self-assembly can indeed be applied in the case of transimination reactions. A recently reported example of dissipative transimination involved the transition between two imine cages from a DCL of a pre-formed cage and a free aromatic polyamine (**Figures I-18**).[98] By the addition of tribromoacetic acid as a chemical fuel, the initially formed [1+1] cage **6** disintegrated immediately due to the protonation and precipitation of the aliphatic amine **7**, while the [4+4] cage **CBC 5** gradually formed. As tribromoacetic acid decomposed to CO_2 and $CHBr_3$ over time, $[\mathbf{7\text{-}H_3}]^+$ was deprotonated and re-dissolved into the solution, inducing a second cage-to-cage transformation process with the re-formation of [1+1] cage **6**. This work illustrates a path towards the design and preparation of dissipative, temporal materials through the dynamic covalent chemistry strategy, demonstrating a way to regulate the composition of constituents and achieve a dissipative off-equilibrium state of a DCL.

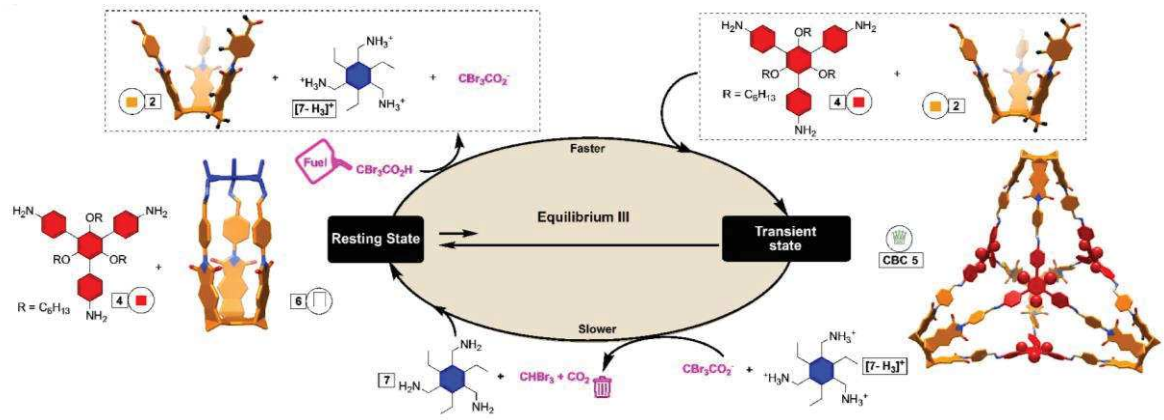

Figure I-18. Dissipative Cage-to-cage transformation via transimination (Figure reproduced from reference[98]).

3. Self-Sorting in Constitutional Dynamic Chemistry

3.1. The concept of self-sorting

The term of "self-sorting" is defined as the selective formation of substructures by a species with a high ability to distinguish itself from non-self in complex systems. It is relevant to most biological processes and is essential for ensuring the realization of sophisticated functions in biological systems. For example, the formation of microtubules requires the self-sorting of α-tubulin and β-tubulin to form tubulin dimers, and the self-sorting of tubulin dimers to generate the orthogonal supramolecular assembly. In living cells, proteins are delivered to their appropriate destinations using a self-sorting process known as protein targeting. Self-sorting also plays a crucial role in the assembly of adenine-thymine (A-T) and cytosine-guanine (C-G) in a certain sequence.

Self-sorting behaviours may provide important clues for understanding the origin of life and for improving the design of artificial biomimetic systems. To better understand the self-sorting phenomenon of living systems in nature, chemists have been working on the construction of artificial self-sorting systems to imitate the highly organized behaviour in competing environments at the supramolecular and molecular levels.

The first actual contact with self-sorting in chemistry was probably Pasteur's discovery of "spontaneous resolution", the separation by crystallisation of optical isomers of sodium ammonium tartrate from its racemic mixture in the 19th century.[99] The simultaneous cogeneration of highly ordered self-organized complex systems (artificial self-sorting system) in solution, was reported by Lehn in the 1990s.[100] It was found that under appropriate conditions, mixing two different tris-bipyridine ligands with 3 equivalents of Cu(I) and 3 equivalents of Ni(II), the two ligands coordinated to Ni(II) or Cu(I) simultaneously and orthogonally from one another, which led to the simultaneous formation of triple or double helix structures, respectively (**Figures I-19**). No other assemblies could be detected by either fast atom bombardment mass spectrometry or ^{1}H NMR. This self-sorting or self-recognition allowed the preferential binding of complementary ligand chains on the metal ion templates regardless of other ligands in the same solution, thus enabling the spontaneous discrimination and self-organization of target molecules from a multi-component mixture at the supramolecular level.

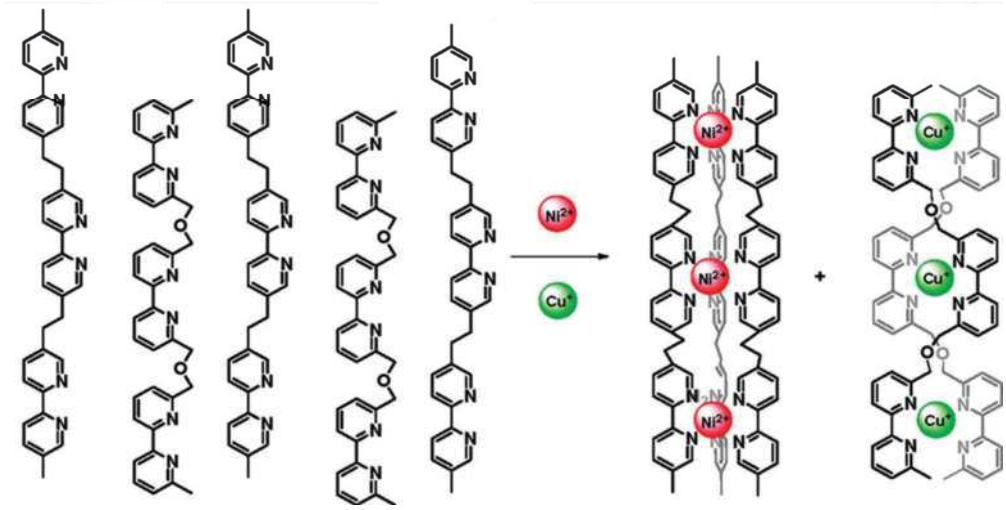

Figure I-19. Cogeneration of triple or double helix assemblies via highly selective self-organization process (Figure reproduced from reference[100]).

Since then, numerous examples have confirmed the precise assembling behaviour of supramolecular architectures in competitive conditions by dynamic non-covalent interactions such as hydrogen bonding,[101–103] metal-ligand interactions,[104–106] and electrostatic interactions[107]. In 1997, Sanders and co-workers first introduced the term of self-sorting in their study of macrocyclization via intermolecular transesterification.[108]

Wu and Issac defined self-sorting as the efficient distinction between imprecise and precise structures, and introduced the concepts of "thermodynamic self-sorting" and "kinetic self-sorting".[109] Thermodynamic self-sorting refers to the self-classification phenomenon that occurs at thermodynamic equilibrium, while other non-thermodynamic equilibrium systems controlled by kinetics are classified as kinetic self-sorting systems. Most of the currently published works on self-sorting can be regarded as thermodynamically controlled systems. They also distinguish self-categorization systems as "narcissistic self-sorting" and "social self-sorting ". The former refers to the case where a particular kind of molecule has a high affinity with itself (**Figure I-20**, pathway B), while the latter is defined as the case where one kind of molecule exhibits a high affinity toward a different kind of molecule (**Figure I-20**, pathways A, C and D). "Narcissistic self-sorting" is also called " homoleptic self- sorting" and "social self-sorting" is also known as "heteroleptic self-sorting".

Schalley *et al*. also categorized self-sorting as "integrative" and "non-integrative".[110,111] Through integrative self-sorting, a mixture of all initial components can assemble into only one assembly. In contrast, by non-integrative self-sorting, all substrates are able to assemble

into a mixture but one that is smaller than the possible set of discrete assemblies at the same time, as shown in pathways B and C of **Figure I-20**.

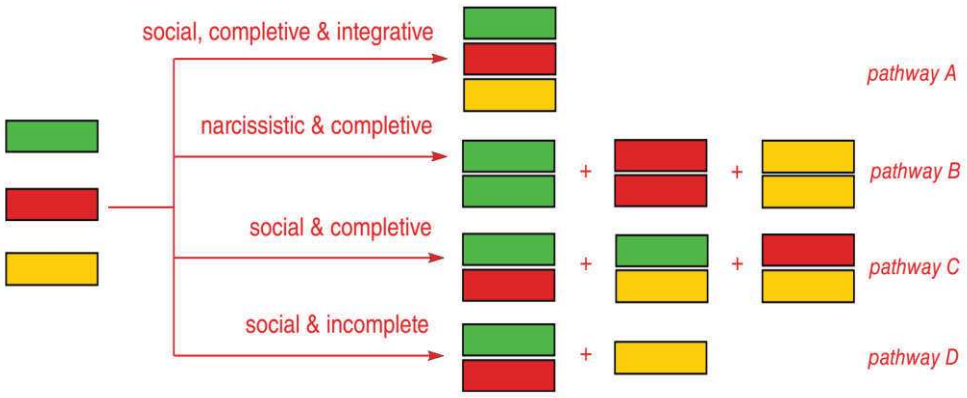

Figure I-20. Classification of self-sorting systems (Figure reproduced from reference[112])

3.2. Self-sorting under metallosupramolecular interactions

Schmittel and co-workers reported a metal-ligand coordinated self-sorting system generated by phenanthroline (**1**) and pyridinediyl aldehyde (**2**) (**Figure I-21**) in the presence of Cu(I).[113] Due to the different number of electron-donor atoms of phenanthroline and pyridine units, the geometric configuration of the produced metallo-supramolecular architectures was affected by the stoichiometry of the metal ion. The 1:1:1 ratio of **1: 2: Cu(I)** resulted in an incomplete homoleptic self-sorting state with grid **S** and free **2**; when 1:1:1.5 ratio was used, an incomplete heteroleptic self-sorting state with triangle **T** and half amounts of **2** was obtained; while a 1:1:2 ratio led to the completive heteroleptic self-sorting of grid **R**. More interestingly, by adding or removing appropriate amounts of Cu(I), fully reversible interconversion between these three distinct self-sorting states was achieved. Thus, a metal-stoichiometry-controlled dynamic switchable self-sorting system was achieved.

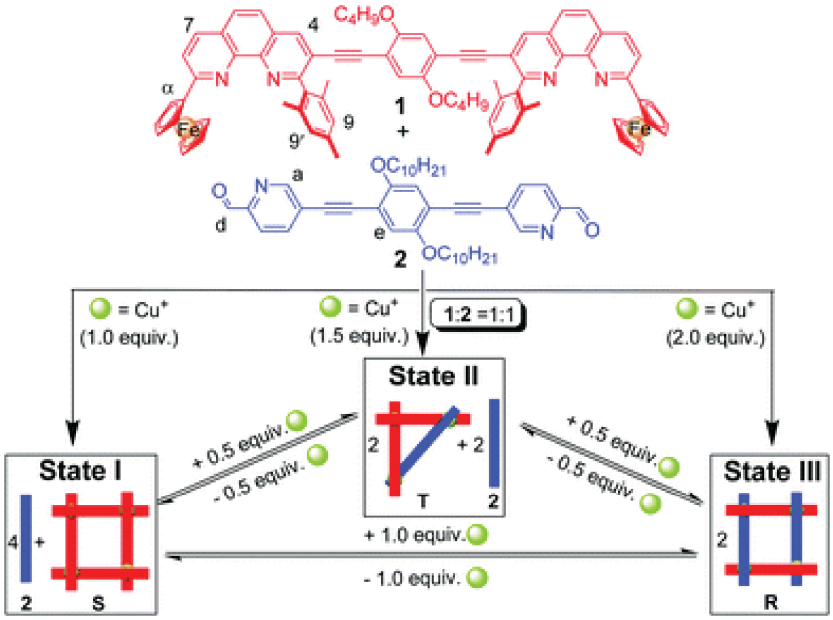

Figure I-21. Three-state cyclic interconversion of the metallosupramolecular complexes S, T and R depending on the Cu+ amount (equiv. refer to the amount of **1**) (Figure reproduced from reference[113])

The group of Reinhoudt characterised a supramolecular self-sorting system based on hydrogen bonding (**Figure I-22**).[114] They reported the co-assembly of bis(melamine)-calix[4]arenes (**b-Calix**) and barbituric acids (**B**) into stable double layer rosette box structures **(b-Calix)$_3$(B)$_6$** connected through 36 hydrogen bonds. Furthermore, a tetra-layer rosette box involving 72 hydrogen bonds could be obtained by replacing bis(melamine)-calix[4]arenes with their dimerized (through bridge X) tetramelamine derivatives (**t-Calix**). Competitive experiments showed that free **b-Calix** caused the disassembly of the tetra-layer rosette box **(t-Calix)$_6$(B)$_{12}$** and led to the generation of a double layer rosette box. Thus, the double layer rosette box is more stable than the tetra-layer one. Thereafter, self-sorting experiments confirmed the efficient simultaneous formation of these two assemblies by mixing **b-Calix** and **t-Calix** in a ratio of 2:1 with a slightly excess of **B**. However, mixing equal amounts of tetramelamine **t-Calix** derivatives (bridge X = -$(CH_2)_6$- or -CH_2(m-C_6H_4)CH_2-) with **B** resulted in scrambling and generation of various heteromeric assemblies containing both tetramelamines.

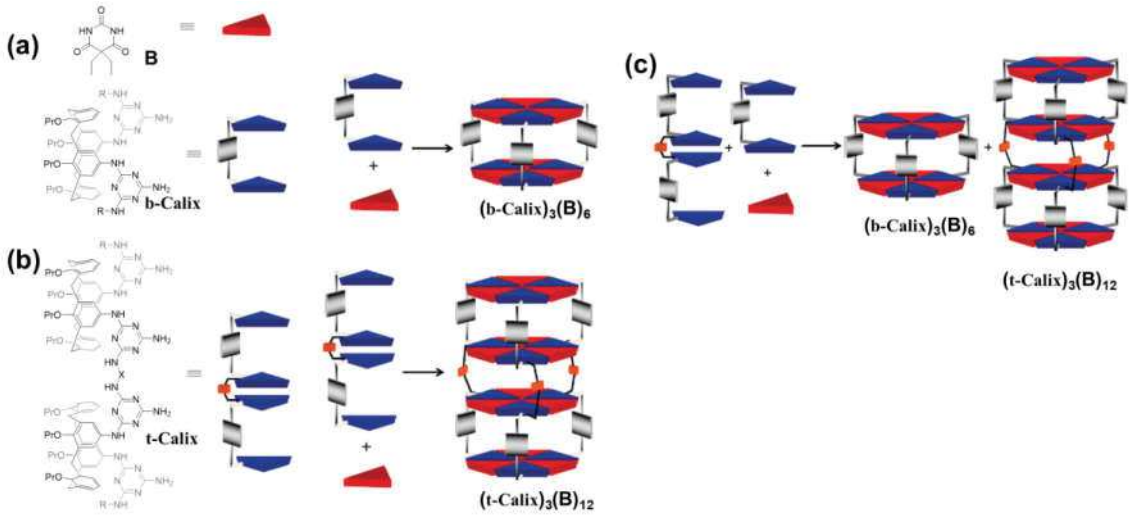

Figure I-22. Schematic representation of the self-assembling of double layer rosette box and self-sorting of double layer and tetra-layer rosette box. (Figure reproduced from reference[114]).

Recently, in a similar manner, Gu and Lehn described a hierarchical two-level self-sorting from a DCL of two Knoevenagel derivatives with two imino-derivatives.[60] This system achieved self-sorting in two levels, self-sorting of constituents into two kinds of discrete hexameric rosettes by hydrogen bonding, and self-sorting of one of the rosettes into a cylindrical supramolecular polymer by stacking (see **Figure I-9**).

3.3. Self-sorting under dynamic covalent chemistry

Self-sorting systems dependent upon the operation of dynamic covalent bonds have also been widely studied. Reversibility of dynamic covalent bonds permits the erasure of undesired intermediates (error correction) through the exchange of components and results in the most thermodynamically stable structures from DCLs.

3.3.1. Metal-imine coordination

The coordination of metal-imine bonds can be used to construct supramolecular structures as well as to produce self-sorting systems.[115–117] Nitschke *et al.* found that the mixing of two pyridine monoaldehydes and two amines (a triamine and a monoamine) in water resulted in a DCL containing 11 imine constituents (**Figure I-23**).[118] Mixing two metal ions, Cu(I) and Fe(II), into this DCL drove the re-equilibration of the constituents and eventually to the simultaneous formation of only two discrete imine complexes. Although the aldehyde substrates structurally differ by only one methyl group, the Cu(I) ion exhibited a

higher selectivity for the more electron-rich methylpyridine, while Fe(II) selectively bonded the pyridine without methyl to reduce unfavourable spatial interactions in the hexadentate imine complex.

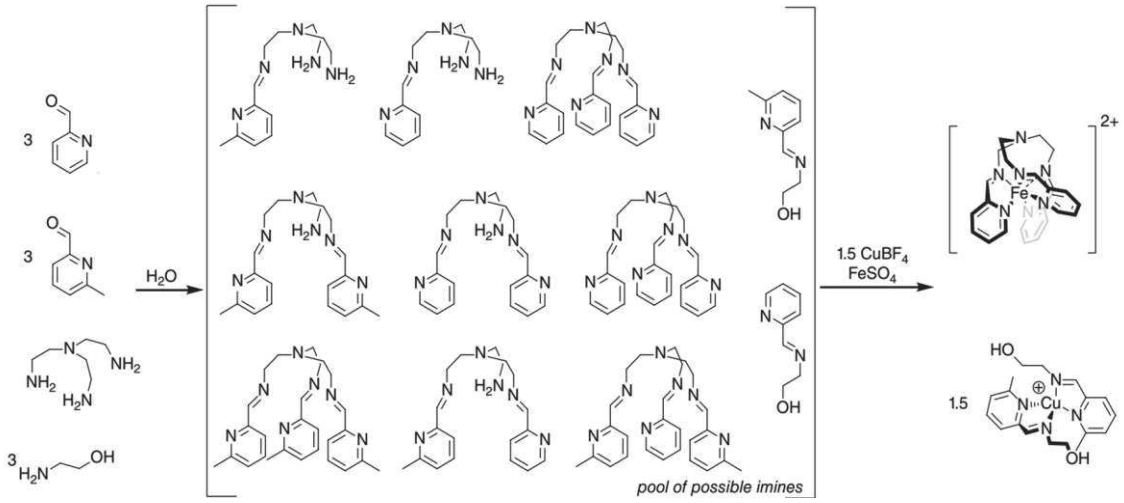

Figure I-23. Coordination driven selection and self-sorting from a DCL of 11 possible imine constituents

3.3.2. Self-sorting resulting in similar structures

Self-sorting can also be achieved in systems without the involvement of metal templates, by taking advantage of the thermodynamic selectivity of imine bonds. Sanders *et al.* first introduced the term self-sorting into chemical systems and reported a thermodynamically controlled self-sorting system based on a transesterification reaction (**Figure I-24**).[108] Two hydroxy esters were mixed and heated at reflux in toluene with a methoxide ion catalyst (MeOK/18-crown-6). In the equilibrium state, one formed a trimer through a three-molecule condensation reaction, while the other one condensed to form a dimer, with only minor amounts of heteroleptic structures present. This work laid the foundation for the construction of thermodynamically controlled self-sorting systems by reversible covalent bonds.

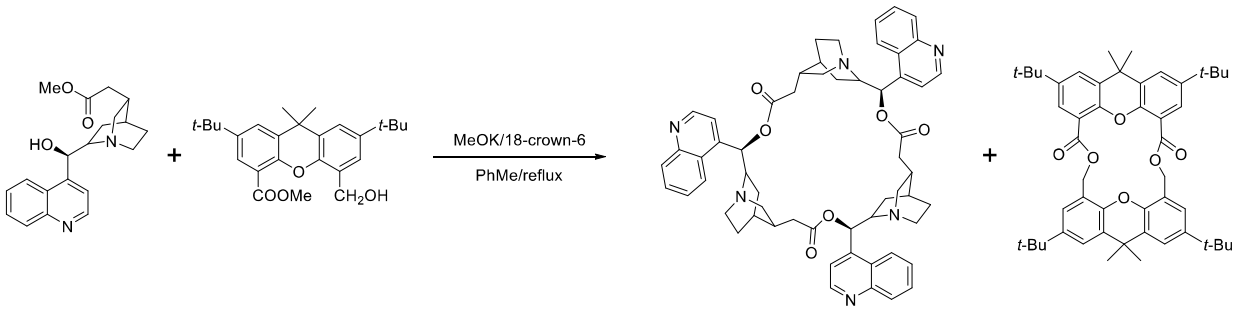

Figure I-24. Self-sorting based on transesterification reaction (from reference 104).

The group of Mukherjee has obtained a series of interesting results in the self-sorting of imino-cages.[119–121] As shown in **Figures I-25**, when two bent dialdehydes **A** and **B** were mixed with two triamines **X** and **Y**, in the molar ratio of 3:3:2:2, a self-sorted output was generated among the four components, which eventually yielded only two [3+2] homoleptic cages. After independent synthetic studies of four homogeneous cages and careful analysis by DFT calculations, they concluded that the whole self-sorting process of producing two homoleptic cages is thermodynamically controlled. Under thermodynamic control, they achieved the conversion of a thermodynamically less stable cage into one with greater stability by introducing another dialdehyde or triamine to replace the disfavoured cage building unit.

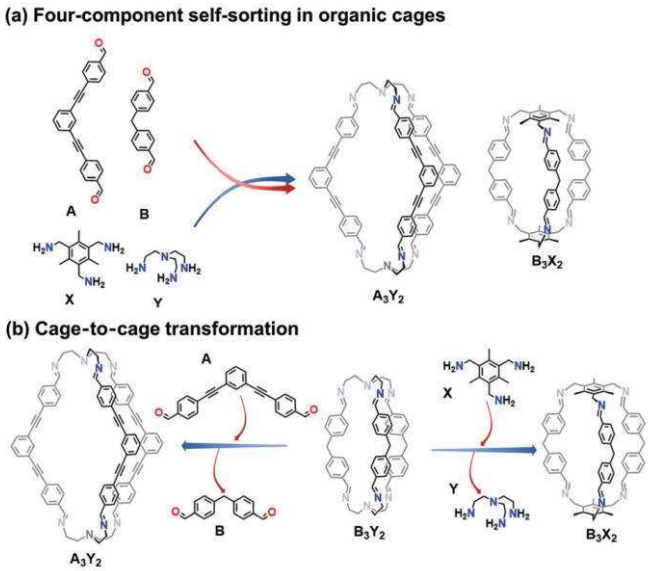

Figure I-25. (a) self-sorting of [3+2] homoleptic cages via imine condensation and (b) cage-to-cage transformation through component exchange (Figure reproduced from reference[121]).

Similarly, Lehn *et al.* reported a selective self-sorting behaviour of imine cages within competitive conditions of two dialdehydes with triamine in a molar ratio of 3:3:2 (3 for each dialdehyde and 2 for triamine).[122]

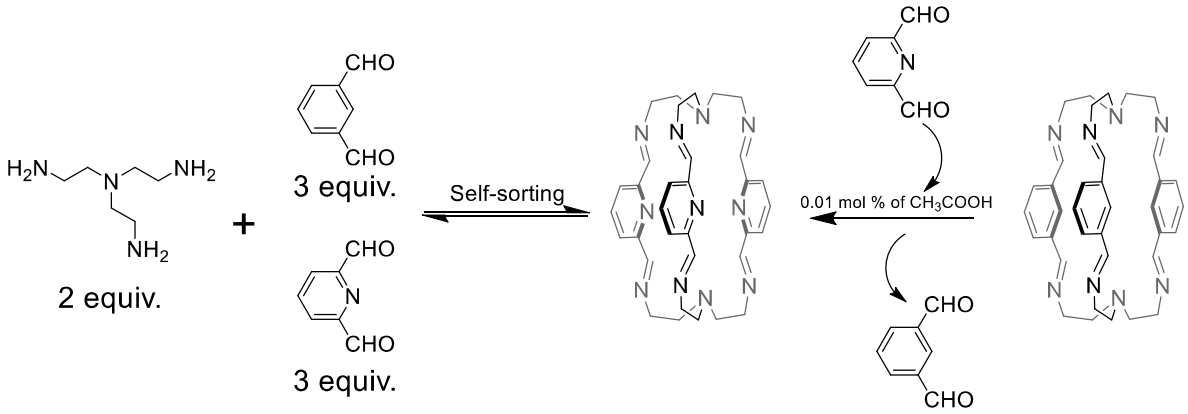

Figure I-26. Incomplete self-sorting and component exchange of imine cages.

3.3.1. Self-sorting resulting in distinct structures

Most known self-sorting systems involve discrimination between similar structures. The generation of distinct structures *via* self-sorting processes is less common and warrants specific consideration.

In 2020, Lehn *et al.* obtained a [2 × 2] grid-like complex and a linear double helix structure simultaneously in DCLs that were generated from two monoamines, two dialdehydes, and two metal ions, as shown in **Figure I-27**.[123] This system demonstrated impressive examples of self-sorting of two distinct supramolecular assemblies at three levels. Firstly, at the molecular level, the self-sorting led to the generation of only two imine bonded ligands. Secondly, at the supramolecular level, the self-sorting of metals and imine ligands was brought about by selective coordination interactions. Finally, the self-sorting of two discrete supramolecular assemblies was obtained by selective self-organization of constituents. This study also demonstrated that the resulting output from DCLs could be influenced by both coordination and structural/conformational characteristics of the initial components.

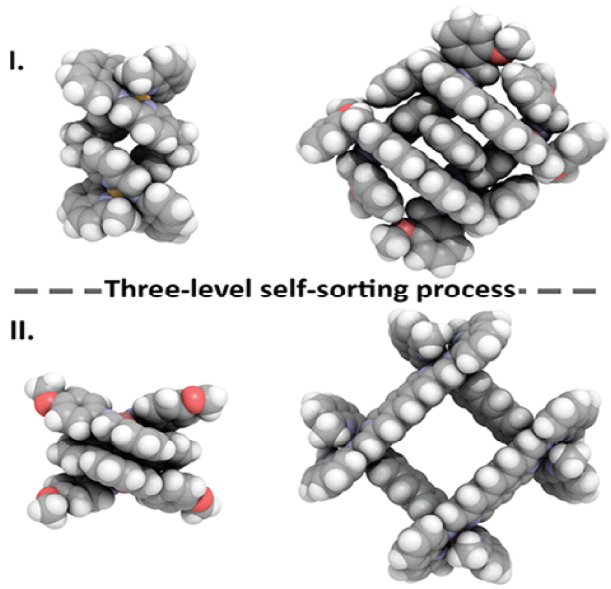

Figure I-27. Self-sorting of a [2 × 2] grid-like complex and a linear double helix (Figure reproduced from reference[123]).

Otto *et al.* studied by HPLC-MS the formation kinetics of a self-sorting system generating foldamers and self-replicators in 2021.[124] The authors found that with different molar ratios of the building blocks, the self-sorting outputs were different. When the molar ratio of **1b:2** (see **Figure I-28**) was less than 6:4, co-generation of self-replicator $(\mathbf{1b})_2\mathbf{2}_1$ and foldamer $\mathbf{2}_{15}$ was observed. The kinetics revealed that foldamer $\mathbf{2}_{15}$ was not generated until all of **1b** was consumed. When the molar ratio of **1b:2** was less than 7:3, no foldamer was detectable and only two self-replicators $(\mathbf{1b})_4$ and $(\mathbf{1b})_2\mathbf{2}_1$ were present. The kinetics revealed that self-replicator $(\mathbf{1b})_4$ was kinetically favoured, reaching its maximum abundance in a relatively short reaction time, during which a little amount of $(\mathbf{1b})_2\mathbf{2}_1$ was produced. Thereafter, the amount of $(\mathbf{1b})_4$ slightly decreased and promoted the formation of $(\mathbf{1b})_2\mathbf{2}_1$. The results revealed that the molar ratio of the substrates could affect the self-sorting reaction process, and lead to various outputs.

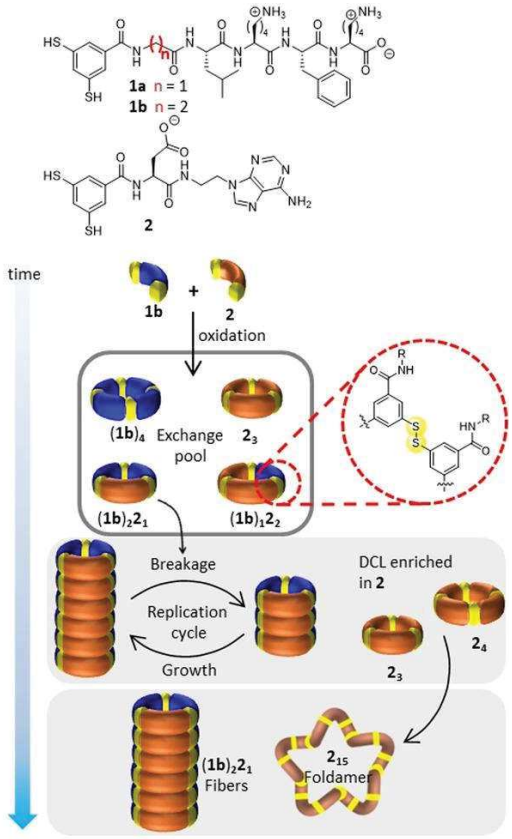

Figure I-28. Self-sorting of foldamers and self-replicators. (Figure reproduced from reference.[124])

3.4. Kinetically controlled self-sorting systems

Self-sorting systems under kinetic control remain a challenge but they are expected to be important models for non-equilibrium biological systems.[125]

Lehn *et al.* carried out a kinetic study on the metal-imine coordinated self-sorting system shown in **Figure I-29**.[126] They found that in a DCL composed of two 2-formylpyridines (**A**, **C**) and two amines (**B**, **D**) at a concentration lower than 3.6 mM, homoleptic complex $[Fe(\mathbf{A},\mathbf{B})_2]^{2+}$ and an almost equal molar amount of heteroleptic complex $[Fe(\mathbf{A},\mathbf{B})(\mathbf{C},\mathbf{D})]^{2+}$, as well as another homoleptic complex $[Cu(\mathbf{C},\mathbf{D})_2]^{+}$ were produced after heating at 60 °C for 18 h. After 20 days of heating at 60 °C, the ratio of homo-to heteroleptic Fe(II) complex increased to 1:0.25, showing that the heteroleptic complex was a kinetic product, and the formation of which led the system to be trapped out-of-equilibrium. The authors also found that by controlling the concentration, electronic and steric parameters of the components, as well as the coordination preferences of the metal cations in the DCL, such kinetically trapped

out-of-equilibrium states could be inhibited.

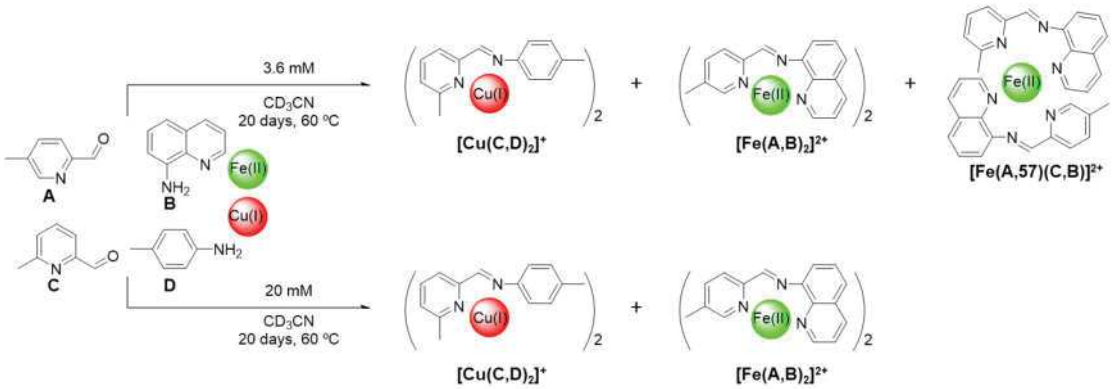

Figure I-29. Kinetically controlled self-sorting of complexes $[Cu(\mathbf{C},\mathbf{D})_2]^+$ and $[Fe(\mathbf{A},\mathbf{B})_2]^{2+}$ via imine condensation of initial reactants (**A**, **B**, **C**, **D**).

One of the objectives of the use of kinetic self-sorting is the elimination of the products from the reversible chemical equilibrium. Allowing the kinetic products to undergo additional irreversible reactions, for instance by the addition of an oxidant I_2, is one of the chemical methods to remove the kinetic products from the reversible equilibrium and thus push the reaction equilibrium towards the formation of the kinetic product.[127] It is also possible to separate the kinetic products by physical methods, such as distillation and precipitation.[128–130] Miljanić *et al.* reported that by sequentially exploiting irreversible stimuli like chemical oxidation, column chromatography, and distillation methods, it was possible to isolate six constituents from a [10 × 10] DCL containing up to 100 imino constituents.[131] As a result, the [10 × 10] DCL was iteratively simplified to a [6 × 6] matrix and the concentration of remaining constituents was amplified more than three times (**Figure I-30**).

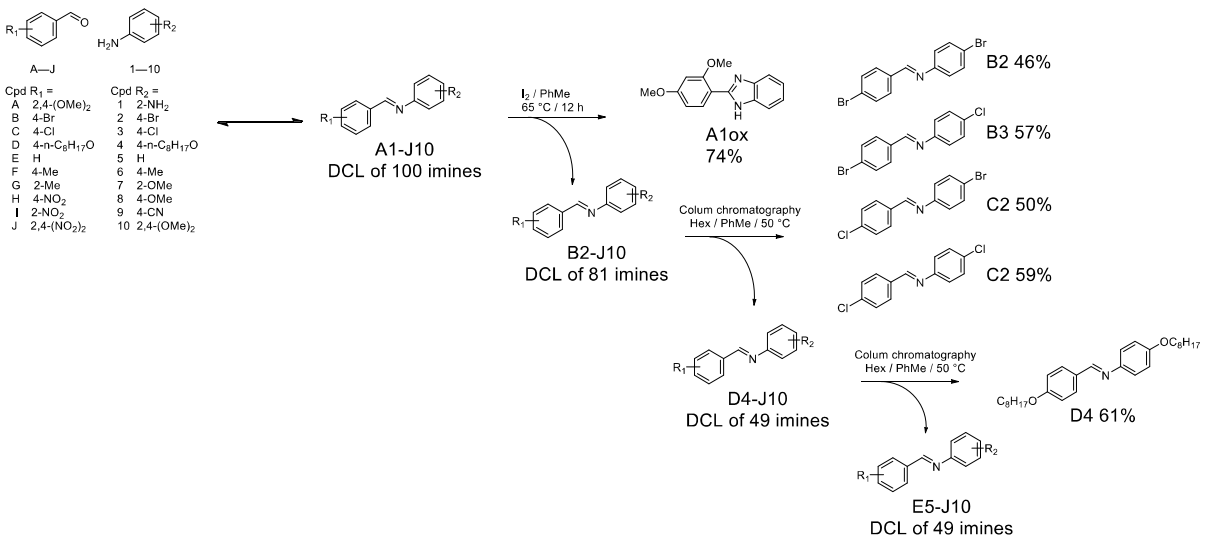

Figure I-30. Simplification of a multi-responsive [10 × 10] DCL via slow addition of iodine, column chromatography, and slow distillation, sequentially.

4. Aim of the thesis

This thesis is intended to provide plausible mechanistic insights into the self-sorting behaviour of dynamic covalent macrocycles and macrobicyclic cages. It includes three major experimental parts which are:

1. The study of self-sorting processes related to the basic laws of rational design of a thermodynamically controlled system.
2. The study of kinetically-controlled self-sorting systems from out-of-equilibrium to equilibrium states, and the time-dependent transition of product distributions from kinetic to thermodynamic forms.
3. Study of the constitutional regulatory behaviour of self-sorting systems in producing isomeric entities from dynamic covalent libraries.

Chapter II. Rules of Self-Sorting

1. Introduction

In recent years, supramolecularly-driven self-sorting processes have attracted much attention and intensive research efforts.[100,109,132] Nonetheless, self-sorting systems constructed by reversible condensation reactions with covalent bonds still need to be thoroughly investigated. This becomes evident if one considers the following features: (i) complex systems generally lead to low selectivities; (ii) reversible self-sorting processes usually generate a wide range of intermediates, which hampers the correct analysis of the whole system. Therefore, the study of the mechanism of reversible covalent self-sorting processes is of great importance for understanding and designing such self-sorting systems. Highly-fidelity self-sorting behaviour for imine bonded 3D molecular cages has been reported by several groups.[121] These preorganized discrete structures obtained by imine condensation reactions from multicomponent DCLs were shown to give self-assembled products reflecting either: 1) homoleptic self-sorting;[119] 2) heteroleptic self-sorting;[133] or 3) statistical mixing of disordered assemblies.[131]

Currently, there is still the necessity to solve the problem of how to rationally control self-sorting systems so that the complexity of molecular libraries increases without leading to untreatable mixtures of compounds as a result of similar energetic distributions. Hence, studying the process of the self-sorting behaviour of dynamic covalent bonds becomes crucial. Rather few studies have focused on the study of self-assembly / self-sorting mechanisms based on dynamic covalent chemistry.[126] When a substrate has multiple reaction sites, a large number of transient intermediates can be generated in the DCL. This can be due to the competition between intra- and intermolecular reactions within the same DCL, increasing the complexity of gathering representative data. To find a means to avoid this potential issue, rational design of the precursors and monitoring of the component abundance at different reaction times should enable the prediction of self-sorting outcomes. This hypothesis motivated us to investigate the self-sorting processes based on dynamic covalent bond formation in the synthesis of compounds containing well-defined cavities.

2. Results and Discussion

Previous work from the Lehn group has described the synthesis and characterization of macrocyclic and macrobicyclic cryptand-type structures, as well as their self-sorting behaviour.[122] As the subject of this thesis, these studies have now been extended to the elucidation of the self-sorting mechanisms of homoleptic macrocycles and macrobicyclic cages through dynamic imine bonds. The formation of the C_2-symmetric tetraimino macrocycles and D_3-symmetric hexaimino macrobicycles shown in **Scheme II-1** was the focus of the initial work. The presence of the desired cyclic structures was confirmed by both nuclear magnetic resonance (NMR) spectroscopy and high-resolution mass spectrometry (HRMS).

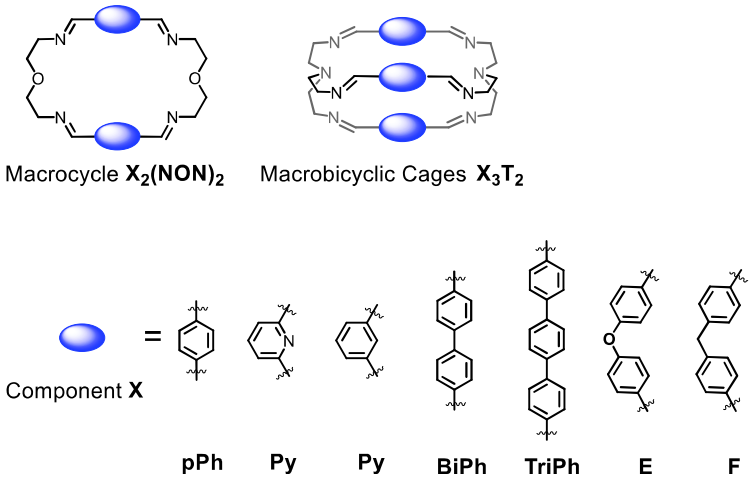

Scheme II-1. Molecular structures of the components (bottom; in italics) and of the homoleptic imine-based [2 + 2] macrocycles and [3 + 2] macrobicyclic cages (top) studied in the present work.

2.1. Formation of macrocycle $pPh_2(NON)_2$

2.1.1. ^{1}H NMR monitoring

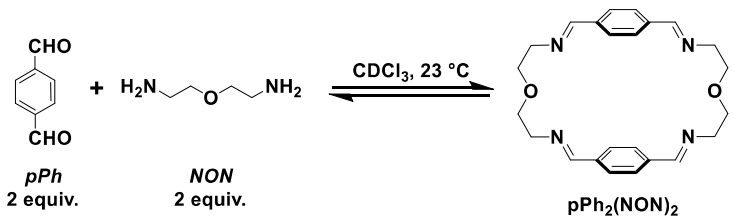

Scheme II-2. Synthesis of macrocycle **$pPh_2(NON)_2$** via [2+2] imine condensation

The multiple condensation reactions involved in the formation of compounds containing several imino groups often lead to the generation of numerous transient intermediates that complicate the monitoring of the generation of the macrocyclic compounds by ^{1}H NMR spectroscopy.

The expected formation of macrocycle **pPh$_2$(NON)$_2$**, using terephthalaldehyde (**pPh**) and 2,2'-oxybis(ethylamine) (**NON**) as precursors, was first studied. To better follow the initiation of the reaction and the conversion of intermediates, the reaction rates were kept to a minimum by treating the chloroform solvent with basic aluminium oxide to remove any traces of acid. As a result, more than a week at room temperature was required before any changes in the spectrum fell below the level of detection (**Figure II-1**). After this time, the two singlets due to the symmetrical terephthalaldehyde reactant had disappeared and two singlets at a higher field consistent with the formation of a symmetrical terephthalaldimine unit as in the macrocyclic structure were the only detectable signals. That the final product was indeed the 2:2 macrocycle was subsequently confirmed by mass spectrometry.

During the ^{1}H NMR measurements, signals assigned to several intermediates were observed. After 120 min of reaction, two singlets at 10.06 and 8.38 ppm, and an AB doublet pair at 7.94 and 7.89 ppm were prominent new features (**Figure II-1**). Some other extremely weak peaks indicated that other species were present but their concentrations never became sufficient to allow characterisation. Signals due to the first detected intermediate rose in intensity up to about 900 min, then declined as new intermediate signals appeared, with the spectrum at 720 min showing two new singlet peaks at 10.03 ppm and 8.30 ppm associated with a doublet pair at 7.86-7.84 ppm and 7.80-7.78 ppm, along with two very weak singlets at 8.33 ppm and 7.78 ppm. In turn, these signals declined as the final product appeared.

While it is possible that the reaction of difunctional molecules in a 1:1 molar ratio could simply give rise to linear polymers, the fact that the final product of the present reaction is the 2:2 macrocycle indicates that polymerisation is not favoured under the given conditions and indeed the NMR spectral changes can be explained in terms of just three simple acyclic intermediates, namely **[pPh+NON]**, **[pPh+2NON]**, and **[2pPh+NON]**, being on the pathway to the macrocycle. No matter what the final reaction state, the [1+1] unsymmetrical **[pPh+NON]** intermediate must form first and its ^{1}H NMR spectrum should show one aldehyde signal, one imine signal, and a doublet pair in the aromatic area. These expected spectroscopic features (including peak integrals) correlate well with the green peaks in **Figure**

II-1. This intermediate can react with either another molecule of terephthalaldehyde to give **[2pPh+NON]**, where the aromatic ring has an unsymmetrical environment, or another molecule of the diamine to give **[pPh+2NON]**, where the aromatic ring has a symmetrical environment. Thus, the orange peaks shown in Figure II-1 were assigned to the former and the two red singlets to the latter. The time evolution of the reaction mixture composition is plotted in **Figure II-2**. It can be seen that the concentration of intermediate **[pPh+NON]** (see **Figure S-II-19** in Chapter VII) significantly increased with time from 7 to 900 min, reaching 30% abundance after ca. 1000 min of reaction. The concentration of this intermediate smoothly decreased for the subsequent 4000 min. The smaller quantities of **[2pPh+NON]** and **[pPh+2NON]** detected showed a similar but somewhat slower time dependence. Significantly, although an acyclic, unsymmetrical intermediate of composition **[2pPh+2NON]** must be a precursor to the final product, no peaks assignable to such a species were evident, indicating that this species, once formed, must rapidly cyclise.

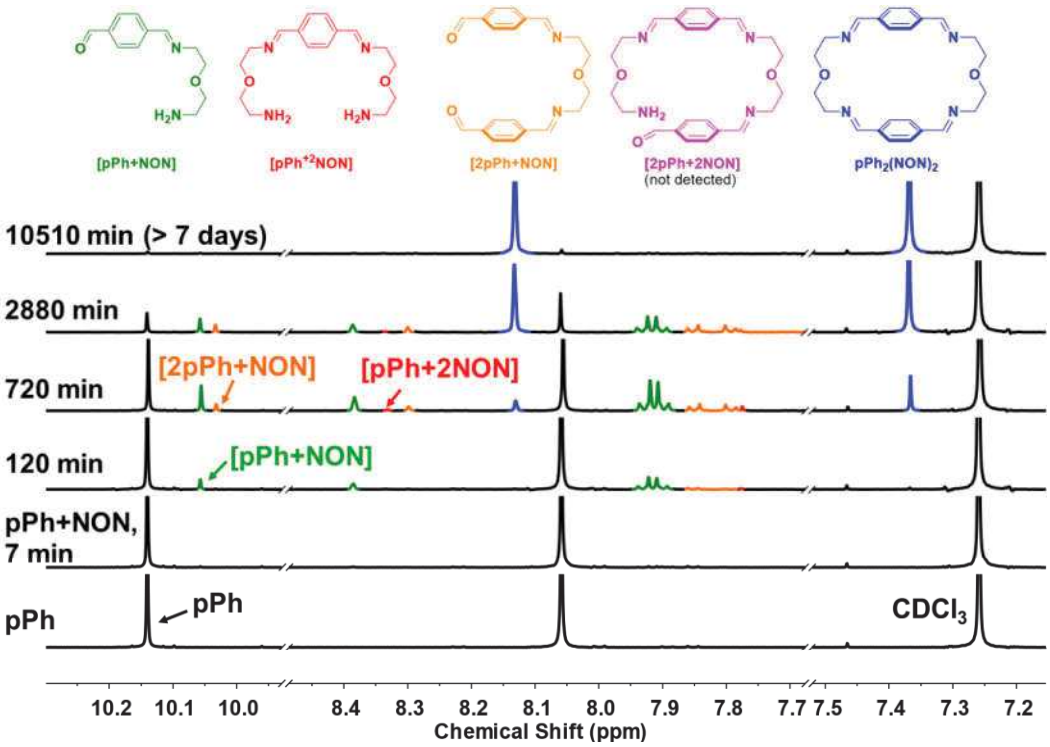

Figure II-1. Time evolution of the ^{1}H NMR spectra (500 MHz, $CDCl_3$, 23 °C) of a 1:1 mixture of **pPh** and **NON** ($[\mathbf{pPh}]_0 = [\mathbf{NON}]_0$ = 3.6 mM) showing the formation of three intermediates and of the final macrocycle **$pPh_2(NON)_2$**. Selected reaction times: 7 min, 120 min, 720 min, 2880 min and 10510 min.

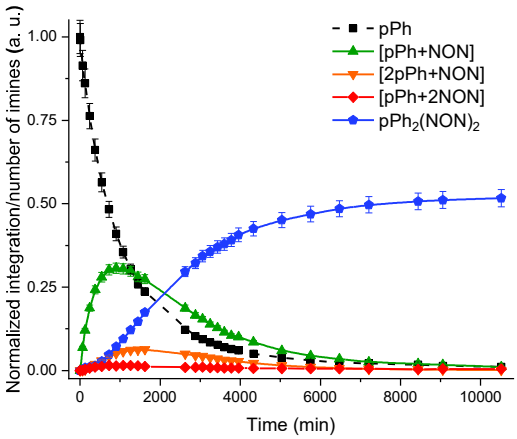

Figure II-2. ^{1}H NMR monitoring of the time evolution (over 10510 min) of the species generated in the reaction between **pPh** and **NON** ([**pPh**]$_0$ = [**NON**]$_0$ = 3.6 mM). Error in ^{1}H-NMR signal integration: ±5%.

2.1.2. HRMS-ESI monitoring

Next, the evolution of intermediates was investigated using HRMS. Anticipating that LC separation might involve further reactions of the intermediates, the direct injection method was used. The ionization processes of different compounds are not identical, and the quantity of ions they produce depends upon a variety of factors such as their ionization potential and the detector sensitivity. Thus, differences in ion currents cannot be used to analyse the concentration differences of different species. Nonetheless, although mass spectrometry is used in most cases for non-quantitative analysis, the concentration of one given compound is positively correlated with the amount of ions it produces.[134]

For the convenience of analysis, the signals attributed to the substrates, intermediates, and products that were observed during the whole assay process are listed in **Table S-II-1** (Chapter VII). As can be seen in **Figure II-3**, the signals with m/z of 105.1025 (**NON**+H$^+$) and 221.1276 (**[pPh+NON]**+H$^+$) were observed at the initial stage of the reaction. With the progress of the reaction, both nearly completely disappeared, while new signals with m/z of 405.2269 (**pPh$_2$(NON)$_2$**+H$^+$) and 427.2088 (**pPh$_2$(NON)$_2$**+Na$^+$) due to macrocyclic species gradually increased.

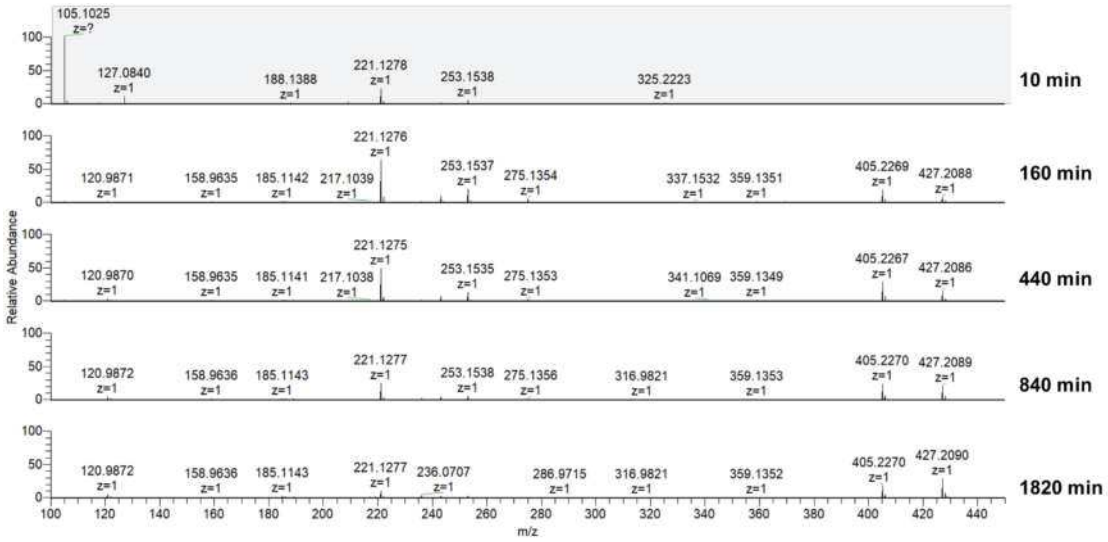

Figure II-3. Time evolution of the HRMS-ESI spectra showing the formation of intermediates and macrocycle **pPh$_2$(NON)$_2$** after 10, 160, 440, 840, and 1820 min.

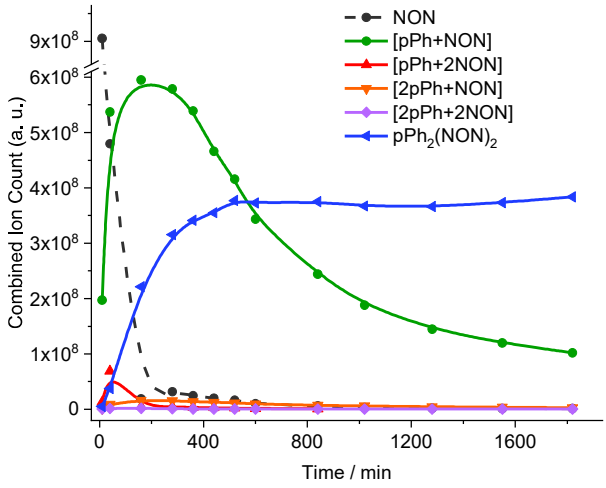

Figure II-4. HRMS-ESI monitoring of the time evolution of the species generated during **pPh$_2$(NON)$_2$** formation from a 1:1 mixture of **pPh** and **NON**. NB: These data do not provide quantitative information about the relative amounts of each species identified by its mass, but, taken separately, they display the evolution of a given identified species during the course of the reaction. The curves are added to guide the eye.

The evolution of their m/z peak intensities over time is plotted in **Figure II-4**. The **[pPh+NON]** (m/z = 221.1276, [M+H$^+$]) intermediate was formed within 10 min, and it reached its highest abundance after 200 min during the reaction process. Thereafter, its

concentration gradually decreased, due to its conversion into other intermediates. Both the ^{1}H NMR and HRMS **(Figures II-2** and **4**) curves for the macrocyclization reaction revealed an induction period, consistent with the formation of at least one intermediate species prior to the cyclization step.[10] (see also the formation of **$BiPh_2(NON)_2$** in Chapter VII, **Figures S-II-20** to **S-II-23**)

2.1.3. Theoretical study

To gain additional insights into the reaction mechanism, theoretical calculations were performed for estimating the free energies of formation of the species (in the gas phase) detected in the synthesis of **$pPh_2(NON)_2$**. For each compound, the lowest-energy conformation was explored with molecular mechanics (Merck molecular force field - MMFF) and density functional theory (DFT) calculations. The free energy of formation for each optimized geometry was then calculated using a simplified MP2 level. The computational results are summarized in **Figure II-5.** Interestingly, the free energy of formation of **[pPh+2NON]** (-11.40 kJ/mol) is higher than that of **[2pPh+NON]** (-22.52 kJ/mol) and **[2pPh+2NON]** (-36.94 kJ/mol).

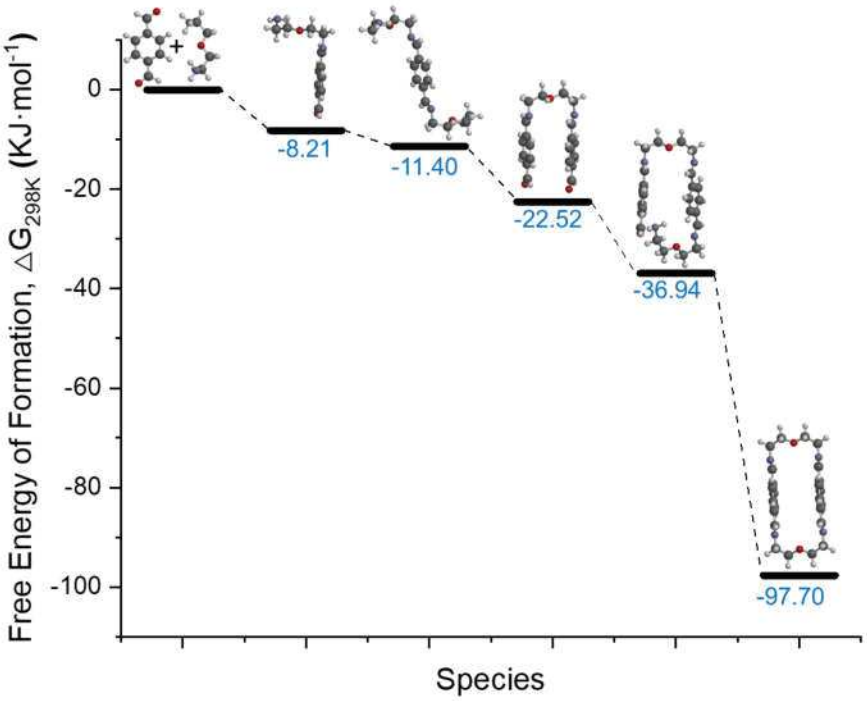

Figure II-6. Free energy of formation (△G) at 25 °C (298K) for the different species detected in the synthesis of macrocycle **$pPh_2(NON)_2$**.

2.1.4. Formation process of the macrocycle $pPh_2(NON)_2$

Based on the above results, a possible self-assembly mechanism for such [2 + 2] covalent organic macrocycles is shown in **Scheme II-3**. The most direct path to form $pPh_2(NON)_2$ after the initial formation of the [1+1] intermediate **[pPh+NON]** would be the dimerization of this species to give **[2pPh+2NON]**, which could then undergo an intramolecular cyclization step to yield the macrocycle. The observation of three intermediates, however, shows that there must be at least three pathways for generating the macrocycle, i) one-step dimerization of two **[pPh+NON]** intermediates; ii) and iii): condensation with an additional component (**pPh** or **NON**) to form intermediates [1 + 2] and [2 + 1]; finally, intramolecular macrocyclization yielding macrocycle $pPh_2(NON)_2$. It must be mentioned that the transformation of the intermediates of odd stoichiometry, namely **[2pPh+NON]** and **[pPh+2NON]**, into the [2+2] macrocycle occurs at relatively slow rates because the concentrations of free **pPh** and **NON** are now quite low compared to the initial values.

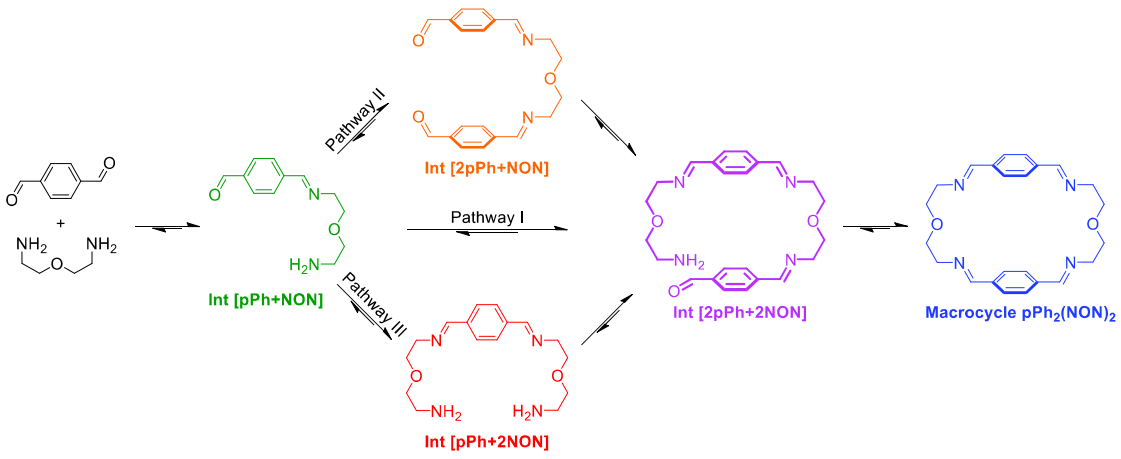

Scheme II-3. Stepwise [2 + 2] imine condensation processes showing the intermediates formed in the generation of the dynamic covalent macrocycle $pPh_2(NON)_2$.

2.2. Self-sorting of macrocycles from a three-component DCL

2.2.1. ^{1}H NMR monitoring

The homo-self-sorting behaviour was investigated for a three-component mixture of two dialdehydes of different lengths, namely **pPh** and **BiPh** (4,4'-biphenyldialdehyde), and **NON** in a 2:2:4 ratio. **Figure II-7** represents the corresponding ^{1}H NMR spectra showing a progressive formation of new species that were assigned to different intermediates. The initial substrate mixture remained almost unchanged for 4 min. After about 720 min, a number of minor peaks - which were difficult to integrate - were observed, but only a small amount of macrocyclic products were formed. As the dialdehydes and **NON** were gradually consumed, a series of intermediates were involved in the oligomerization and intramolecular cyclization reactions leading to the ultimate production of the macrocycles **pPh$_2$(NON)$_2$** and **BiPh$_2$(NON)$_2$** only.

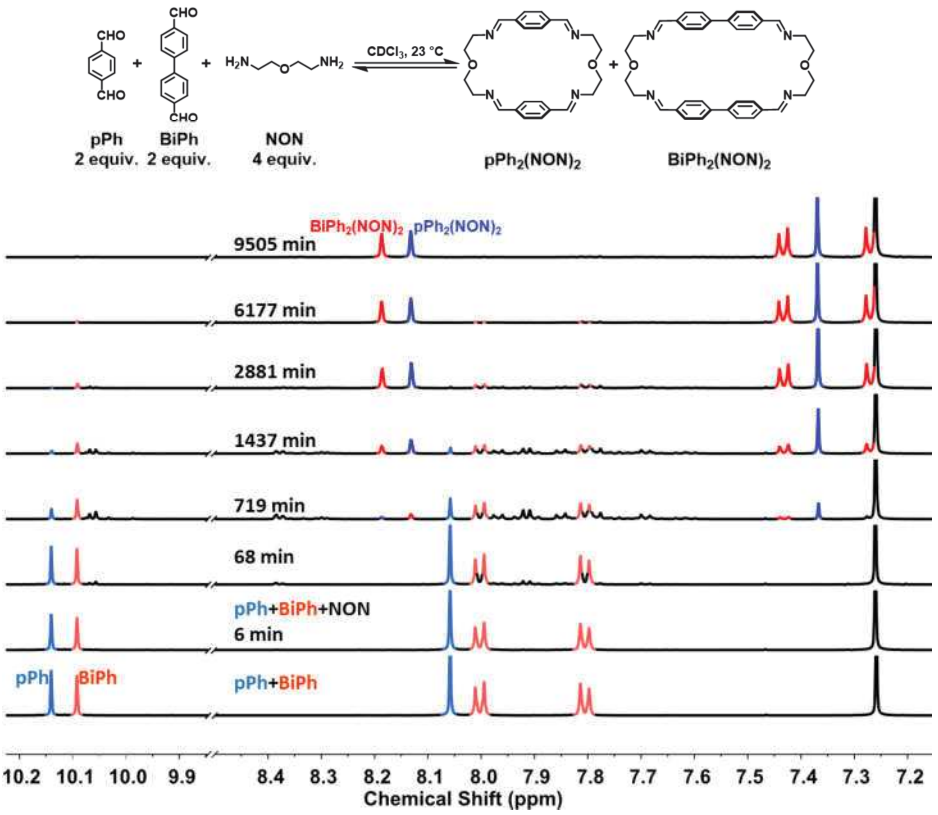

Figure II-7. Time evolution of the partial ^{1}H NMR spectra (400 MHz, $CDCl_3$, 23 °C) for the reaction 2**pPh** + 2**BiPh** + 4**NON** ([**pPh**]$_0$ = [**BiPh**]$_0$ = 3.6 mM; [**NON**]$_0$ = 7.2 mM) over 9505 min. The two bottom spectra correspond to the isolated macrocycle **pPh$_2$(NON)$_2$** and **BiPh$_2$(NON)$_2$**

The consumption of **pPh** and **BiPh** as well as the generation of the two macrocycles are plotted versus reaction time in **Figure II-8**. The formation of macrocycle **pPh$_2$(NON)$_2$** was faster than that of **BiPh$_2$(NON)$_2$** and followed the faster initial consumption of **pPh** in comparison with that of **BiPh**. The formation rate of **pPh$_2$(NON)$_2$**, **BiPh$_2$(NON)$_2$** in the self-sorting **pPh:BiPh:NON** system (half-consumption $t_{1/2}^F$ of **pPh$_2$(NON)$_2$** = 1350 min, $t_{1/2}^F$ of **BiPh$_2$(NON)$_2$** = 2000 min) was two-times faster than the one observed in their separated formation ($t_{1/2}^F$ of **pPh$_2$(NON)$_2$** = 2200 min, $t_{1/2}^F$ of **BiPh$_2$(NON)$_2$** = 4030 min). This may be due to the doubled initial concentration of **NON** in the self-sorting system. The composition of the system after 9505 min (158 h) was 51% of **pPh$_2$(NON)$_2$**, 49% of **BiPh$_2$(NON)$_2$**, and less than 1% of unreacted **BiPh**. The high yields attained for both macrocycles indicated the high-fidelity of the self-sorting and confirmed the absence of heteroleptic macrocycles.

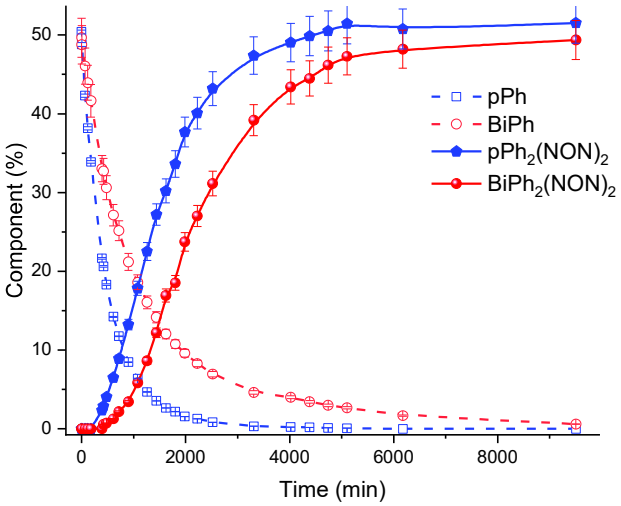

Figure II-8. ^{1}H NMR monitoring of dialdehydes **pPh**, **BiPh** and macrocycles **pPh$_2$(NON)$_2$** and **BiPh$_2$(NON)$_2$** over 9505 min.

Focusing on the process of reaction, one can observe several signals belonging to neither the identified intermediates of the **pPh**/**NON** reaction nor those of the **BiPh**/**NON** reaction (**Figure II-9**). They may be the result of the formation of several heteroleptic intermediates (e.g., **[pPh+BiPh+NON]**, **[pPh+BiPh+2NON]**). Unfortunately, the concentration of these intermediates was rather low and their aromatic regions overlapped with the signals of other intermediates, making it difficult to elucidate their precise composition/structure.

Notwithstanding, no heteroleptic macrocycles could be detected after equilibration, indicating that correction and dissociation processes were taking place.[134]

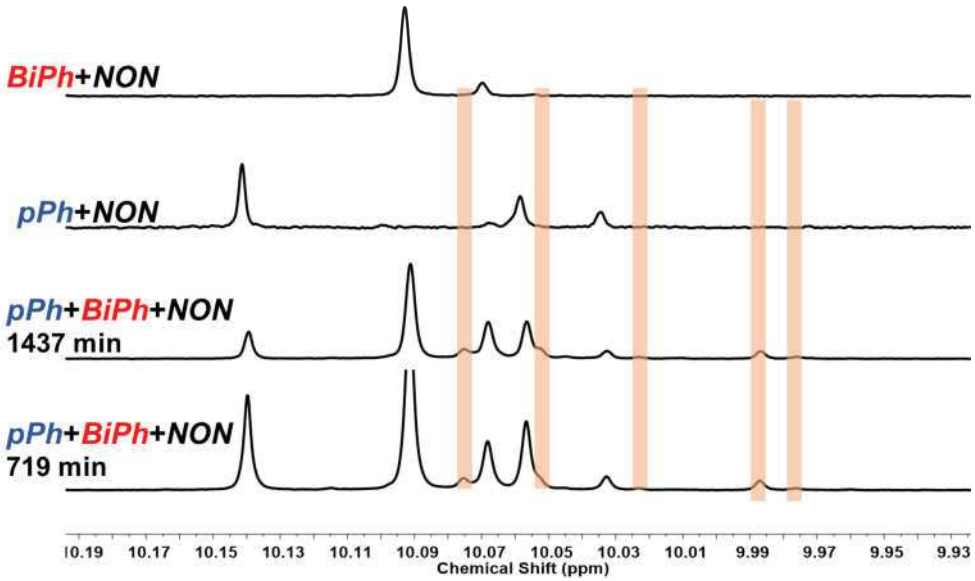

Figure II-9. ^{1}H NMR spectra comparison of the **pPh/BiPh/NON** self-sorting experiment with **pPh/NON** and **BiPh/NON** separated reactions. The top two spectra correspond to the **pPh/NON** reaction at 2880 min and **BiPh/NON** reaction at 4384 min.

2.2.2. HRMS-ESI monitoring

HRMS was also used to identify some intermediates and to follow their evolution as a function of time. The intermediates **[pPh+NON]**, **[BiPh+NON]**, and **[pPh+2NON]** were very rapidly formed after mixing the solutions of the three components. They reached their highest abundance after 180 min of reaction, being afterwards transformed into the homoleptic macrocycles. After 24 h, two prominent peaks with m/z of 405.2276 and 557.2900 were attributed to macrocycles $[\mathbf{pPh_2(NON)_2}+H]^+$ and $[\mathbf{BiPh_2(NON)_2}+H]^+$, respectively. The intermediates **[pPh+BiPh+NON]** and **[pPh+BiPh+2NON]**, as well as the macrocycle **(pPh)(BiPh)(NON)$_2$**, were also detected in the course of the reaction. Due to the poor thermodynamic stability of the heteroleptic species, macrocycle **(pPh)(BiPh)(NON)$_2$** disappeared later on. No signals corresponding to heteroleptic macrocycles could be observed at the end of the reaction, indicating again the occurrence of a self-correcting process.

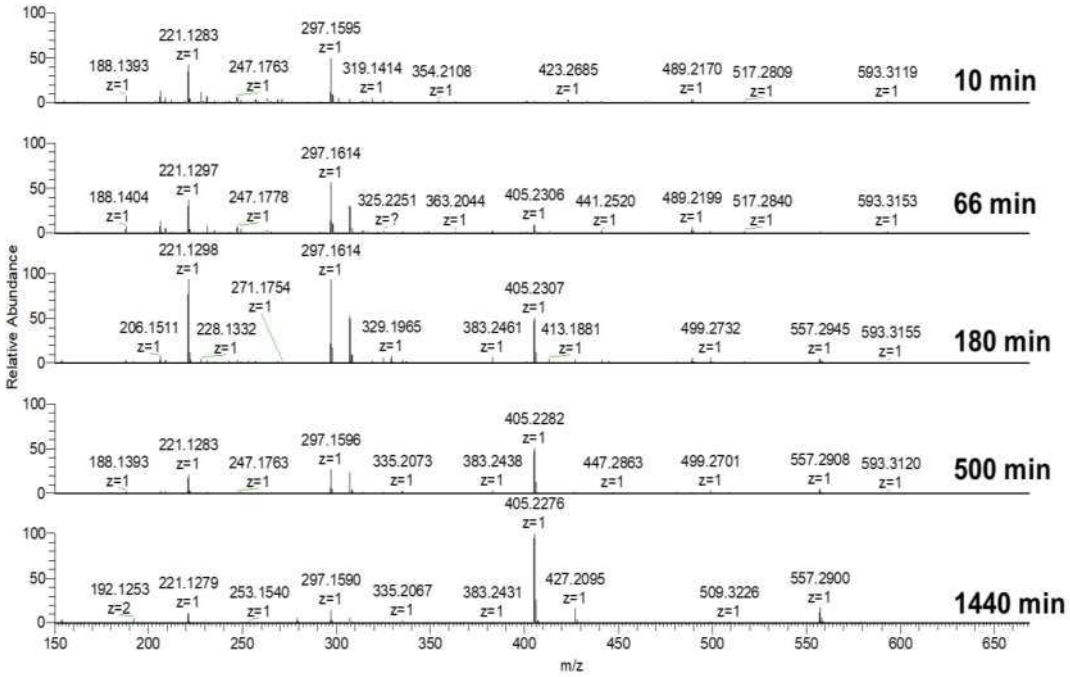

Figure II-10. Evolution of HRMS-ESI(+) spectra of the 2/2/4 mixture of **pPh** (2 mM), **BiPh** (2 mM) and **NON** (2 mM), in 50%-50% $CHCl_3$/MeOH. Selected reaction times: 10, 66, 180, 500, and 1770 min.

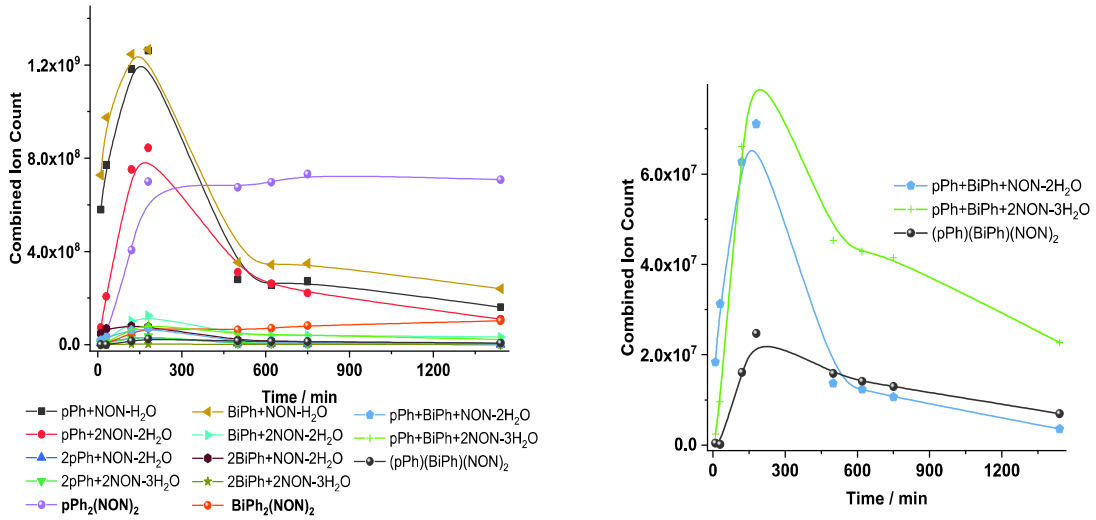

Figure II-11. HRMS-ESI kinetic evolution of the species generated during the self-sorting process of 2**pPh** + 2**BiPh** + 4**NON** (50%-50% $CHCl_3$/MeOH, r.t) as a function of time over 1440 min. NB: These data do not provide quantitative information about the relative amounts of each species identified by its mass, but, taken separately, they display the evolution of a given identified species during the course of the reaction. The curves are added to guide the eye.

2.2.3. Self-sorting processes of macrocycles $pPh_2(NON)_2$ and $BiPh_2(NON)_2$

On the basis of the results above, a plausible self-sorting process may be suggested. In an initial step, the diamine **NON** reacts with the aldehydes **pPh** or **BiPh** to form the corresponding [1+1] intermediate; this intermediate can convert directly to the homoleptic macrocycle, namely $\mathbf{pPh_2(NON)_2}$ or $\mathbf{BiPh_2(NON)_2}$ by dimerization but, as discussed above. (**Scheme II-3**) at least two other pathways are possible. In the mixed aldehyde system, heteroleptic intermediates do appear to form but are removed by self-correction processes leading to the high-fidelity homo-self-sorting (**Scheme II-4**). At least two heteroleptic intermediates, **[pPh+BiPh+NON]** and **[pPh+BiPh+2NON]**, were observed transiently and their final absence shows that their formation must be reversible.

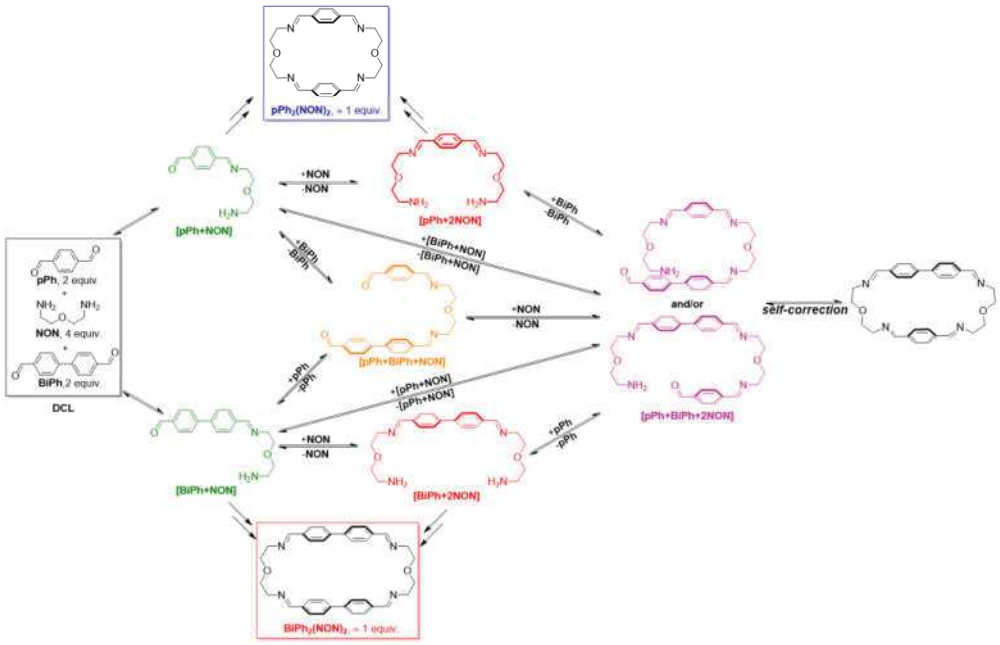

Scheme II-4. Self-correction and dissociation processes showing the conversion of heteroleptic intermediates into the desired homoleptic macrocycles $\mathbf{pPh_2(NON)_2}$ and $\mathbf{BiPh_2(NON)_2}$.

2.3. Self-sorting of macrocycles from a four-component DCL

A four-component DCL composed of **pPh**, **BiPh**, **TriPh** (4,4"-terphenyldialdehyde) and **NON** in a 2:2:2:6 ratio was investigated (**Figure II-12**). The ^{1}H NMR time evolution indicated that the reaction equilibrium was reached after 5510 min of heating at 40 °C. The generation of macrocycles followed the rate sequence $\mathbf{pPh_2(NON)_2}$ > $\mathbf{BiPh_2(NON)_2}$ ≥

TriPh$_2$(NON)$_2$. The composition of the final equilibrium solution was 36% **pPh$_2$(NON)$_2$**, 32% **BiPh$_2$(NON)$_2$**, and 32% **TriPh$_2$(NON)$_2$**, inferring that the three macrocyclic species presented similar energies of formation. The production of the three macrocycles was also confirmed by HRMS (Chapter VII, **Figure S-II-32**).

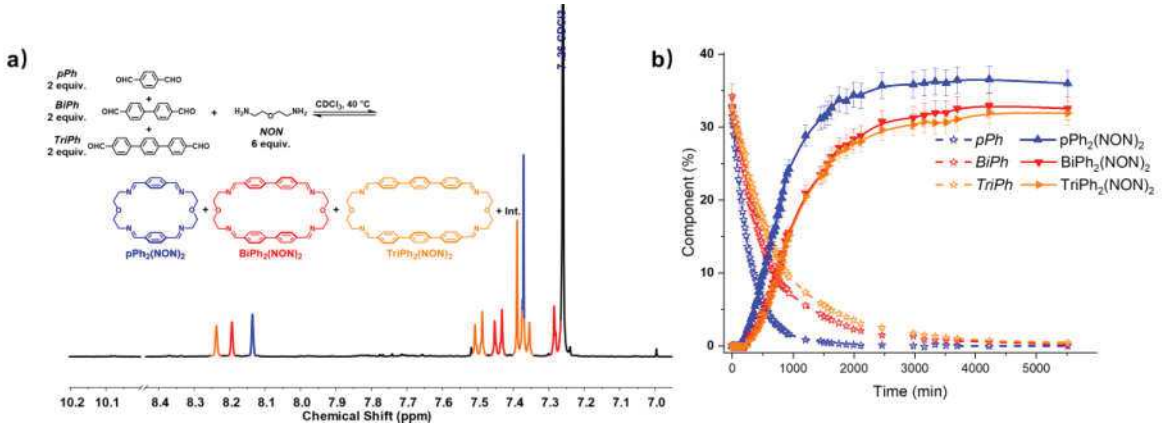

Figure II-12. (a) Partial ^{1}H NMR spectrum (after 5510 min at 40 °C, 400 MHz, $CDCl_3$) of the parallel formation of a mixture of macrocycles **pPh$_2$(NON)$_2$**, **BiPh$_2$(NON)$_2$** and **TriPh$_2$(NON)$_2$** from the self-sorting experiment between 2**pPh** + 2**BiPh** +2**TriPh** + 6**NON**. (b) Component abundance (macrocycles **pPh$_2$(NON)$_2$**, **BiPh$_2$(NON)$_2$** and **TriPh$_2$(NON)$_2$**) as measured using ^{1}H NMR (t_{max} = 5510 min).

2.4. Formation of the macrobicyclic cage pPh$_3$T$_2$ (T = tris(aminomethyl)amine = "tren")

2.4.1. ^{1}H NMR monitoring

The assembly of cage **pPh$_3$T$_2$** (**Figure II-13**) was first monitored by ^{1}H NMR spectroscopy. In the ^{1}H NMR spectra, signals due to several intermediates were observed. As there may be at least eight possible intermediates for the generation of a cage, it is not surprising that the spectra are more complicated than in the case of the macrocycles. Hence, only the simplest **[pPh+T]** (**Figure II-14**) was assigned. After 118 min, about 55% **pPh** was involved in the reaction, of which 35% **pPh** was converted to **[pPh+T]**, while only 2% cage **pPh$_3$T$_2$** was generated, indicating that the remaining intermediates contained about 13% **pPh**. After that, the concentration of **[pPh+T]** gradually decreased and up to 96% cage **pPh$_3$T$_2$** was

generated. (see Chapter VII, **Figures S-II-26** and **Figure S-II-27** for the observation of the self-assembly reaction between **T** and **BiPh**).

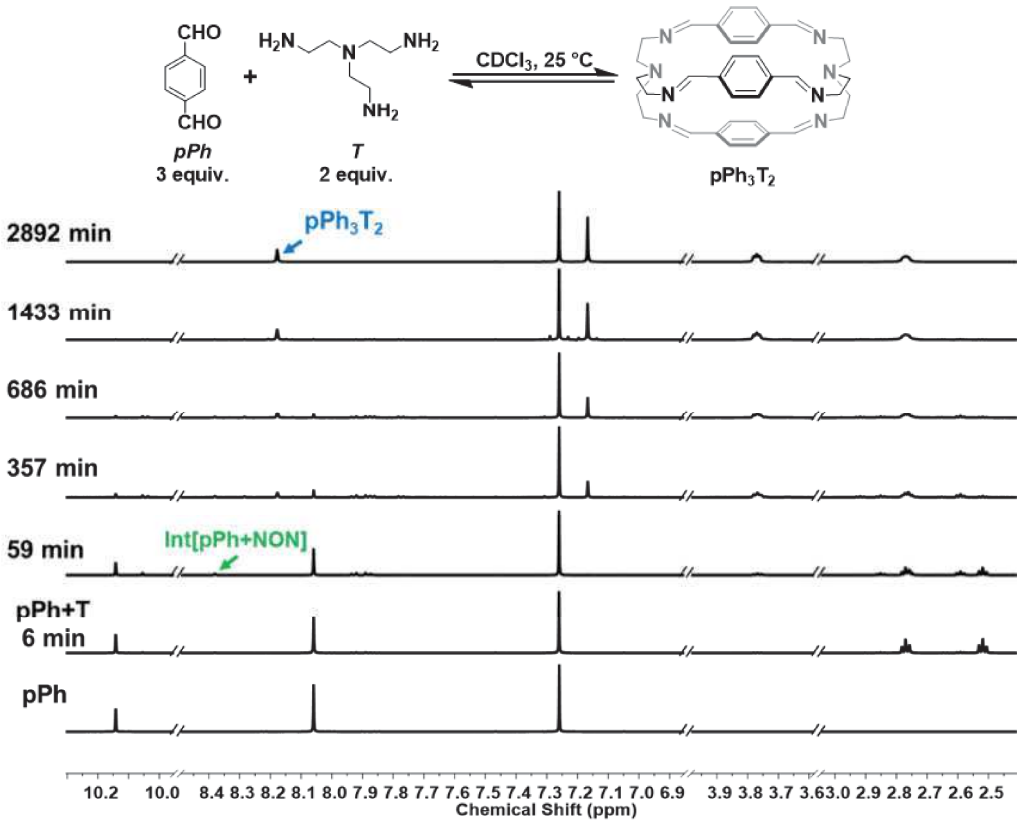

Figure II-13. Evolution of the ^{1}H NMR spectra (500 MHz, $CDCl_3$) of a 3:2 mixture of **pPh** (3.6 mM) and **T** (2.4 mM) showing the formation of intermediate **[pPh+T]** and of the final macrobicyclic cage **pPh_3T_2**.

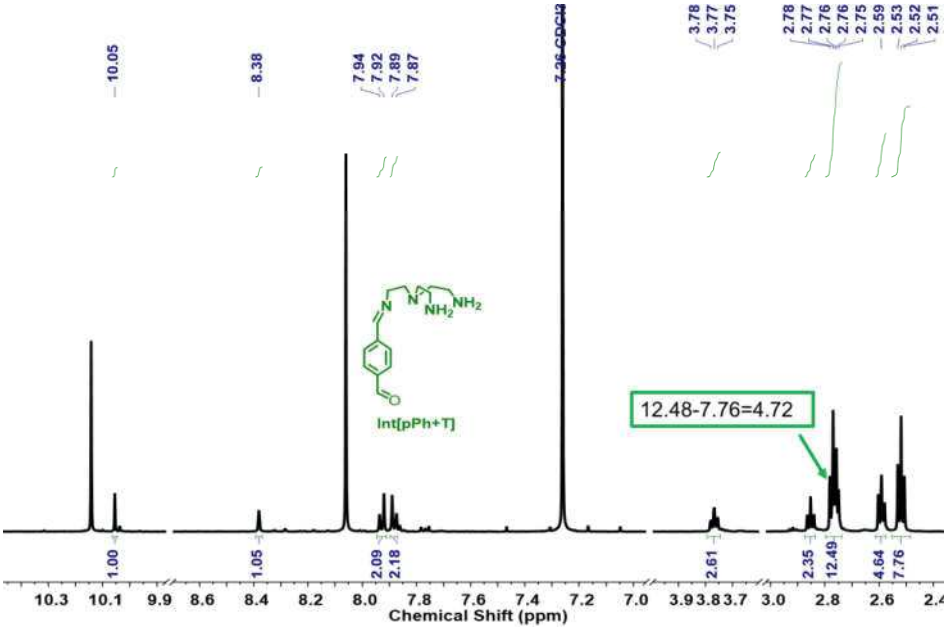

Figure II-14. ^{1}H NMR spectrum (400 MHz, $CDCl_3$) showing the generation of the intermediate [**pPh**+**T**] after 59 min of condensation reaction between **pPh** (3.6 mM) and **T** (2.4 mM).

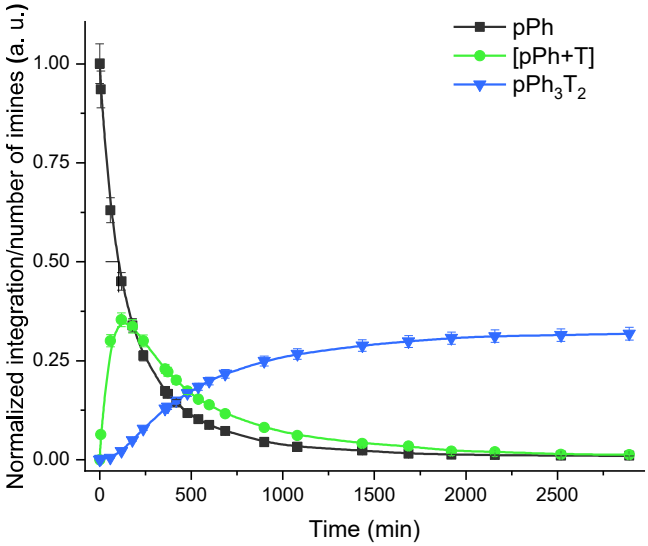

Figure II-15. Time evolution of the species generated during the synthesis of **pPh_3T_2** as measured using ^{1}H NMR. Error in ^{1}H-NMR signal integration: ±5%.

2.4.2. HRMS-ESI monitoring

The HRMS monitoring defined a similar trend to that observed in the ^{1}H NMR

monitoring. From **Figures II-16** and **II-17**, it can be seen that after mixing the two reactants, the [1+1] type of intermediate (i.e., **[pPh+T]**) was formed first and gradually reached its highest abundance. As expected, the [2+2] type of intermediate **[2pPh+2T]** reached its maximum concentration slightly later than **[pPh+T]**. Although the absolute intensities of the other four intermediates **[2pPh+T]**, **[pPh+2T]**, **[3pPh+T]**, and **[3pPh+2T]** were quite low, their abundance trend could still be determined thanks to the high sensitivity of the HRMS equipment. (see Chapter VII, **Figure S-II-27** for the formation of cage $\mathbf{BiPh_3T_2}$).

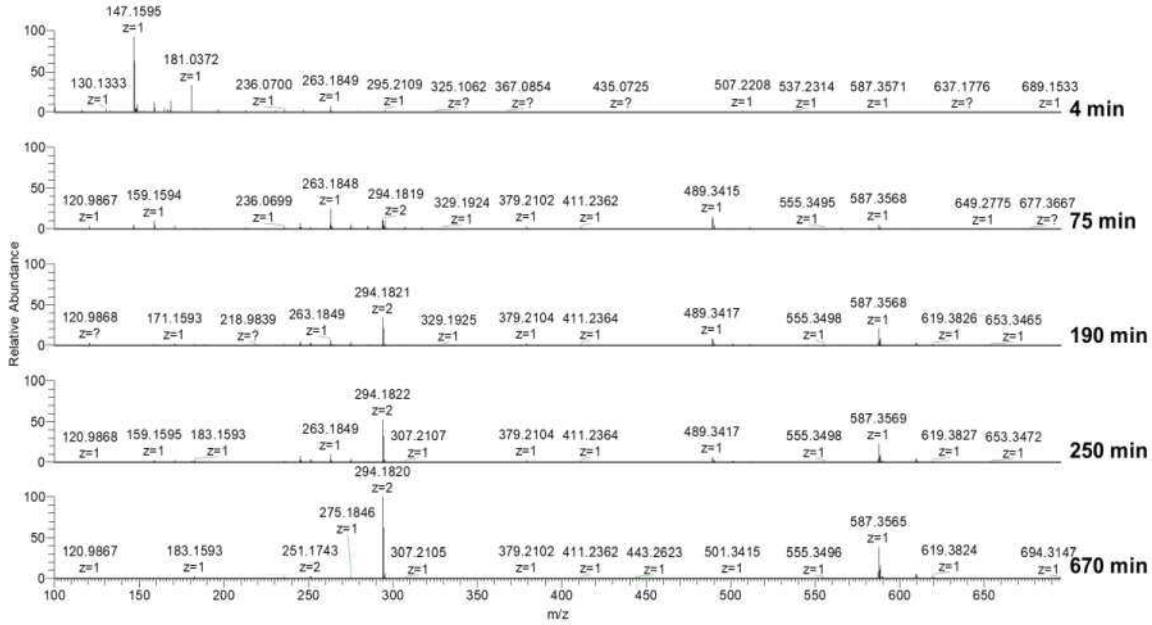

Figure II-16. Evolution of the HRMS-ESI spectra of the 3:2 mixture of **pPh** (2 mM) and **T** (1.3 mM) in 50%-50% $CHCl_3$/MeOH.

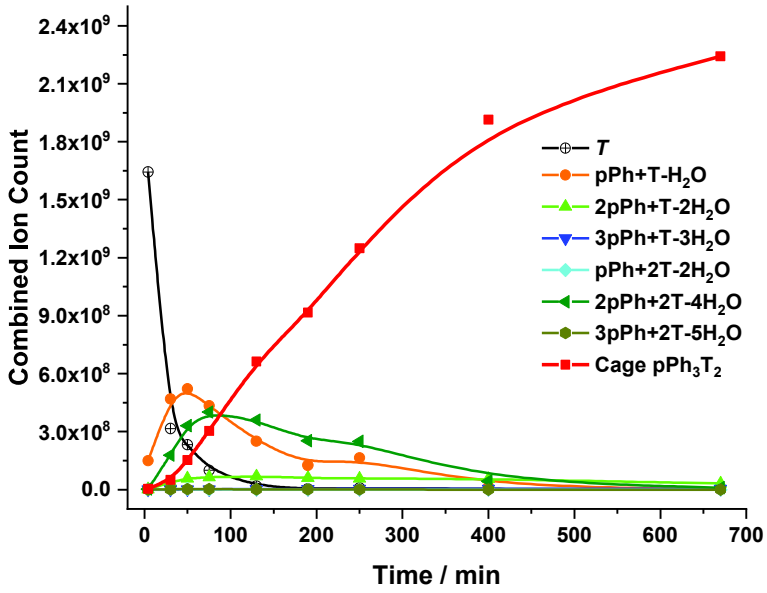

Figure II-17. HRMS-ESI kinetic profiles for the species generated during the self-assembly of **pPh** (2 mM) and **T** (50%-50% $CHCl_3$/MeOH, r.t) as a function of time. NB: These data do not provide quantitative information about the relative amounts of each species identified by its mass, but, taken separately, they display the evolution of a given identified species during the course of the reaction. The curves are added to guide the eye.

2.4.3. Formation processes of the macrobicyclic cage pPh_3T_2

Pathways for the generation of this [3+2] cage (i.e., **pPh_3T_2**) were then assessed. Figure **II-18** illustrates all the imine species possibly involved in the dynamic self-assembling process (nine intermediates as well as two reagents and a cage product), although some of them were not detected by HRMS-ESI. In the initial stages of the reaction, only the dialdehyde **pPh** and the tetramine **T** were present in the solution, along with slowly increasing quantities of the [1+1] type of intermediate.

The proposed cage formation process involves sequential reactions with free **pPh** and/or **T**, first with the [1+1] species, then with each higher species, increasing the number of imine bonds and number of linking bridges until the precursor to the desired [3+2] cage is formed (blue-line pathway) and undergoes intramolecular cyclisation. Some of these [1+1] intermediates may connect directly with themselves or other [1+1] or [2+1] type of

intermediates to form [2+2] or [3+2] type of intermediates, respectively (orange-line pathway).

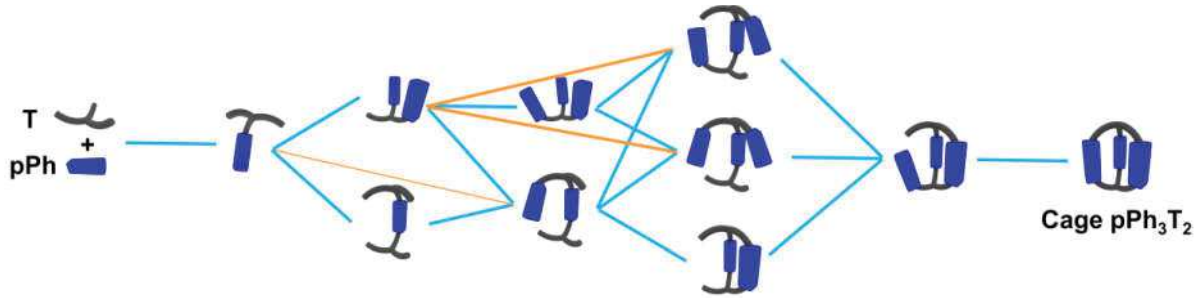

Figure II-18. Stepwise [3 + 2] imine condensation processes showing the intermediates on the way to the formation of the dynamic covalent macrocyclic cage.

2.5. Self-sorting of macrobicyclic cages from a three-component DCL

2.5.1. ^{1}H NMR monitoring

A three-component self-sorting experiment resulting in the parallel formation of two cages was set up from a **pPh:BiPh:T** mixture in a 3:3:4 ratio. **Figure II-19** and **Figure II-20** show that after mixing the components, the concentration of **pPh** rapidly decreased. Simultaneously, new broad signals appeared and progressively disappeared as the reaction proceeded, indicating that they were due to intermediate species. After ca. 240 min, some additional low-intensity peaks were noted, together with signals assigned to the imine bond CH of both the small cage **pPh_3T_2** and the large cage **$BiPh_3T_2$**, while both **pPh** and **BiPh** were progressively further consumed. The aldehyde **pPh** was nearly fully consumed after 720 min, time at which 9% **BiPh** remained unreacted. The consumption sequence was in accordance with their corresponding cage formation rates. NMR yields of 51% for **pPh_3T_2** and 46% for **$BiPh_3T_2$** were attained after about 4157 min (69 h), with the final mixture containing 2% of unreacted **BiPh**. The final spectrum indicated the high-fidelity self-sorting and confirmed the absence of any heteroleptic cages.

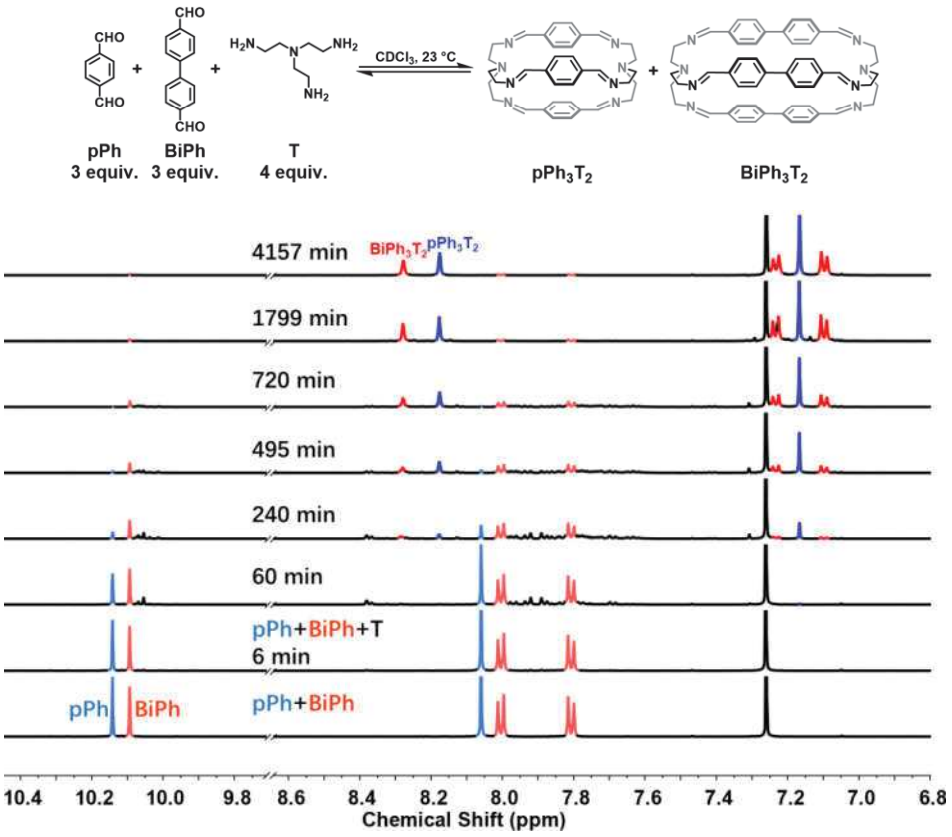

Figure II-19. Time evolution of the partial ^{1}H NMR spectra (400 MHz, $CDCl_3$, 23 °C) of the reaction **3pPh** + **3Biph** + **4T** ($[\mathbf{pPh}]_0$ = $[\mathbf{BiPh}]_0$ = 3.6 mM, $[\mathbf{T}]_0$ = 4.8 mM). The two bottom spectra correspond to the isolated macrobicyclic cages $\mathbf{pPh_3T_2}$ and $\mathbf{BiPh_3T_2}$.

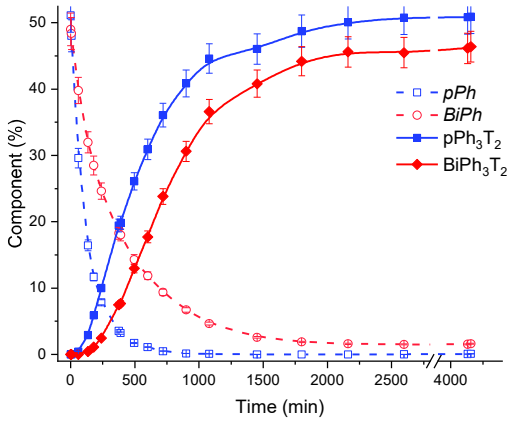

Figure II-20. ^{1}H NMR monitoring of dialdehydes **pPh, BiPh** and cages $\mathbf{pPh_3T_2}$, $\mathbf{BiPh_3T_2}$ over 1800 min. The component distribution (%) was obtained by integration of the aromatic and aldehyde CHO proton signals in the 400 MHz ^{1}H NMR spectra. Error in ^{1}H-NMR signal integration: ±5%.

2.5.2. HRMS-ESI monitoring

To gain some additional information about the mechanism of the macrobicycle self-sorting processes, intermediates formed during the reaction were characterised by their HRMS spectra. **Table S-II-3** lists all identified intermediates and cages detected in time dependent HRMS experiments. The evolution of the spectra over time is shown in **Figure II-22** and it revealed qualitative trends for these species. After 4 min of mixing, the [1+1] type intermediates (i.e., **[pPh+T]** and **[BiPh+T]**) were generated, and their concentrations reached their maximum intensity at about 30-60 min, and then gradually decreased. The [2+2] intermediates followed a similar tendency but slightly slower than that of [1+1] intermediates. In general, a cascade reaction was triggered by the rapid appearance of **[pPh+T]** and **[BiPh+T]**, resulting ultimately in the simultaneous formation of $\mathbf{pPh_3T_2}$ and $\mathbf{BiPh_3T_2}$.

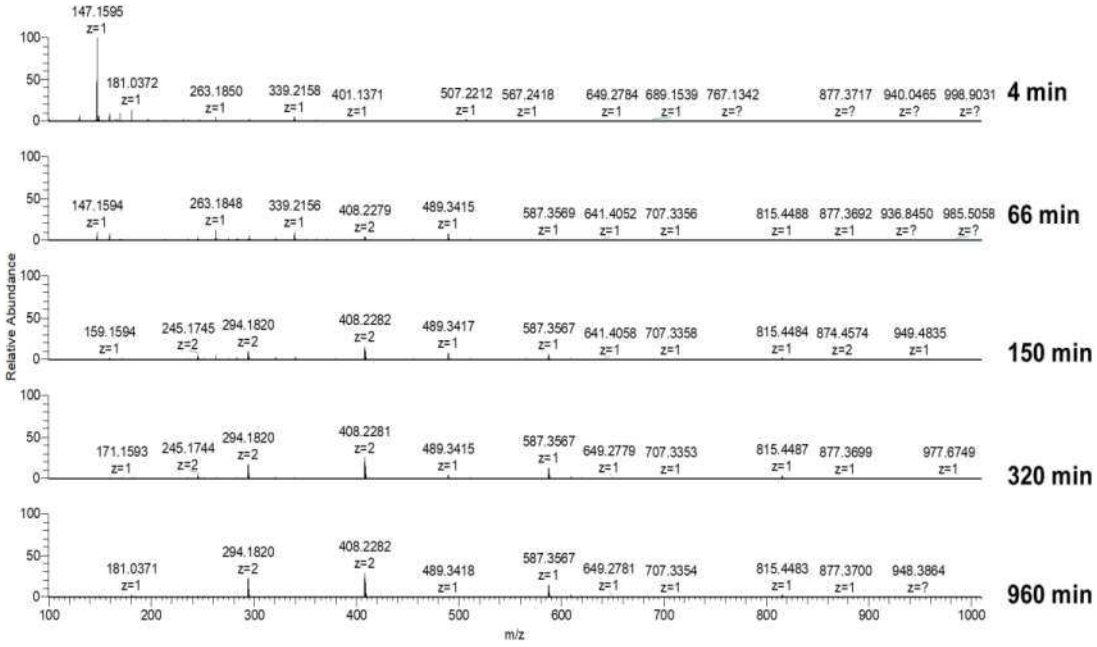

Figure II-21. Evolution of the HRMS-ESI spectra of the 3:3:4 mixture of **pPh** (2 mM), **BiPh** (2 mM) and **T** in 50%-50% $CHCl_3$/MeOH after 4 minutes, 66 minutes, 150 minutes, 320 minutes and 960 minutes.

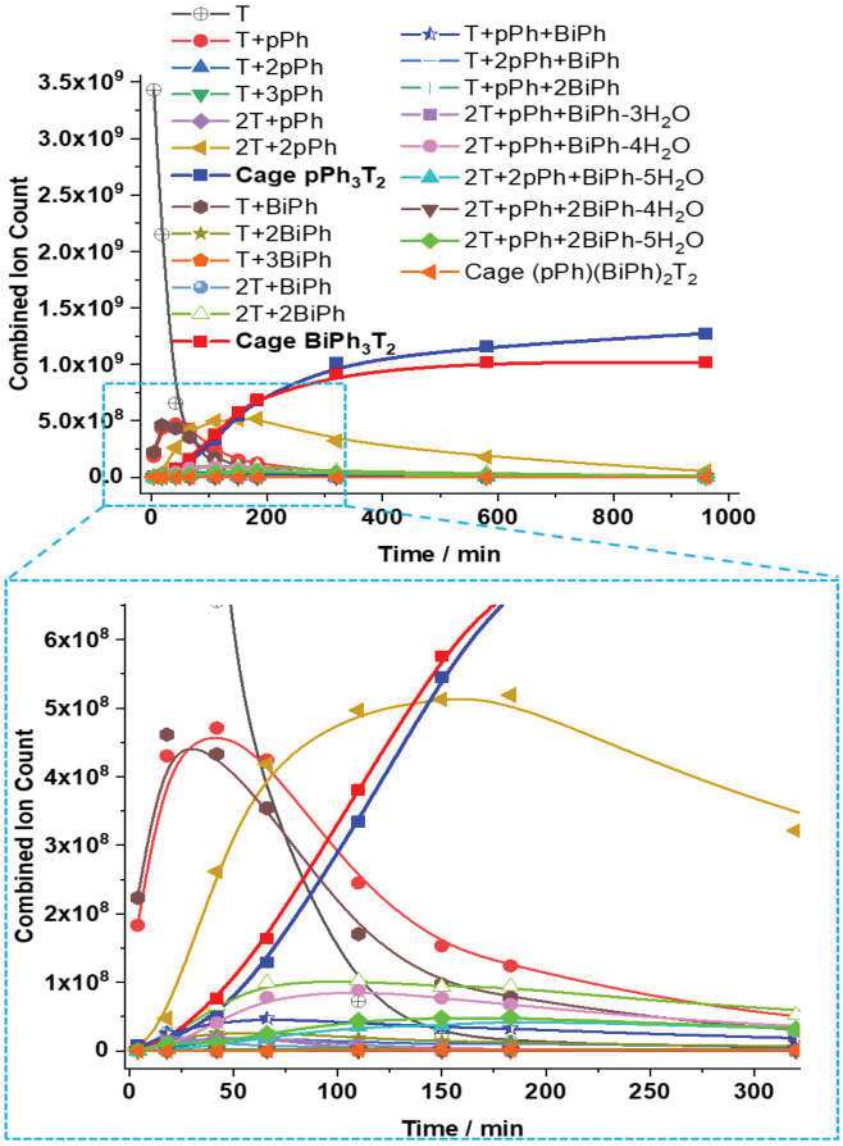

Figure II-22. HRMS-ESI monitoring of the evolution of the species generated during the reaction of 3**pPh** + 3**BiPh** + 4**T** (50%-50% $CHCl_3$/MeOH, r.t) as a function of time over 960 min. NB: These data do not provide quantitative information about the relative amounts of each species identified by its mass, but, taken separately, they display the evolution of a given identified species during the course of the reaction. The curves are added to guide the eye.

Several heteroleptic intermediates appeared which subsequently underwent conversion to other species before disappearing from the final spectra. Studying the HRMS plot in higher detail (under high amplification of the axis, **Figure II-23**) revealed a decrease in the

concentration of the heteroleptic cage (i.e., **(pPh)(Biph)$_2$T$_2$**) after its formation, indicating a self-correction process as a result of the poor stability of such heteroleptic species.

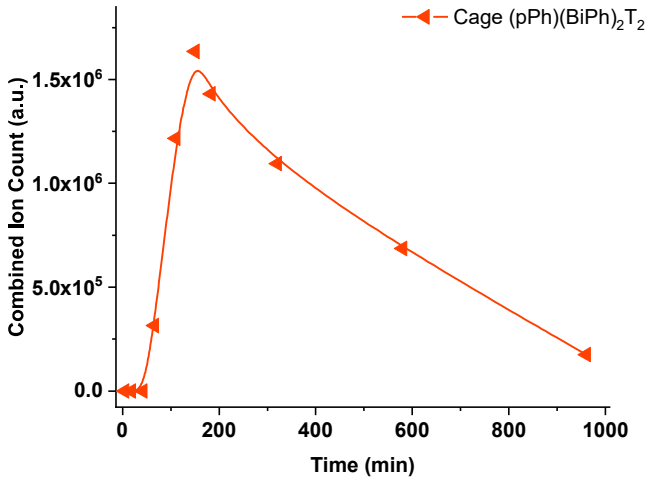

Figure II-23. Amplified HRMS-ESI plot showing the evolution of cage **(pPh)(BiPh)$_2$T$_2$** as a function of time. NB: These data do not provide quantitative information about the relative amounts of each species identified by its mass, but, taken separately, they display the evolution of a given identified species during the course of the reaction. The curves are added to guide the eye.

2.5.3. Stepwise self-sorting experiment through component recombination

The previous "one-pot" self-sorting experiment was performed in two steps to gain more insight into the recombination process of the intermediates (**Scheme II-5**).

The ^{1}H-NMR study indicated that in a solution prepared by mixing 3 equiv. **BiPh** and 4 equiv. **T**, 36% of the initial **T** was converted into the cage **BiPh$_3$T$_2$**. After 24h, as no CHO signal of free **BiPh** remained, the rest of **BiPh** appeared to have formed **[BiPh+2T]** (10% by **T**) and **[2BiPh+2T]** (15% by **T**), accompanied by the remaining free **T** (40%). This composition did not change over another 4 days. Then, on the addition of 3 equiv. **pPh** to this solution, all intermediates and free **T** were converted into > 47% (concerning the internal reference) of each of the two macrobicycles **pPh$_3$T$_2$** and **BiPh$_3$T$_2$** (**Figure II-24**). These results indicated that the reaction between i) the added **pPh**, ii) the **[BiPh+2T]** and **[2BiPh+2T]** intermediates, and iii) the remaining free **T** gave the **pPh$_3$T$_2$** cage together with the additional **BiPh$_3$T$_2$** cage. Taken together, they confirm that self-correction did indeed take

place by component recombination driven by the thermodynamically-favoured formation of the **pPh$_3$T$_2$** cage.

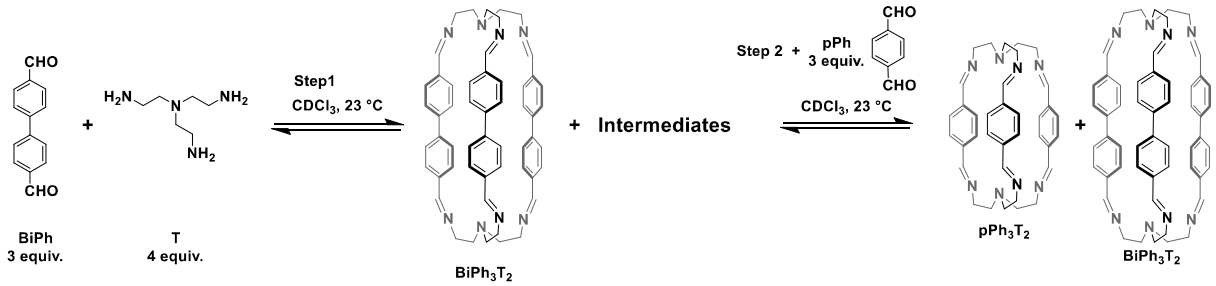

Scheme II-5. Component recombination by addition of 3 equiv. **pPh** to the 3**BiPh** + 4**T** solution.

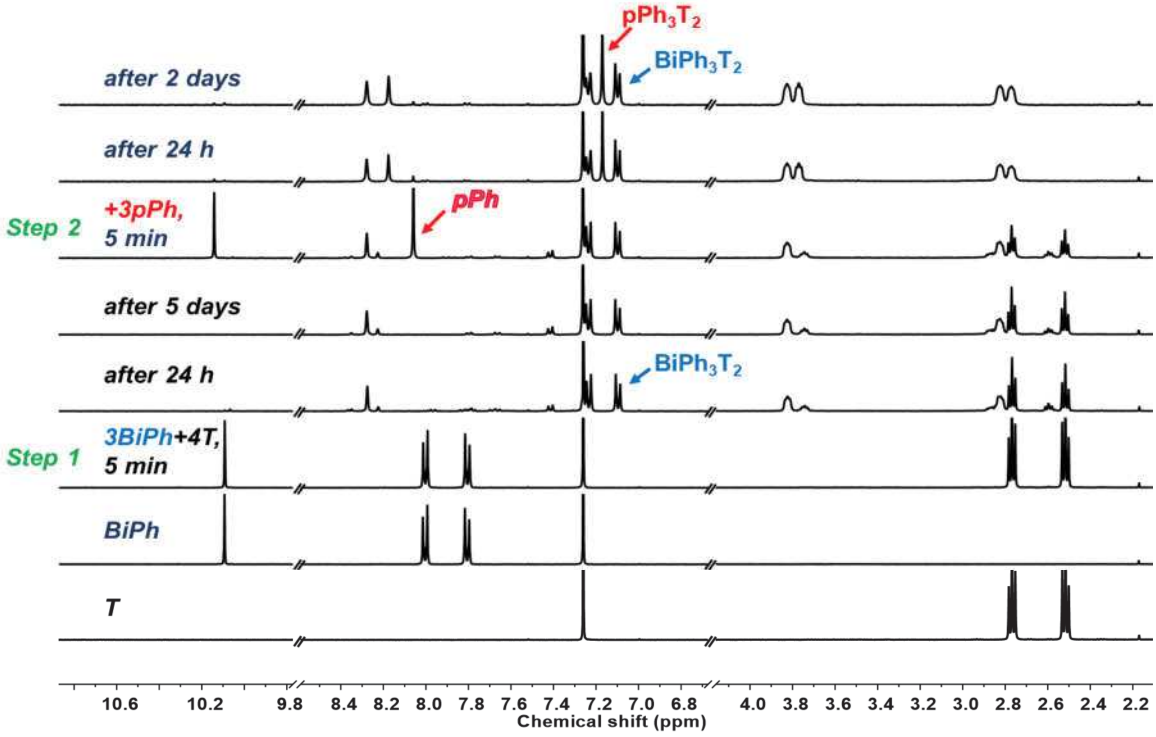

Figure II-24. Evolution of the ^{1}H NMR (400 MHz, $CDCl_3$, 23 °C) spectra of stepwise self-sorting by addition of 3 equiv. **pPh** to the 3**BiPh** + 4**T** solution (the initial concentration of **BiPh** is 3.6 mM, **T** is 4.8 mM).

2.5.4. Self-sorting processes of macrobicyclic cages pPh_3T_2 and $BiPh_3T_2$

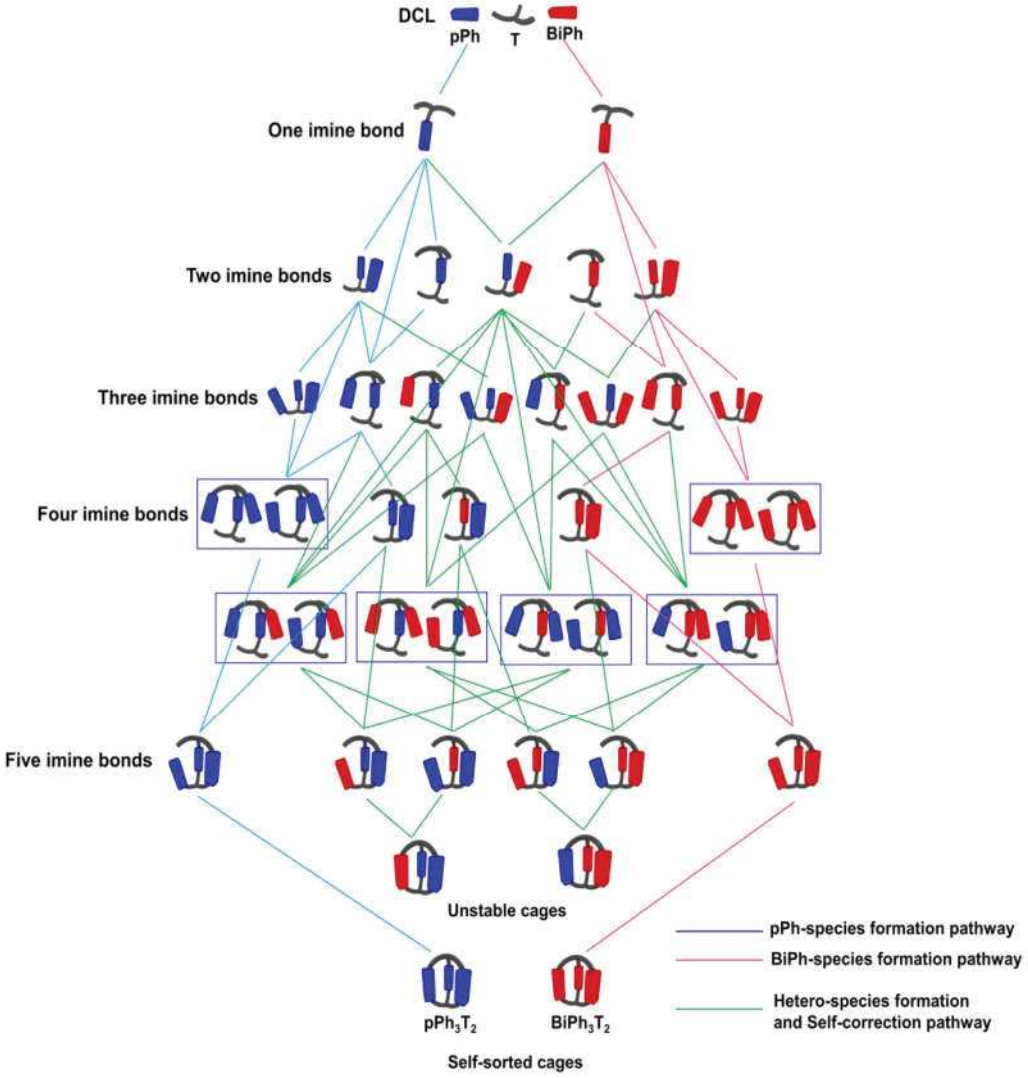

Figure II-25. Possible reaction pathways in the three-component [3+2] imine-cage self-sorting system. Blue and red cuboid represent the dialdehyde units, the three-jaw figure represent the triamine **T.** Cyan and pink lines correspond to the homoleptic reactions to form **[*x*pPh+*y*T]** and **[*x*BiPh+*y*T]** species, respectively. Green lines correspond to the heteroleptic pathways and self-correction pathways.

The self-sorting of cages defined a progressive evolution towards the final homoleptic structures along a sequence of steps which may involve up to 38 intermediates (**Figure II-25**): the [1+1] intermediate was formed initially in high abundance, and then it converted into three-component intermediates [1+2] and [2+1]. These intermediates of odd stoichiometry were then transformed into four- (i.e., [2+2] and [1+3]) and five-component (i.e., [2+3]) larger

intermediates, which finally led to the formation of the desired homoleptic cage structures. Self-correction of the heteroleptic species must take place at different steps within the reaction sequence to yield the pure homoleptic macrobicyclic structures **pPh$_3$T$_2$** and **BiPh$_3$T$_2$**.

2.6. Principles of self-sorting

2.6.1. Effect of component size

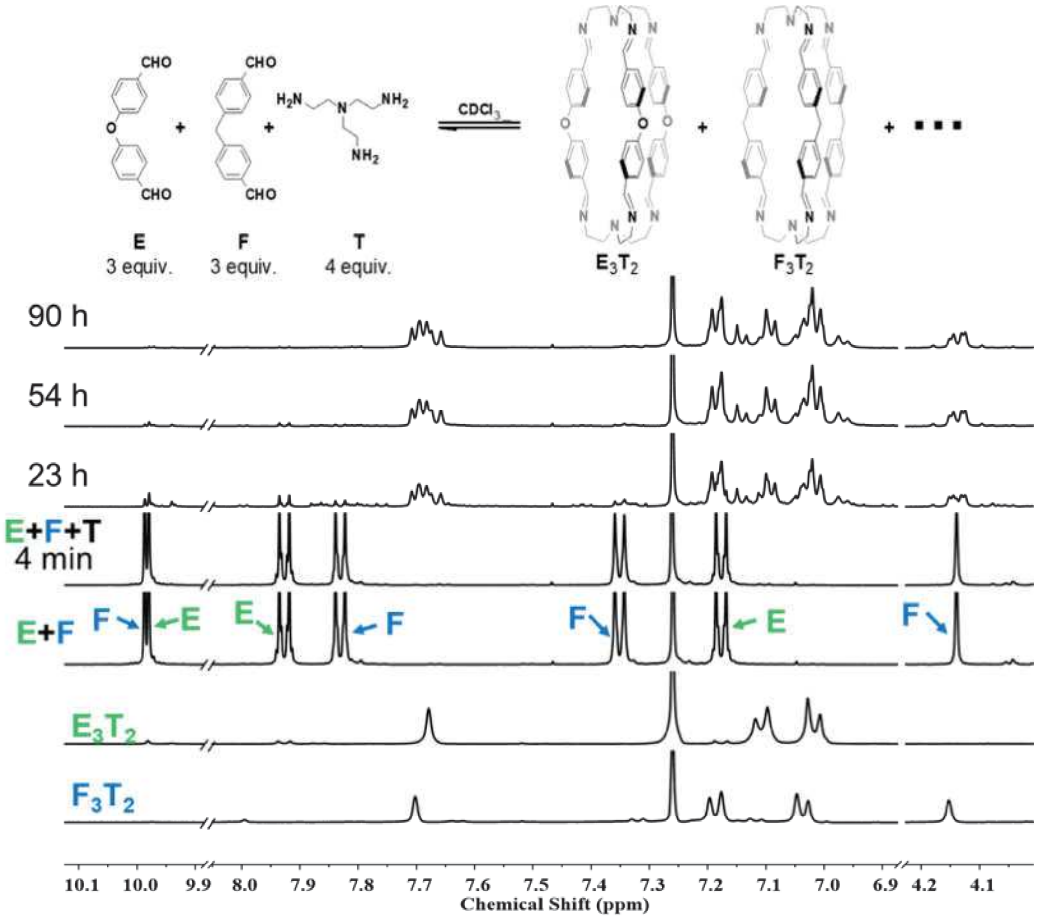

Figure II-26. Time evolution of the ^{1}H NMR (400 MHz, $CDCl_3$, 23 °C) spectra of 3**E** + 3**F** + 4**T** reaction.

The previous results (for instance, the self-sorting of **T** with **pPh** and **BiPh**) inferred self-sorting behaviours between components of different lengths. Here we explored the self-sorting capacity of two dialdehydes of similar length (**E**, **F**) at the ratio of **E:F:T** = 3:3:4 **(Figure II-26)**. Upon equilibration, aside from the signals of cage **E$_3$T$_2$ and F$_3$T$_2$**, it became evident in the view of the ^{1}H NMR signals that some additional species were produced (see

for instance the 7.8-7.6 ppm in **Figure II-26**). Although the structure of these side-products signals could not be identified by NMR, it was sufficient to demonstrate that the current system did not exhibit the high-fidelity self-sorting phenomenon that we expected. This experiment thus reveals that minor variations in precursor length can crucially affect the self-sorting outcome.

2.6.2. Effect of stoichiometry

2.6.2.1. Stoichiometry effects on the self-sorting of components in different length

The self-sorting behaviour of cages in a competitive environment with insufficient amounts of **T** was then investigated. The reactions were monitored by ^{1}H NMR by mixing **pPh:BiPh:T** in different stoichiometric ratios.

Table II-1. Outcomes of self-sorting experiments in **pPh:BiPh:T** mixtures with different ratios of **T.**[a]

	pPh:BiPh:T		
Constitutent	3:3:2 (%)	3:3:3 (%)	3:3:4 (%)
Unreacted **pPh**	10	4	< 1
Unreacted **BiPh**	36	25	< 1
Cage **pPh_3T_2**	36	45	51
Cage **$BiPh_3T_2$**	8	23	46

[a.] The component distribution (%) was obtained by integration of the aromatic and aldehyde CHO proton signals in the 400 MHz or 500 MHz ^{1}H NMR spectra. Error in ^{1}H-NMR signal integration: ±5%.

The outcomes of the reactions at equilibrium are summarized in **Tables II-1**. It can be seen that (i) when there is an insufficient amount of **T**, the system preferred to form the relatively smaller cage **pPh_3T_2**, indicating that such cage is thermodynamically more stable than the bigger one; (ii) all experiments exhibited excellent self-sorting behaviour, with good overall NMR yields.

2.6.2.2. Stoichiometry effects on the self-sorting of components in similar length

Lehn et al. have reported a highly selective incomplete self-sorting phenomenon from mixtures of dialdehydes of similar length (pyridine-2,6-dicarboxaldehyde, **Py** and m-

phenylenedicarboxaldehyde, **mPh**).[12] They demonstrated that from a mixture of **Py**:**mPh**:**T** in a 3:3:2 ratio, the outcome showed a preference for cage $\mathbf{Py_3T_2}$ with up to 92% yield. This motivated us to examine the self-sorting selectivity of **Py**:**mPh**:**T** in a 3:3:4 ratio.

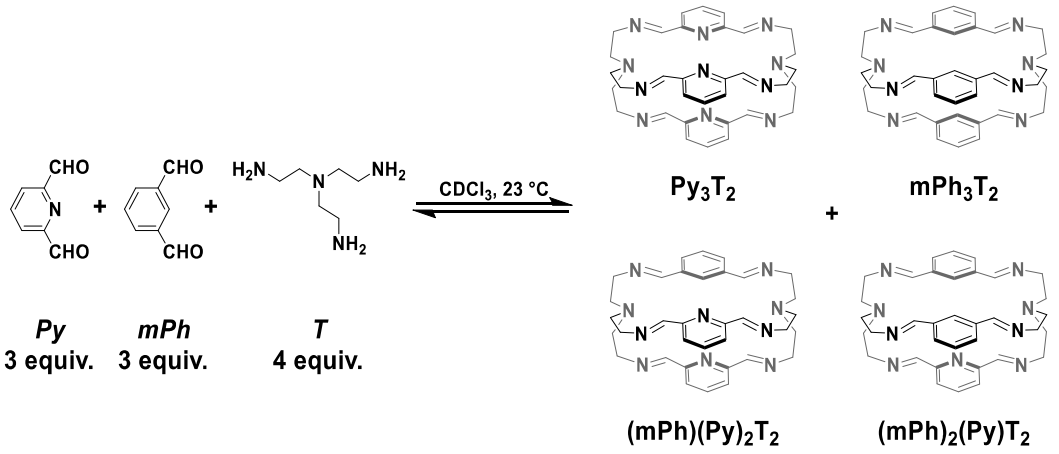

Scheme II-5. Precursors and possible products for the dynamic library: 3**Py** + 3**mPh** + 4**T**

The ^{1}H NMR spectra (**Figure II-27**) showed that after mixing all components, it was evident that the consumption of **mPh** was significantly slower than that of **Py**. As the reaction course proceeded, complex uninterpretable signals appeared around the characteristic peaks of cages $\mathbf{Py_3T_2}$ and $\mathbf{mPh_3T_2}$. The careful analysis led to attributing two singlets with chemical shifts at 5.2 and 5.3 ppm to the two heteroleptic cages $\mathbf{(Py)(mPh)_2T_2}$ and $\mathbf{(Py)_2(mPh)T_2}$, respectively. The existence of these heteroleptic macrobicycles was further confirmed by HRMS-ESI (**Figure II-28**). After 8 days of equilibration, the composition of each constituent as indicated by the ^{1}H NMR remained unchanged, which was: $\mathbf{mPh_3T_2}$ (20%), $\mathbf{(Py)(mPh)_2T_2}$ (25%), $\mathbf{(Py)_2(mPh)T_2}$ (32%), $\mathbf{Py_3T_2}$ (20%) and 3% unreacted **mPh**. In comparison with previous reports, this experiment demonstrates that the stoichiometric ratio of the initial library of components is an essential factor that determines the outcome of self-sorting (ordered) or unsorting (disordered).

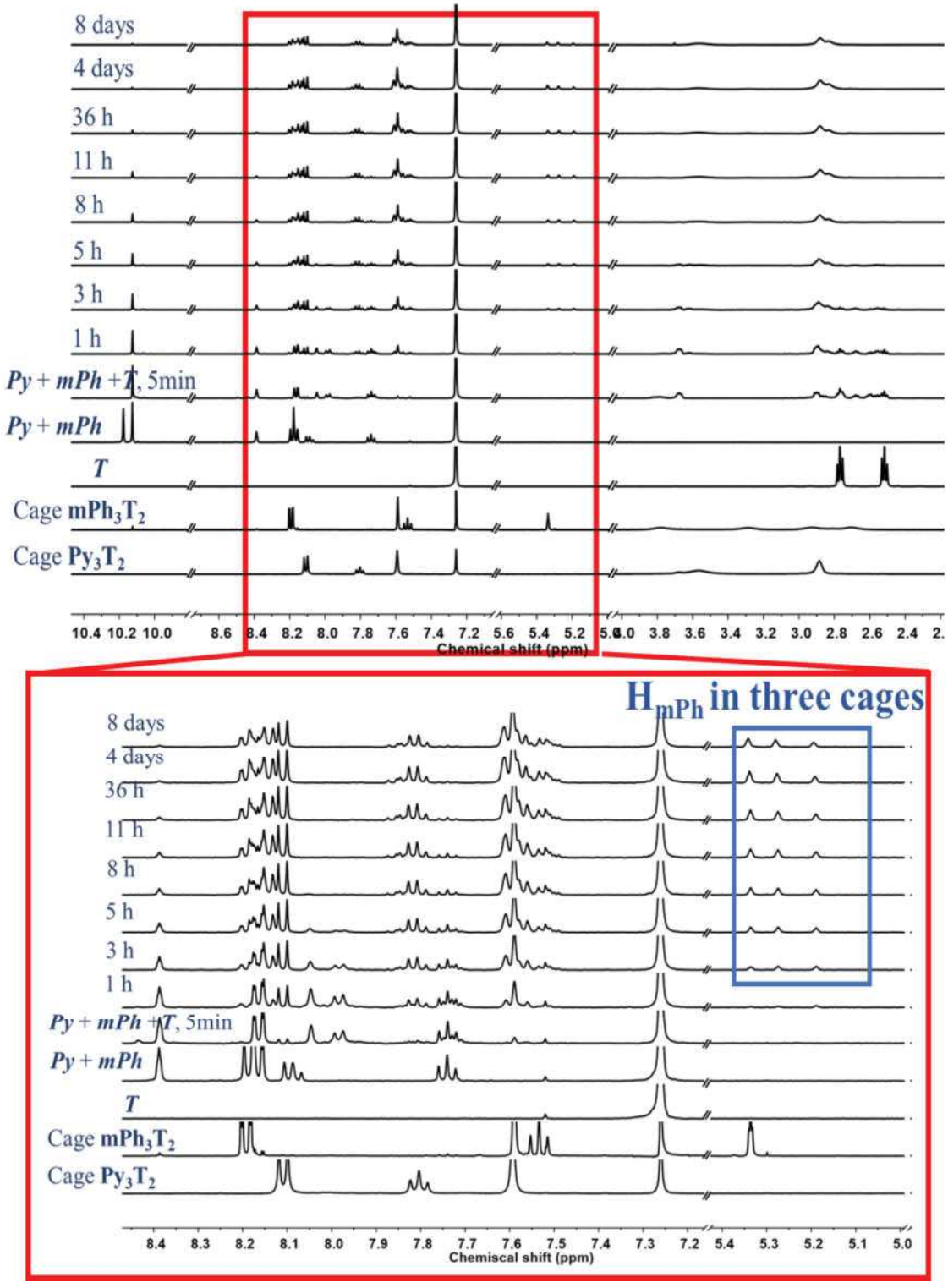

Figure II-27. Time evolution of the ^{1}H NMR spectra (400 MHz, $CDCl_3$, 23 °C) of the reaction 3**Py** + 3**mPh** + 4**T** ($CDCl_3$, 23 °C). The two bottom spectra correspond to the isolated $\mathbf{Py_3T_2}$ and $\mathbf{mPh_3T_2}$ cages.

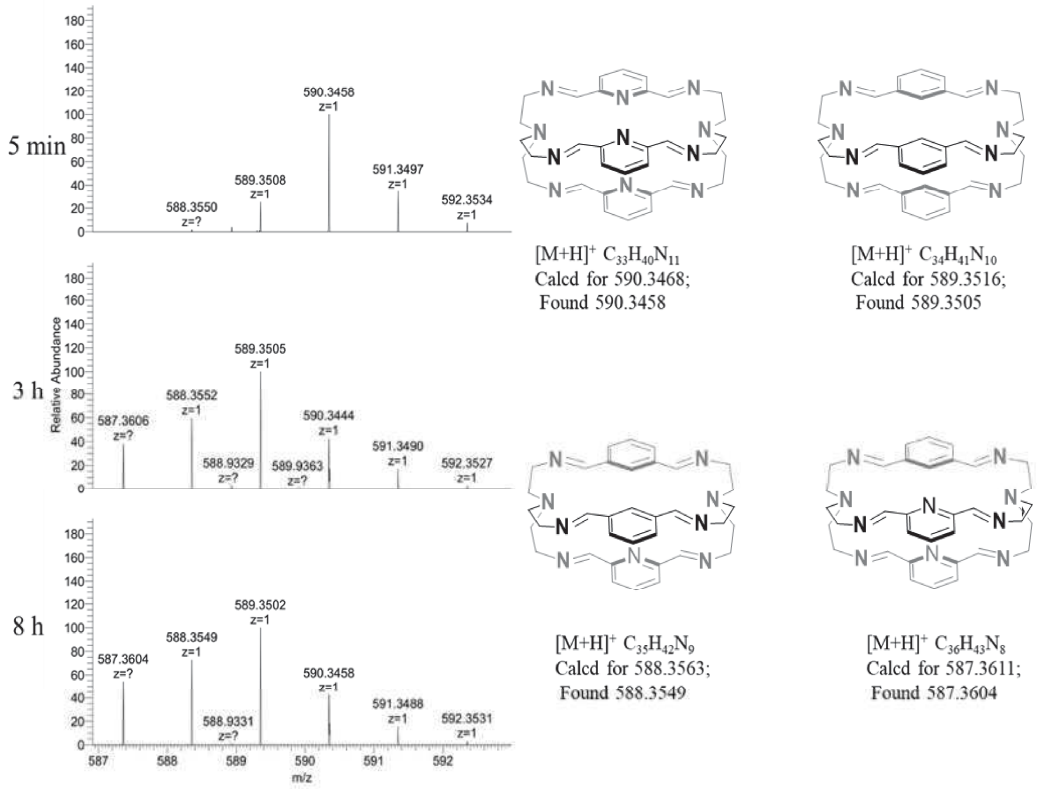

Figure II-28. Time evolution of the partial HRMS-ESI spectra for the reaction crude of the dynamic self-assembly between 3**Py** + 3**mPh** + 4**T**

2.7. Self-sorting of macrobicyclic cages from a four-component DCL

In another case, a four-component DCL composed of **pPh**, **BiPh**, **TriPh** and **T** in a 3:3:3:6 ratio was investigated in $CDCl_3$ (**Figure II-29**). The time evolution was monitored by ^1H NMR at 40 °C. Again, the reactant concentrations decreased uniformly with time, in a similar manner to the appearance of the characteristic peaks assigned to cages **pPh_3T_2**, **$BiPh_3T_2$** and **$TriPh_3T_2$**, following the sequence of relative rates **pPh_3T_2** ≥ **$BiPh_3T_2$** ≥ **$TriPh_3T_2$**. After 900 min, signals corresponding to macrobicyclic cages **pPh_3T_2**, **$BiPh_3T_2$**, and **$TriPh_3T_2$** were clearly apparent and the distribution was 29% **pPh_3T_2**, 26% **$BiPh_3T_2$**, 26% **$TriPh_3T_2$**, together with <1% unreacted **BiPh** and <1% unreacted **TriPh**. The production of the three macrocycles was also confirmed by HRMS (Chapter VII, **Figure S-II-34**). These results indicate that with an appropriate choice of precursor components, self-sorting systems of higher diversity can be efficiently designed.

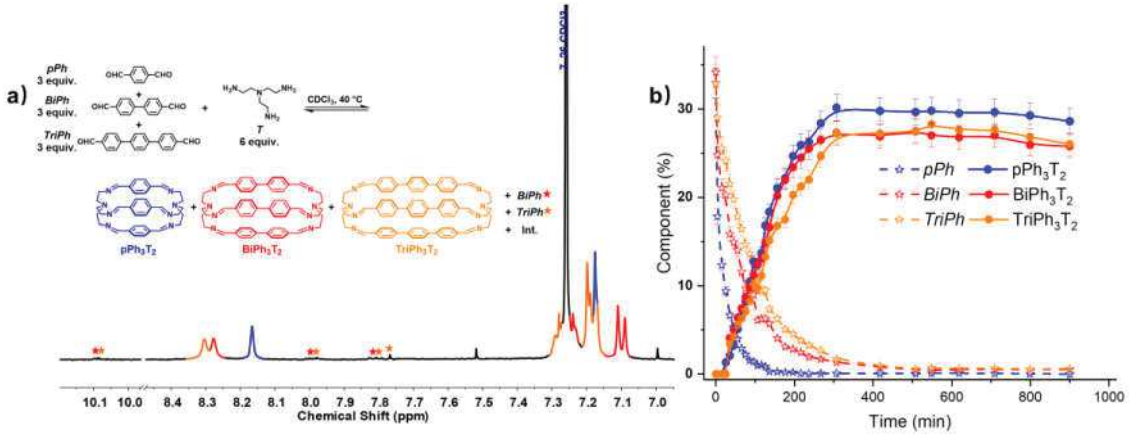

Figure II-29. (a) Partial ^{1}H NMR spectrum (400 MHz, $CDCl_3$) of the parallel formation of macrobicyclic cages **pPh$_3$T$_2$**, **BiPh$_3$T$_2$,** and **TriPh$_3$T$_2$** through the self-assembly of 3**pPh** + 3**BiPh** +3**TriPh** + 6**T** after 900 min at 40 °C. (b) ^{1}H NMR monitoring of the formation of the cages **pPh$_3$T$_2$**, **BiPh$_3$T$_2$**, and **TriPh$_3$T$_2$** over 900 min. Error in ^{1}H-NMR signal integration: ±5%. The signals of free dialdehydes **BiPh** and **TriPh** are indicated by red and orange stars, respectively.

3. Summary of the chapter

We have studied the formation and self-sorting processes of either [2+2] tetraimino macrocycles or [3+2] hexaimino macrobicyclic cages using ^{1}H NMR and HRMS-ESI to clarify the intrinsic rationale of self-sorting.

At the beginning of the chapter, the work focuses on the mechanistic studies of the [2+2] imine-based macrocycles formation. After the kinetic investigations, a plausible three-pathway cyclization mechanism towards the formation of [2+2] covalent organic macrocycles was suggested. The results demonstrated that the heteroleptic intermediates randomly generated during this process can be corrected through dissociation and recombination (i.e., self-correction process) leading to the parallel generation of two or three homoleptic macrocycles.

The rest of the chapter describes the study of the self-assembly process of dynamic molecular cages and several factors to influence their self-sorting behaviour. The generation of macrobicyclic cages is more complicated than that of macrocycles, when macrobicyclic cages are implemented into a three-component self-sorting system, at least 43 species with

numerous internal reactions could be generated. To ensure the precise recognition of self and non-self and to eliminate metastable heteroleptic species, an intrinsic self-correction process is indispensable. In addition, the structural and stoichiometric effects were confirmed to be the two key factors for the rendering of high-fidelity self-sorting. With this approach, the simultaneous generation of three macrocycles or cages was successfully achieved from four-component DCLs.

The results highlight the essential role played by structural features as well as stoichiometry in controlling both the kinetic and thermodynamic parameters to balance a sorted versus a scrambled outcome.

Chapter III. Dynamic Covalent Self-Sorting and Kinetic Switching Processes in Two Cyclic Orders: Macrocycles and Macrobicyclic Cages

1. Introduction

A further step towards systems of higher complexity resides in the design and exploration of DCLs presenting time dependence that would autonomously adapt to their inherent kinetic factors and display self-recognition processes in the buildup of their constitution through component self-sorting processes, leading to the emergence of higher states of complex behaviour.[126,135,136]

Recently, He and Lehn described a series of time-dependent DCLs that were generated from mixtures of two aldehydes and two amino compounds through the formation of reversible C＝N bonds, either in the absence or presence of metal ions as shown in **Figure III-1**.[30] Based on the internal kinetic and thermodynamic properties of the selected components as well as their related constituents, these DCLs underwent an evolution from an initial kinetic distribution to the final thermodynamic one as a function of time. As a result, the overall evolution exhibited a kinetically-controlled orthogonal switching from one diagonal to the other diagonal of the [2 × 2] CDN. This report led to the present efforts to incorporate such interesting kinetically controlled evolution into self-sorting systems.

In Chapter II, self-sorting processes in one type of topology, either macrocycles or cages have been described. That antecedent project led to the exploration of DCLs of higher complexity by, for instance: (i) implementing self-sorting in two cyclic orders (e.g., concurrent formation of macrocycles and macrobicyclic cages); (ii) evaluation of time-dependent switching behaviours in the self-sorting processes of macrocycles and macrobicyclic cages.

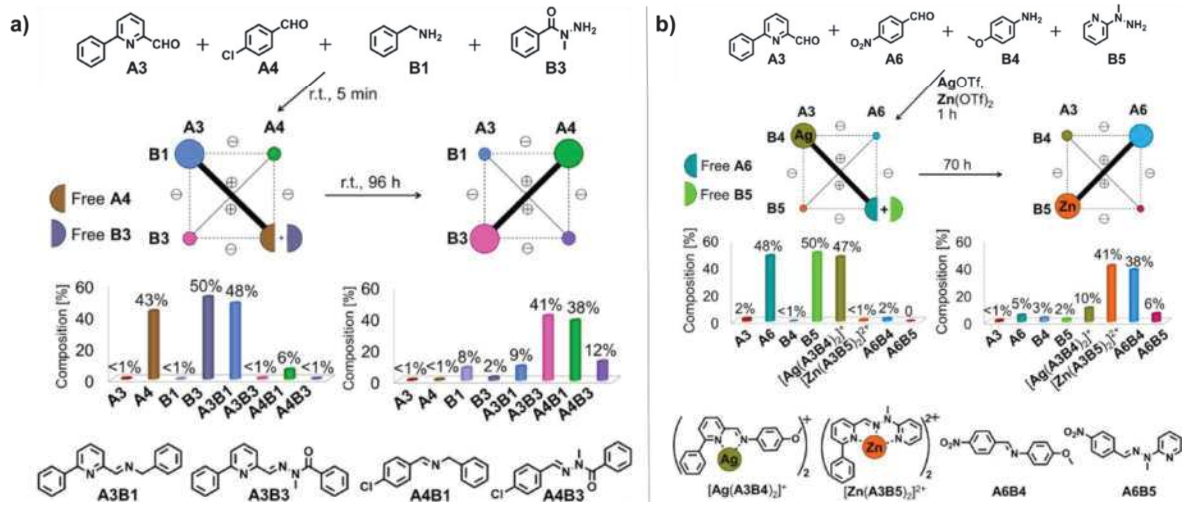

Figure III-1. Kinetic orthogonal switching of the [2 × 2] CDNs (**a**) in the absence and (**b**) in the presence of metal cations (Figure reproduced from reference[30]).

2. Results and Discussion

2.1. Self-sorting in two cyclic orders

As shown in Chapter II, the main driving force for efficient self-sorting arises from the differential reaction rates of the substrates involved. The reactivity of triamine **T** is known to be higher than that of diamine **NON**, and the formation of **T**-cages is proven to be faster than that of **NON**-macrocycles. These two polyamines were therefore chosen to examine the possibility of parallel generation of constituents with different topologies *via* self-sorting processes.

2.1.1. Self-sorting from three components Py/T/NON

To start with, the relatively reactive pyridine 2,6-dicarboxaldehyde (**Py**) was chosen to react with a mixture of **T** and **NON**. Considering that **T** contains three reactive amino groups and **NON** contains two amino groups, in order to allow all amines to fully react with the aldehyde, the three precursors were mixed in a molar ratio of **Py:T:NON**=5:2:2. Upon simultaneous addition of **T** and **NON** into a **Py** solution in an NMR tube, the tube was shaken and the reaction was monitored by ^{1}H NMR spectroscopy. Component **T** was almost completely consumed after only 5 min of reaction, with the expected coupled decrease in the amount of unreacted **Py**. The ^{1}H NMR spectra taken over this period showed a large number

of complicated signals which were difficult to interpret, indicating that several intermediates were formed from the reaction of **Py** and **T**.

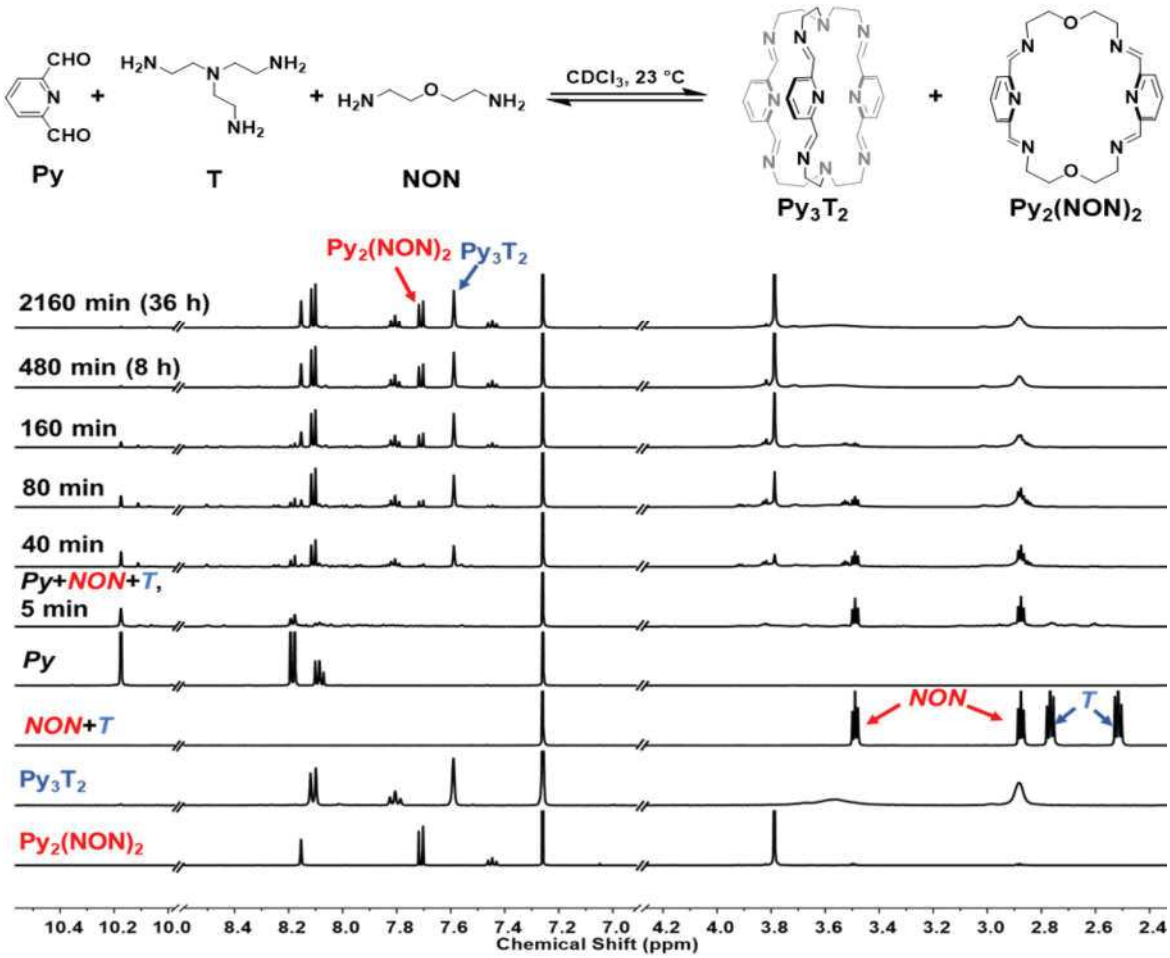

Figure III-2. ^{1}H NMR (500 MHz, $CDCl_3$, 23 °C) monitoring of the self-sorting behaviour of the reaction 5**Py** + 2**T** + 2**NON**, where the initial concentration of **Py** is 9.0 mM and the initial concentration of both **T** and **NON** is 3.6 mM. The two bottom NMR spectra are the spectra of pure **$Py_2(NON)_2$** and **Py_3T_2** and have been included for comparison.

Study of the reaction progress described in Chapter II showed that the self-sorting of organic cages and macrocycles involves an induction period with multiple condensation reactions generating a number of unidentified intermediates. In accordance with this, as **NON** was gradually consumed, another series of intermediates was detected in solution and presumed to be involved in different oligomerization and cyclization reactions. Once equilibrium was reached (after 36 h), almost all of the starting materials had been converted

to macrocycle **$Py_2(NON)_2$** and macrobicyclic cage **Py_3T_2**.

The rate curve (**Figure III-5a**) showed that (i) after mixing, more than 50% of **Py** was immediately consumed and no cyclic product was formed; (ii) the rate of formation of cage **Py_3T_2** was higher than that of macrocycle **$Py_2(NON)_2$**; (iii) the outcome in which 60% of **Py** was converted into cage **Py_3T_2** and 37% into **$Py_2(NON)_2$** agreed well with the stoichiometric ratio of the initial components.

2.1.2. Self-sorting from three components BiPh/T/NON and E/T/NON (E = diphenylether dialdehyde)

2,6-pyridinedicarboxaldehyde was replaced by the longer but less reactive 4,4'-biphenyldicarboxaldehyde, **BiPh**, to examine the effect of the dialdehyde length and reactivity on the self-sorting outcome. Throughout the reaction (**Figure III-3**), a large number of signals corresponding to intermediate compounds appeared. After 700 min, all the **T** had been consumed and converted into the cage **$BiPh_3T_2$**, while **NON** had not been entirely consumed. At equilibrium after 3830 min, the two predominant species were cage **$BiPh_3T_2$** and macrocycle **$BiPh_2(NON)_2$**.

The rate plot (**Figure III-5b**) showed that (i) the rate of consumption of **BiPh** was significantly slower than that of **Py** in the previous system; (ii) the formation rate of **$BiPh_3T_2$** was faster than that of **$BiPh_2(NON)_2$**; (iii) the concentration of cage **$BiPh_3T_2$** remained unchanged during the slow formation of **$BiPh_2(NON)_2$**. When equilibrium was reached, about 60% of **BiPh** was converted to cage **$BiPh_3T_2$** and about 33% of **BiPh** was converted to macrocycle **$BiPh_2(NON)_2$**, with the rest of the **BiPh** in the form of side products.

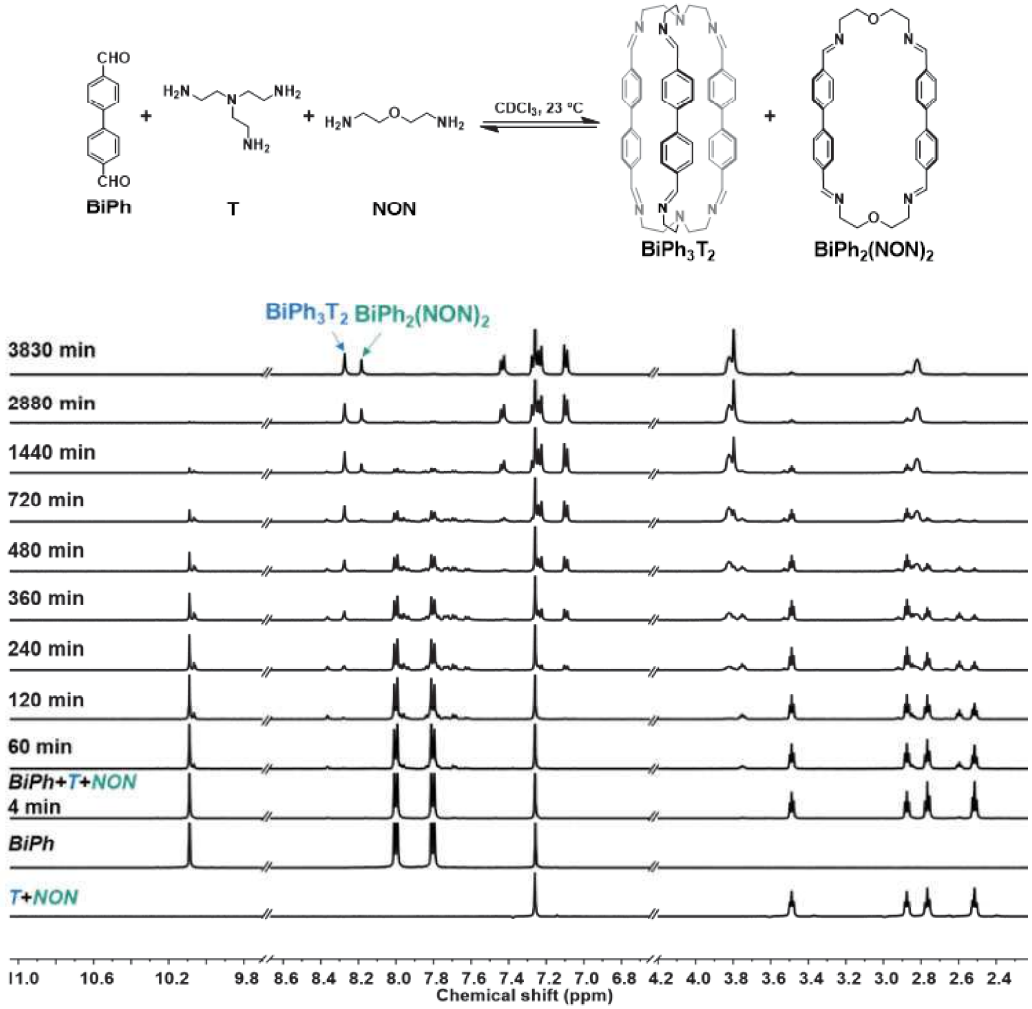

Figure III-3. ^{1}H NMR (500 MHz, $CDCl_3$, 23 °C) spectra of the self-sorting behaviour of reaction 5**BiPh** + 2**T** + 2**NON**, where the initial concentration of **BiPh** was 9.0 mM and the initial concentration of both **T** and **NON** was 3.6 mM.

The self-sorting behaviour of **E/T/NON** was also examined. After 24 h of reaction at room temperature, the resultant solution was heated to 50 °C. At equilibrium, the dominant species present were cage $\mathbf{E_3T_2}$ (65 %) and macrocycle $\mathbf{E_2(NON)_2}$ (30 %) The above results prove that self-sorting of macrocycles and macrobicyclic cages can be achieved from a mixture of the selected dialdehyde with **T** and **NON** (**Figure III-4** and **5c**).

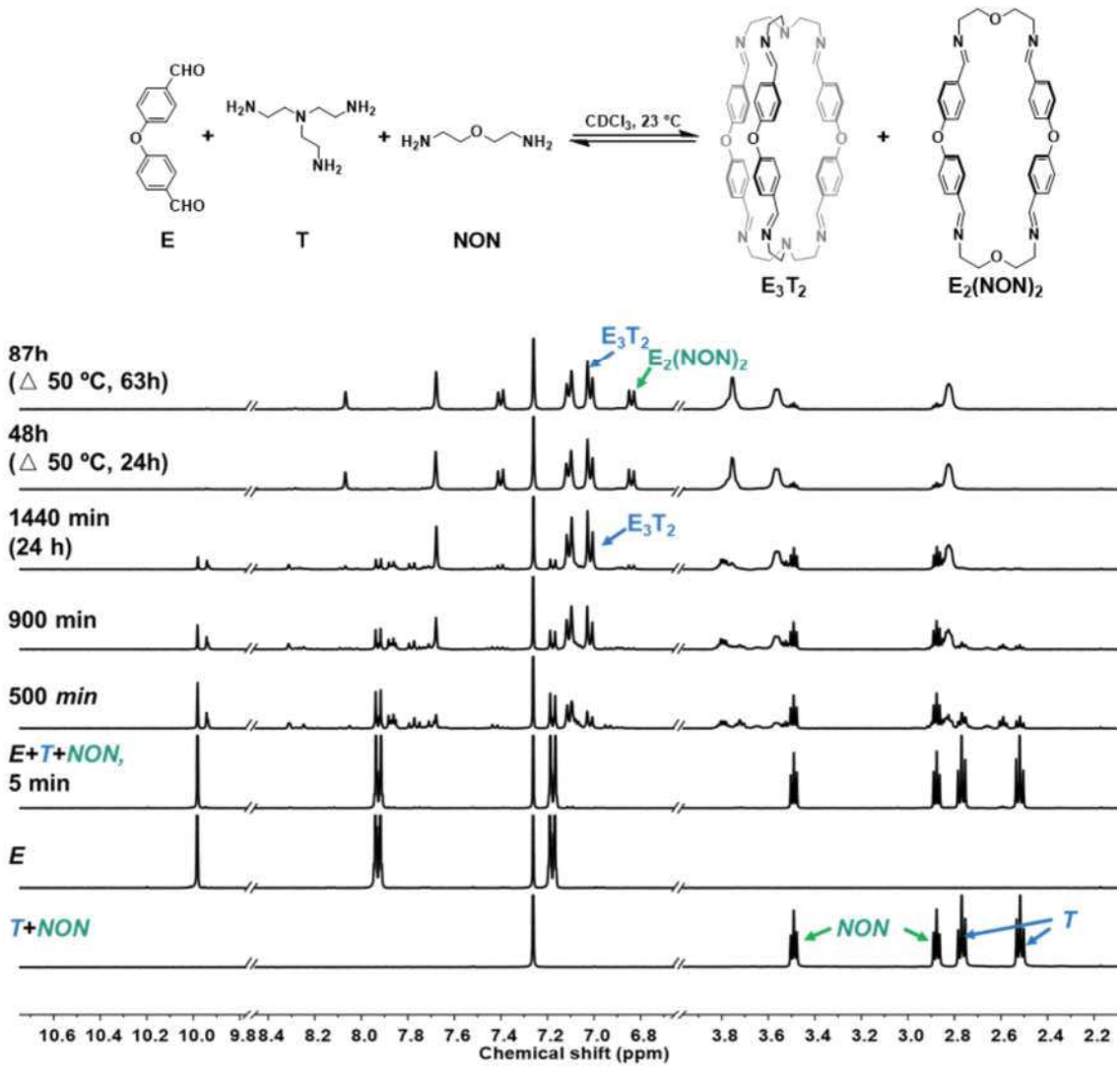

Figure III-4. ^{1}H NMR (400 MHz, CDCl3, 23 °C) monitoring of the self-sorting behaviour of reaction 5**E** + 2**T** + 2**NON**, where the initial concentration of E is 9.0 mM and the initial concentration of both T and NON is 3.6 mM.

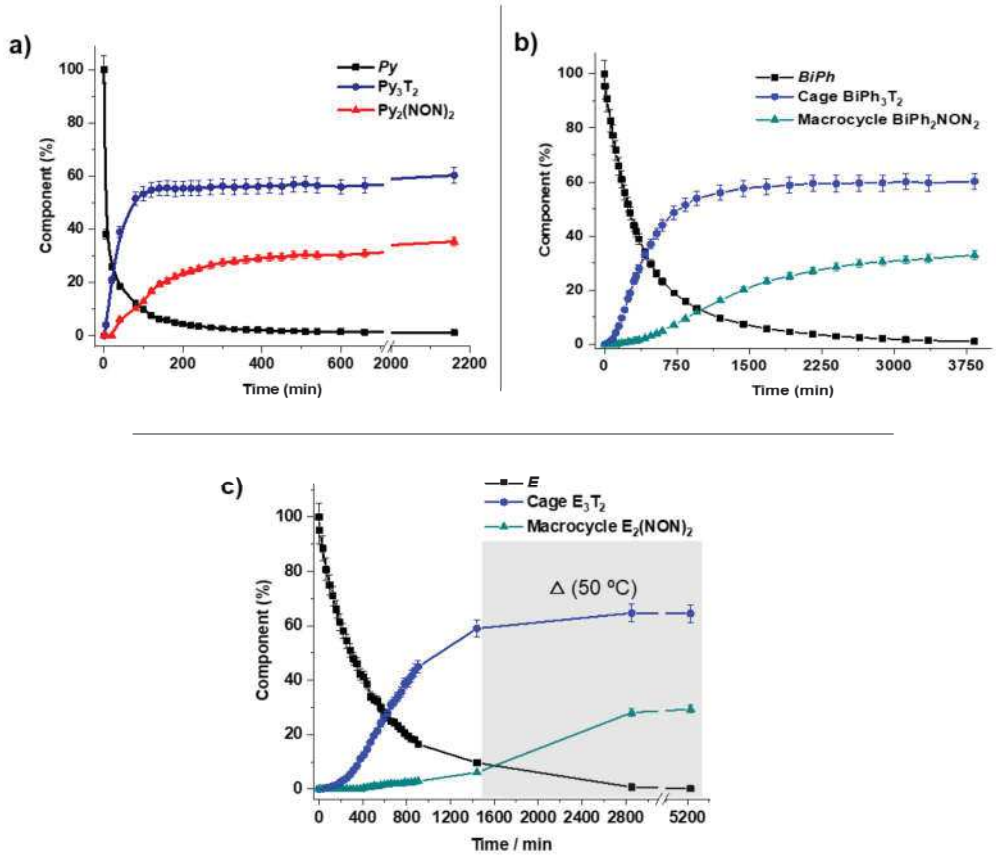

Figure III-5. Rate plots of the time evolution of a) **Py**, **$Py_2(NON)_2$**, and **Py_3T_2**, b) **BiPh**, **$BiPh_2(NON)_2$**, and **$BiPh_3T_2$**, c) **E**, **$E_2(NON)_2$**, and **E_3T_2**. The compositions (%) have been obtained by the integration of specific signals in the ^{1}H NMR spectra. Error in ^{1}H-NMR signal integration: ±5%.

2.1.3. DCL[1] generated from four components: Py/BiPh/T/NON.

First of all, the self-sorting within the four-component (**DCL[1]**) was studied for two distinct-in-shape aldehydes (**Py**/**BiPh**), **T**, and **NON** (**Scheme III-1**). Here, the molar ratio was set as 5 (**Py**):5 (**BiPh**):4 (**T**):4 (**NON**).

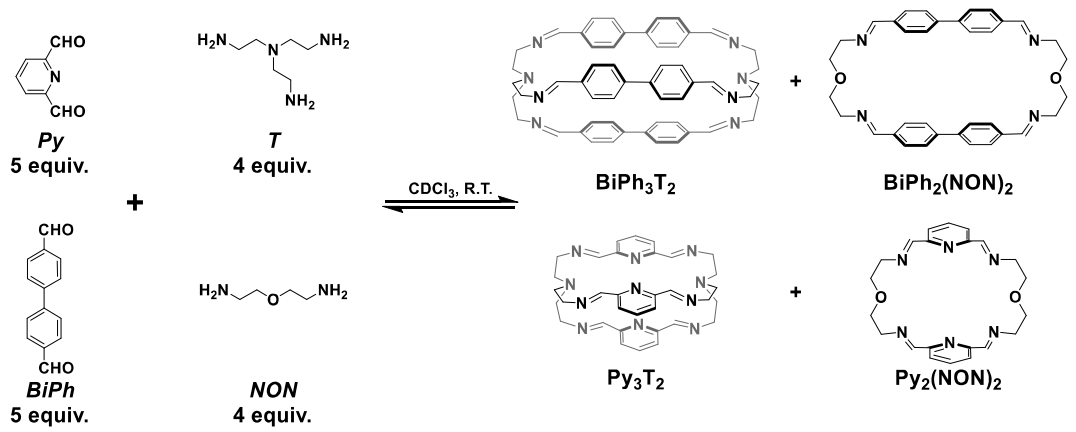

Scheme III-1. Precursors and possible products for the dynamic library: 5**Py** + 5**BiPh** + 4**T**+ 4**NON** (**DCL[1]**)

The ^{1}H NMR spectra revealed the formation of the four expected constituents, with a composition of 12%, 47%, 32%, and 5% for **$BiPh_3T_2$**, **Py_3T_2**, **$BiPh_2(NON)_2$** and **$Py_2(NON)_2$**, respectively. Therefore, the system was clearly following a high-fidelity homo-self-sorting behaviour as no heteroleptic cage/macrocycle was present in the equilibrium state (**Figure III-6**).

Furthermore, the ^{1}H NMR spectra showed that the consumption of the **Py** component occurred much faster than the appearance of the **Py_3T_2** product. This behaviour suggested again the occurrence of sequential reactions during which a number of open-chain intermediates was generated. The presence of such intermediates can be better appreciated in the amplified version of the ^{1}H NMR spectrum after 5 min (**Figure III-6b**), as well as in the corresponding high resolution mass spectrum (**Figure III-7**).

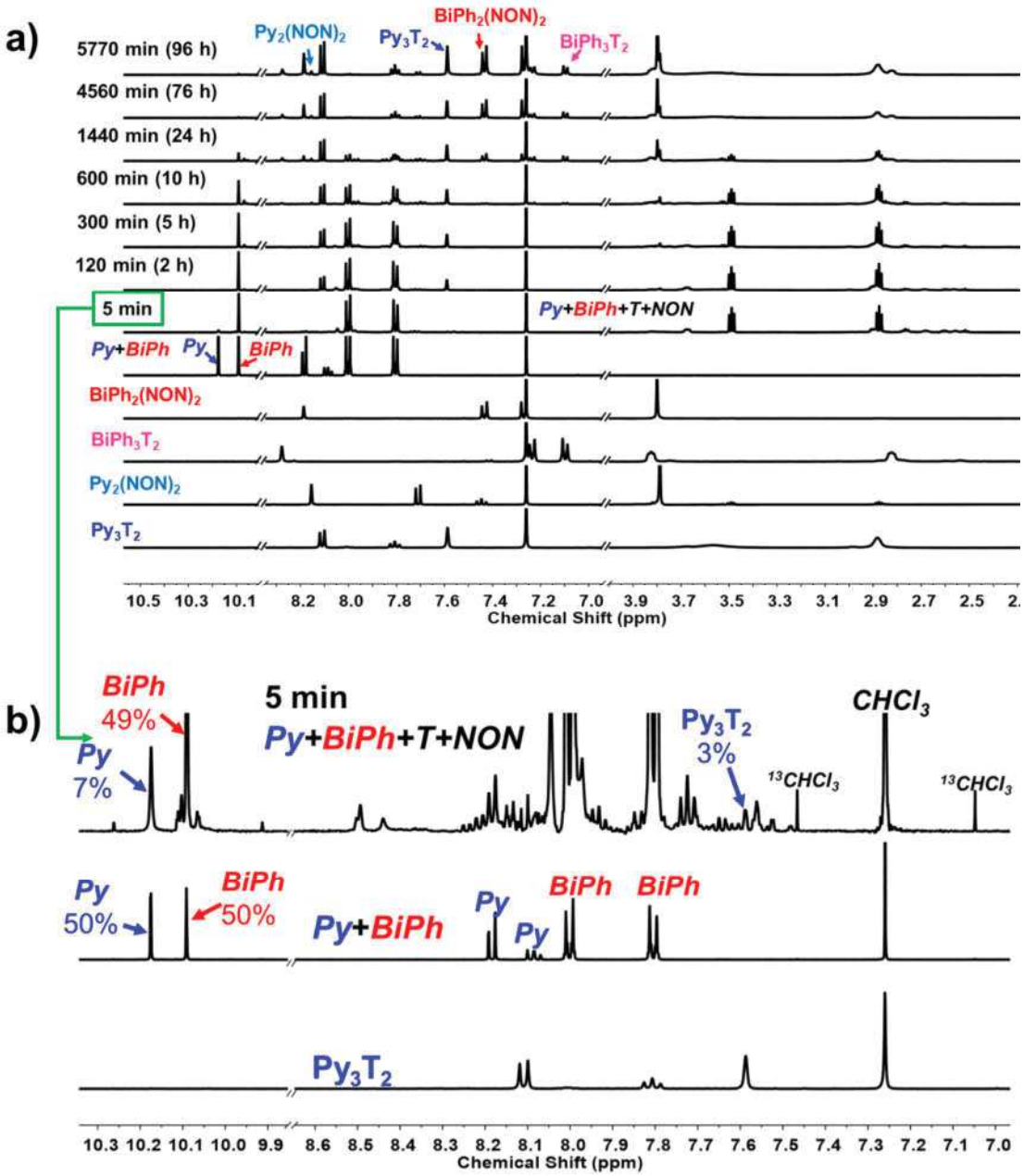

Figure III-6. (a) Time evolution of the ^{1}H NMR (500 MHz, $CDCl_3$, 25 °C) of the reaction 5**Py** + 5**BiPh** + 4**T**+ 4**NON** ($[\mathbf{Py}]_0 = [\mathbf{BiPh}]_0$ = 3.6 mM; $[\mathbf{T}]_0 = [\mathbf{NON}]_0$ =2.9 mM). The four bottom traces correspond to the isolated cage $\mathbf{Py_3T_2}$, macrocycle $\mathbf{Py_2(NON)_2}$, cage $\mathbf{BiPh_3T_2}$, and macrocycle $\mathbf{BiPh_2(NON)_2}$. (b) Partially amplified ^{1}H NMR spectra of the reaction 5**Py** + 5**BiPh** + 4**T**+ 4**NON** after 5 minutes of mixing. The two bottom traces correspond to the isolated cage $\mathbf{Py_3T_2}$ and the component mixture **Py** + **BiPh**.

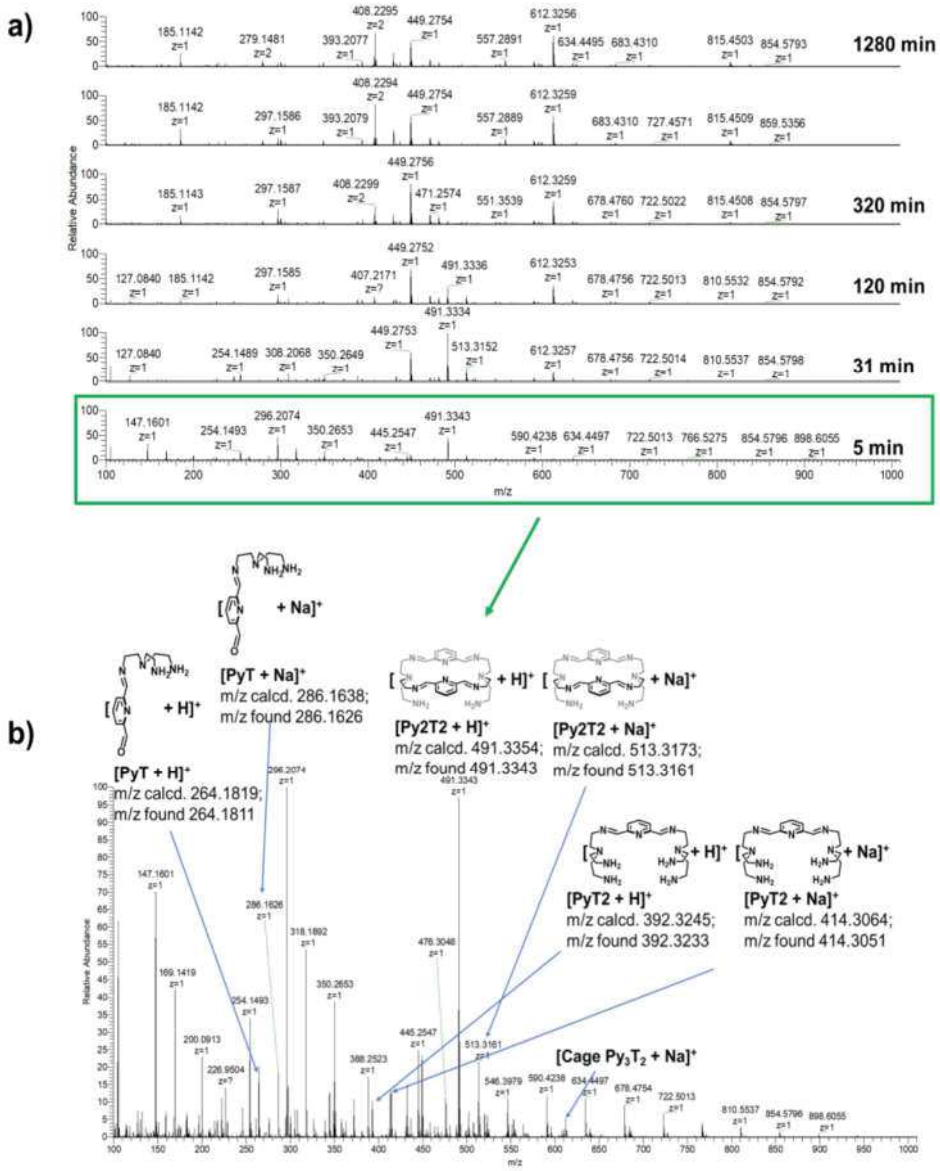

Figure III-7. (a) Time evolution of the HRMS-ESI spectra for the reaction between 5**Py** + 5**BiPh** + 4**T** + 4**NON** ($[\mathbf{Py}]_0 = [\mathbf{BiPh}]_0$ = 2.0 mM; $[\mathbf{T}]_0 = [\mathbf{NON}]_0$ =1.6 mM; 25 °C) in 50%-50% $CHCl_3$/MeOH after 5, 31, 120, 320, 630, and 1280 min. (b) Amplified high resolution mass spectrum of the reaction between 5**Py** + 5**BiPh** + 4**T**+ 4**NON** after 5 minutes.

These and previous observations show **Py** to be more reactive (better electrophile) than **BiPh**, and **T** to be a better nucleophile than **NON.** The central nitrogen of **T** might also participate in proton transfer events. That the macrobicyclic cage $\mathbf{Py_3T_2}$was the first one to be formed (**Figure III-8**) must be considered quite remarkable, taking into account that the formation of such macrobicycle requires more condensation reactions (i.e., 6) than for the

generation of macrocycles (i.e., 4) (**Figure III-8**).

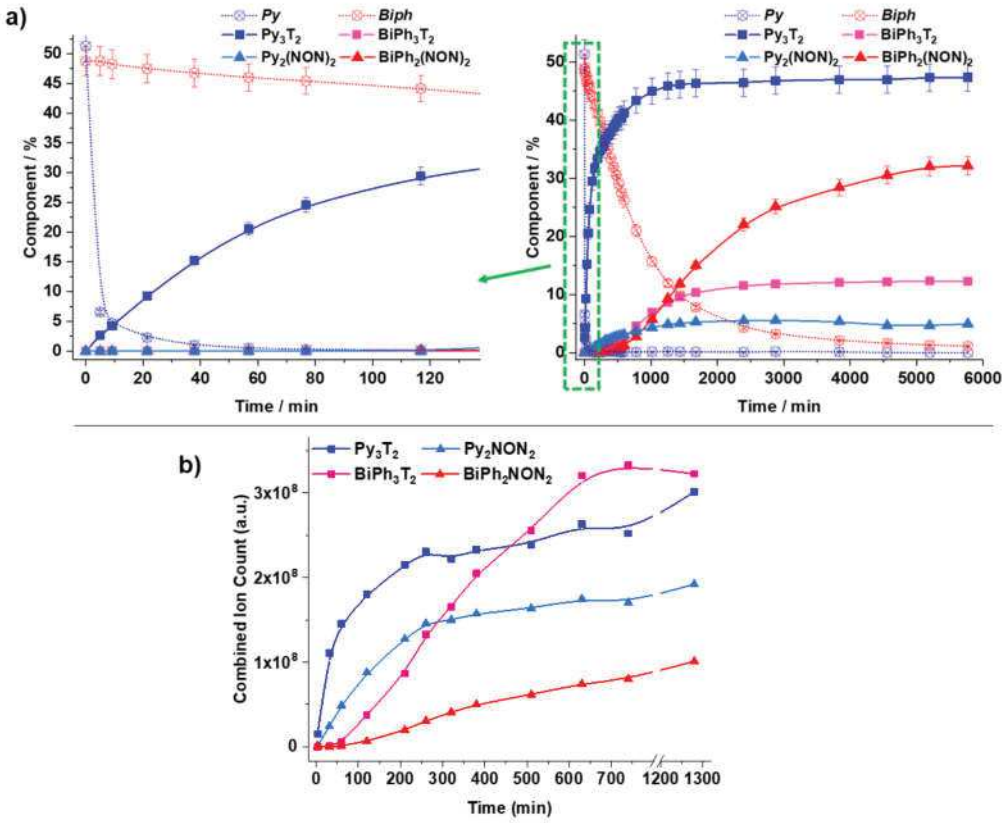

Figure III-8. Rate plots showing the time evolution of the abundance of dialdehydes **Py** and **BiPh**, cages $\mathbf{Py_3T_2}$ and $\mathbf{BiPh_3T_2}$, and macrocycles $\mathbf{Py_2(NON)_2}$ and $\mathbf{BiPh_2(NON)_2}$**.** (a) ^{1}H NMR monitoring over 5770 min. The composition % was obtained by integration of the aromatic area for cage $\mathbf{BiPh_3T_2}$, macrocycle $\mathbf{Py_2(NON)_2}$, imine proton for cage $\mathbf{Py_3T_2}$, macrocycle $\mathbf{BiPh_2(NON)_2}$ and aldehyde CHO proton signals in the 500 MHz ^{1}H NMR spectra ($CDCl_3$, 25 °C). Error in ^{1}H-NMR signal integration: ±5%. (b) HRMS-ESI monitoring over 1280 min. NB: These data of HRMS do not provide quantitative information about the relative amounts of each species identified by its mass, but, taken separately, they display the evolution of a given identified species during the course of the reaction. The curves are added to guide the eye.

Py, **BiPh** and **T** were then mixed in a molar ratio of 3:3:2 to investigate the thermodynamic stability of cages $\mathbf{Py_3T_2}$ and $\mathbf{BiPh_3T_2}$. As expected, cage $\mathbf{Py_3T_2}$ was preferentially generated during the course of the reaction until equilibrium was reached, with up to 94% of the **Py** component being transformed into cage $\mathbf{Py_3T_2}$. In contrast, **BiPh**

remained unreacted and no **$BiPh_3T_2$** product was observed. This competition experiment agrees well with the previously reported case for the **Py**/isophthalaldehyde **(mPh)/T** system in a 3:3:2 molar ratio.[122] Thus, the formation of cage **Py_3T_2** seems to be both kinetically and thermodynamically favoured. The intramolecular interactions between the imine C-H bonds and the N lone pair may have played a crucial role in stabilising cage **Py_3T_2**.[122]

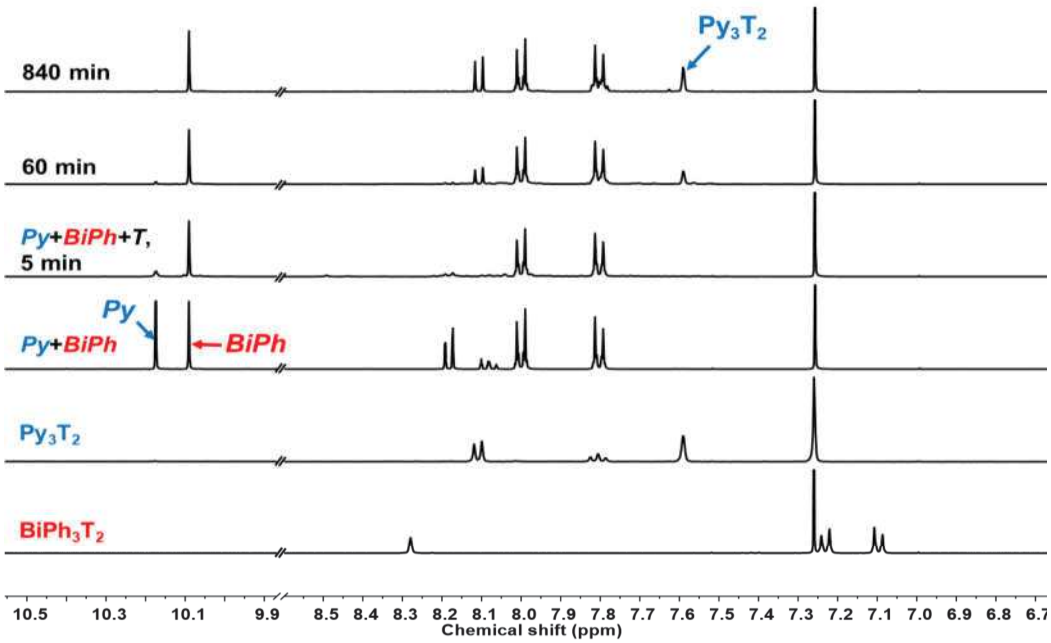

Figure III-9. (a) Time evolution of the ^{1}H NMR (400 MHz, $CDCl_3$, 25 °C) of the reaction between 3**Py**+3**BiPh**+2**T** 5 ($[Py]_0$ = $[BiPh]_0$ = 3.6 mM; $[T]_0$ = $[NON]_0$ =2.9 mM). The two bottom traces correspond to the isolated cages **Py_3T_2**, and **$BiPh_3T_2$**.

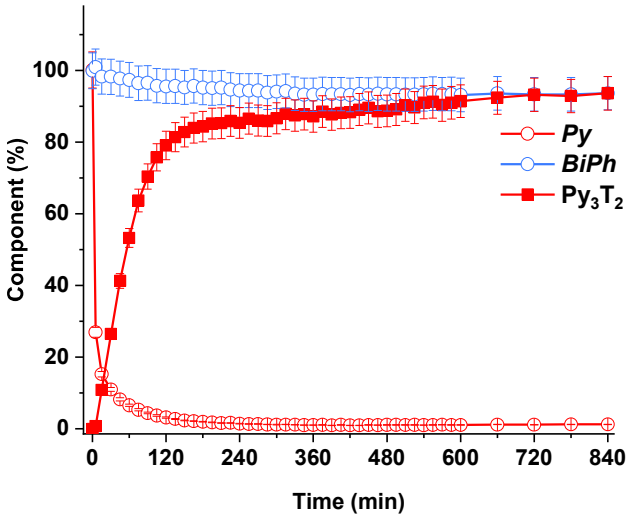

Figure III-10. Rate plots showing the time evolution of dialdehydes **Py** and **BiPh**, and cages $\mathbf{Py_3T_2}$, and $\mathbf{BiPh_3T_2}$.

2.1.4. DCL[2] generated from four components pPh/BiPh/T/NON.

DCL[2] was built up starting from **pPh**, **BiPh**, **T** and **NON** under the same conditions as used for **DCL[1]** (**Scheme III-2**).

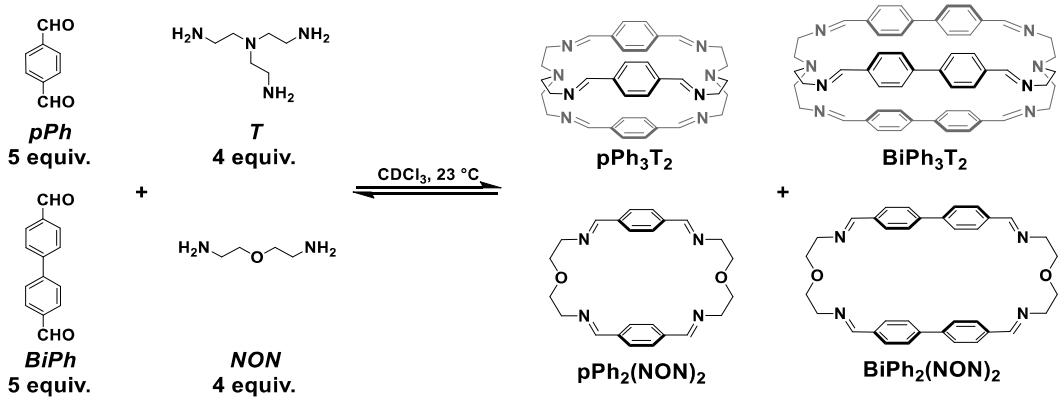

Scheme III-2. Precursors and possible products for the dynamic library : 5**pPh** + 5**BiPh** + 4**T**+ 4**NON** (**DCL[2]**)

The time evolution of the species monitored using ^{1}H NMR revealed that the consumption of initial components was slower than previously observed for **Py**, suggesting

that **pPh** also presents a lower reactivity than **Py** (**Figures III-11** and **III-13a**). After ca. 3 h, the ^{1}H NMR showed the presence of cage **pPh$_3$T$_2$** (11%), cage **BiPh$_3$T$_2$** (<3%), macrocycle **pPh$_2$(NON)$_2$** (<2%), macrocycle **BiPh$_2$(NON)$_2$** (<1%), unreacted **pPh** (10%), and unreacted **BiPh** (27%). The sum composition of the assignable signals was about 54%, therefore unidentified intermediates or other products contained nearly 46% of the building blocks. As the reaction proceeded, all precursors and unidentified intermediates were consumed and were gradually converted into about 20% of each homoleptic macrocycle and 30% of each macrobicycle. Here the compositions are presented on the basis of the percentages of the dialdehyde components (component %). Considering that each macrobicyclic cage is composed of three dialdehyde molecules and each macrocycle contains only two dialdehyde molecules, the corresponding molar ratio of the actual compounds themselves is almost 1:1:1:1.

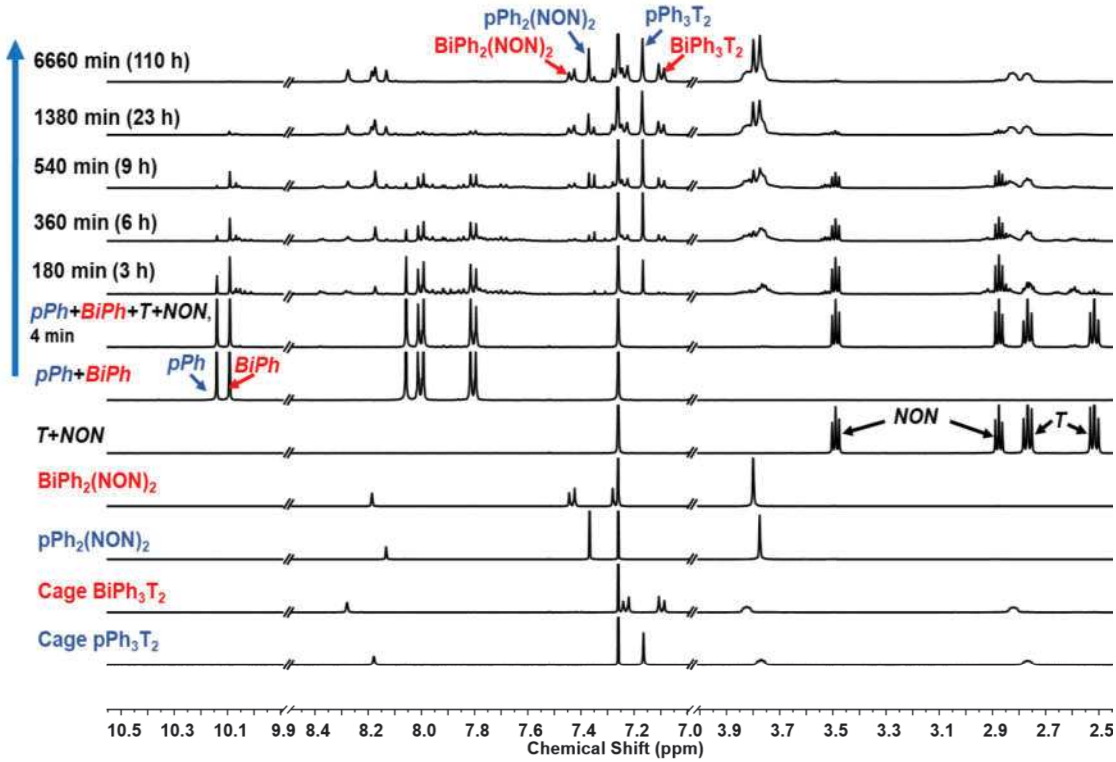

Figure III-11. Time evolution of the ^{1}H NMR spectra (500 MHz, $CDCl_3$, 25 °C) of the reaction 5**Py** + 5**BiPh** + 4**T**+ 4**NON** (**[Py]$_0$** = **[BiPh]$_0$** = 3.6 mM; **[T]$_0$** = **[NON]$_0$** =2.9 mM). The four bottom traces correspond to the isolated cage **Py$_3$T$_2$**, macrocycle **Py$_2$(NON)$_2$,** cage **BiPh$_3$T$_2$** and macrocycle **BiPh$_2$(NON)$_2$**.

Subsequently, we followed the rate of formation of **DCL[2]** through HRMS-ESI analyses. The possible molecular ions of the four products are listed in **Table S-III-2** (Chapter VII). As shown in **Figure III-12**, two intense signals for dipositively charged species at m/z 294.1841 and 408.2308 were observed and were attributed to $\mathbf{[pPh_3T_2+2H]^+}$ and $\mathbf{[BiPh_3T_2+2H]^+}$, respectively. Within the measured period (**Figure III-11b**), the intensity of these two species gradually increased, indicating the progressive formation of $\mathbf{pPh_3T_2}$ and $\mathbf{BiPh_3T_2}$. However, the formation of macrocycles $\mathbf{pPh_2(NON)_2}$ and $\mathbf{BiPh_2(NON)_2}$ was less obvious, likely as a result of their weaker response intensity. In general, the HRMS rate profiles showed similar patterns to those of the ^{1}H NMR rate curves.

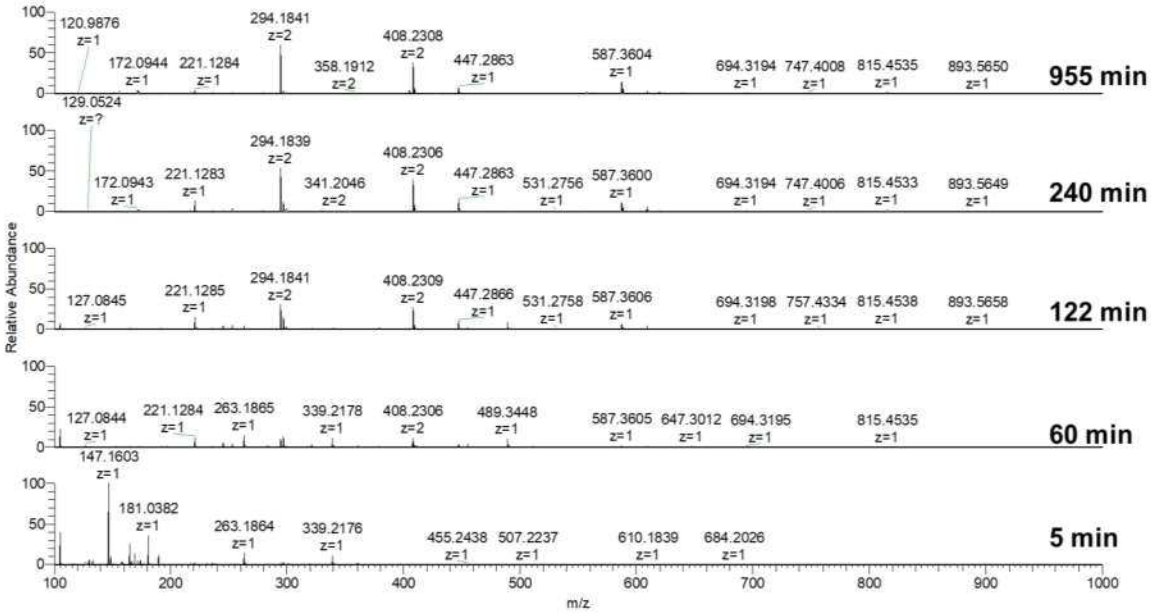

Figure III-12. Time evolution of the HRMS-ESI spectra of 5**pPh** + 5**BiPh** + 4**T** + 4**NON** ($\mathbf{[pPh]_0}$ = $\mathbf{[BiPh]_0}$ = 2.0 mM; $\mathbf{[T]_0}$ = $\mathbf{[NON]_0}$ =1.6 mM; 25 °C) in 50%-50% $CHCl_3$/MeOH after 5, 60, 122, 240, and 955 min.

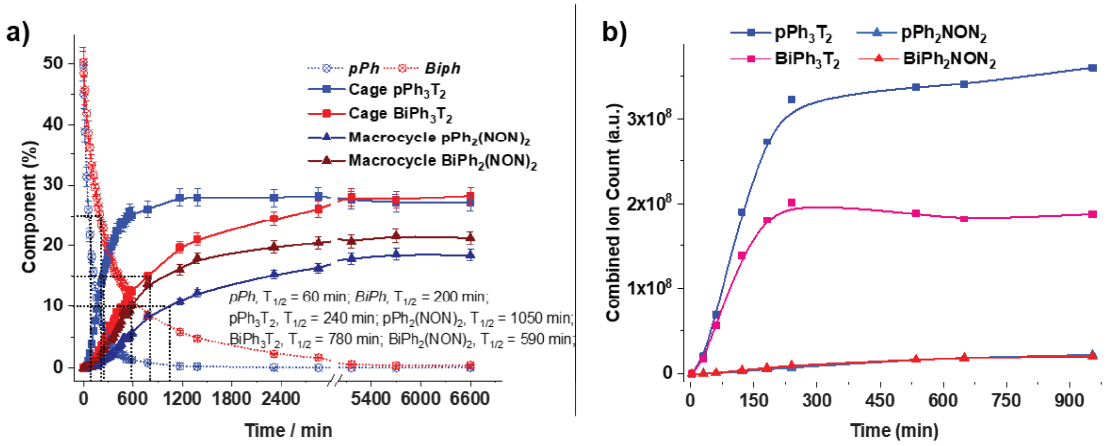

Figure III-13. Kinetic plots of the evolution of dialdehyde **pPh**/**BiPh**, cages **pPh_3T_2**/**$BiPh_3T_2$**, and macrocycles **$pPh_2(NON)_2$**/**$BiPh_2(NON)_2$** as a function of time (a) ^{1}H NMR monitoring over 6600 min. (b) HRMS-ESI monitoring over 955 min. NB: These data of HRMS do not provide quantitative information about the relative amounts of each species identified by its mass, but, taken separately, they display the evolution of a given identified species during the course of the reaction. The curves are added to guide the eye.

2.1.5. DCL[3] generated from four components Py/mPh/T/NON.

In Chapter II, the effect of the stoichiometric ratio of reactants on the self-sorting outcome of the **mPh** + **Py** + **T** system has been described. Mixing **mPh/Py/T** in a 3:3:4 ratio allowed for the formation of the statistically distributed constituents. Conversely, when an **mPh/Py/T**=3:3:2 ratio was used, **T** selectively reacted with **Py** because of its higher reactivity, to give only cage **Py_3T_2**.

Hence, one may surmise that the statistically self-sorted outcome would be observed by adding **NON** into the reaction of **mPh/Py/T** = 3:3:2. The ^{1}H NMR spectra in **Figure III-14** indeed show that after equilibration of the mixture, cage **Py_3T_2** (28%) and macrocycle **$mPh_2(NON)_2$** (25%) were the two major constituents. However, there were unassigned signals still present in the spectrum of the whole reaction mixture. These signals are assigned to heteroleptic cages/macrocycles that had not been removed during the self-sorting process. The reason may be that the reactivity differences between **Py** - **mPh** and **T** - **NON** are not large enough to allow for the specific selection of components. As a result, a random combination of non-self-sorted products was produced.

In light of these results, it can be concluded that achieving high-fidelity self-sorting requires the use of reactants with significantly distinct structures which give products of significantly different stability.

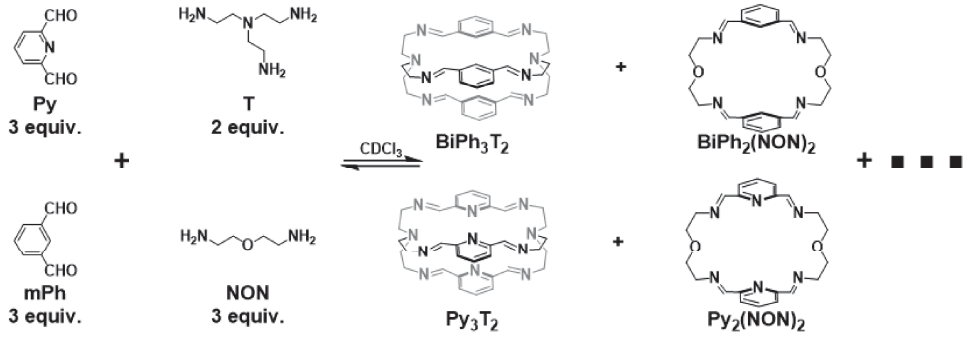

Scheme III-3. Precursors and possible products for the dynamic library :3**Py** + 3**mPh** + 2**T**+ 3**NON** (**DCL[3]**)

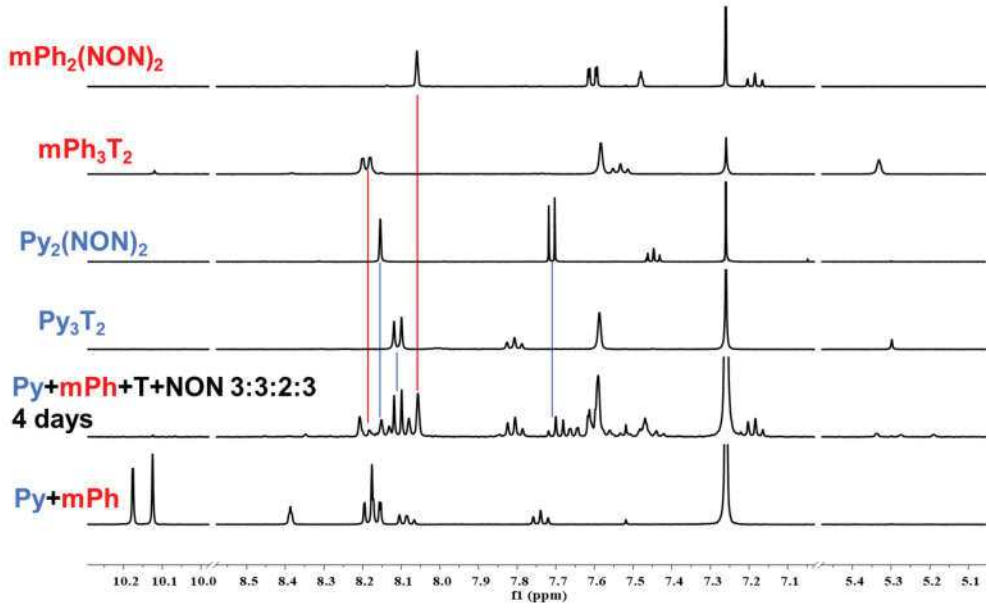

Figure III-14. ^{1}H NMR spectra (400 MHz, $CDCl_3$, 23 °C) of the reaction 3**Py** + 3**mPh** + 2**T**+ 3**NON** ($[\mathbf{Py}]_0 = [\mathbf{BiPh}]_0$ = 3.6 mM) after equilibration for 4 days. The four bottom traces correspond to the isolated cage $\mathbf{Py_3T_2}$, macrocycle $\mathbf{Py_2(NON)_2}$, cage $\mathbf{mPh_3T_2}$, and macrocycle $\mathbf{mPh_2(NON)_2}$.

2.1.6. DCL[4] generated from [3 × 2] five components of Py, BiPh, TriPh, T, NON

To further increase the complexity of the system, the number of initial components of the library was again increased. A series of five-component [3 × 2] DCLs was built by mixing

three dialdehydes with **T** and **NON** in a molar ratio of 3：3：3：2(**T**)：6(**NON**) at 40 °C.

Firstly, three dialdehydes, **namely Py**, **BiPh** and **TriPh**, differing in length were selected (**Scheme III-4**). Since **Py** is the most reactive one among the aldehydes and **T** is more reactive than **NON**, a large amount of **T** should first form cage $\mathbf{Py_3T_2}$. The reaction was followed by ^{1}H NMR (**Figures III-15** and **Figures III-16**). After 90 min, all **Py** was completely consumed, giving 23% of $\mathbf{Py_3T_2}$ and 2% of $\mathbf{Py_2(NON)_2}$. Meanwhile, a large amount of **BiPh** and **TriPh** remained unreacted and no macrocycles and cages containing **BiPh** or **TriPh** could be detected. After 720 min, the distribution of constituents was **BiPh** (<5%), **TriPh** (<7%), $\mathbf{Py_3T_2}$ (30%), $\mathbf{Py_2(NON)_2}$ (6%), $\mathbf{BiPh_3T_2}$ (2%), $\mathbf{BiPh_2(NON)_2}$ (12%), $\mathbf{TriPh_3T_2}$ (< 6%), $\mathbf{TriPh_2(NON)_2}$ (10%), and the rest of the missing components was present in solution as intermediates. On further progress of the reaction, macrocycles $\mathbf{BiPh_2(NON)_2}$ and $\mathbf{TriPh_2(NON)_2}$ increased in concentration, while that of cages $\mathbf{BiPh_3T_2}$ and $\mathbf{TriPh_3T_2}$ decreased. After 2340 min, the distribution was **BiPh** (<1%), **TriPh** (<1%), $\mathbf{Py_3T_2}$ (29%), $\mathbf{Py_2(NON)_2}$ (6%), $\mathbf{BiPh_3T_2}$ (<1%), $\mathbf{BiPh_2(NON)_2}$ (30%), $\mathbf{TriPh_3T_2}$ (<1%), $\mathbf{TriPh_2(NON)_2}$ (28%). This experiment also proved that by using components of different length, self-sorting can be efficiently reached for the five-component [3×2] DCL.

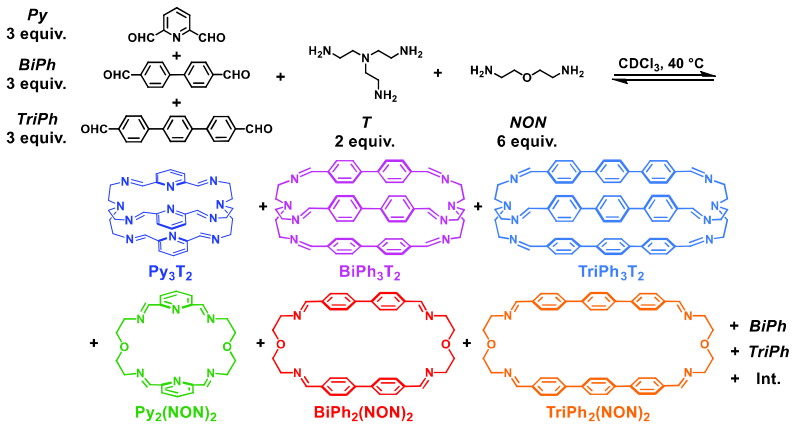

Scheme III-4. Precursors and possible products for the dynamic library : 3**Py** + 3**BiPh** +3**TriPh** + 2**T**+ 6**NON** (**DCL[4]**)

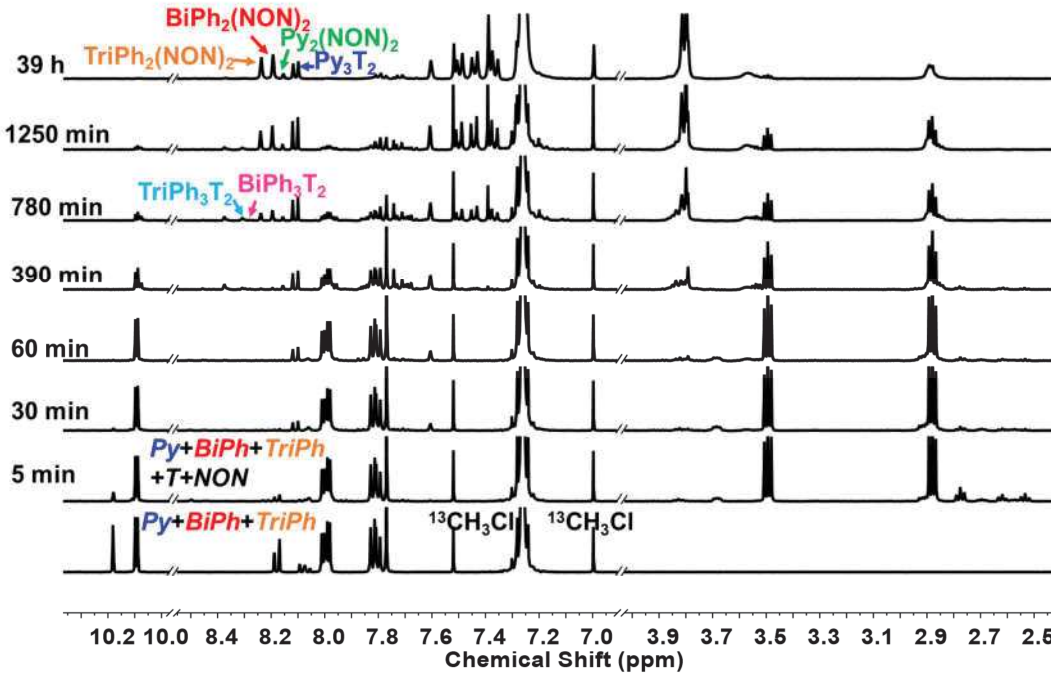

Figure III-15. Time evolution of the ^{1}H NMR spectra (400 MHz, $CDCl_3$, 40 °C) for the reaction between 3**Py** + 3**BiPh** +3**TriPh** + 2**T**+ 6**NON**. The initial concentration of each dialdehyde was 1.0 mM.

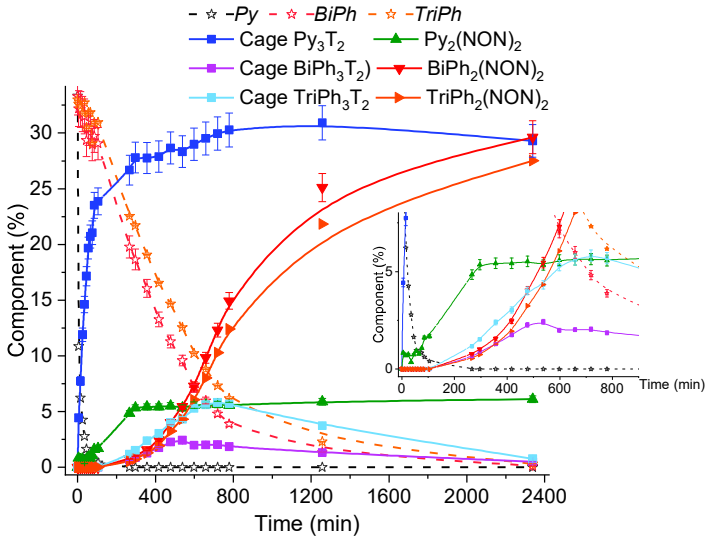

Figure III-16. Kinetic plots of the evolution of dialdehyde **Py**, **BiPh**, **TriPh**, macrocycles and macrocyclic cages over 2340 min. Error in ^{1}H-NMR signal integration: ±5%.

2.1.7. DCL[5] generated from [3 × 2] five components of Py, pPh, BiPh, T, NON

A similar system was designed starting from the precursors **Py**, **pPh**, **BiPh**, **T** and **NON**

under the same conditions as before (**Scheme III-5**). After 13 h, equilibrium of the reaction was reached (**Figure III-17**), with a distribution of constituents: **BiPh** (3%), **Py_3T_2** (23%), **$Py_2(NON)_2$** (5%), **pPh_3T_2** (0%), **$pPh_2(NON)_2$** (23%), **$BiPh_3T_2$** (2%), **$BiPh_2(NON)_2$** (23%). The total amount of assignable species of the system was approximately 79%, which might be because the similar length of **Py** and **pPh** precluded correction of the heteroleptic species. This system adopted self-sorting behaviour to some extent, but the overall result was less than satisfactory.

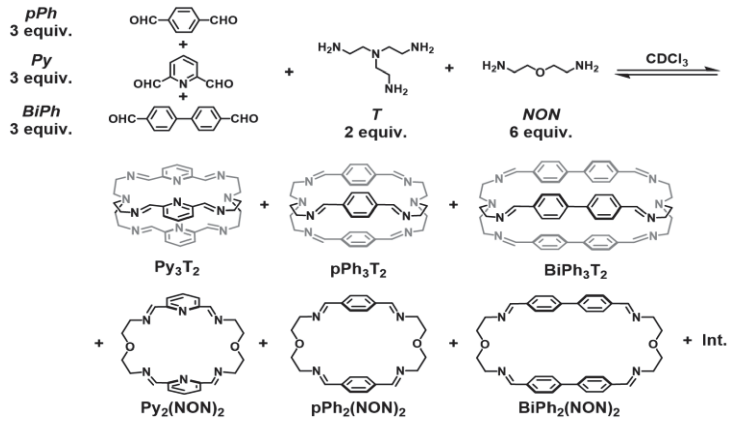

Scheme III-5. Precursors and possible products for the dynamic library : 3**Py** + 3**pPh** +3**BiPh** + 2**T**+ 6**NON** (**DCL[5]**)

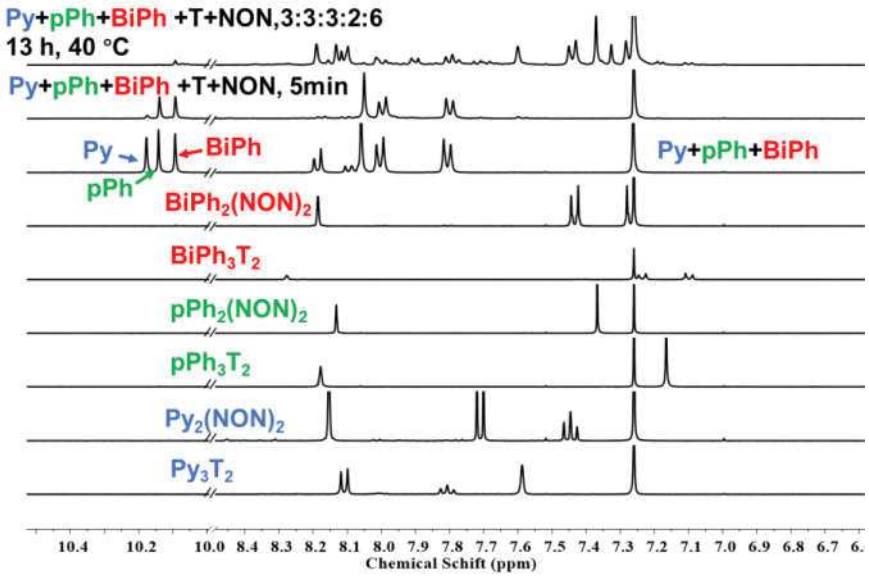

Figure III-17. Time evolution of the ^{1}H NMR spectra (400 MHz, $CDCl_3$, 40 °C) of the reaction 3**Py** + 3**pPh** + 3**BiPh** + 2**T**+ 6**NON**. The initial concentration of each dialdehyde was 1.0 mM.

2.1.8. DCL[6] generated from [4 × 2] six components: Py, pPy, BiPh, TriPh, T, NON

Finally, the self-sorting behaviour of **DCL[6]** (**Scheme III-6**) built up from six components (**Py, pPy, BiPh, TriPh, T, NON** in a ratio of 3:3:3:2:6) was studied at 40 °C for 3 days. The equilibrated solution (**Figure III-18**) gave **BiPh** (1%), **TriPh** (2%), **Py_3T_2** (21%), **$Py_2(NON)_2$** (4%), **$pPh_2(NON)_2$** (17%), **$TriPh_3T_2$** (2%), **$BiPh_2(NON)_2$** (21%), and **$TriPh_2(NON)_2$** (17%). These products contained approximately 85% of the initial reactants. These results further corroborated the proposed important role of structural features towards achieving precise self-sorting of DCLs.

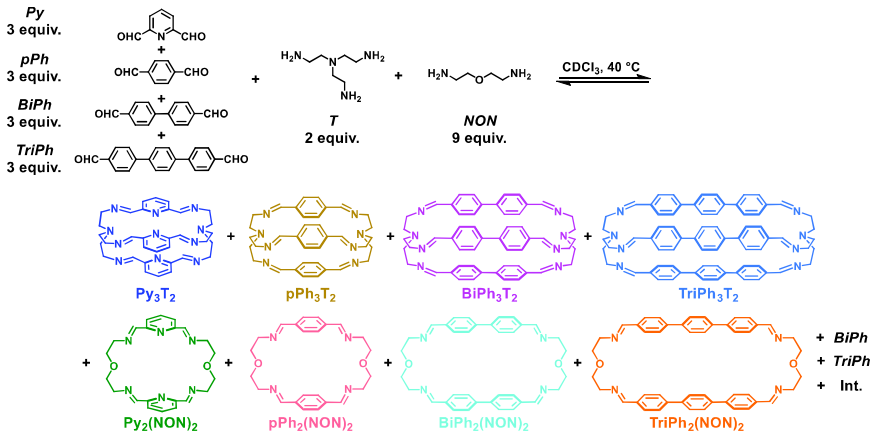

Scheme III-6. Precursors and possible products for the dynamic library : 3**Py** + 3**pPh** + 3**BiPh** + 3**TriPh** +2**T**+ 9**NON** (**DCL[6]**)

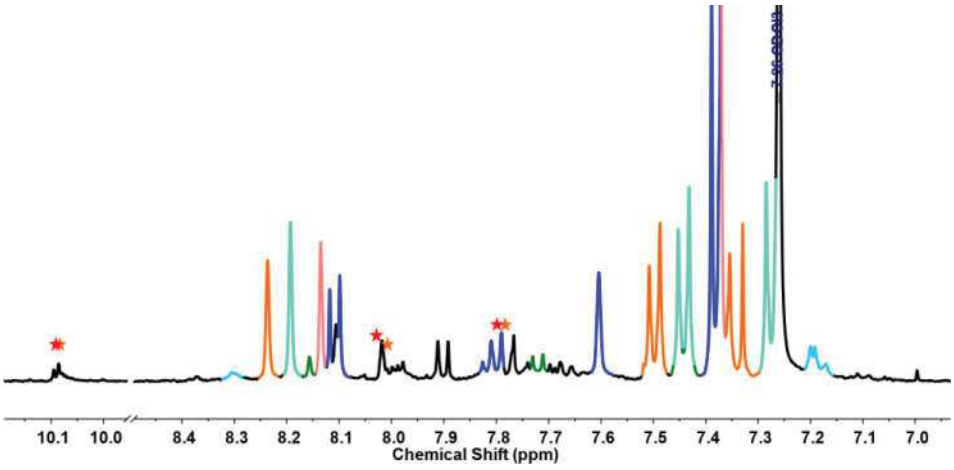

Figure III-18. Time evolution of the ^{1}H NMR spectra (400 MHz, $CDCl_3$, 40 °C) of the reaction 3**Py** + 3**pPh** + 3**BiPh** + 3**TriPh** +2**T**+ 9**NON**. The initial concentration of each dialdehyde was 2.0 mM. The signals of free dialdehydes **BiPh** and **TriPh** are indicated by red and orange stars, respectively.

2.2. Dynamic switching of CDNs of macrocycles and macrobicyclic cages

The component selectivity of **DCL[1]** exhibited the amplified formation of a pair of agonistic constituents, namely cage **Py_3T_2** and macrocycle **$BiPh_2(NON)_2$**. From this outcome, it is quite evident that the initial kinetically favoured formation of cage **Py_3T_2** promoted the generation of its agonistic macrocycle **$BiPh_2(NON)_2$**. The results of the competition experiment between **Py/Biph/T** also revealed that cage **Py_3T_2** presents a higher thermodynamic stability than cage **$BiPh_3T_2$**. However, the thermodynamic disparities between the macrocycle and cage of **BiPh** remained unclear. Therefore, to elucidate the thermodynamic properties of each constituent in **DCL[1]**, the following component recombination experiments were performed.

2.2.1. Transformation from macrocycle $BiPh_2(NON)_2$ to cage $BiPh_3T_2$

To investigate the difference in thermodynamic stability of macrocycle **$BiPh_2(NON)_2$** and cage **$BiPh_3T_2$**, the first step was to explore if any macrocycle-to-cage transformation could be attained. Thus, **T** (4 equiv.) was added to the pre-synthesized macrocycle **$BiPh_2(NON)_2$** (3 equiv.) in solution, and the reaction process was monitored by ^{1}H NMR spectroscopy (**Figure III-19**), the kinetic curve of this reaction being shown in **Figure III-20**. **NON** units of macrocycle **$BiPh_2(NON)_2$** were gradually replaced by **T**, which resulted in a progressive transformation of macrocycle **$BiPh_2(NON)_2$** to cage **$BiPh_3T_2$**. After about 400 min, the amounts of macrocyclic **$BiPh_2(NON)_2$** and cage **$BiPh_3T_2$** remained constant indicating that equilibrium of the reaction was reached, corresponding to 20% of macrocycle **$BiPh_2(NON)_2$** and 43% of cage **$BiPh_3T_2$**. 8% of **[Biph+2T]**, 6% of **[2Biph+2T]**. The remaining 23% of **BiPh** was present as soluble side products that could not be identified.

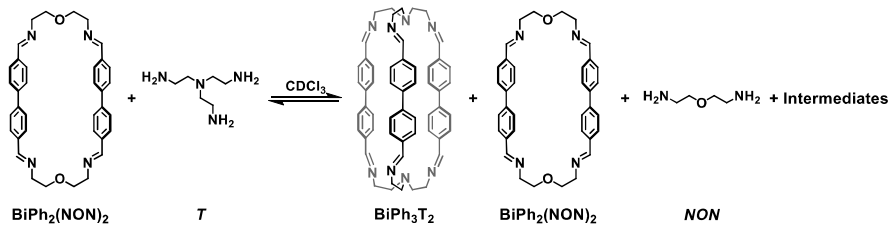

Scheme III-7. Macrocycle-to-cage transformation experiment

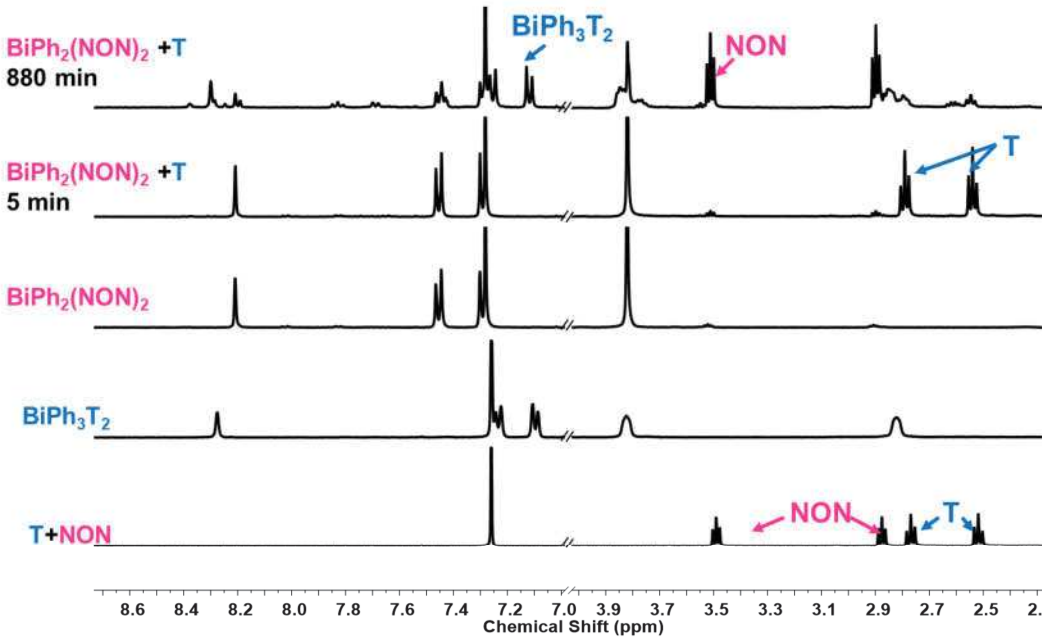

Figure III-19. Time evolution of the ^{1}H NMR spectra (400 MHz, $CDCl_3$, 23 °C) showing the macrocycle **$BiPh_2(NON)_2$** to macrocyclic cage **$BiPh_3T_2$** transformation.

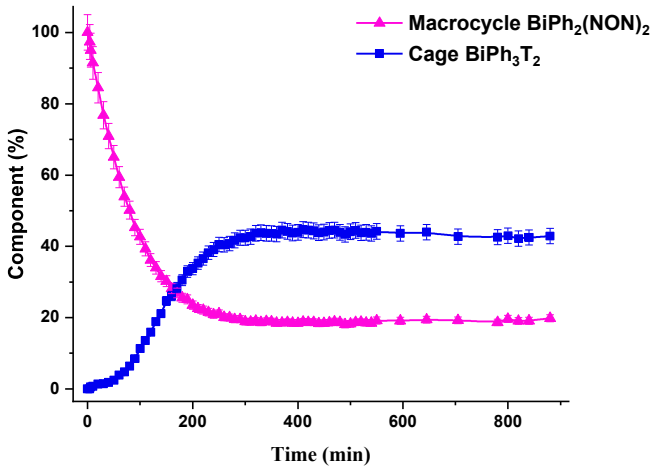

Figure III-20. Component abundance as calculated by ^{1}H NMR for macrocycle **$BiPh_2(NON)_2$** and cage **$BiPh_3T_2$** over time.

2.2.2. Stepwise self-sorting and component recombination of Py/BiPh/NON and T

The second experiment consisted of mixing three components **Py/BiPh/NON** (2 equiv. of each, **Figure III-21**). The equilibrium was reached after 13 h, where 81% of **Py** and **NON**

had reacted to give macrocycle **$Py_2(NON)_2$** as the main product with 14% of **Py** and 94% of **BiPh** remaining unreacted. After 5 days of the addition of an appropriate amount of **T** (4/3 equiv.) to this initial solution, the amount of macrocycle **$Py_2(NON)_2$** was significantly reduced and the equilibrium under these new conditions was shifted in favour of cage **Py_3T_2**, with a constituent distribution of **$BiPh_3T_2$** (10%), **Py_3T_2** (45%), **$BiPh_2(NON)_2$** (33%) and **$Py_2(NON)_2$** (9%), together with unreacted **BiPh** (1%). This experiment demonstrated that (i) **$Py_2(NON)_2$** is more thermodynamically stable than **$BiPh_2(NON)_2$** and cage **Py_3T_2** is more thermodynamically stable than both **$Py_2(NON)_2$** and **$BiPh_3T_2$**; (ii) the less thermodynamically stable constituents can be transformed to more stable ones by component recombination.

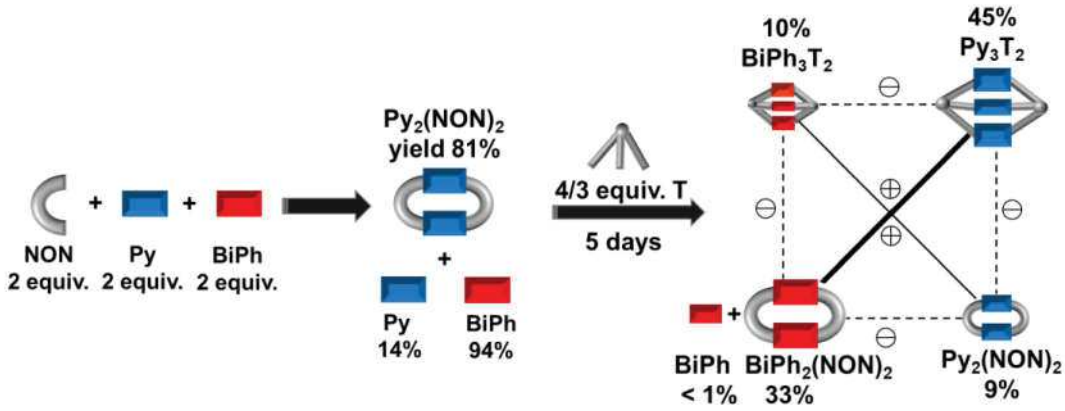

Figure III-21. Stepwise self-sorting by the addition of **T** into a preequilibrated solution of **Py**/**BiPh**/**NON**. Data obtained from the ^{1}H NMR spectra (400 MHz, 25 ºC, $CDCl_3$).

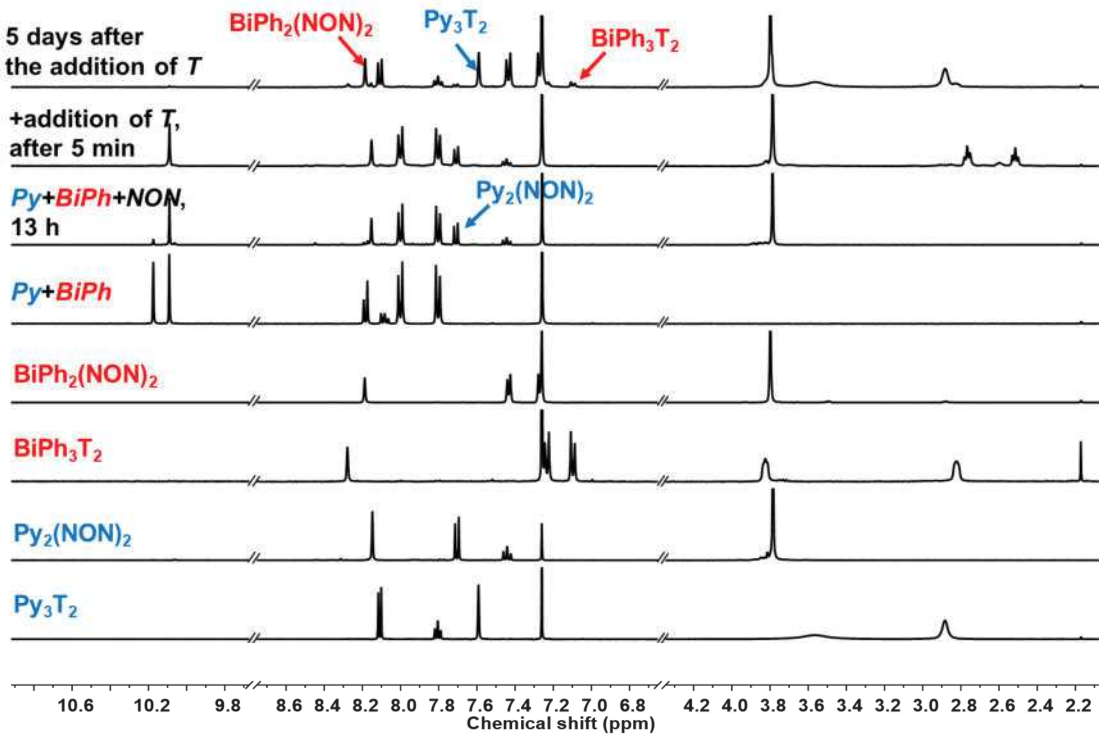

Figure III-22. Time evolution of the ^{1}H NMR spectra (400 MHz, 25 ºC, $CDCl_3$) for the stepwise self-sorting by the addition of 2/3 equiv. of **T** into an equilibrated solution of **NON** (3.6 mM, 2 equiv.), **Py** (3.6 mM, 2 equiv.) and **BiPh** (3.6 mM, 2 equiv.). The four bottom traces correspond to the isolated **$BiPh_2(NON)_2$**, **$BiPh_3T_2$**, **$Py_2(NON)_2$** and **Py_3T_2**.

2.2.3. Imine metathesis within pre-formed cages and macrocycles

The above experiments confirm that such imine-based macrocycles can be transformed into cages by component exchange. In a similar fashion, the dynamic nature of the imine bonds provides the capacity to realize a cage-to-cage transformation by the addition of another building block.[119,122] Such transformation may also take place between preformed macrocycles and macrobicyclic cages. To further explore this behaviour in a four-component self-sorting system, two [2 × 2] Macrocycle-Macrobicyclic Cage Constitutional Dynamic Networks (CDNs), namely **DCL[7]** and **DCL[8]** (**Figure III-25**), were designed. The CDNs were built up from mixtures of the separately prepared macrobicyclic cages and macrocycles in the presence of 5 mol% dimethylamine hydrochloride (DMA·HCl) as an exchange catalyst.

DCL[7] was constructed by mixing two agonistic constituents macrocycle **$Py_2(NON)_2$** and cage **$BiPh_3T_2$** (1:1 concerning dialdehyde units) using dimethylamine hydrochloride

(DMA-HCl) as the catalyst. After 10 days of equilibration, a composition of 6%, 41%, 41%, and 5% for **$BiPh_3T_2$**, **Py_3T_2**, **$BiPh_2(NON)_2$**, and **$Py_2(NON)_2$**, respectively, was attained. The agonistic constituents **Py_3T_2** and **$BiPh_2(NON)_2$** were clearly the major products, reflecting an orthogonal distribution switching in the [2× 2] CDN (**Figure III-23**). Since no released **T** or **NON** was observed during this process, the cage and macrocycle had broken up and recombined to the preferred structures concomitantly by component exchange or imine metathesis driven by the formation of the most stable cage **Py_3T_2**.

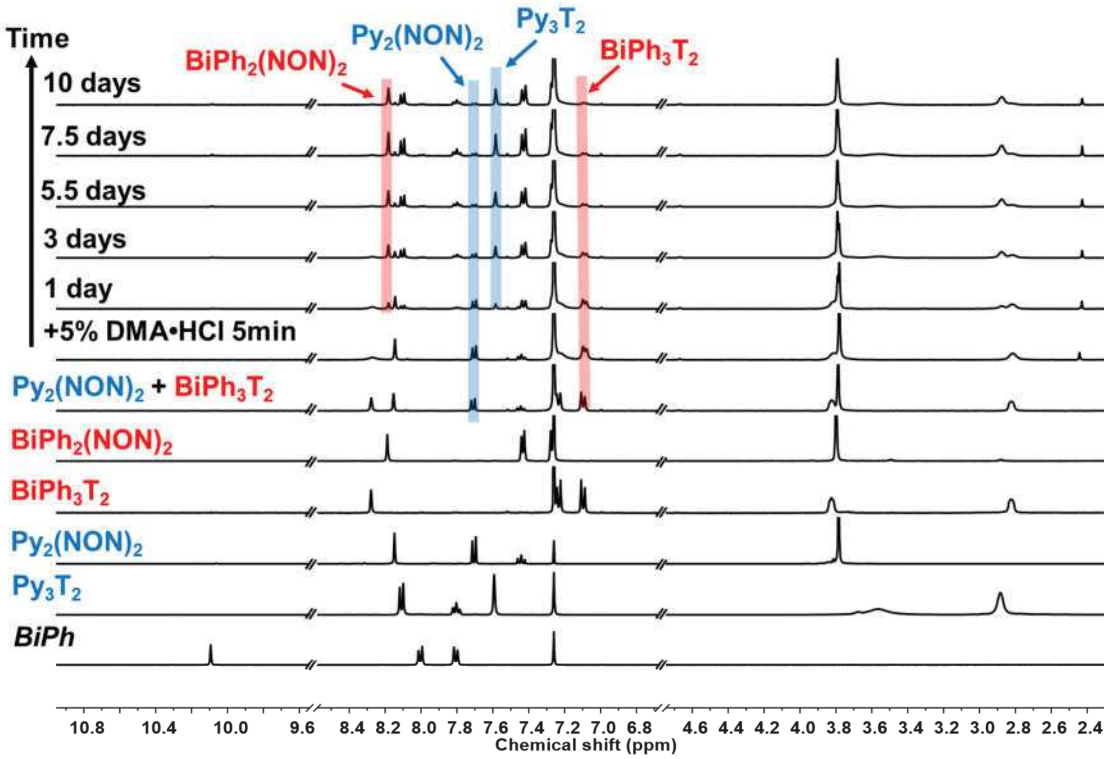

Figure III-23. Time evolution for the ^{1}H NMR spectra (400 MHz, r.t.) of the mixture of macrocycle **$Py_2(NON)_2$** (1.6 mM), cage **$BiPh_3T_2$** (1.1 mM), and 5 mol% dimethylamine hydrochloride (DMA·HCl) after 5 minutes, 1 day, 3 days, 5.5days, 7.5 days, and 10 days (six top traces). The five bottom traces correspond to the isolated **$BiPh_2(NON)_2$**, **$Py_2(NON)_2$**, **$BiPh_3T_2$**, **Py_3T_2**, and **BiPh**.

Importantly, macrocycle **$BiPh_2(NON)_2$** was considered to be the least thermodynamically stable amongst the four constituents of the library (i.e., **Py_3T_2**, **$Py_2(NON)_2$**, **$BiPh_3T_2$**, and **$BiPh_2(NON)_2$**) and its generation would be precluded in such a competitive environment. However, with the appropriate design of the CDN, the formation of the unfavoured product can be driven by the generation of the agonistic one

(thermodynamically favoured).

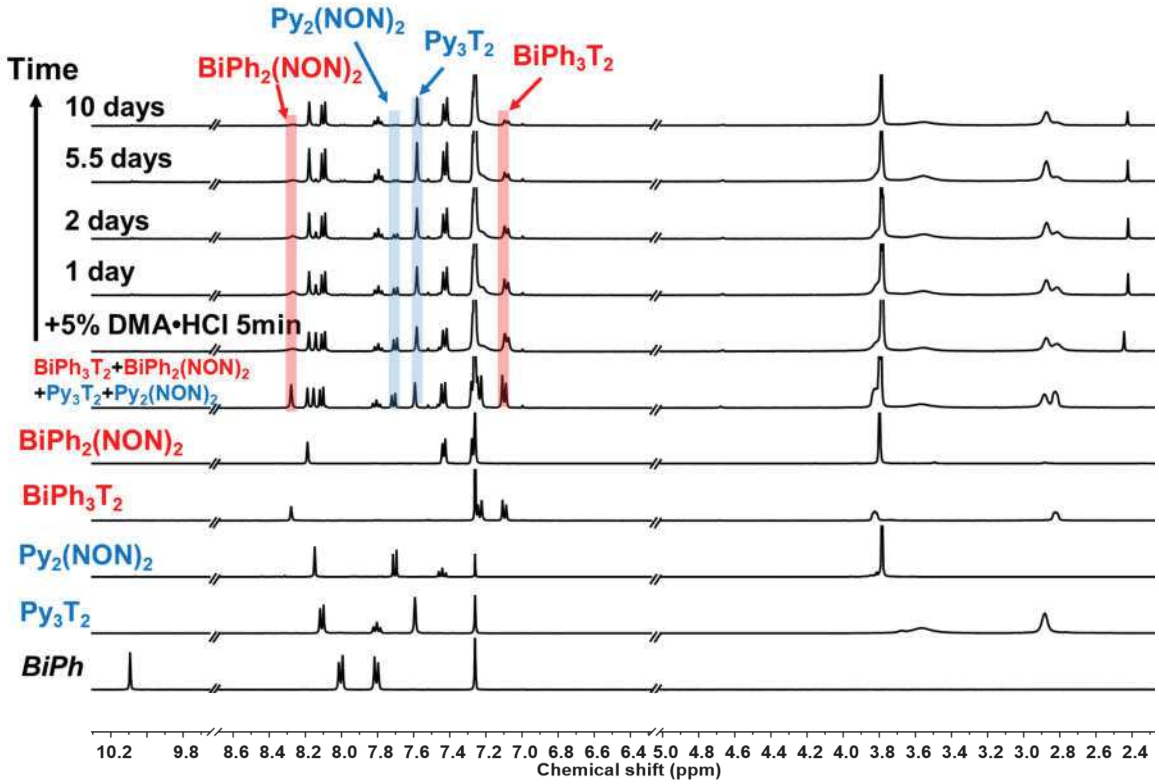

Figure III-24. Time evolution of the ^{1}H NMR spectra (400 MHz, r.t.) for the mixture of **$BiPh_2(NON)_2$**, **$Py_2(NON)_2$**, **$BiPh_3T_2$** and **Py_3T_2** (0.9 mM each) and 5 mol% (in terms of dialdehyde components) dimethylamine hydrochloride (DMA·HCl) after 5 minutes, 1 day, 2 days, 5.5 days, and 10 days (six top traces). The five bottom traces correspond to the isolated **$BiPh_2(NON)_2$**, **$Py_2(NON)_2$**, **$BiPh_3T_2$**, **Py_3T_2** and **BiPh**.

DCL[8] consisting initially of an appropriate mixture of the four preformed entities **Py_3T_2**, **$BiPh_3T_2$**, **$Py_2(NON)_2$** and **$BiPh_2(NON)_2$** (20% of each macrocycle and 30% of each macrobicycle concerning dialdehyde units, 25% of each concerning molecules) was set up to investigate component redistribution among these four constituents in the same conditions. After 10 days of self-organization, a composition of 10%, 46%, 37%, and 2% for **$BiPh_3T_2$**, **Py_3T_2**, **$BiPh_2(NON)_2$**, and **$Py_2(NON)_2$** was attained, showing that the agonistic constituents **Py_3T_2** and **$BiPh_2(NON)_2$** had become the predominant products (**Figure III-24**).

In a similar trend to that of **DCL[7], DCL[8]** was thus undergoing evolution from the initial distribution to the preferred self-sorted distribution, dominated by the cage **Py_3T_2** generation and the amplification of the agonistic species interrelated through the same

diagonal of the square DCL (i.e., **$BiPh_2(NON)_2$**). These experiments confirmed that these macrocyclic and macrobicyclic structures based on multiple imine bonds exhibited excellent self-sorting properties under acid catalysis to render them dynamic. Besides, they also exemplified that the use of agonistic and antagonistic relationships of constituents in a CDN can force the expression of thermodynamically unfavourable products.

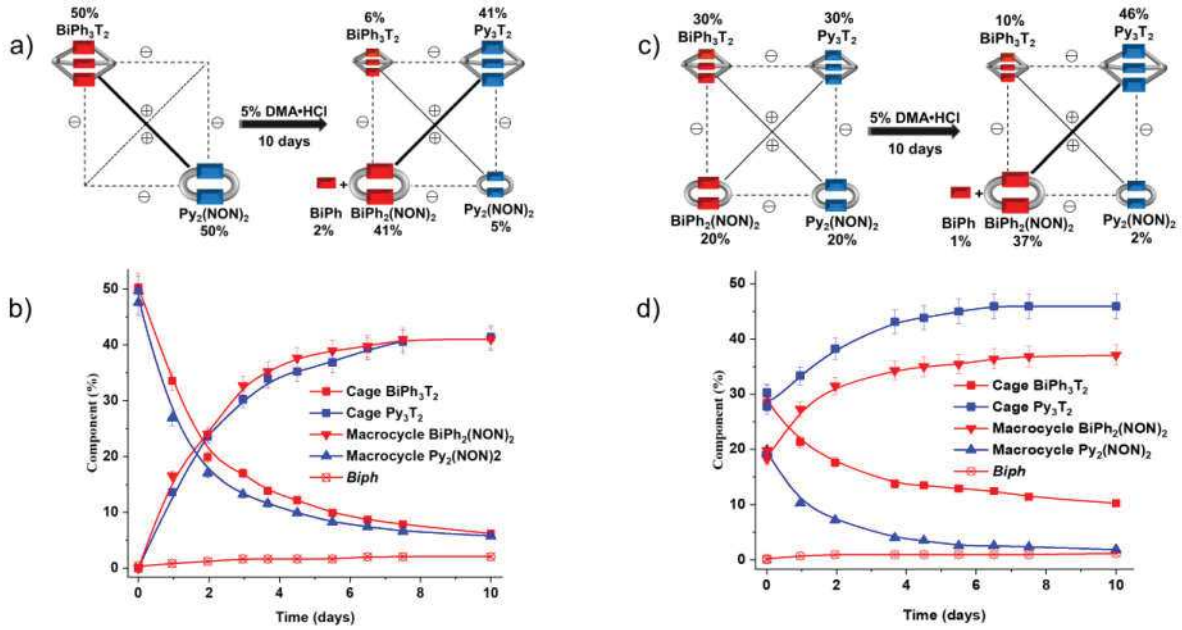

Figure III-25. Network switching in **DCL[7]** (**a,b**), **DCL[8]** (**c,d**) by component rearrangement from the starting distribution of preformed constituents (left square) to the final distribution (right square). Experiments were performed over 10 days in the presence of 5 mol% of dimethylamine hydrochloride (DMA·HCl) as an exchange catalyst. (b) and (d) reveal the time evolution of the component abundance during the rearrangement for **DCL[7]** and **DCL[8]**, respectively, as measured by ^{1}H NMR. The processes were further followed for 300 days, with some decomposition of the constituents being observed.

2.3. Constitutional dynamic network switching from kinetic to thermodynamic distributions of self-sorting dynamic macrocycles and macrobicyclic cages

The behaviour of the CDNs constructed from pre-synthesized constituents provoked

efforts to explore time-dependent DCLs that might undergo switching between agonistic and antagonistic constituents under kinetic control.

2.3.1. Component selection

In order to successfully design kinetically switchable dynamic self-sorting systems, the following parameters were considered for selecting the components: (i) the shape difference between the aldehyde components to optimize the self-sorting ability (e.g., one or two aromatic groups: 2,5-Furandicarbaldehyde (**Fur**) and 2,2'-bipyridine-6,6'-dicarbaldehyde (**BiPy**)); (ii) dialdehydes of different reactivities (e.g., carbonyl group activated by a neighbouring nitrogen site, as in **BiPy**); (iii) the lower thermodynamic stability for the kinetically-trapped species formed. For instance, in a [2 × 2] CDN consisting of four constituents (**AB, AB′, A′B** and **A′B′**), if the diagonally located agonistic constituents **AB** and **A′B′** are initially formed as kinetic products from the four components (**A**, **B**, **A′** and **B′**), the antagonistic orthogonal pair **AB′** and **A′B** is expected to be gradually generated as the thermodynamic product over time.[30] Competition between macrobicyclic cages and macrocycles was chosen as a model because of the differences in the cyclic order of the compounds and in their thermodynamic stabilities.

Three sets of self-sorting experiments were carried out involving: (i) the competition of two dialdehydes **BiPy** and **Fur** (in 2:2:2 molar ratio) towards the diamine **NON** [three components generating two macrocycles]; (ii) the competition of two dialdehydes **BiPy** and **Fur** (or **mPh**) towards **T** (in 3:3:2 molar ratio) [three components generating two cages]; and (iii) a four constituent [2 × 2] CDN made up of two macrocycles and two macrobicycles with competition between four components.

2.3.2. Time-dependent macrocycle switching from DCL[9] of three components Fur/BiPy/NON

A competitive self-sorting experiment generating two macrocycles was carried out for a DCL containing the aldehydes **BiPy** and **Fur** together with the diamine **NON** in a 2:2:2 molar ratio in $CDCl_3$ at 23 °C (**Figure III-26**). **BiPy** was immediately transformed upon mixing and after about 35 min, the compound distribution was **BiPy** (10%), **Fur** (33%), **$BiPy_2(NON)_2$** (40%) and **$Fur_2(NON)_2$** (<1%), with the remaining species being unidentified intermediates.

The reaction was then equilibrated for 9 days with a decrease in the concentration of **$BiPy_2(NON)_2$** accompanied by a steady increase of **$Fur_2(NON)_2$** and a release of **BiPy**, resulting in a final distribution of **BiPy** (22%), **Fur** (7%), **$BiPy_2(NON)_2$** (17%) and **$Fur_2(NON)_2$** (19%). (**Figure III-27**)

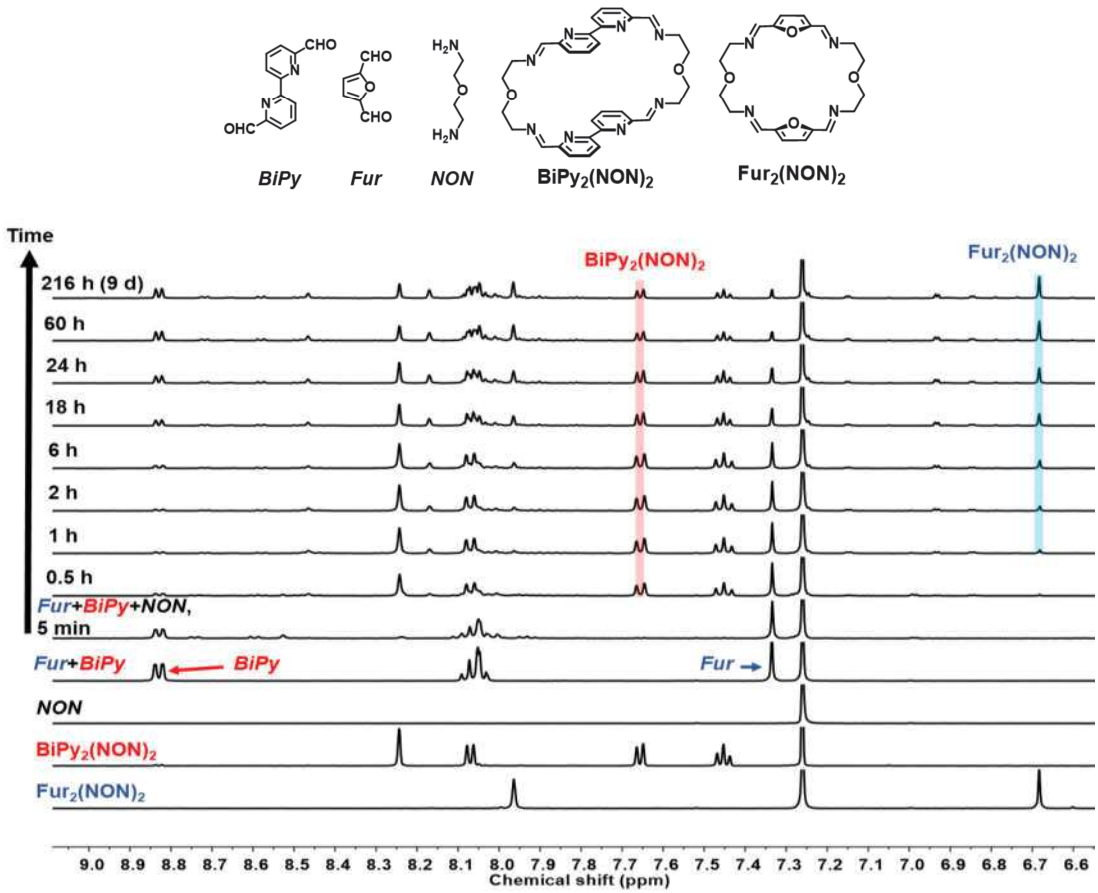

Figure III-26. Time evolution of the ^{1}H NMR (400 MHz, $CDCl_3$, 25 °C) for a mixture 2**Fur**+2**BiPy**+2**NON** (**[Fur]$_0$** = **[BiPy]$_0$** = 3.6 mM) after 5 min, 0.5 h, 1 h, 2 h, 6 h, 18 h, 24 h, 60 h and 216 h (nine top traces). The two bottom traces correspond to the isolated **$BiPy_2(NON)_2$** and **$Fur_2(NON)_2$**.

To summarize, the more reactive dialdehyde **BiPy** first reacted with **NON** in a rather short time leading to the formation of the kinetic product **$BiPy_2(NON)_2$** (kinetic self-sorting). Thereafter, the latter decreased and the **$Fur_2(NON)_2$** macrocycle was slowly formed, indicating that it was the more stable macrocycle (thermodynamic self-sorting), although the reaction had not yet reached its equilibrium. After about 9 days, **$BiPy_2(NON)_2$** remained in solution, suggesting that the thermodynamic features of **$BiPy_2(NON)_2$** and **$Fur_2(NON)_2$** must

be somewhat similar, as evidenced by their final ca. 1:1 ratio.

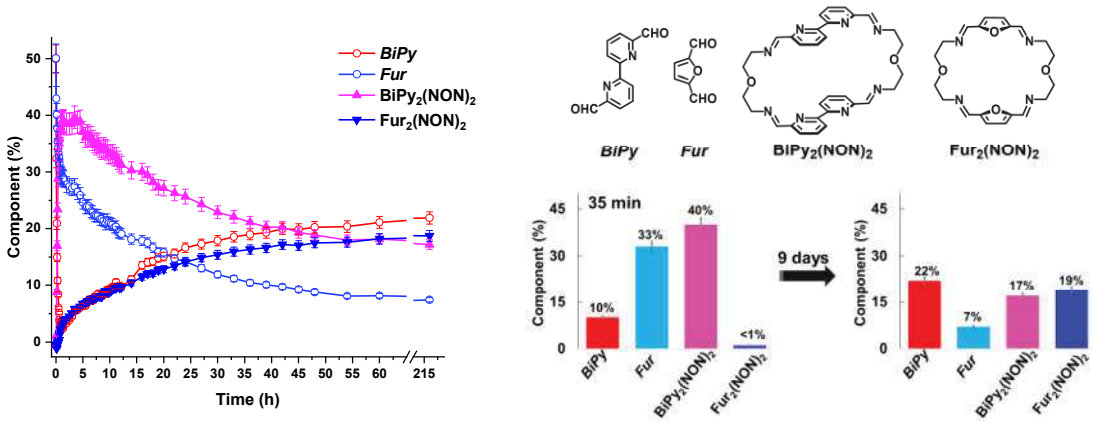

Figure III-27. Structure and distribution of macrocycles **$BiPy_2(NON)_2$** and **$Fur_2(NON)_2$** generated from a mixture of 2**Fur** + 2**BiPy** + 2**NON** (% calculated based on the components; Error in ^{1}H-NMR signal integration: ±5%).

2.3.3. Time-dependent macrobicyclic cage switching from a library of three components

To investigate the selective self-sorting in the formation of macrobicyclic cages in competitive environments, a set of experiments was carried out for libraries containing **BiPy** together with another aldehyde competing for **T** in a 3:3:2 ratio.

2.3.3.1. DCL[10]: 3BiPy+3Fur+2T

The first case of study was the system based on **BiPy/Fur/T** in a molar ratio of 3/3/2. ^{1}H NMR experiments (**Figure III-28**) revealed that after **T** was added into a mixture of **BiPy** and **Fur,** the signals for free **T** immediately began to diminish in conjunction with a significant decrease of the ones for **BiPy** and **Fur**. At this time (5 min of reaction), the integration of the CHO ^{1}H NMR signals at 10.19 and 9.86 ppm corresponded to 31% of each free **BiPy** and **Fur**, but the desired cages **$BiPy_3T_2$** and **Fur_3T_2** were still almost undetectable. Hence, the initial condensation reactions clearly resulted in the formation of intermediates. The concentration of **BiPy** then dropped to 13% after about 1 h. Meanwhile, the concentration of cage **$BiPy_3T_2$** increased to its peak value of 22%, together with 5% of the

[2+2] intermediate **Int[BiPy$_2$T$_2$]** (identified by ^{1}H NMR and HRMS, see **Figures S-III-1** and **S-III-2** in Chapter VII). In contrast, the concentration of unreacted **Fur** decreased smoothly to 26%, and only 1.5% of cage **Fur$_3$T$_2$** was detected. Interestingly, further progress of the reaction revealed a slow decrease in the concentration of **BiPy$_3$T$_2$**, whereas the concentration of **Fur$_3$T$_2$** and free **BiPy** progressively increased, suggesting a transformation from **BiPy$_3$T$_2$** to **Fur$_3$T$_2$**. After about 384 h (around 16 days) the solution contained **BiPy** (42%), **Fur** (4%), **BiPy$_3$T$_2$** (3%) and **Fur$_3$T$_2$** (48%), with **Fur$_3$T$_2$** as the major product. This behaviour is illustrated in **Figure III-29**.

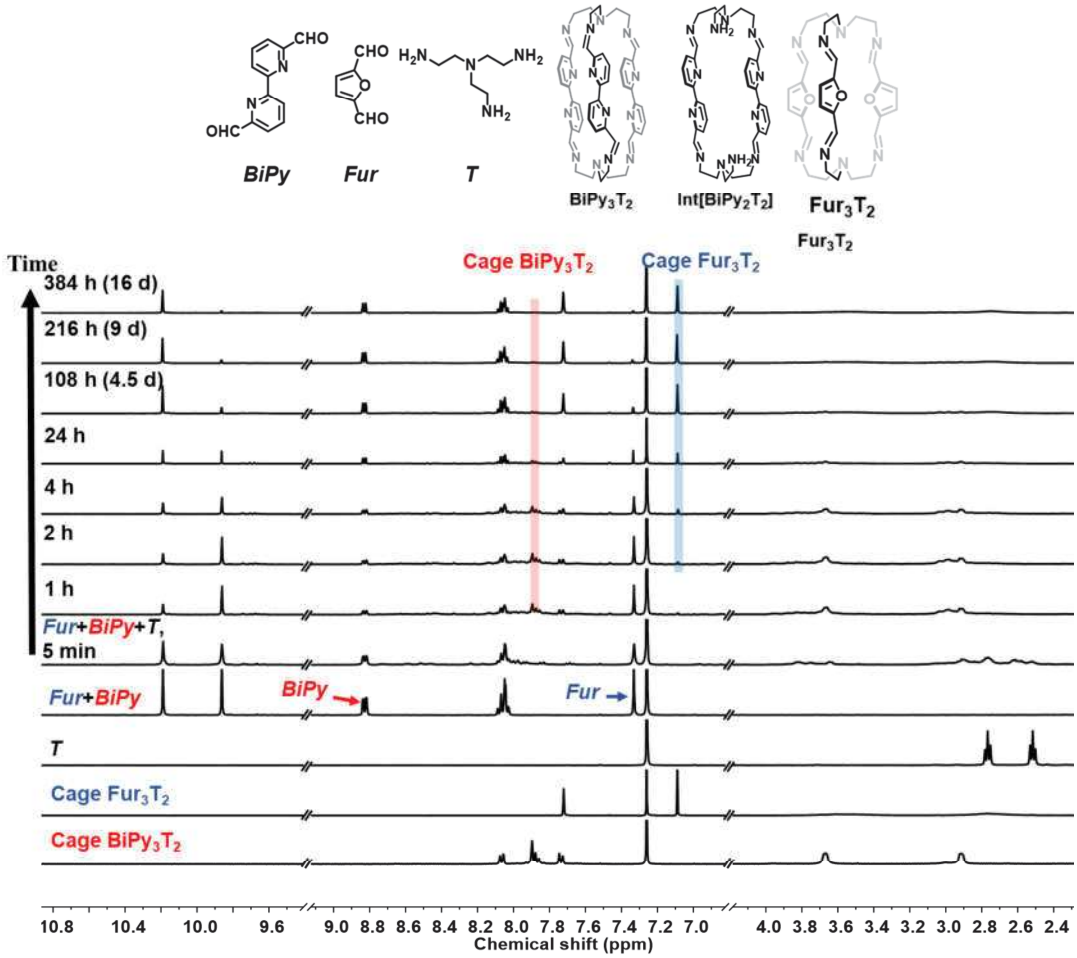

Figure III-28. Evolution of the ^{1}H NMR spectra for 3**Fur**+3**BiPy**+2**T** (**[Fur]$_0$** = **[BiPy]$_0$** = 3.6 mM, $CDCl_3$, 23 °C) after 5 min, 1 h, 2 h, 4 h, 24 h, 108 h, 216 h and 384 h (eight top traces). The two bottom traces correspond to the isolated cage **Fur$_3$T$_2$**, and cage **BiPy$_3$T$_2$**.

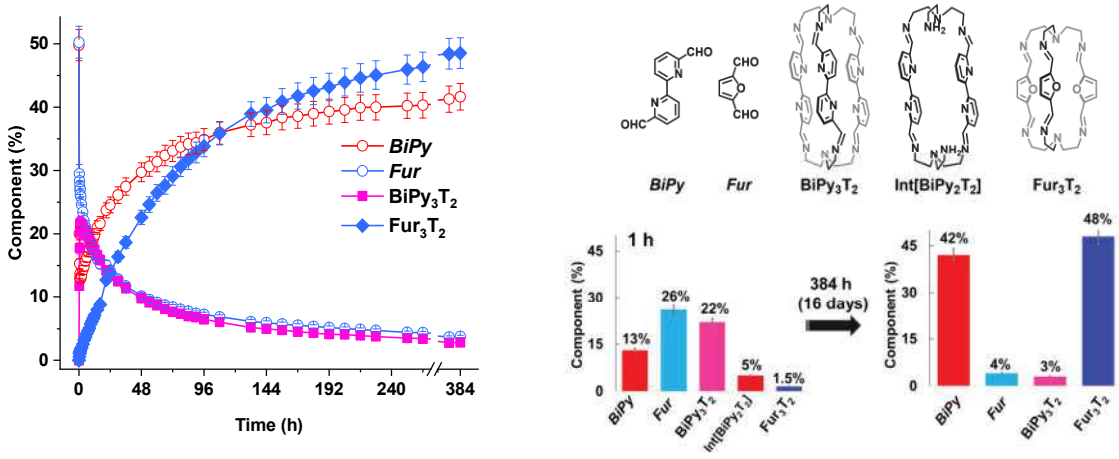

Figure III-29. (left) ^{1}H NMR monitoring and (right) abundance distribution of the time-dependent mixture of 3**BiPy** + 3**Fur** + 2**T** in $CDCl_3$ at 23 °C (% calculated based on the components; Error in ^{1}H-NMR signal integration: ±5%)

In order to examine any temperature effect, the same experiments were performed at 40 °C. Integration of ^{1}H NMR signals indicated a mixture of **BiPy$_3$T$_2$** (19%), **Fur$_3$T$_2$** (2%), 12% unreacted **BiPy** and 27% unreacted **Fur** after 1h. Notably, after 12 days, the distribution was 2% **BiPy$_3$T$_2$**, 46% **Fur$_3$T$_2$**, 38% unreacted **BiPy** and 5% unreacted **Fur**. As expected, a higher temperature accelerated the transformation from **BiPy$_3$T$_2$** to **Fur$_3$T$_2$**, but it did not increase the final amount of **BiPy$_3$T$_2$** (**Figures III-30** and **III-31**).

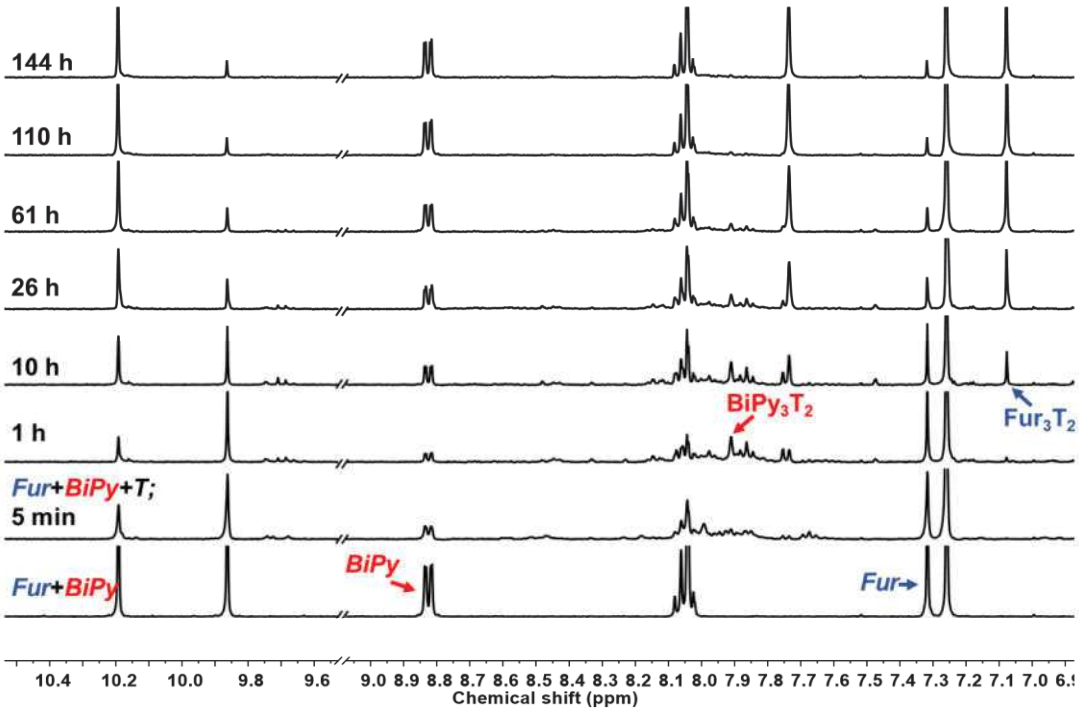

Figure III-30. Evolution of the ^{1}H NMR (400 MHz, CDCl3, 40 °C) spectra for 3**Fur**+3**BiPy**+2**T** ($[\mathbf{Fur}]_0 = [\mathbf{BiPy}]_0$ = 3.6 mM) after 5 min, 1 h, 10 h, 26 h, 61 h, 110 h and 144 h.

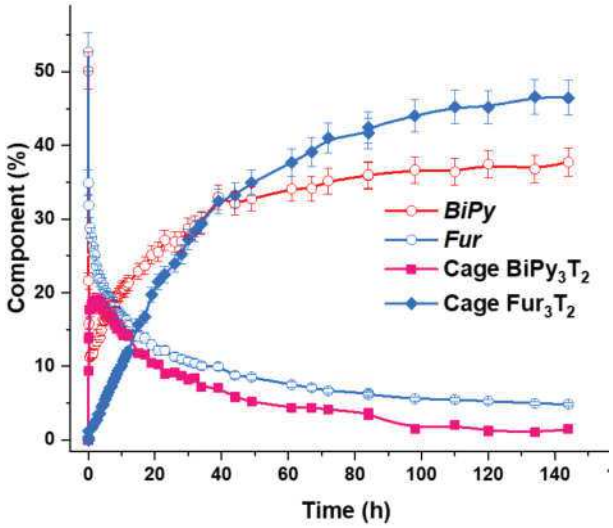

Figure III-31. ^{1}H NMR monitoring for the time evolution of the reaction 3**Fur**+3**BiPy**+2**T** ($[\mathbf{Fur}]_0 = [\mathbf{BiPy}]_0$ = 3.6 mM, CDCl3, 40 °C), as obtained from aromatic proton signals in the ^{1}H NMR spectra. Error in ^{1}H-NMR signal integration: ±5%.

2.3.3.2. DCL[11]: 3mPh+3BiPy+2T

Starting from a mixture of **BiPy** and **mPh** (3 equiv. each) with **T** (2 equiv.) at room temperature, **BiPy** was consumed as soon as **T** was added to the solution (**Figure III-32**). As can be seen from **Figure III-33**, the distribution after 2 h was **BiPy** (7%), **mPh** (46%), **$BiPy_3T_2$** (30%) as well as **Int[$BiPy_2T_2$]** species (6%), but no signals corresponding to **mPh_3T_2** were detected. After about 14 days, the amounts of **$BiPy_3T_2$**, **Int[$BiPy_2T_2$]** and **mPh** decreased to 12%, 3%, and 32% respectively, while those of **BiPy** and **mPh_3T_2** increased to 27% and 22%, respectively. Although the conversion from **$BiPy_3T_2$** to **mPh_3T_2** was very slow and was continuing even after 14 days, it was sufficient to demonstrate that the system underwent a transformation from kinetic to thermodynamic products.

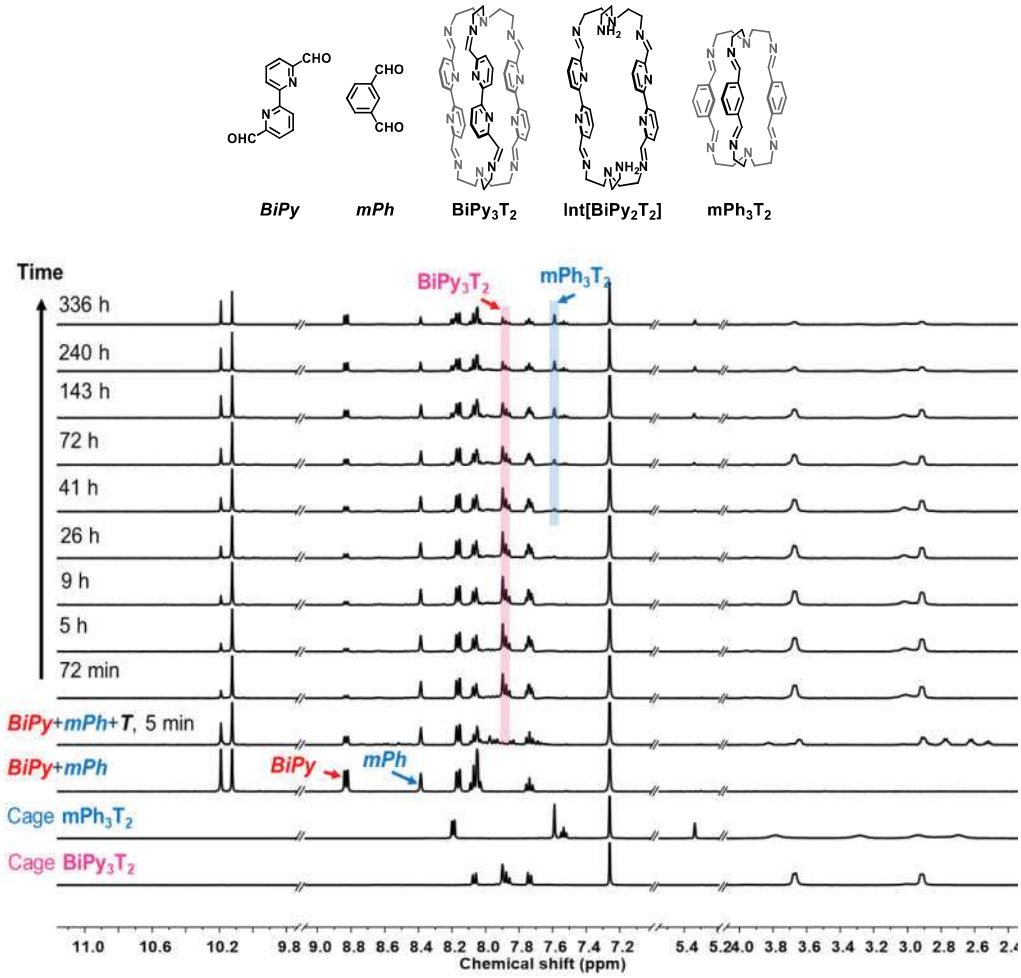

Figure III-32. Time evolution of the ^{1}H NMR spectra of 3**mPh**+3**BiPy**+2**T** (**$[mPh]_0$** = **$[BiPy]_0$** = 3.6 mM, 400 MHz, $CDCl_3$, 25 °C) after 5 min, 72 min, 5 h, 9 h, 26 h, 41 h, 72 h, 143 h, 240 h and 336 h (ten top spectra). The two bottom traces correspond to the isolated cage **mPh_3T_2** and cage **$BiPy_3T_2$**.

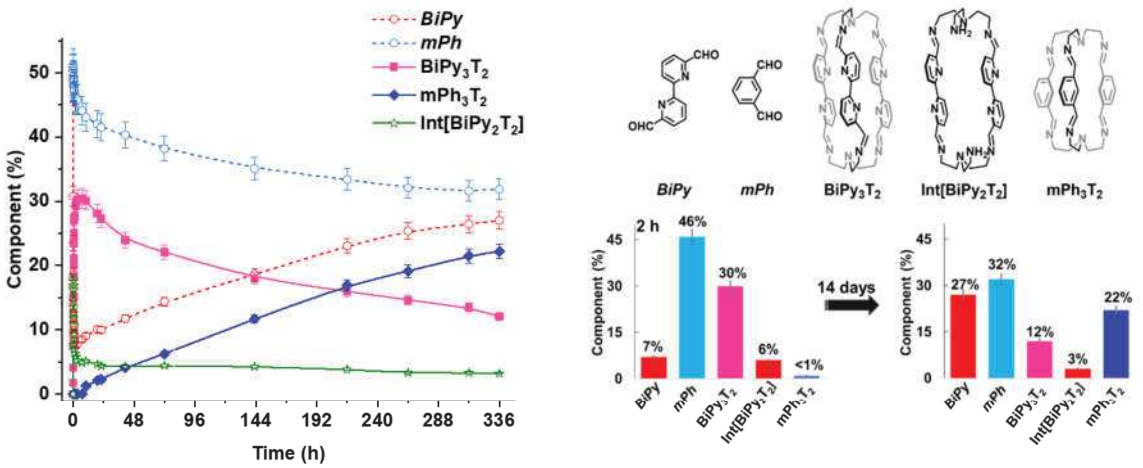

Figure III-33. (left) ^{1}H NMR monitoring of the time evolution of the species abundance. (right) Structure and distribution of macrobicyclic cages **mPh$_3$T$_2$**, **BiPy$_3$T$_2$** and **Int[BiPy$_2$T$_2$]** generated from a mixture of 3**mPh** + 3**BiPy** + 2**T** (% calculated on the basis of the components; Error in ^{1}H-NMR signal integration: ±5%)

2.3.3.3. DCL[12]: 3Py+3BiPy+2T

In all these cases, a fast selective formation of cage **BiPy$_3$T$_2$** was observed at the beginning of the reaction; however, **T** exhibited a preference to transform into the thermodynamically favoured cage containing monoaromatic bridges. The main reason for the time-dependent switching achieved in the previous sets of experiments can be attributed to the lower reactivity of **Fur** and **mPh** (in comparison with **BiPy**) but the higher stability of their corresponding products compared to those of **BiPy**.

To investigate the effect of reactivity differences within substrates, a more reactive pyridine dialdehyde **Py** was selected to replace **Fur** and **mPh** under the same conditions. After mixing, the concentration of both **Py** and **BiPy** decreased, but **Py** was consumed more rapidly and cage **Py$_3$T$_2$** was generated more quickly than cage **BiPy$_3$T$_2$**. As can be seen from the ^{1}H NMR monitoring (**Figure III-35**), the amount of cage **Py$_3$T$_2$** was always higher than that of cage **BiPy$_3$T$_2$**. Overall, this system did not exhibit a time-dependent switching process, illustrating the importance of reactivity differences within substrates.

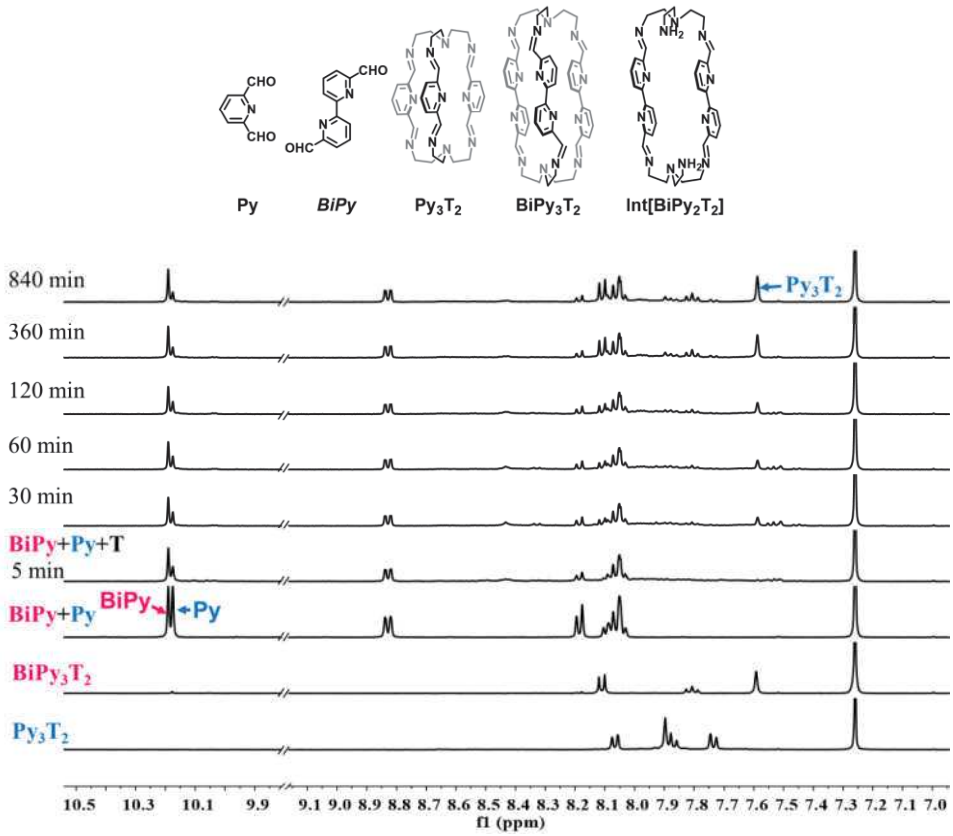

Figure III-34. Time evolution of the ^{1}H NMR spectra for 3**Py**+3**BiPy**+2**T** ($[\mathbf{mPh}]_0 = [\mathbf{BiPy}]_0$ = 3.6 mM, 400 MHz, $CDCl_3$, 23 °C). The two bottom traces correspond to the isolated cages $\mathbf{Py_3T_2}$ and $\mathbf{BiPy_3T_2}$.

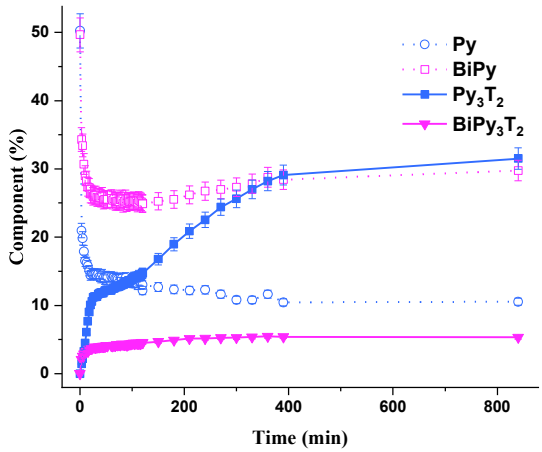

Figure III-35. ^{1}H NMR monitoring of the time-dependent evolution of cages generated from a mixture of 3**Py**+3**BiPy**+2**T** (Error in ^{1}H-NMR signal integration: ±5%)

2.3.3.4. DCL[13]: 3BiPh+3BiPy+2T

Next, systems with substrates of similar lengths were investigated. The reaction of a mixture of **BiPh**, **BiPy** and **T** in a molar ratio of 3:3:2 was followed by ^{1}H NMR spectroscopy as a function of time (**Figure III-36**). After mixing, **BiPy** was rapidly transformed into **[BiPy$_2$T$_2$]**. After 15 min, **[BiPy$_2$T$_2$]** reached its highest abundance, which was about 24%. The composition of the system at this point also contained 13% of unreacted **BiPy**, 48% of unreacted **BiPh**, and 13% of cage **BiPy$_3$T$_2$**. After 60 min, it was difficult to detect the intermediate **[BiPy$_2$T$_2$]**, indicating that it had been fully converted to cage **BiPy$_3$T$_2$** (new abundance = 31%). In contrast, only 2% of cage **BiPh$_3$T$_2$** was generated at this point. Thereafter, the system gradually reached equilibrium, with a distribution of **BiPy** (6%), **BiPh** (44%), **BiPy$_3$T$_2$** (39%), and **BiPh$_3$T$_2$** (2%). The rate plot is shown in **Figure III-37**. Again, the system did not exhibit time-dependent conversion behaviour throughout the course of the reaction, showing that **BiPy$_3$T$_2$** was both kinetically and thermodynamically favoured.

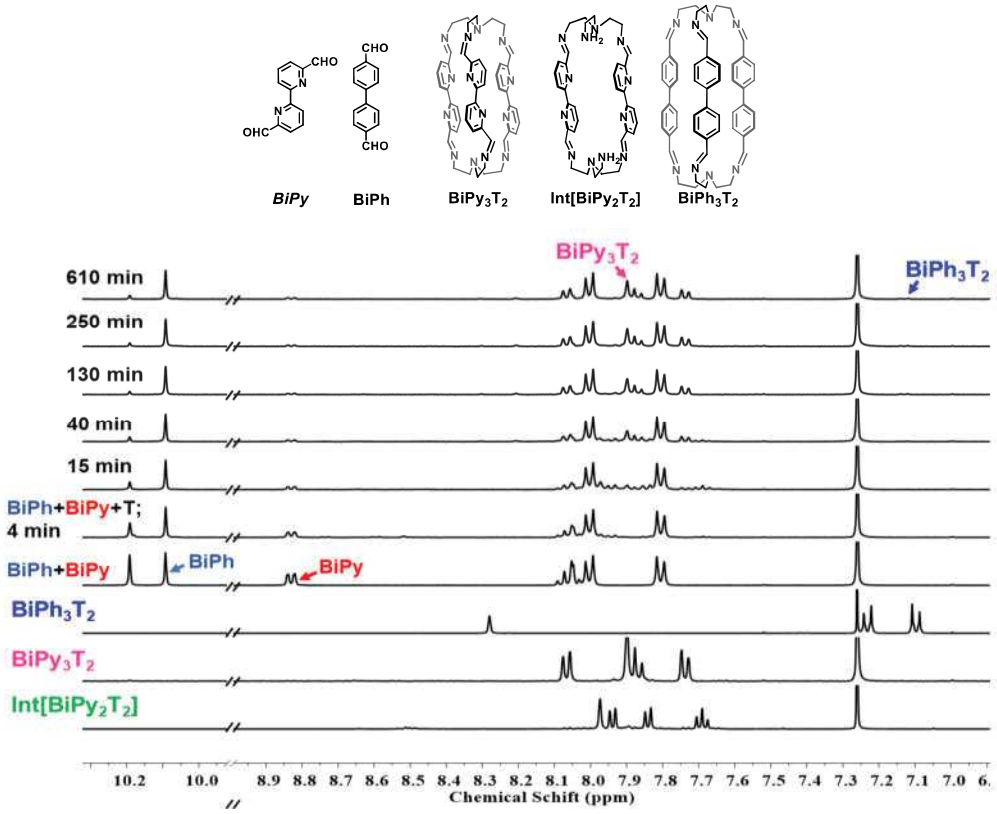

Figure III-36. Time evolution of the ^{1}H NMR spectra for 3**BiPh**+3**BiPy**+2**T** (**[BiPh]$_0$** = **[BiPy]$_0$** = 3.6 mM, **[T]$_0$** = 2.4 mM 400 MHz, $CDCl_3$, 25 °C).

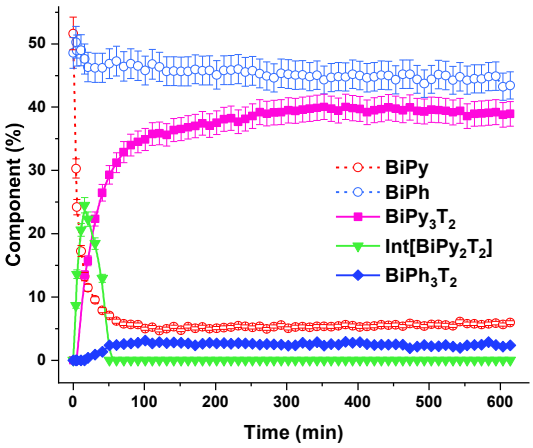

Figure III-37. ^{1}H NMR monitoring of the time-dependent evolution of cages generated from a mixture of 3**BiPh**+3**BiPy**+2**T**. Error in ^{1}H-NMR signal integration: ±5%.

In summary, from the results for all the different experiments, we can state that when **BiPy** was treated with **T** in the presence of **Fur** or **mPh**, the reaction mixture contained predominantly **BiPy$_3$T$_2$** at early times (kinetic self-sorting), but the system slowly underwent component exchange towards the generation of the corresponding thermodynamic product, namely **Fur$_3$T$_2$** or **mPh$_3$T$_2$** (thermodynamic self-sorting), with the release of the dialdehyde component **BiPy**. However, when **Py** was used instead, the first cage formed (i.e., **Py$_3$T$_2$**) was also the thermodynamically stable product, precluding its conversion into cages containing other linkages. Finally, dialdehydes of similar size produced cages of similar thermodynamic stability. In all cases, smaller cages were shown more stable than larger ones.

Hence, the key features for designing and operating self-sorting under kinetic control can be concluded as follows: (i) linkages should have different sizes; (ii) the longer linkages should be more reactive than the shorter ones.

2.3.4. Switching from kinetic to thermodynamic distributions in a [2 × 2] CDN of two macrocycles and two macrobicyclic cages

Extending the above studies, a [2 × 2] CDN containing four constituents, two macrocycles and two macrobicyclic cages, was generated from two aldehydes and two amino compounds.

DCL[14] containing the components **BiPy**, **Fur**, **T** and **NON** in a 5:5:4:4 molar ratio

was first investigated. The expected antagonistic products cage **$BiPy_3T_2$** and macrocycle **$BiPy_2(NON)_2$** share the dialdehyde **BiPy**, while cage **Fur_3T_2** and macrocycle **$Fur_2(NON)_2$** share the dialdehyde **Fur**. As seen from **Figure III-38** and **Figure III-39**, after 2.5 h of reaction, a complex mixture was obtained: the dominant product **$BiPy_3T_2$** reached its maximum abundance of ca. 16%, together with 6% of intermediate **[$BiPy_2T_2$]**. There was only a very small amount of its agonistic **$Fur_2(NON)_2$** (2%) accompanied by 13% of unreacted **Fur**. Small amounts of the two other products **Fur_3T_2** and **$BiPy_2(NON)_2$** were formed, 4% and 9% respectively, and unreacted **BiPy** (2%) remained. After 15 h, free **BiPy** had disappeared, and the constituents detected were **$BiPy_3T_2$** (14%), **Fur_3T_2** (14%), **$BiPy_2(NON)_2$** (17%) and **$Fur_2(NON)_2$** (8%), as well as some free **Fur** (2%). After 36 h, the composition of the mixture was **$Fur_2(NON)_2$** (9%) together with **$BiPy_3T_2$** (13%), **Fur_3T_2** (22%) and **$BiPy_2(NON)_2$** (20%). At short times the largest fraction of components was contained in unidentified intermediates. Finally, after 18 days, a simpler distribution (probably close to equilibrium) was reached containing **$BiPy_3T_2$** (5%), **Fur_3T_2** (47%), **$BiPy_2(NON)_2$** (35%) and **$Fur_2(NON)_2$** (1%). A minor amount (ca. 12%) of the components was still present as unidentified species. ESI-HRMS monitoring also confirmed such a reaction process (**Figure III-40**). The details for the MS signal assignation of MS can be found in Chapter VII, **Table S-III-3**. From HRMS, **[$BiPy_2T_2$]** and cage **$BiPy_3T_2$** reached their highest concentrations in about 1 h, and then gradually decreased. The highest-in-intensity peak (m/z 427.2439) was attributed to the cyclic intermediate **[$Fur_2T(NON)$]**. New signals with m/z of 385.1858 and 407.1676 also appeared, attributed to the formation of macrocycle **$Fur_2(NON)_2$**.

When 10 mol% dimethylamine hydrochloride (DMA·HCl), was added as an acid catalyst to **DCL[14],** the self-sorting was significantly faster, giving a distribution of 4%/42%/34%/1%/7%/1% for **$BiPy_3T_2$/Fur_3T_2/$BiPy_2(NON)_2$/$Fur_2(NON)_2$/BiPy/Fur** after 5.5 days, with ca. 11% of unidentified materials (**Figure S-III-5** in Chapter VII).

Overall, in the course of the process, **$BiPy_3T_2$** was rapidly formed and then its concentration decreased progressively in favour of **Fur_3T_2** and **$BiPy_2(NON)_2$**, indicating a switching from the initial incomplete kinetic distribution network in which the fast formed **$BiPy_3T_2$** dominates to a thermodynamically preferred distribution with amplification of the agonistic constituents **Fur_3T_2** and **$BiPy_2(NON)_2$**. The process represents an orthogonal switching from one diagonal to the other one of the square network.

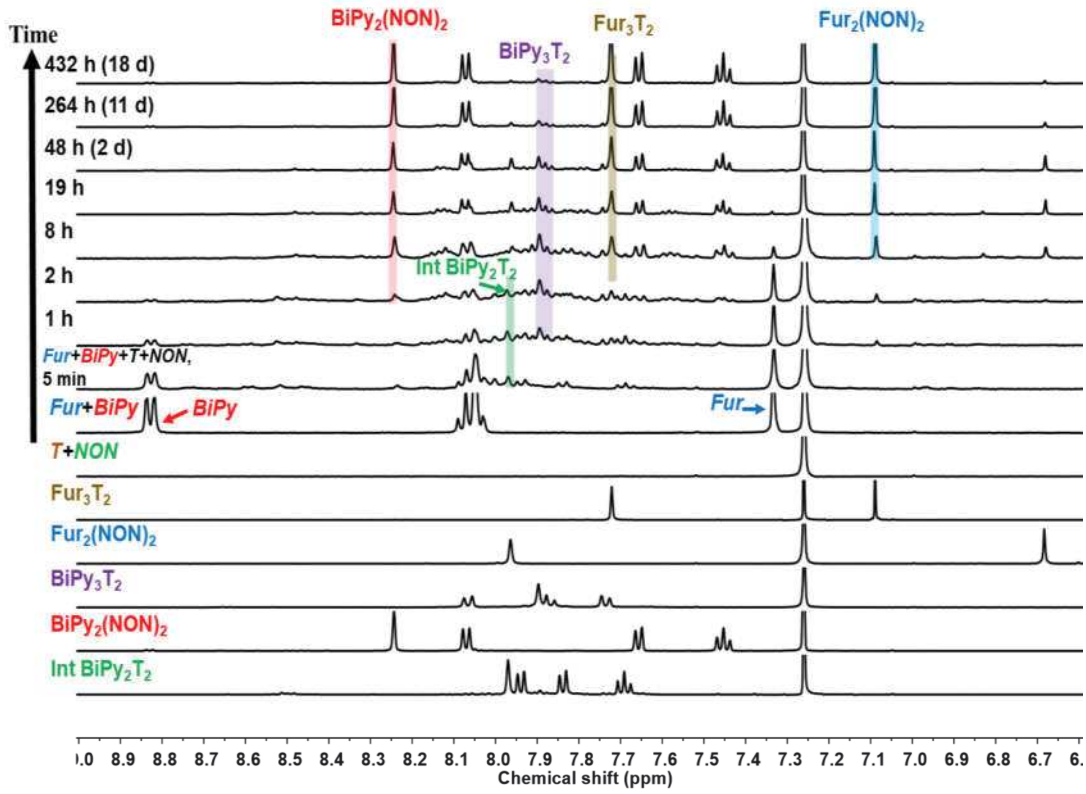

Figure III-38. Evolution of the ^{1}H NMR spectra for 5**Fur** + 5**BiPy** + 4**T**+ 4**NON** (**DCL[14]**) ($[\mathbf{Fur}]_0$ = $[\mathbf{BiPy}]_0$ = 3.6 mM, $CDCl_3$, 25 °C) after 5 min, 2 h, 8 h, 19 h, 48 h, 264 h and 432 h (eight top traces). The five bottom traces correspond to the isolated $\mathbf{Fur_3T_2}$, $\mathbf{Fur_2(NON)_2}$, $\mathbf{BiPy_3T_2}$,$\mathbf{BiPy_2(NON)_2}$ and $\mathbf{[BiPy_2T_2]}$.

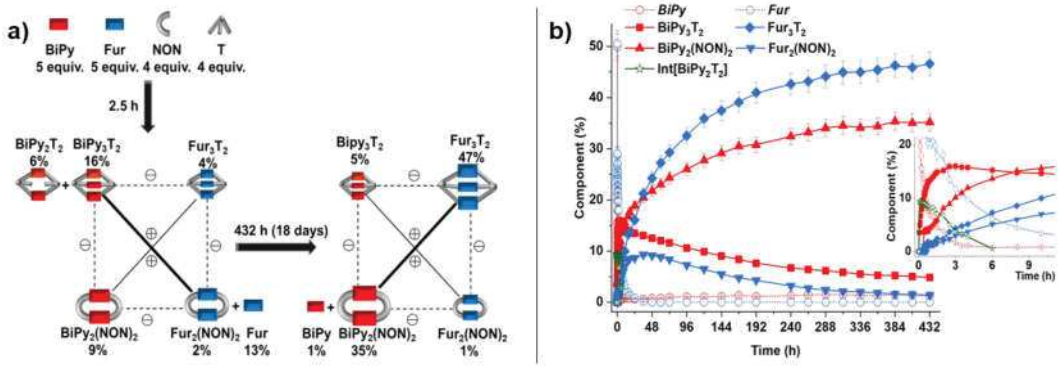

Figure III-39. (a) Component distribution in **DCL[14]** showing the orthogonal switching from a kinetic to a thermodynamic distribution of constituents over 18 days. (b) ^{1}H NMR monitoring the time evolution of macrocycle $\mathbf{BiPy_2(NON)_2}$ and macrobicycle $\mathbf{Fur_3T_2}$ with orthogonal switching of constituents from a mixture of 5**BiPy** + 5**Fur** + 4**T** + 4**NON** in $CDCl_3$ at 25 °C. (insert): amplified initial period. $[\mathbf{BiPy}]_0$ = $[\mathbf{Fur}]_0$ = 3.6 mM. (% calculated on the basis of components; Error in ^{1}H-NMR signal integration: ±5%)

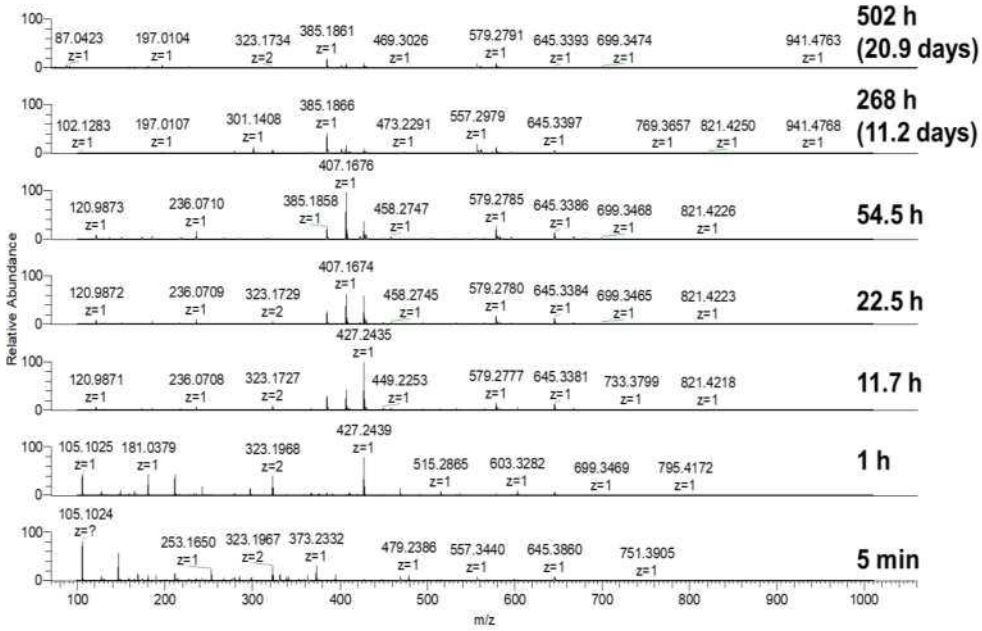

Figure III-40. Time evolution of the HRMS-ESI spectra for 5**Fur** + 5**BiPy** + 4**T** + 4**NON** ($[\mathbf{Fur}]_0$ = $[\mathbf{BiPy}]_0$ = 2.0 mM; $[\mathbf{T}]_0$ = $[\mathbf{NON}]_0$ =1.6 mM; 25 °C) in 50%-50% $CHCl_3$/MeOH.

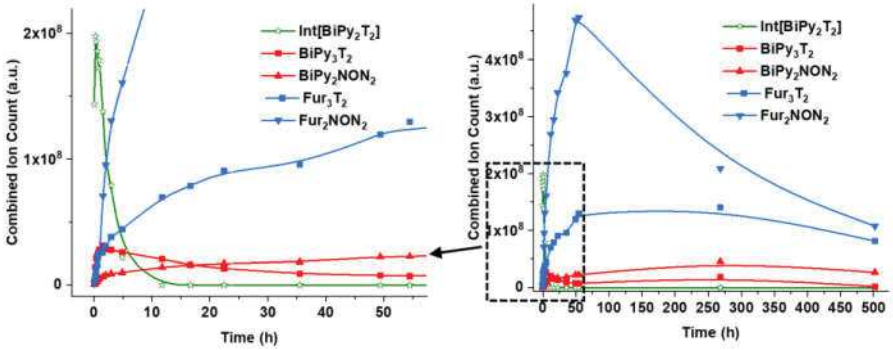

Figure III-41. HRMS-ESI monitoring the time-dependent generation of Intermediate $[\mathbf{BiPy_2T_2}]$, cages $\mathbf{BiPy_3T_2}$ and $\mathbf{Fur_3T_2}$, and macrocycles $\mathbf{BiPy_2NON_2}$ and $\mathbf{Fur_2(NON)_2}$ from the reaction between 5**Fur** + 5**BiPy** + 4**T** + 4**NON** ($[\mathbf{Fur}]_0$ = $[\mathbf{BiPy}]_0$ = 2.0 mM; $[\mathbf{T}]_0$ = $[\mathbf{NON}]_0$ =1.6 mM; 25 °C) as a function of time (over 502 h). NB: These data do not provide quantitative information about the relative amounts of each species identified by its mass, but, taken separately, they display the evolution of a given identified species during the course of the reaction. The curves are added to guide the eye.

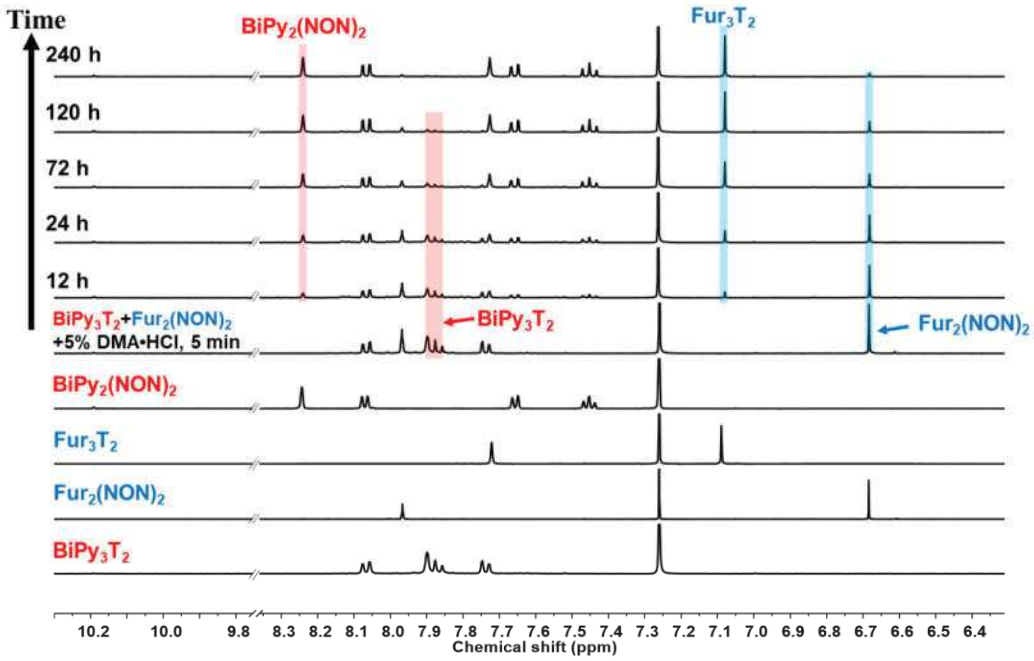

Figure III-42. Partial ^{1}H NMR spectra (aromatic region, 400 MHz, 25 °C) for the mixture of **$BiPy_3T_2$**, and **$Fur_2(NON)_2$** (50% of each, on basis of dialdehyde components) and 5 mol% dimethylamine hydrochloride (DMA·HCl) after 5 min, 12 h, 24 h, 72 h, 120 h and 240 h (six top traces). The four bottom traces correspond to the isolated **$BiPy_3T_2$**, **$Fur_2(NON)_2$**, **Fur_3T_2** and **$BiPy_2(NON)_2$**.

Similar observations were made of the behaviour of **DCL[15],** starting from a mixture of two agonistic constituents, (i.e., cage **$BiPy_3T_2$** and macrocycle **$Fur_2(NON)_2$**) in a ratio of 1:1 (concerning dialdehyde units). After 10 days, the system reached a composition of 3%, 45%, 47%, and 3% for **$BiPy_3T_2$**, **Fur_3T_2**, **$BiPy_2(NON)_2$** and **$Fur_2(NON)_2$**, respectively. Thus, it is evident that the agonistic constituents macrobicyclic cage **Fur_3T_2** and macrocycle **$BiPy_2(NON)_2$** became the major products as a result of a distribution switching to the orthogonal diagonal of the [2 × 2] CDN (**Figure III-42** and **Figure III-43**).

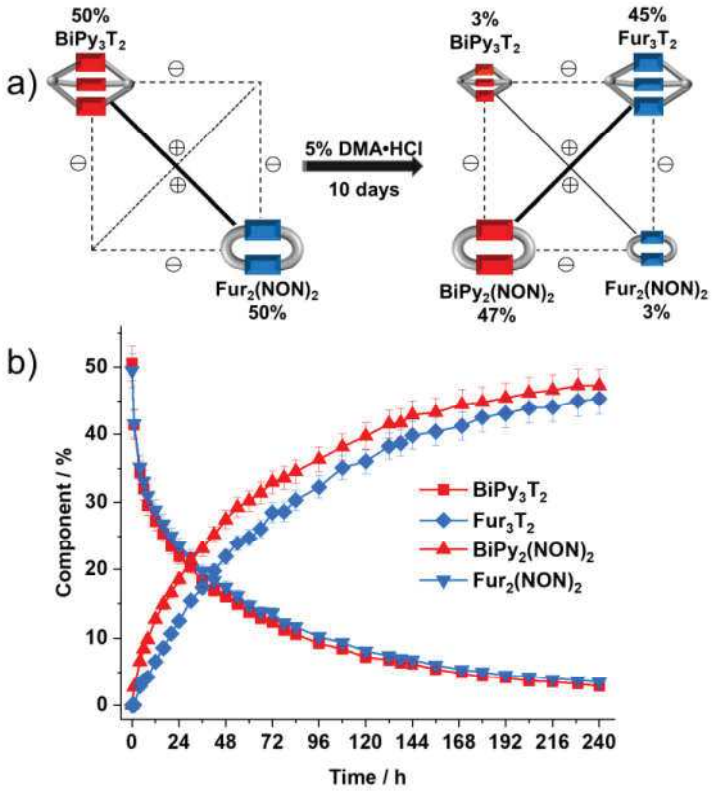

Figure III-43. (a) Network switching in the **DCL[15]** through component exchange from preformed macrocycle **$Fur_2(NON)_2$** (50%) and cage **$BiPy_3T_2$** (50%) (left) to the final distribution over 10 days in presence of 5 mol% DMA·HCl (concerning the dialdehyde components) as exchange catalyst (right). (b) ^{1}H NMR monitoring the time-dependent switching evolution in **CDN-7** over 10 days. Error in ^{1}H-NMR signal integration: ±5%.

3. Summary of the chapter

In conclusion, this chapter involves: (i) the self-sorting of two model architectures of different cyclic order, namely macrocycles and macrobicyclic cages; and (ii) the kinetic switching from the initially fast formed self-sorted kinetic product to the thermodynamic one.

The first section demonstrates the high-fidelity formation of macrocycles and cages performed under thermodynamic control by mixing triamine (**T**) or diamine (**NON**) with dialdehydes of a different type. Since the cages were generated before the macrocycles in all DCLs, the selectivity and fidelity of self-sorting processes are governed by the cages' stability and the formation rate of macrocycles in the system.

The rest of the chapter suggested a time-dependent dual-stage process for the different DCLs. Firstly, an initial kinetic non-equilibrium state was generated containing the rapidly-generated constituent together with a mixture of unreacted components, incomplete intermediates, and small amounts of other cages and macrocycles. Secondly, the non-equilibrium state evolved towards equilibrium and resulted in a thermodynamically controlled switching process from this kinetic distribution to the thermodynamic one. Many efforts have been devoted in this chapter to studying how time-dependent switching of constituents in a DCL can be achieved by controlling the size and reactivity of initial components.

Moreover, the rational design and utilization of kinetic and thermodynamic features of macrocycles and macrobicyclic cages permitted to demonstrate that several CDNs can adapt over time either from separately prepared constituents or by in situ imine condensation from their components. This switching behaviour in CDNs thus revealed an orthogonal switching from one diagonal to the other diagonal of the [2 × 2] network square or, in other words, from an out-of-equilibrium distribution to the equilibrium one.

In general terms, the diverse kinetic and thermodynamic features of the dynamic system drive the redistribution of all inter-connected constituents through component exchange, thus illustrating the regulation and self-correction ability of constitutional dynamic networks.

explore DCLs based on unsymmetric components with different structural and electronic properties for each macrobicyclic lid.

2. Results and Discussion

2.1. Formation of cage isomers

The unsymmetrical dialdehyde **Py-Ph** was allowed to react with **T** in $CDCl_3$ at room temperature for 24 h. The reaction mixture, as monitored by ^1H NMR, showed three signals between 8.6 and 8.9 ppm, indicating the presence of at least three different imines (**Figure V-1a**). The solution was further analysed by HRMS and the only signal found correlated well with the presence of the [3+2] imine cage. Combining both the ^1H NMR and HRMS results, the only possibility is the coexistence of two isomeric cages, namely **bbp** and **bbb.** As shown in scheme **V-2**, cage **bbb** describes the stereoisomer containing all dialdehyde units pointing in the same direction, whereas cage **bbp** denotes the species in which one of the dialdehydes is present in the reverse direction.

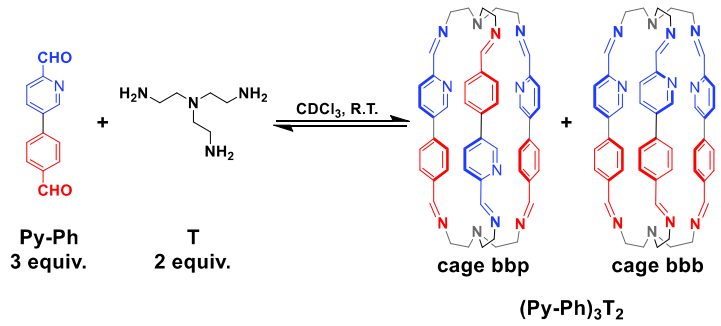

Scheme V-2. Formation of two isomeric cages via imine condensation of unsymmetric dialdehyde **Py-Ph** and **T**.

A structural comparison of the two isomeric cages suggested four kinds of coordination sites which depend on the number of N-donor atoms (from both imine and pyridine scaffolds). One of the 3D-arrangements within the cavity of cage **bbb** contained six N-donor sites, allowing for octahedral coordination of metallic cores. It was envisaged at this point that the separation of the two isomers could be achieved by making use of the anticipated solubility difference between monometallic and uncoordinated cages.

Indeed, after the addition of $Zn(OTf)_2$ (1 equiv.) into a suspension of both macrobicyclic

isomers in MeCN/$CHCl_3$ only one isomer, namely **cage bbp**, remained insoluble. Significant differences can be observed in the ^{1}H NMR spectra when comparing the isolated isomer (**Figure V-1c**) with the initial isomeric mixture. Integration of imine signals from the ^{1}H NMR spectrum for the *in situ* generated mixture in $CDCl_3$ revealed a distribution of **bbp** (67%) and **bbb** (33%). Even a more favourable formation of cage **bbp** (83%) was observed when the reaction was carried out in MeOH (**Figure V-1b**). Therefore, the reaction presented selectivity towards the generation of **cage bbp**, rather than a statistical 1:1 mixture of the two isomers. This selectivity may be due to the mutual repulsion of the electron-rich N atoms present in the pyridine rings that triggers the directional rotation of one linkage unit to minimize this unfavourable conformation.

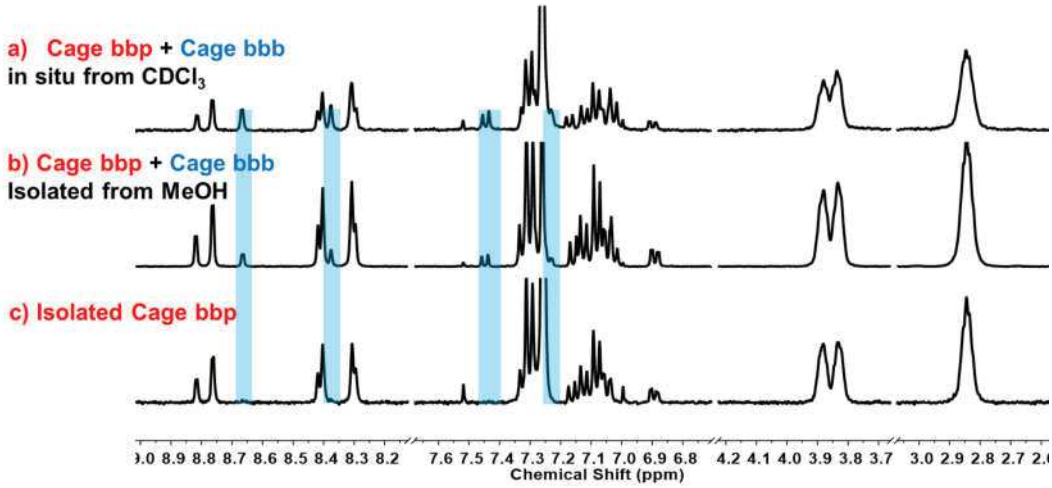

Figure V-1. Comparison of ^{1}H NMR spectra (400 MHz, $CDCl_3$, 23 °C) of (a) isomeric mixture obtained *in situ* from $CDCl_3$; (b) isomeric mixture obtained from MeOH; (c) isolated **cage bbp**. The blue stripes highlight some characteristic signals of **cage bbb**.

Colourless crystals were obtained when performing the reaction in a 1:1 ratio of $CHCl_3$/MeOH. Although the X-ray structure determination was modelled in terms of the cage **bbp** (**Figure V-2**), the ^{1}H NMR spectrum of this crystalline solid in $CDCl_3$ showed a mixture of both isomeric cages to be present. The difficulty in distinguishing C from N by X-ray diffraction is well known and assuming that the two cages could adopt essentially identical conformations, it is quite possible that both could be present in the one crystal.

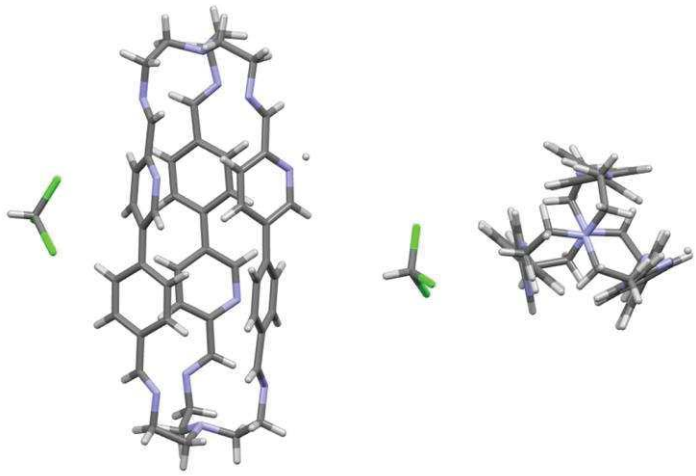

Figure V-2. Single-crystal X-ray structure interpreted as that of the macrobicyclic cage **bbp**. Colour scheme: carbon (grey), hydrogen (white), nitrogen (blue), chlorine (green).

2.2. Metallo-selective amplification of cage bbb

DCLs displaying a selection of components and amplification of constituents in response to metal cations pave the way towards adaptive systems presenting higher levels of application.[56,146] To investigate the metallo-adaptation ability of the current system, $Zn(OTf)_2$ solution (0.5 equiv.) was added to the mixture of two stereoisomeric cages (2 equiv. total isomeric concentration). The octahedral coordination preference of Zn(II) was expected to favour its complexation in the hexadentate site of **cage bbb** (coordination of Zn(II) with three N atoms of imines and three N atoms of pyridinyl units). Indeed, the **cage bbp** gradually transformed into the thermodynamically-favoured **cage bbb-Zn** complex, and the distribution was **cage bbb-Zn(II)** (90%) and **cage bbp** (10%) after 7 days at room temperature in the presence of 0.2 equiv. of dimethylamine hydrochloride (DMA·HCl).

The use of 2 equiv. of Zn(II) and other cations like Fe(II), Cd(II), Cu(I) were also tested (**Figures S-V-12 to S-V-15**). However, in these cases, the ^{1}H NMR spectra showed no significant changes after several days of reaction, indicating that no cage-to-cage conversion occurred.

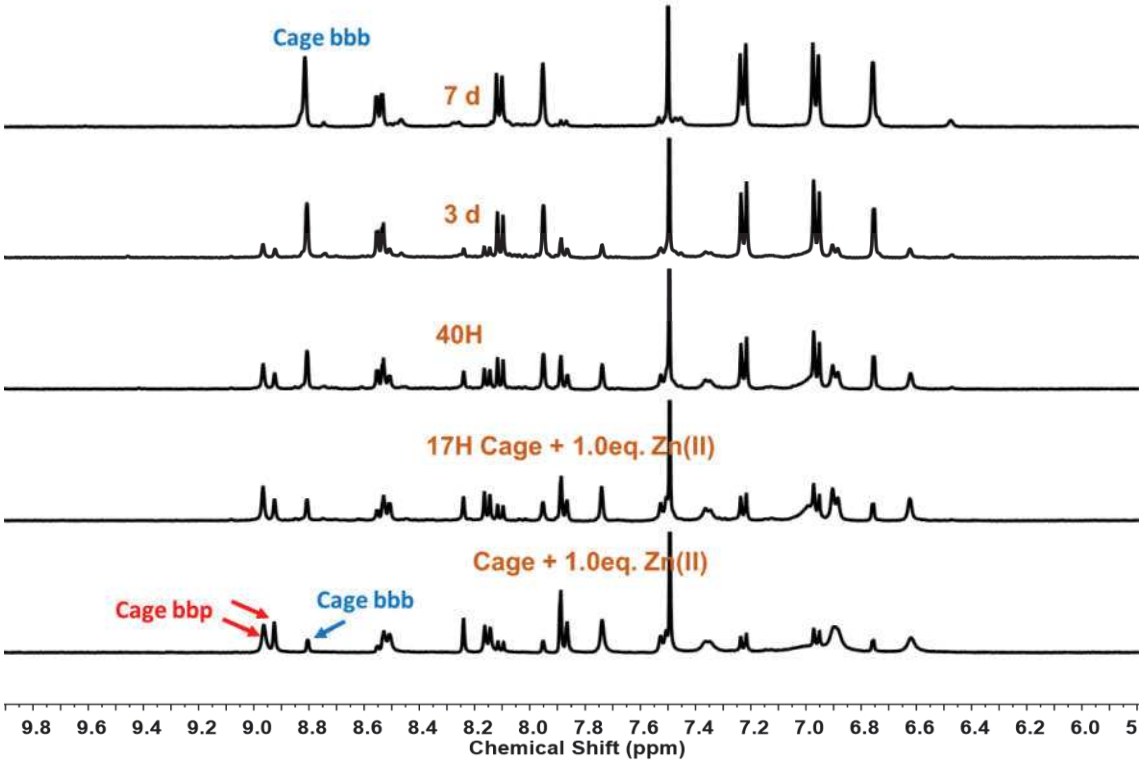

Figure V-3. Comparison of ^{1}H NMR spectra (500 MHz, 60%-40% CD_3CN-$CDCl_3$, 23 °C) showing the cage-to-cage conversion upon Zn(II) addition to the initial isomeric mixture in the presence of 0.2 equiv. of dimethylamine hydrochloride (DMA·HCl).

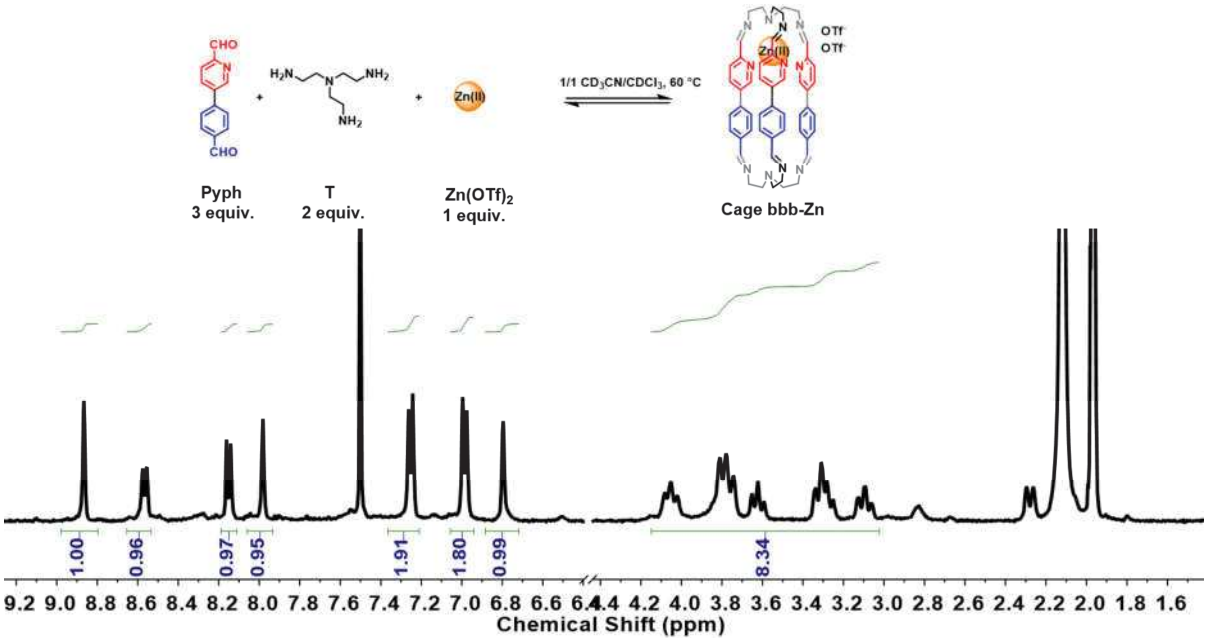

Figure V-4. ^{1}H NMR spectrum (400 MHz, 60%-40% CD_3CN-$CDCl_3$, 23 °C) showing the templated

formation of **cage bbb-Zn(II)** *via* imine condensation of unsymmetric dialdehyde **Py-Ph** (3 equiv.) and **T** (2 equiv.) in the presence of $Zn(OTf)_2$ (1 equiv.).

Considering the adaptive behaviour of the isomeric cages in the presence of Zn(II), the selective synthesis of **cage bbb-Zn** complex by using Zn(II) as a template was attempted. After mixing 1 equiv. $Zn(OTf)_2$ with 3 equiv. of dialdehyde **Py-Ph** and 2 equiv. of **T** at 60 °C for 48 h, **cage bbb-Zn(II)** complex was obtained as the predominant product, with the absence of the undesired isomeric **cage bbp** (**Figure V-4**). This experiment demonstrates the selective assembling and self-sorting of unsymmetric components in the presence of a chemical effector.[147,148]

2.3. Coordinated bimetallic cages

Coordination cages are well-known for their excellent performance in enantiomeric separations, catalysis, sensing, and drug delivery.[149–153] Such remarkable outcomes are the direct result of their well-defined structure, specific size, and tunable cavities.[154–156] To investigate potential applications for these two isomeric cages, the formation of their complexes with different metal ions was explored.

2.3.1. Synthesis of cage bbp complex

Cadmium has two NMR active isotopes with 1/2 nuclear spin, ^{111}Cd and ^{113}Cd. Therefore, cadmium complexes may exhibit proton-cadmium spin-spin coupling in their ^{1}H NMR spectra.[157] Addition of $Cd(OTf)_2$ (2 equiv.) into a 1/1 MeCN-$CHCl_3$ solution of **cage bbp** resulted in the formation of a **cage bbp-2Cd(II)** complex. As shown in the ^{1}H NMR (**Figure V-5**), the imine signals showed a merged $J_{(H\text{-}Cd)}$ coupling in which the difference between the ^{111}Cd and ^{113}Cd coupling constants with ^{1}H were too small to be correctly determined. The differences in the chemical shift in the ^{113}Cd NMR spectrum of -367.01 ppm and -438.93 ppm, both referenced to $CdCl_2$, proved the inequality in coordination geometry (**Figure V-6**). The bimetallic complex was characterised by ^{13}C NMR and ^{113}Cd-^{1}H HMBC (**Figures S-V-9** and **S-V-10** in Chapter VII).

In a similar manner, the **cage bbp-2Pb(II)** species was also synthesized (**Figure V-7** and **Figure S-V-11** in Chapter VII). In this case, ^{1}H-^{207}Pb spin-spin couplings were observed, enabling the calculation of the corresponding coupling constants.

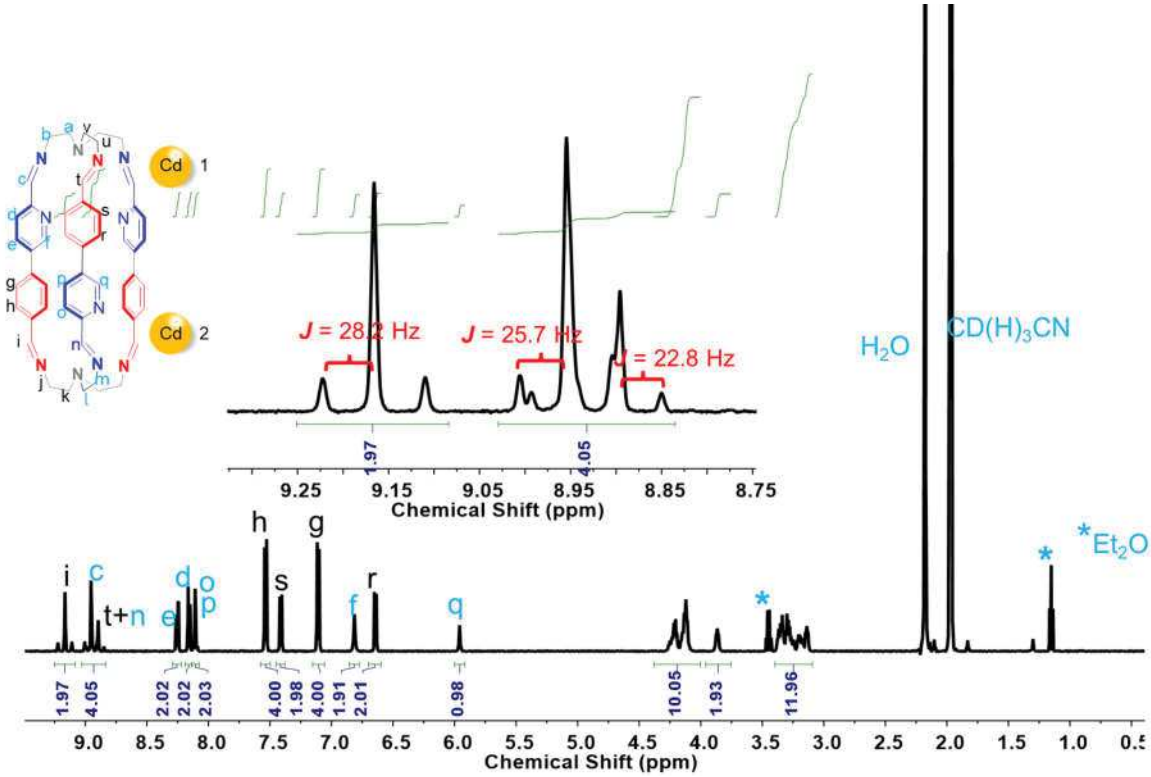

Figure V-5. ^{1}H NMR spectrum (500 MHz, CD_3CN, 23 °C) of complex **bbp-2Cd(II)** showing the coupling of ^{1}H with ^{111}Cd and ^{113}Cd.

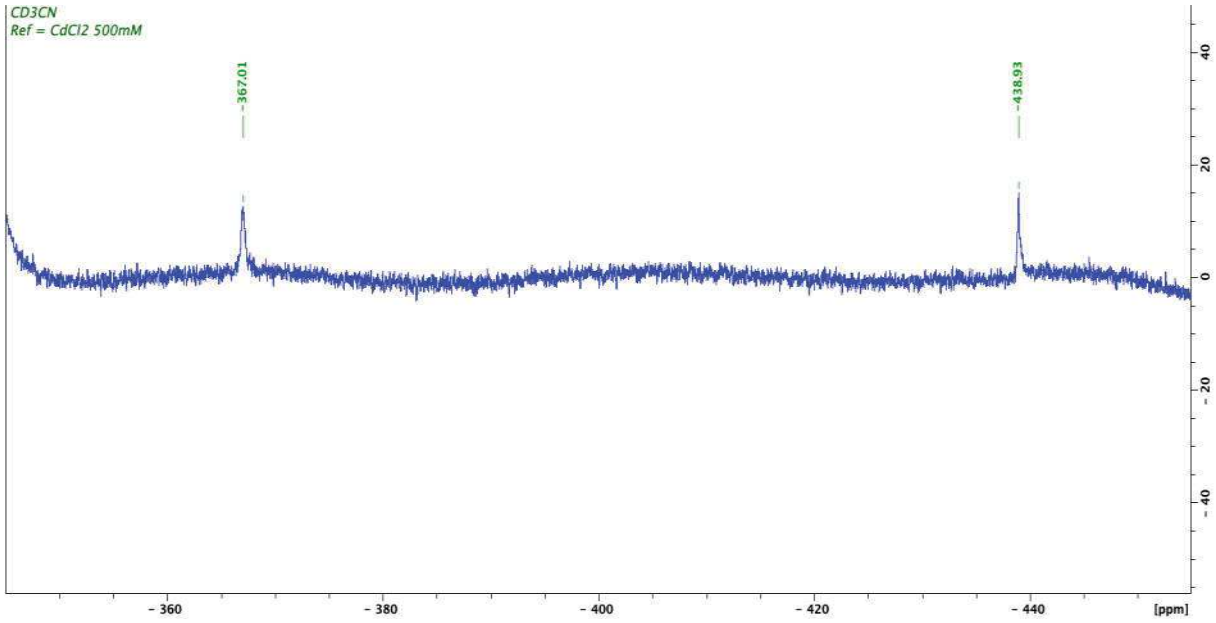

Figure V-6. ^{113}Cd NMR spectrum (CD_3CN, 23 °C) of complex **bbp-2Cd(II)**

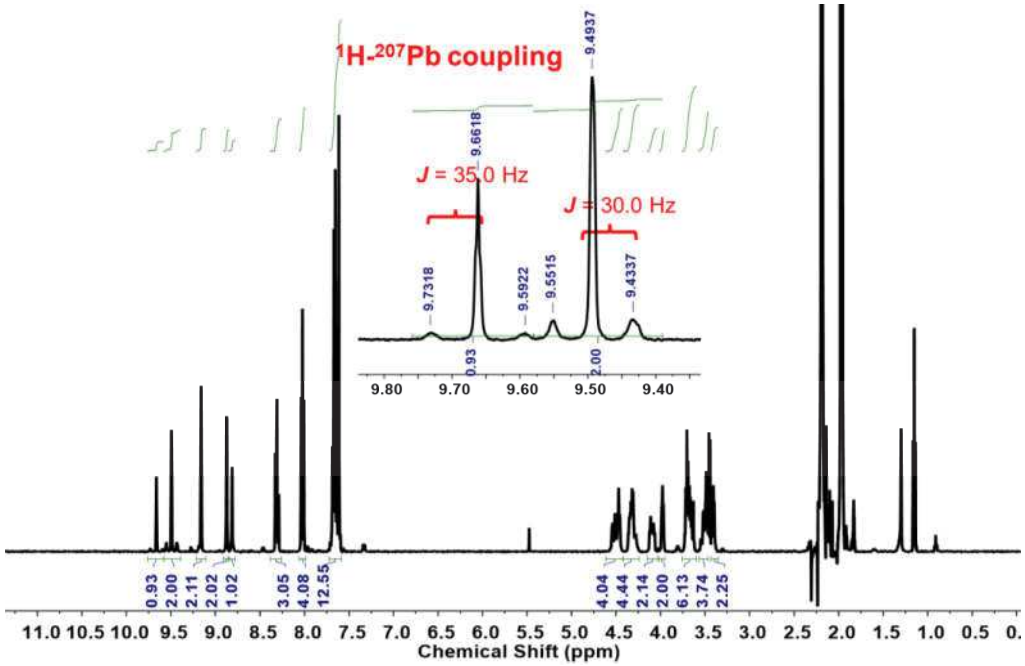

Figure V-7. ^{1}H NMR spectrum (500 MHz, CD_3CN, 23 °C) of complex **bbp-2Pb(II)** showing the single coupling of ^{1}H with ^{207}Pb.

2.3.2. Synthesis of heterometallic cage

The construction of metal-coordinated cages comprising multiple metal ions is of particular interest as the synergic effect between the heterometals could provide promising advantages for catalytic applications.[158] However, the synthesis of such heterometallic complexes requires rational design of the ligands and appropriate stepwise metal ion introduction to avoid the generation of kinetic trapped or homometallic assembled mixtures.

As described above, **cage bbb-Zn(II)** could be obtained either by its separation from isomeric cage mixtures or by metal-templated self-sorting from initial components. It must be mentioned that this unsymmetrical cage provides two different coordination sites that might permit to host two distinct metal ions. Hence, the synthesis of heterobimetallic macrobicyclic complexes was investigated. Addition of Cu(I) (1 equiv.) into a 1/1 MeCN-$CHCl_3$ solution of **cage bbb-Zn(II)** resulted in the formation of heterometallic **cages bbb-Zn(II)-Cu(I)**. The cage complexes were preliminarily characterized preliminarily by ^{1}H NMR spectroscopy (**Figure V-8**).

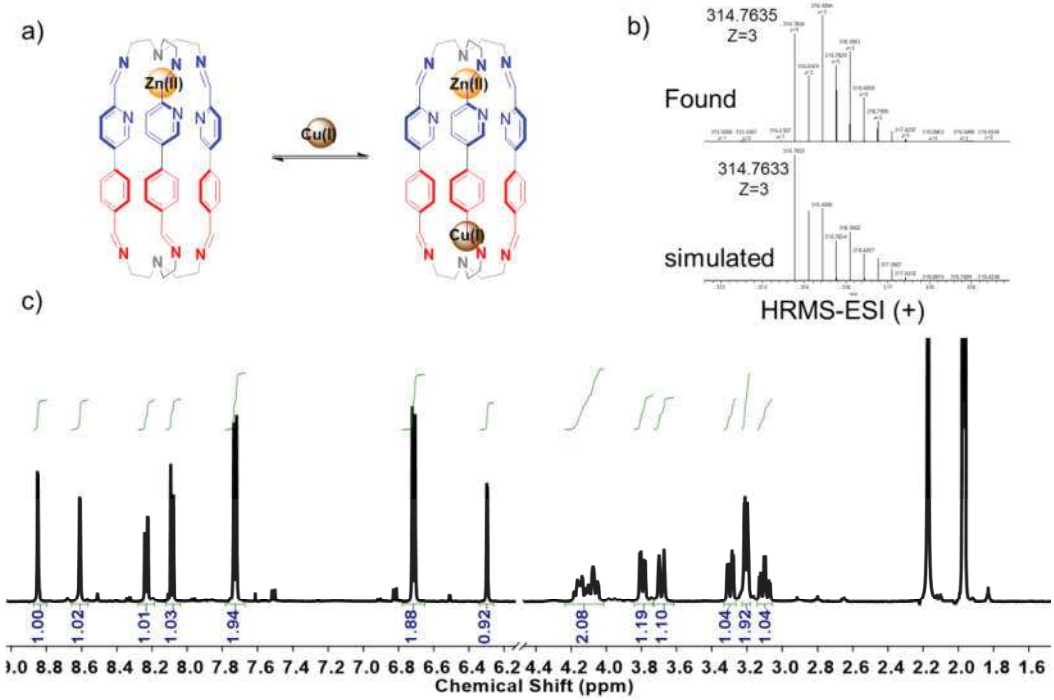

Figure V-8. (a) Chemical structure, (b) ESI(+)-HRMS spectrum and (c) ^{1}H NMR (400 MHz, 60%-40% CD_3CN-$CDCl_3$, 23 °C) spectrum of heterometallic complex **cage bbb-Zn(II)-Cu(I).**

3. Summary of the chapter

In this chapter, the formation of two isomeric cages by imine condensation of unsymmetric dialdehyde **Py-Ph** with **T** has been described. Due to the intrinsic N···N repulsion within the macrobicyclic cavity, cage **bbp** seems to be thermodynamically favoured over its isomeric cage **bbb**. In addition, the different coordination ability of these isomeric cages rendered an ideal scenario for metallo-driven self-sorting. In fact, the imino microenvironment of **cage bbb** seemed to be preferential for the formation of its Zn(II) complex. With this approach, the pure organic **cage bbp** and metal complex **cage bbb-Zn** could be separated by taking advantage of their different solubility. Besides, the dynamic features of imine bonds allowed for the interconversion of **cage bbp** into **cage bbb-Zn** complex in the presence of the metallic core. Similarly, the **cage bbb-Zn** complex could be synthesized through metallo-templated self-assembly of initial components.

The unsymmetrical structural units provided two different chemical environments that were used for heterobimetallic complexations. This work showed that the introduction of isomeric constituents through unsymmetric components into DCLs promoted

interconnections at the challenging stereoisomeric level. The present results may provide a new aspect for developing DCLs of higher complexity with constituents presenting not only “agonistic-antagonistic” relations, but also isomeric interconnections.

Chapter VI. Conclusion and Perspectives

The spontaneous formation of multiple self-organized assemblies via the self-sorting process has a significant impact on the exploration of highly complex biochemical pathways. The study of self-sorting systems under different controlled conditions, and in particular their behaviour under kinetic control, may pave the way to understanding their intrinsic properties and the intricacy of matter. The objective of this thesis was to provide plausible mechanistic insights into the self-sorting behaviour of a set of dynamic covalent libraries of macrocycles and macrobicyclic cages. The four major studies involved:

(i) In Chapter II, the time evolution of imine-based dynamic covalent libraries and their corresponding self-sorting processes involved in the generation of two types of preorganized structures, macrocycles or macrobicyclic cages. On the way to the self-sorted outcome, the formation of heteroleptic intermediates was observed. Thereafter, error-correction processes allowed for the conversion of less stable heteroleptic into homoleptic species through component exchange. A thorough study was also performed for evaluating the importance of structural and stochiometric effects on the final outputs.

(ii) In Chapter III, the self-sorting ability between compounds of two cyclic orders, namely macrocycles and molecular cages. This enabled the generation of [2 × 2] CDNs. Monitoring the kinetic and thermodynamic features of constituents provided an improved understanding of the orthogonal switching from one diagonal to another of the [2 × 2] network occurring as a function of time.

(iii) In Chapter VI, a triply adaptive DCL of macrocyclic constituents was investigated. The composition of the DCL could be modulated by controlling time, the presence of metal ions, and the feeding of an external reactant. By exploiting the adaptative behaviour, the DCL was proved to undergo a cyclic sorting/amplification of constituents to unsorting/statistic distribution process through component exchange.

(iv) Chapter V involved the interconversion between two isomeric dynamic covalent cages that were obtained in the dynamic self-assembly of unsymmetric bridging ligands. Furthermore, the synthesis of their homo- and heterometallic complexes was also attained. The study gave another approach towards reaching higher complexities from simple molecules.

It is also of great importance to be aware of the principles of self-sorting governed by the kinetic and thermodynamic properties of the constituents in the DCLs. The present study applied these basic principles of self-sorting into DCLs, both under kinetic and thermodynamic control. The results illustrated as well how the evolution of self-sorting can be affected by the structural and reactivity properties of initial components.

In conclusion, it can be stated that achieving systems of increasing complexity requires the investigation of constitutional dynamic systems that possess time-dependent adaptive behaviour. This adaptation allows for evolution as a function of time from a non-equilibrium to the equilibrium state, which is of great importance for understanding biological evolution and for developing new types of complex systems.

Chapter VII. Experimental Part

4. General Procedures

4.1. Instrumentation and measurement general procedures

NMR spectra were recorded on Bruker Avance 400 (400 MHz for ^{1}H and 100 MHz for ^{13}C), Bruker Avance III 400 (400 MHz for ^{1}H and 100 MHz for ^{13}C) and Bruker Ascend Spectroscope Avance Neo-500 (500 MHz for ^{1}H and 125 MHz for ^{13}C). MestReNova 10 software was used for the treatment of the NMR spectra. Chemical shifts are given in ppm scale. Residual solvent proton peaks were taken as reference ($CDCl_3$: 7.26 ppm; CD_3CN: 1.94 ppm; TCE-d_2: 6.00 ppm). ^{1}H NMR shifts were measured by using hexamethyldisilane as internal standard. The error in ^{1}H-NMR integration amounts to about ±5%. The coupling constants J are listed in Hz. Peaks are described as singlet (s), doublet (d), triplet (t), doublet of doublet (dd) and multiplet (m). Unless otherwise noted, spectra were recorded at 23 °C

HRMS-ESI (High-Resolution Mass Spectrometry-Electro-Spray Ionisation) mass spectra were recorded by direct injection into a ThermoFisher Exactive Plus EMR Orbitrap mass spectrometer.

X-Ray crystallography was performed at the service de radiocristallographie, University of Strasbourg. The diffraction data collection was carried out on a Bruker PHOTON-III DUO Kappa CPAD diffractometer.

Commercially available chemicals were generally purchased from Sigma-Aldrich, Alfa Aesar, Fluorochem, TCI and were used without further purification. Solvents and reagent of pharmaceutical grade quality were purchased from Carlo Erba, and solvents of spectroscopic grade were purchased from Sigma-Aldrich and Fisher Chemical. $CDCl_3$ was purchased from Euriso-TOP and filtered through basic alumina to remove traces of acid before use.

4.2. Experimental method

4.3. Time-dependent ^{1}H NMR studies

A stock solution of internal standard was made by adding 1.5 μL hexamethyldisilane into 2 mL $CDCl_3$. The stock solutions of amines (**NNN**, **NON**, **NCN**, **T**) and dialdehydes were freshly prepared in $CDCl_3$ and quantified by reference to the internal standard (hexamethyldisilane). For all the cases, dialdehydes and polyamines were mixed in NMR tubes according to reaction conditions indicated in the spectrum. The reaction solution was monitored by ^{1}H NMR until changes reached undetectable levels, at which time it was assumed that equilibrium had been reached. The composition of species was calculated on the basis of the integration of the imine and aromatic proton peaks

NOTE: The time dependent course of the reactions was sensitive to the experimental conditions. The chloroform was passed through basic aluminium oxide to remove trace amounts of acid every time before use. The reaction times $t_{1/2}$ were markedly affected by the aluminium oxide used to treat the $CDCl_3$ (acidity and water) used as the solvent. For example, in the case of the **pPh/NON** system, the half-consumption of **pPh** could vary from 270 min (for old-treated alumina $CDCl_3$) to 720 min (for freshly-treated alumina $CDCl_3$) and the half formation time of the **$pPh_2(NON)_2$** macrocycle from 660 min to 2200 min in the same conditions. We verified that with different qualities of alumina giving these different time dependence curves, the sequence of reaction processes remained the same, with the sequence of three intermediates, and finally, yielded nearly 99% of **$pPh_2(NON)_2$** macrocycle as illustrated in greater detail in section 5.5.6.

4.4. Time-dependent HRMS studies

The 30 mM stock solutions of amines (**NON**, **T**) and dialdehydes were freshly prepared in 50%-50% $CHCl_3$/MeOH. For all the cases, HRMS kinetic experiments were carried out under a dialdehyde concentration of 2 mM and were monitored as a function of time.

5. Chapter II. Rules of Self-Sorting

5.1. Synthesis

5.1.1. Synthesis of 6,6′-diformyl-2,2′-bipyridine (BiPy)

6,6′-diformyl-2,2′-bipyridine was prepared from 6,6′-dimethyl-2,2′-bipyridine according to previously reported procedures. Generally, SeO_2 (3 g, 27 mmol) was added to 6,6′-dimethyl-2,2′-bipyridine (500 mg, 3 mmol) in 40 mL glacial acetic acid. The reaction mixture was refluxed for 48 hours. The oxide residue was separated from the solution by vacuum filtration on a filtered glass funnel. The light brown filtrate was concentrated under reduced pressure, and then the remaining light brown solid was subjected to silica gel column chromatography (CH_2Cl_2/MeOH, 24:1). The product was isolated as a white powder (172 mg, 30%) after evaporation of the solvent. Its properties were consistent with the literature values.[159]

^{1}H NMR (400 MHz, $CDCl_3$): δ 10.19 (s, 2 H), 8.84-8.82 (dd, 2 H), 8.07−8.03 (m, 4 H) ppm.

5.1.2. Synthesis of [1,1':4':1'']Terphenyl-4,4''-dicarbaldehyde

[1,1':4':1'']Terphenyl-4,4''-dicarbaldehyde was prepared via Suzuki–Miyaura Cross-coupling according to previously reported procedures.[160] Its properties were consistent with the literature values.

^{1}H NMR (400 MHz, $CDCl_3$): δ 10.08 (s, 2H), 8.00-7.98 (d, 8Hz, 4H), 7.83-7.81 (d, 8Hz, 4H), 7.77 (s, 4H)

5.1.3. Synthesis of macrocycles

Macrocycles were synthesized according to reference with slight modifications.[161] Normally, **NON** (2,2'-oxybis(ethylamine)) (0.20 mmol) in MeCN (2 mL) was added dropwise in 1 hour at room temperature to dicarboxaldehyde (0.20 mmol) MeCN (8 mL) solution. The mixed solution remained clear for up to 1-2 days, until a white suspension formed. The reaction mixture was stirred at room temperature for another 5 days. The suspension was filtered and the white precipitate collected, washed with MeCN and dried under vacuum.

5.1.4. Synthesis of macrocycle $\mathbf{Fur_2(NON)_2}$

Macrocycle **$Fur_2(NON)_2$** was synthesized directly in $CDCl_3$ without isolation. For this purpose, 2 equiv. **Fur** and 2 equiv. **NON** were mixed in $CDCl_3$ in an NMR tube. The final concentration of **Fur** was 3.6 mM. The characterizations of macrocycles are described below.

5.1.5. Synthesis of macrocycle $\mathbf{TriPh_2(NON)_2}$

[1,1':4':1"]Terphenyl-4,4"-dicarbaldehyde (**TriPh**) (36.41 mg; 0.13 mmol) was dissolved in 8 mL $CHCl_3$. The solution was further diluted with 5 mL MeCN before a MeCN (3 mL) solution of 2,2'-oxybis(ethylamine) (**NON**) (12.90 mg; 0.12 mmol) was added in five portions for 20 minutes. The reaction mixture was stirred at room temperature for 7 days. After removal of the solvent by centrifugation, the crude product was washed with MeCN and dried under vacuum to afford macrocycle **$TriPh_2(NON)_2$** as an ivory solid (38.97 mg, 88 %).

5.1.6. Synthesis of macrobicyclic cages

Macrobicyclic cages were synthesised as described in published work based on this thesis.[122] Macrobicyclic cage **$BiPy_3T_2$** were synthesised in $CDCl_3$ without isolation. For this purpose, 3 equiv. **BiPy** and 2 equiv. **T** (for cage) o were mixed in $CDCl_3$ in an NMR tube. The final concentration of **BiPy** was 3.6 mM.

5.1.7. Synthesis of macrobicyclic cage $\mathbf{TriPh_3T_2}$

[1,1':4':1"]Terphenyl-4,4"-dicarbaldehyde (**TriPh**) (33.15 mg; 0.12 mmol) was dissolved in 8 mL $CHCl_3$. Then, the solution was further diluted with 3 mL MeOH before a MeOH (2 mL) solution of tris(2-aminoethyl)amine (**T**) (11.07 mg; 0.076 mmol) was added in five portions over 20 minutes. The reaction mixture was stirred at room temperature for 3 days. After removal of the solvent by centrifugation, the crude product was washed with 1 mL $CHCl_3$ and MeOH, then dried under vacuum to afford the macrobicyclic cage **$TriPh_3T_2$** as a yellow solid (30.21 mg, 76 %).

5.2. Spectroscopic data of macrocycles and macrobicyclic cages that have been used in chapters II and III

Macrocycle $pPh_2(NON)_2$: The white precipitate was obtained in an isolated yield of 62%.

^{1}H NMR (500 MHz, $CDCl_3$, 25 °C): δ = 8.13 (s, 4H), 7.37 (s, 8H), 3.77 (s, 16H);

^{13}C NMR (125 MHz, $CDCl_3$, 25 °C): δ = 162.50, 137.66, 127.96, 68.77, 60.53;

HRMS (ESI+): m/z calcd for $C_{24}H_{28}N_4O_2$ $[M+H]^+$ 405.2285, found 405.2284.

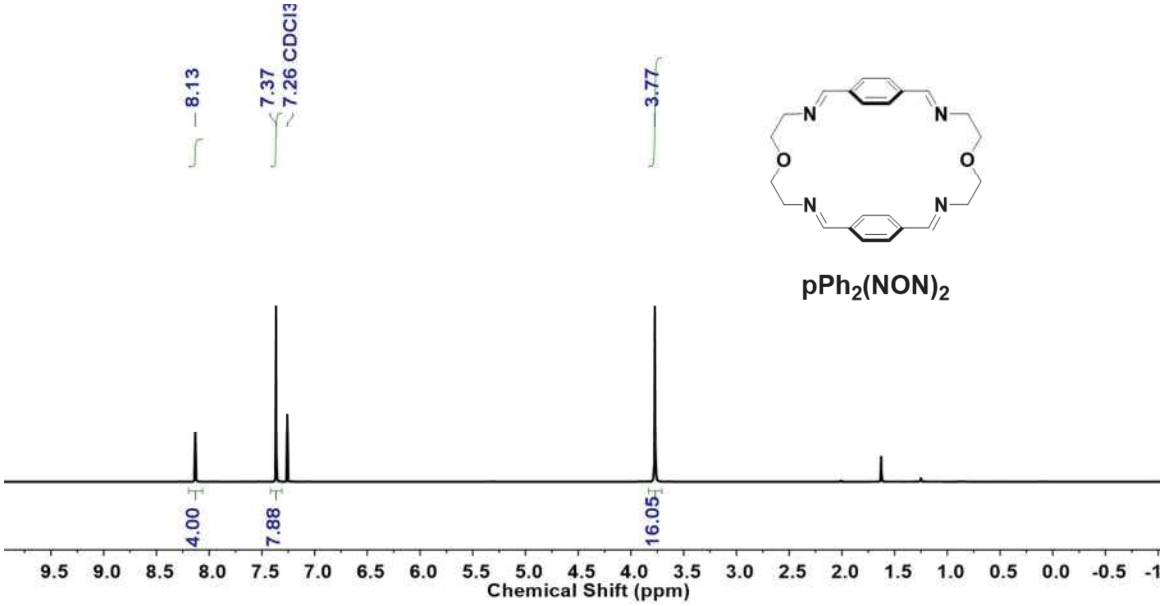

Figure S-II-1. ^{1}H NMR spectrum (500 MHz, $CDCl_3$, 25 °C) of macrocycle **$pPh_2(NON)_2$**.

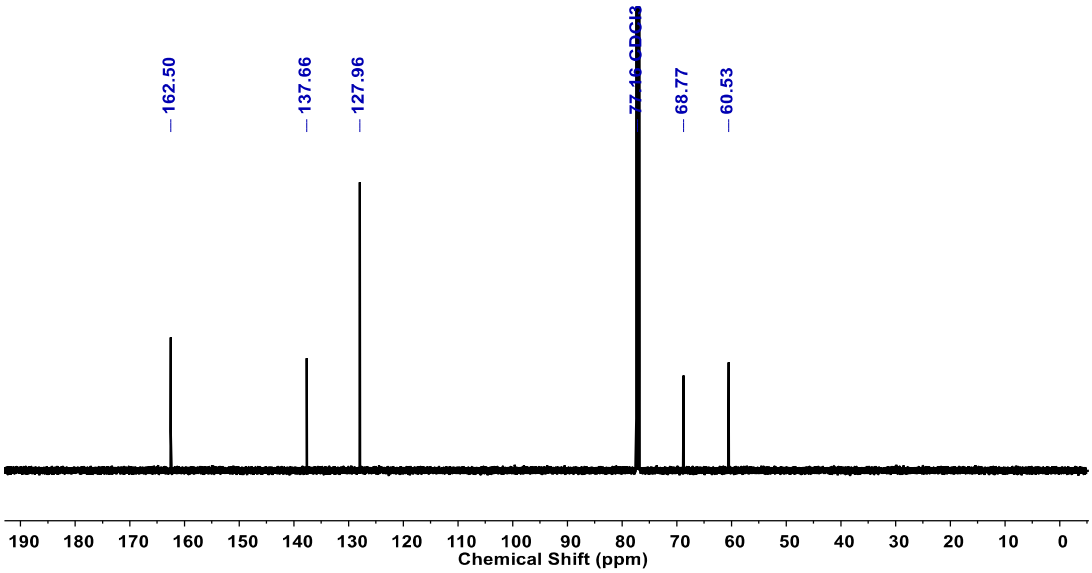

Figure S-II-2. ^{13}C NMR spectrum (125 MHz, $CDCl_3$, 25 °C) of macrocycle **$pPh_2(NON)_2$**.

Macrocycle $Py_2(NON)_2$: The white precipitate was obtained in an isolated yield of 70%.

^{1}H NMR (500 MHz, $CDCl_3$, 25 °C): δ = 8.15 (s, 4H), 7.70 (d, J = 7.7 Hz, 4H), 7.44 (t, J = 7.7 Hz, 2H), 3.78 (s, 16H);

^{13}C NMR (125 MHz, $CDCl_3$, 25 °C): δ = 163.53, 154.02, 136.61, 121.55, 69.02, 61.10;

HRMS (ESI+): m/z calcd for $C_{22}H_{26}N_6O_2$ $[M+2H]^{2+}$ 407.2190, found 407.2188.

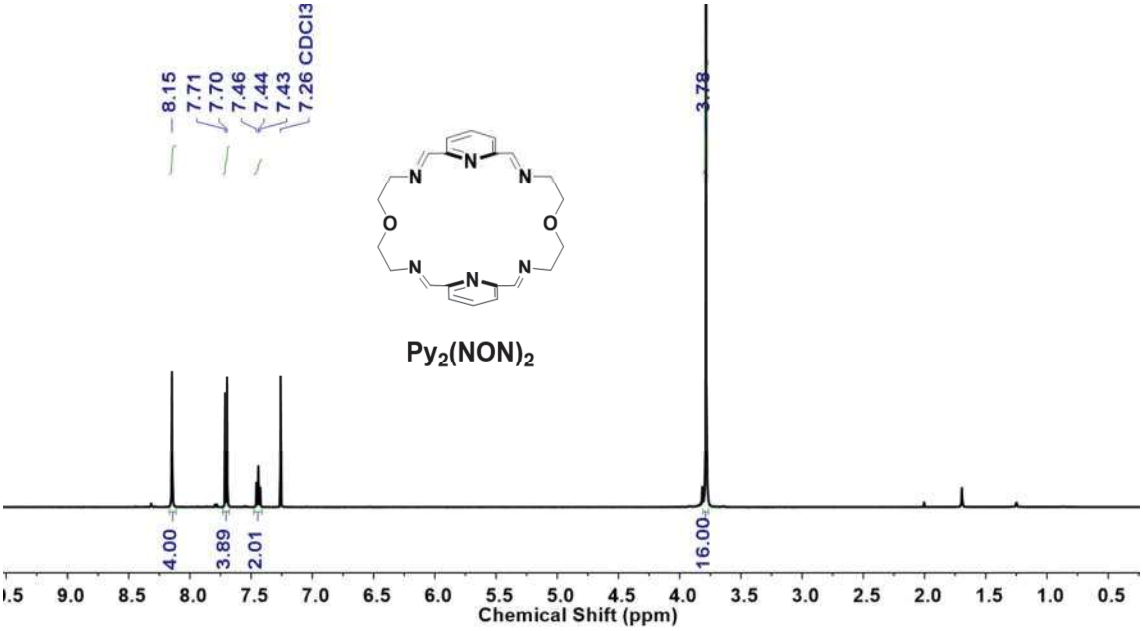

Figure S-II-3. ^{1}H NMR spectrum (500 MHz, $CDCl_3$, 25 °C) of macrocycle **$Py_2(NON)_2$**.

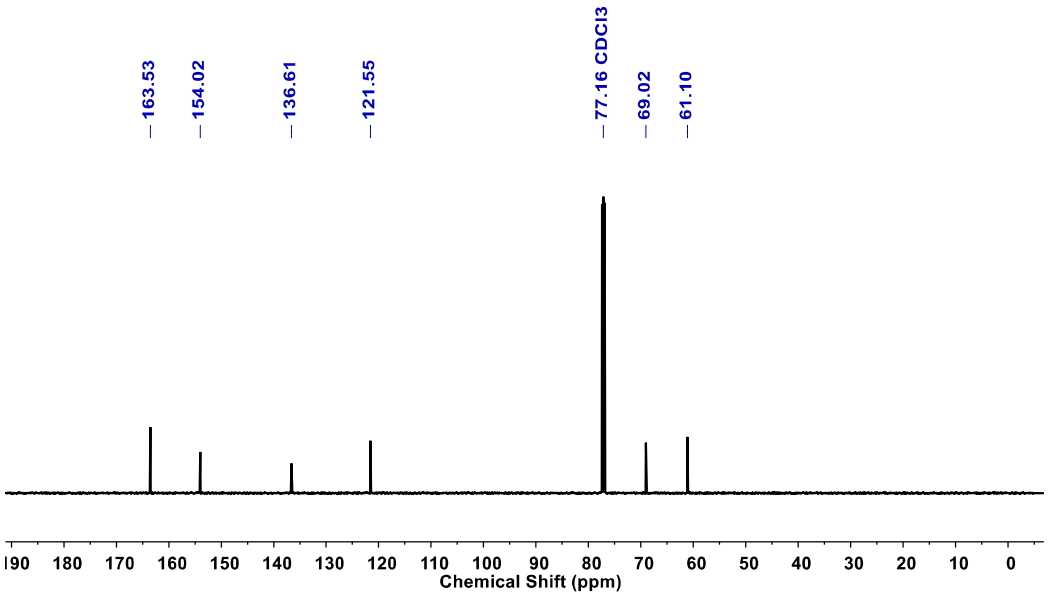

Figure S-II-4. ^{13}C NMR spectra (125 MHz, $CDCl_3$, 25 °C) of macrocycle **$Py_2(NON)_2$**.

Macrocycle $Fur_2(NON)_2$: (^{1}H NMR yield 99%)

^{1}H NMR (500 MHz, $CDCl_3$, 25 °C): δ = 7.96 (s, 4H), 6.68 (s, 4H), 3.77 – 3.74 (m, 8H), 3.72 – 3.71 (m, 8H);

^{13}C NMR (125 MHz, $CDCl_3$, 25 °C): δ = 146.83, 145.85, 107.71, 62.84, 55.09;

HRMS (ESI+): m/z calcd for $C_{20}H_{24}N_4O_4$ $[M+H]^+$ 385.1870, found 385.1870.

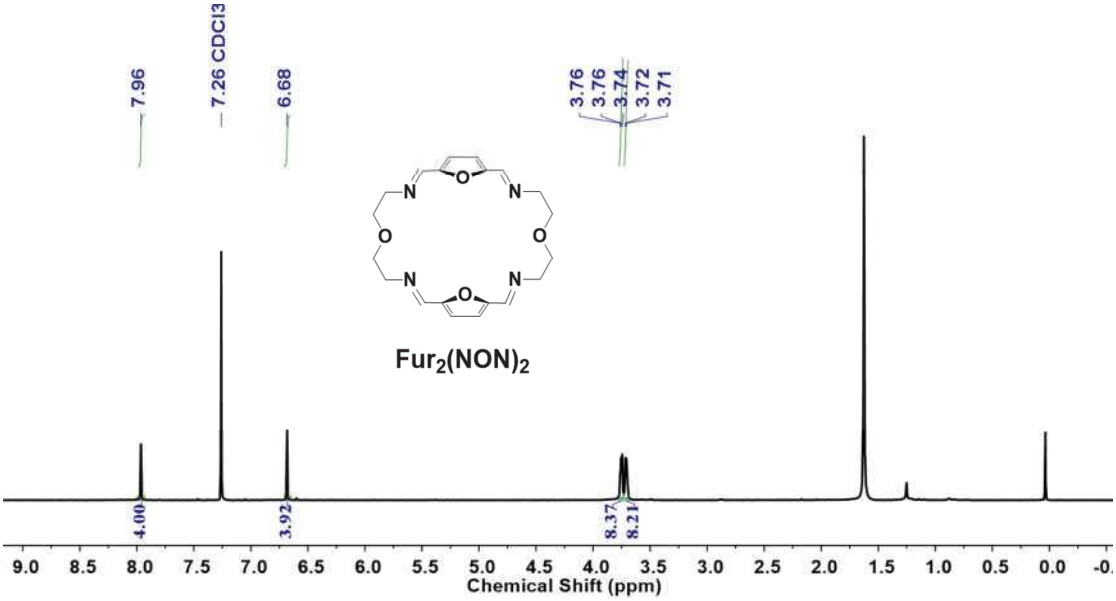

Figure S-II-5. Equilibrium state ^{1}H NMR spectra (500 MHz, $CDCl_3$, 25 °C) of macrocycle **$Fur_2(NON)_2$** obtained *in situ* from 1/1 mixture of **Fur** and **NON.**

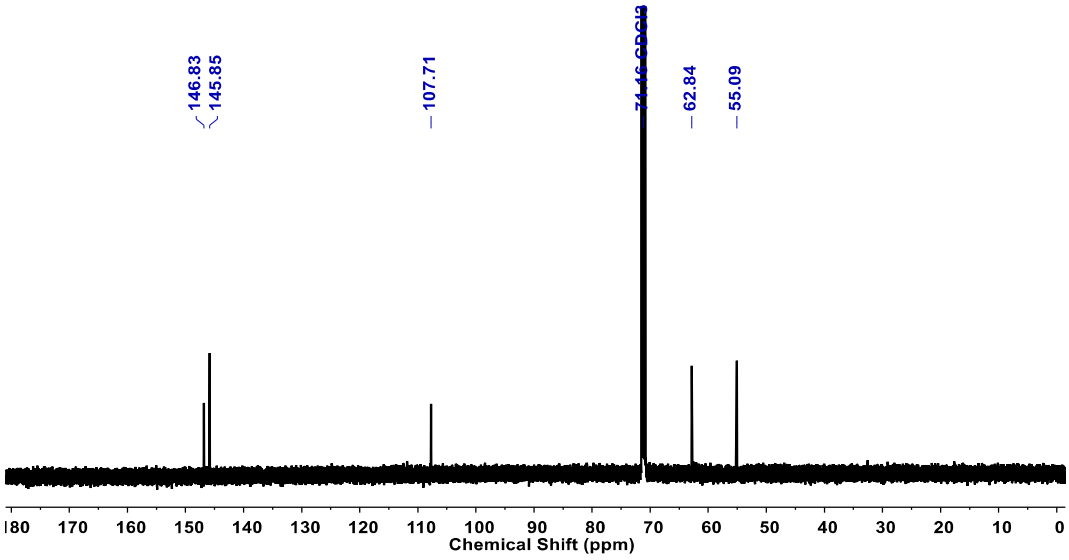

Figure S-II-6. Equilibrium state ^{13}C NMR spectra (125 MHz, $CDCl_3$, 25 °C) of macrocycle **$Fur_2(NON)_2$** obtained *in situ* from 1/1 mixture of **Fur** and **NON.**

Macrocycle $BiPh_2(NON)_2$: The white precipitate was obtained in an isolated yield of 89 %.

^{1}H NMR (500 MHz, $CDCl_3$, 25 °C): δ = 8.19 (s, 4H), 7.43 (d, J = 8.2 Hz, 8H), 7.27 (d, J = 9.5 Hz, 8H) 3.80(s, 16H);

^{13}C NMR (125 MHz, $CDCl_3$, 25 °C): δ = 162.51, 141.94, 135.32, 128.42, 126.85, 69.11, 60.53;

HRMS (ESI+): m/z calcd for $C_{36}H_{36}N_4O_2$ $[M+2H]^{2+}$ 279.1492, found 279.1493.

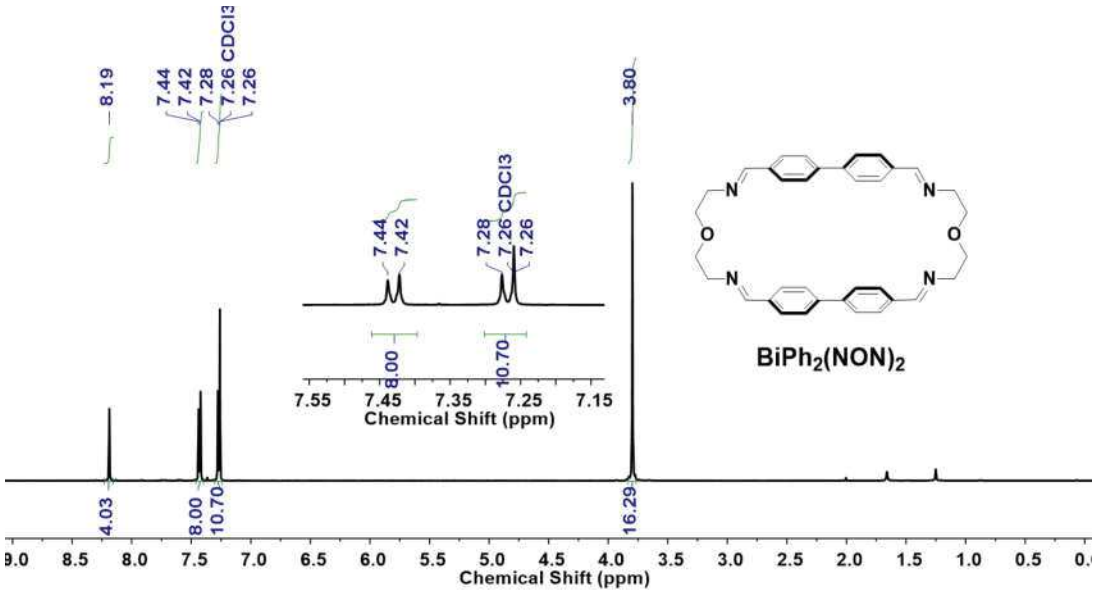

Figure S-II-7. ^{1}H NMR spectra (500 MHz, $CDCl_3$, 25 °C) of macrocycle **$BiPh_2(NON)_2$**.

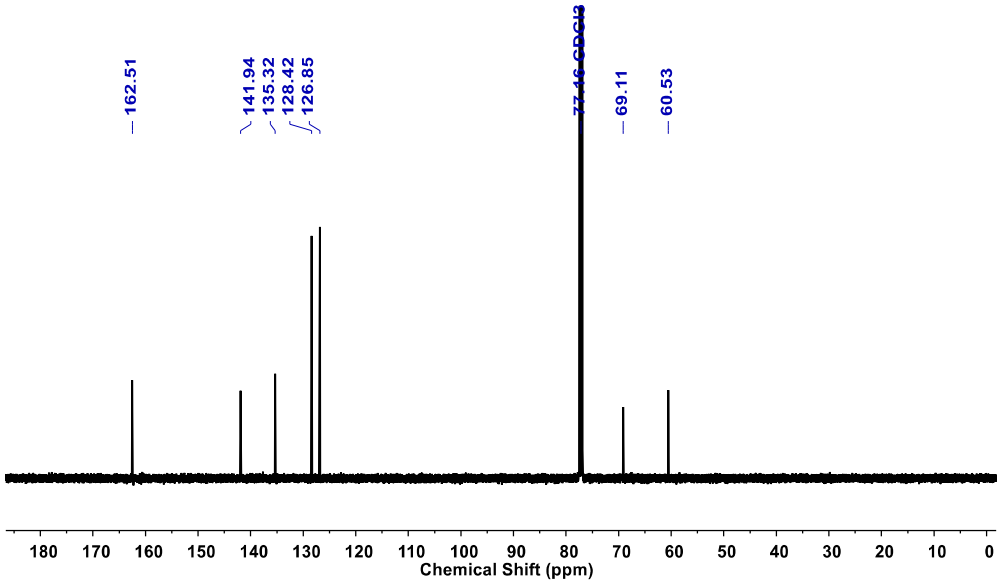

Figure S-II-8. ^{13}C NMR spectra (125 MHz, $CDCl_3$, 25 °C) of macrocycle **$BiPh_2(NON)_2$**.

Macrocycle $BiPy_2(NON)_2$: The white precipitate was obtained in an isolated yield of 78%.

^{1}H NMR (500 MHz, $CDCl_3$, 25 °C): δ = 8.24 (s, 4H), 8.07 (d, J = 7.7 Hz, 4H), 7.66 (d, J = 7.7 Hz, 4H), 7.45 (t, J = 7.7 Hz, 4H), 3.83 (s, 16H);

^{13}C NMR (125 MHz, $CDCl_3$, 25 °C): δ = 164.36, 154.48, 153.61, 136.77, 121.56, 120.25,69.15, 60.95;

HRMS (ESI+): m/z calcd for $C_{32}H_{32}N_8O_2$ $[M+2H]^{2+}$ 281.1397, found 281.1395; $[M+H]^+$ 561.2721, found 561.2712.

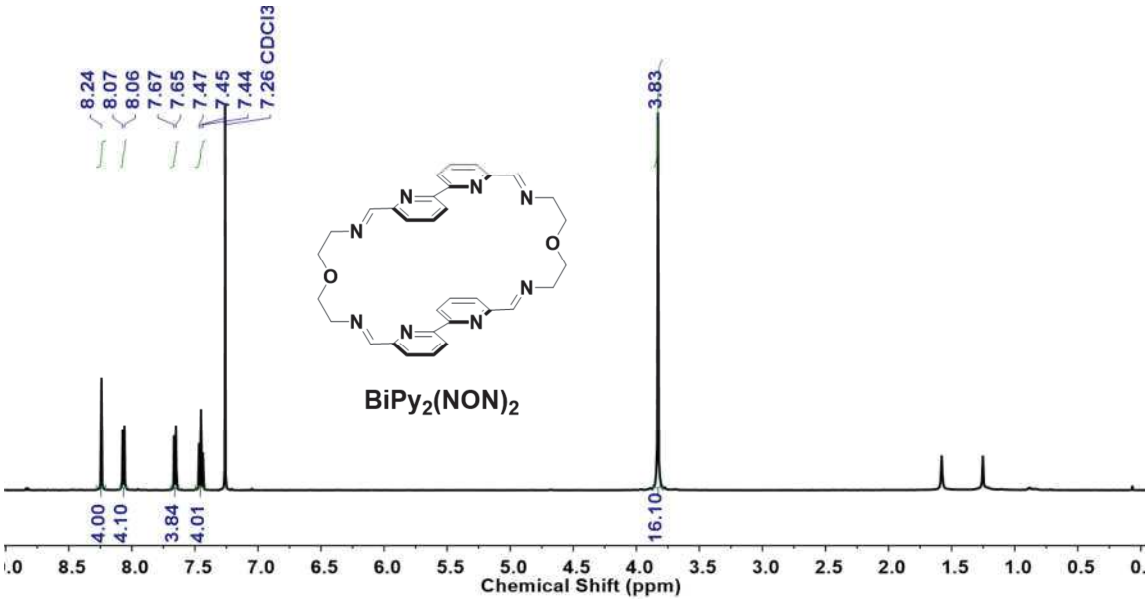

Figure S-II-9. ^{1}H NMR spectra (500 MHz, $CDCl_3$, 25 °C) of macrocycle **$BiPy_2(NON)_2$**.

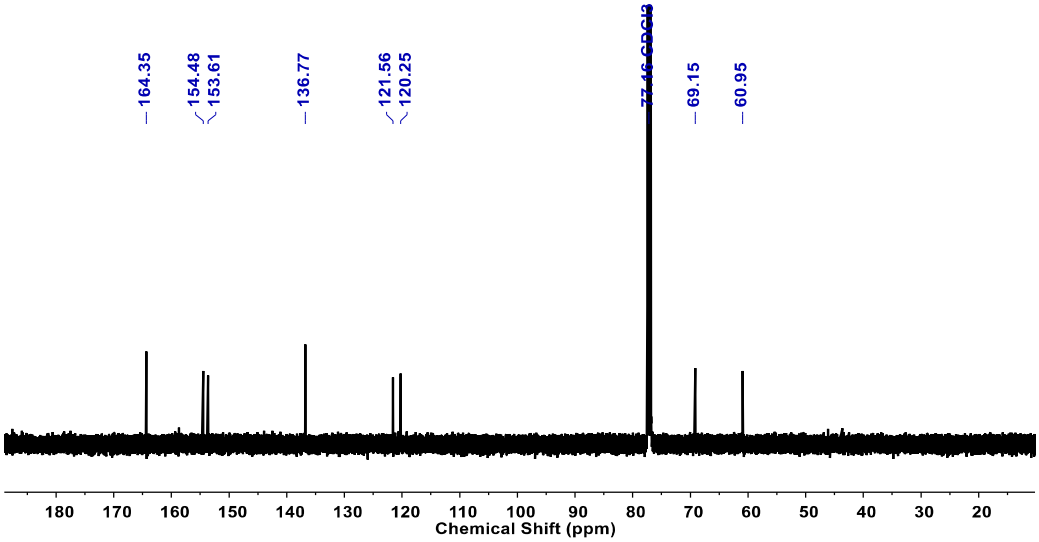

Figure S-II-10. ^{13}C NMR spectra (125 MHz, $CDCl_3$, 25 °C) of macrocycle **$BiPy_2(NON)_2$**.

Macrocycle $E_2(NON)_2$: The white precipitate was obtained in an isolated yield of 61%.

^{1}H NMR (500 MHz, $CDCl_3$, 25 °C): δ = 8.07 (s, 4H), 7.40 (dt, J = 8.7 Hz, 8H), 6.84 (dt, J = 8.6 Hz, 8H), 3.80 – 3.70 (m, 16H);

^{13}C NMR (125 MHz, $CDCl_3$, 25 °C): δ = 161.87,158.30, 131.86, 129.78, 118.64,69.34, 60.63;

HRMS (ESI+): m/z calcd for $C_{36}H_{36}N_4O_4$ $[M+2H]^{2+}$ 295.1441, found 295.1440.

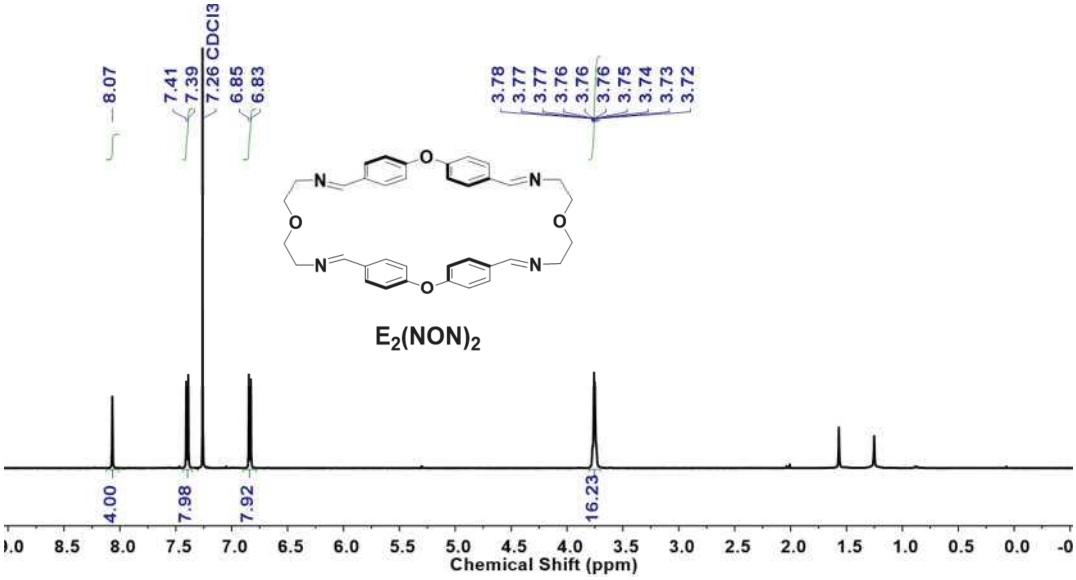

Figure S-II-11. ^{1}H NMR spectra (500 MHz, $CDCl_3$, 25 °C) of macrocycle **$E_2(NON)_2$**.

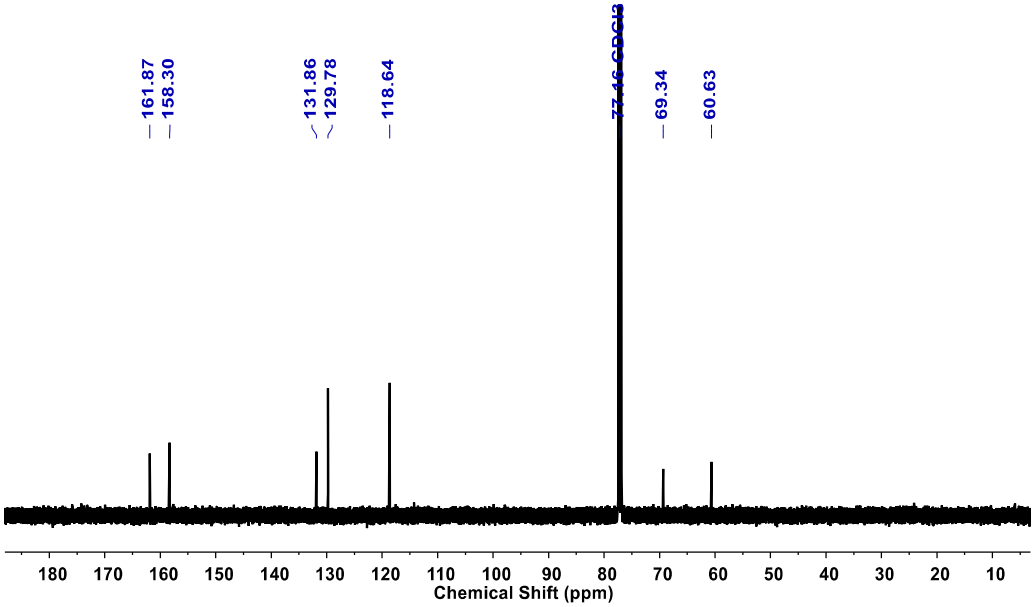

Figure S-II-12. ^{13}C NMR spectra (125 MHz, $CDCl_3$, 25 °C) of macrocycle **$E_2(NON)_2$**.

Macrocycle TriPh$_2$(NON)$_2$:

^{1}H NMR (500 MHz, CDCl$_3$, 25 °C): δ = 8.23 (s, 4H), 7.48 (t, J = 7.5 Hz, 8H), 7.38–7.35 (m, 16H), 3.80–3.70 (m, 16H)

HRMS (ESI+): m/z calcd for $C_{36}H_{36}N_4O_2$ $[M+Na]^+$ 731.3356, found 731.3339

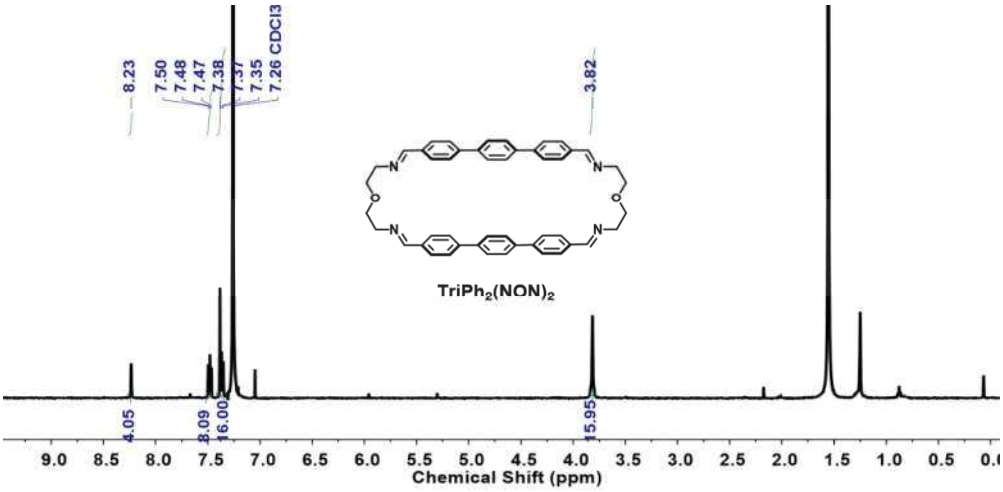

Figure S-II-13. ^{1}H NMR spectra (500 MHz, $CDCl_3$, 25 °C) of macrocycle **TriPh$_2$(NON)$_2$**.

Macrobicyclic cage TriPh$_3$T$_2$:

^{1}H NMR (400 MHz, CDCl$_3$, 25 °C): δ = 8.30 (s, 6H)，7.31-7.22 (m, $CDCl_3$ included)，7.19-7.16 (m, 24H)，3.85 (m, 12H)，2.84 (m, 12H)

HRMS (ESI+): m/z calcd for $[M+H]^+$ 1043.5483, found 1043.5463.

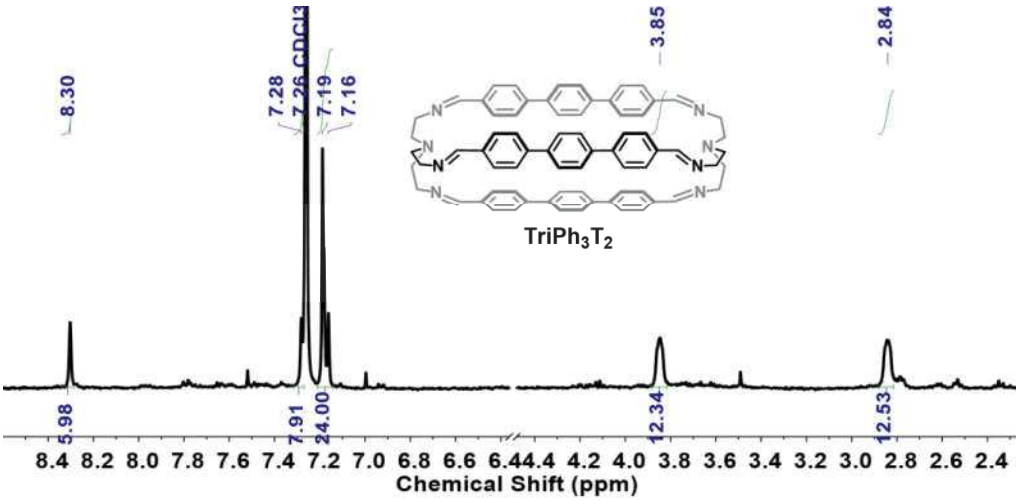

Figure S-II-14. ^{1}H NMR spectra (500 MHz, $CDCl_3$, 25 °C) of macrobicyclic cage **TriPh$_3$T$_2$**

Macrobicyclic cage $BiPy_3T_2$ (^{1}H NMR yield 90%)

^{1}H NMR (500 MHz, $CDCl_3$, 25 °C): δ = 8.07 (d, J = 7.2 Hz, 6H), 7.92, (m, 12H), 7.74 (d, J = 7.7 Hz, 6H), 3.67 (d, J = 4.9 Hz, 12H), 2.97–2.85 (m, 12H).

^{13}C NMR (125 MHz, $CDCl_3$, 25 °C): δ = 163.32, 154.51, 153.51, 136.65, 122.72, 120.34, 59.85, 56.41;

HRMS (ESI+): m/z calcd for $C_{48}H_{48}N_{14}$ $[M+2H]^{2+}$411.2166, found 411.2164; $[M+H]^+$ 821.4259, found 821.4247

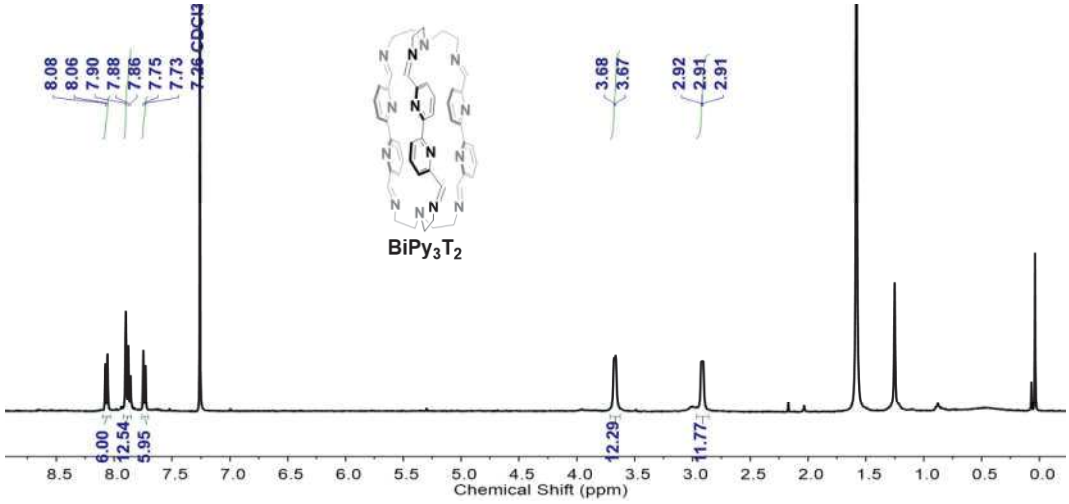

Figure S-II-15. Equilibrium state ^{1}H NMR spectra (400 MHz, $CDCl_3$, 25 °C) of macrobicyclic cage **$BiPy_3T_2$** obtained in situ from 3**BiPy** + 2**T**.

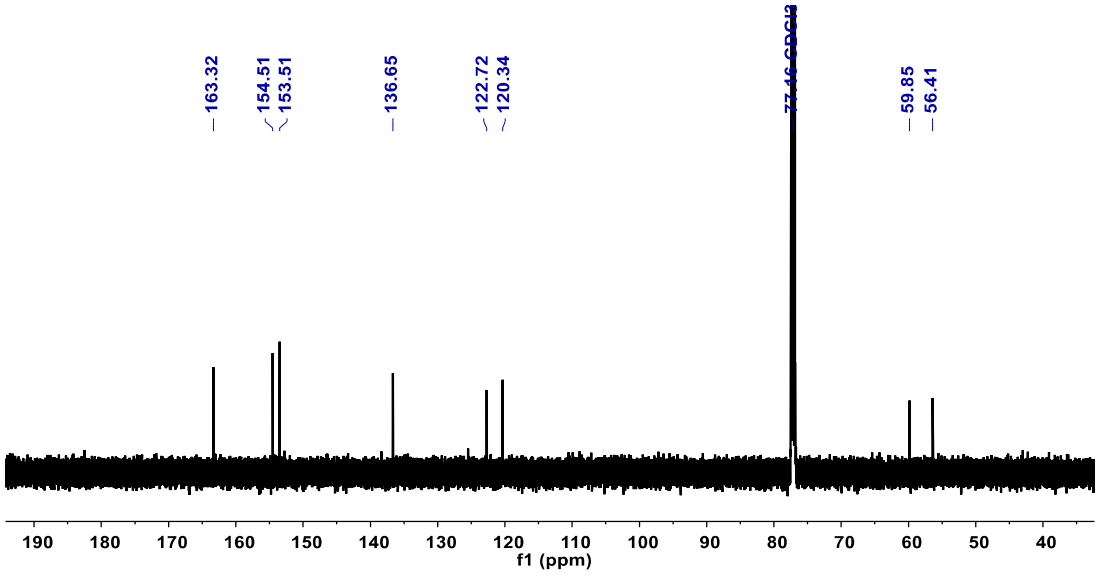

Figure S-II-16. ^{13}C NMR spectra (125 MHz, $CDCl_3$, 25 °C.) of macrobicyclic cage **$BiPy_3T_2$** obtained in situ from 3**BiPy** + 2**T.**

Assignment of intermediate [2Ph+NON]

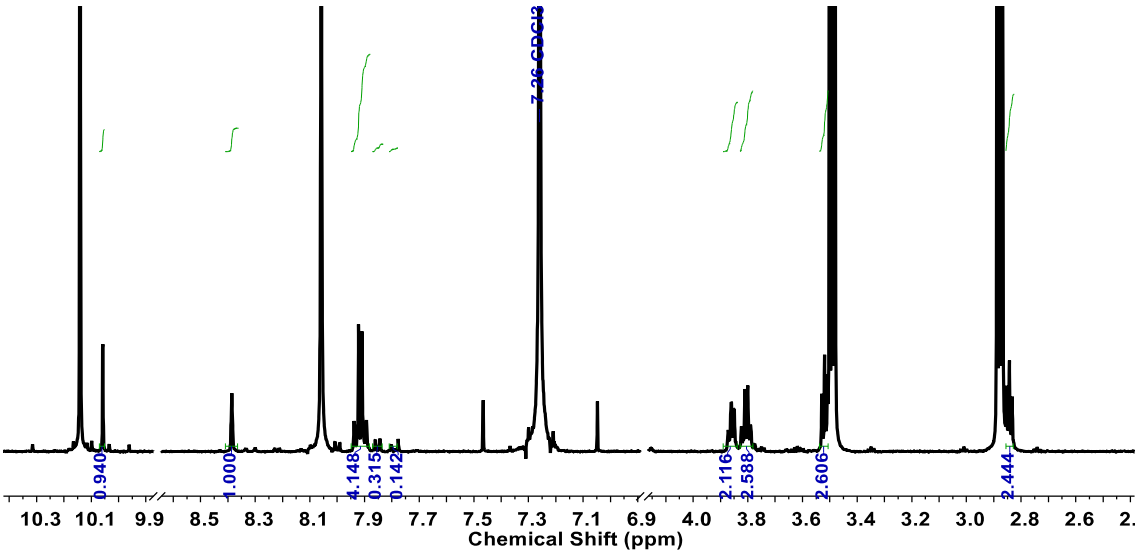

Figure S-II-19. ^{1}H NMR spectrum (500 MHz, $CDCl_3$, 23 °C) of intermediate **[2Ph+NON]**.

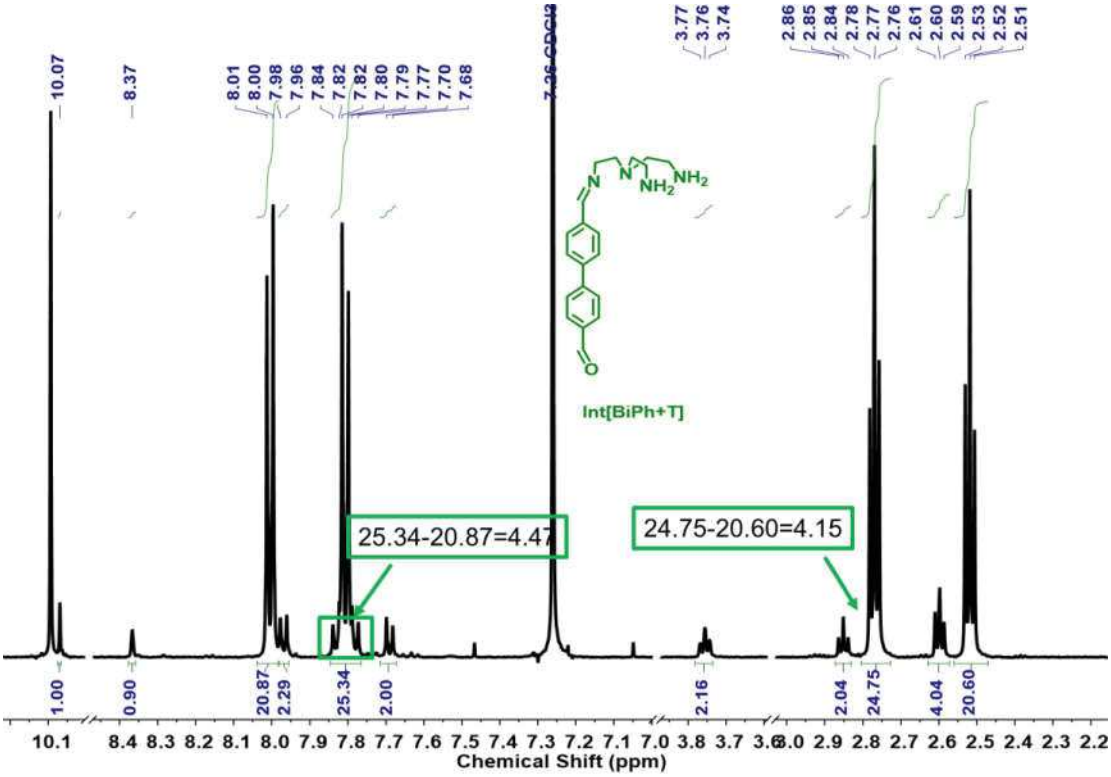

Figure S-II-20. ^{1}H NMR spectra (500 MHz, $CDCl_3$) of the intermediate [**BiPh**+**T**] after 168 min condensation of **BiPh** (3.6 mM) and **T** (2.4 mM).

Assignment of [BiPh+2T] and [2BiPh+2T]

Firstly, the aromatic protons in **[2BiPh+2T]** will be shielded because the protons experience a lower external magnetic field than that of **[BiPh+2T]**, so the chemical shift of the former moves further downfield.

Secondly, the assignment can be verified by a linear equation in two variables based on the integrals shown in Figure S-II-21 shown below. Let the integration of imine protons (H_c) in **[BiPh+2T]** be represented by x, and the integration of imine protons (H_j) in **[2BiPh+2T]** be represented by y. Therefore, the integration of H_f in **[BiPh+2T]** could be represented by $4x$, the integration of H_m in **[2BiPh+2T]** could be represented by y. Considering that only H_m+H_f can give two overlapped triplet signals at chemical shifts 2.61-2.57 ppm, a linear equation with binary variables can be generated: $4x + y = 0.62$, where, from the integrals shown, x, y could have the values of either $x_1 = 0.08$, $y_1 = 0.25$ or $x_2 = 0.25$, $y_2 = 0.08$ but only the former is compatible with the methylene group integral.

Based on the above discussion, we can assign the protons in the spectrum of figure S55.

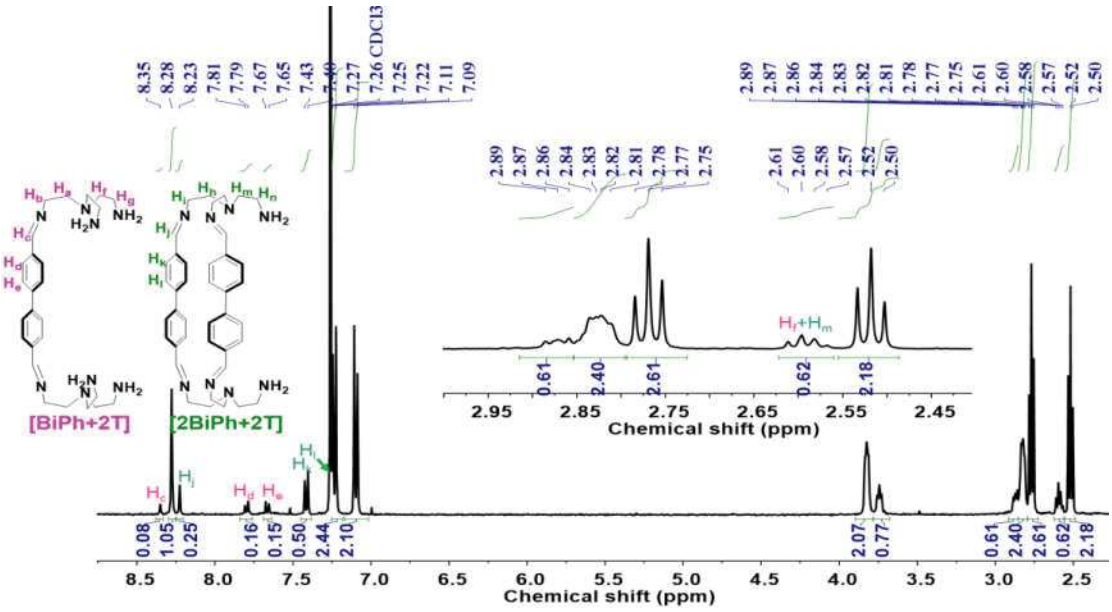

Figure S-II-21. Equilibrated ^{1}H NMR (400 MHz, $CDCl_3$, 23 °C) spectrum of 3**BiPh** + 4**T** reaction at 48 h.

5.3. Formation of the separate macrocycles

5.3.1. Time-dependent ^{1}H NMR spectral changes in the formation of macrocycle $BiPh_2(NON)_2$

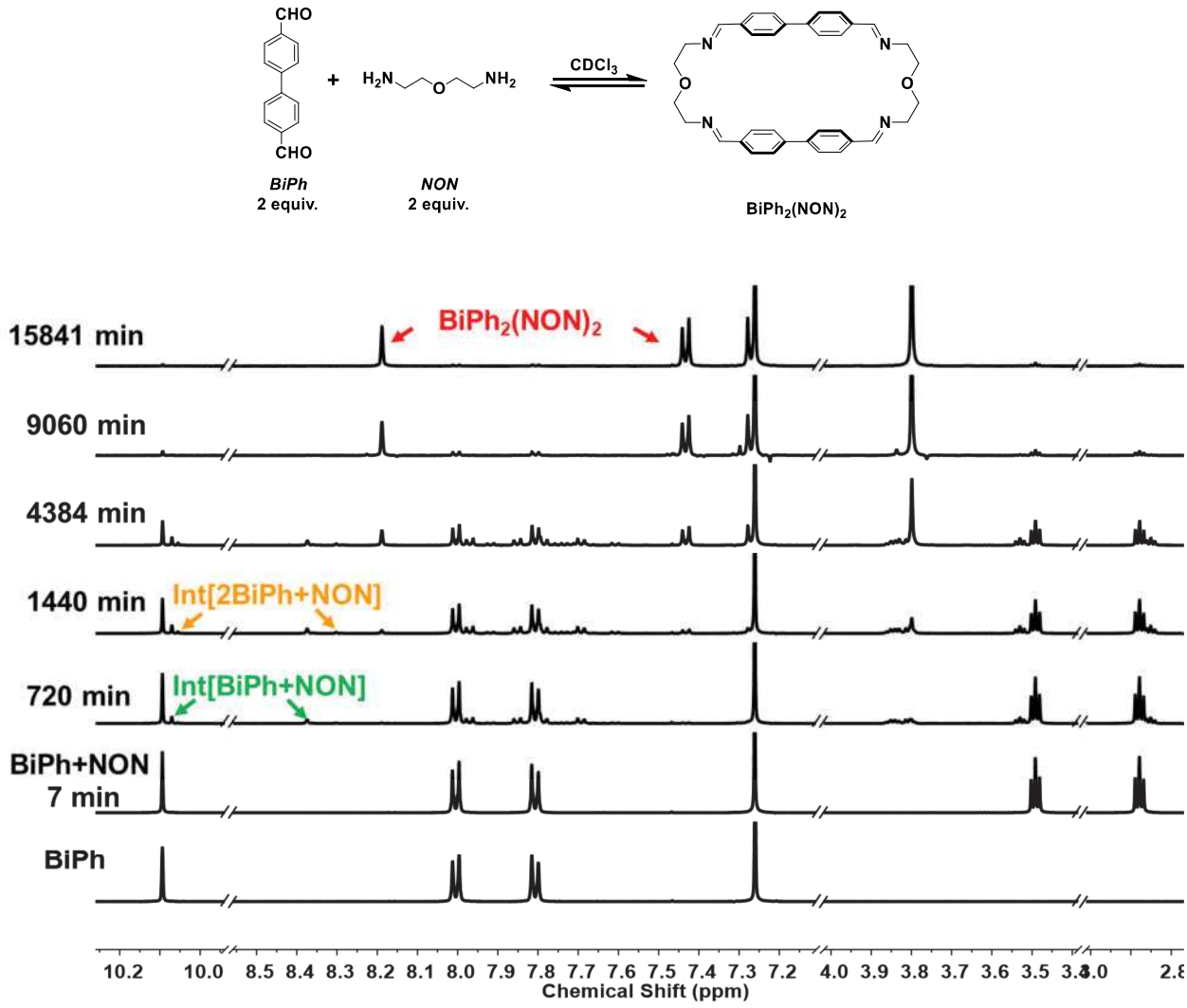

Figure S-II-22. Evolution of the ^{1}H NMR spectra (500 MHz, $CDCl_3$) of a 1/1 mixture of **BiPh** and **NON** (3.6 mM) showing the formation of two intermediates and of the final macrocycle **$BiPh_2(NON)_2$**.

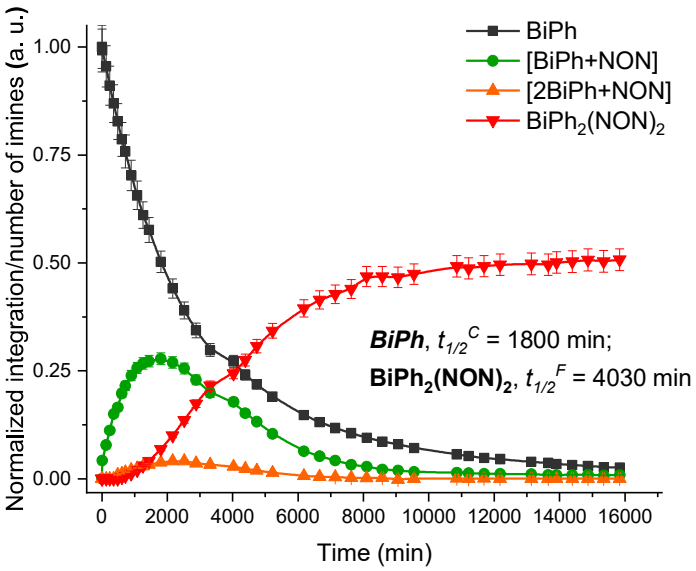

Figure S-II-23. ^{1}H NMR monitoring of the evolution of a 1/1 mixture of components **BiPh** and **NON** (3.6 mM each in $CDCl_3$) as a function of time as obtained from integration of the imine CH=N and dialdehyde CHO proton signals in the 500 MHz ^{1}H NMR spectra.

5.3.2. Time-dependent HRMS changes in the formation of macrocycle $pPh_2(NON)_2$

Table S-II-1. HRMS-ESI assignments of the key species identified during the formation process of macrocycle **$pPh_2(NON)_2$**

Entry	assignment	formula	Combined ion	m/z calcd.	m/z found
1	**NON**	$C_4H_{12}N_2O$	$+H^+$	105.1022	105.1024
			$+Na^+$	127.0842	127.0840
2	[**pPh**+**NON**]-H_2O	$C_{12}H_{16}N_2O_2$	$+H^+$	221.1285	221.1276
			$+Na^+$	243.1104	243.1095
			$+2H^+$	111.0679	N/A[a.]
3	[**pPh**+2**NON**]-$2H_2O$	$C_{16}H_{26}N_4O_2$	$+H^+$	307.2129	307.2115
			$+Na^+$	329.1948	329.1934
			$+2H^+$	154.1101	154.1095
4	[2**pPh**+**NON**]-$2H_2O$	$C_{20}H_{20}N_2O_3$	$+H^+$	337.1547	337.1531
			$+Na^+$	359.1372	359.1351
			$+2H^+$	169.0810	N/A
5	[2**pPh**+2**NON**]-$3H_2O$	$C_{24}H_{30}N_4O_3$	$+H^+$	423.2391	N/A
			$+Na^+$	445.2210	445.2193
			$+2H^+$	212.1232	212.1386

6	[2**pPh**+2**NON**]-4H_2O	$C_{24}H_{28}N_4O_2$	$+H^+$	405.2285	405.2269
			$+Na^+$	427.2104	427.2089
			$+2H^+$	203.1179	N/A

N/A: Unable to read the mass-to-charge ratio (m/z) abundance as it has an extremely close m/z value to other more abundant ion-combined species.

5.3.3. Time-dependent HRMS changes in the formation of macrocycle $BiPh_2(NON)_2$

Table S-II-2. HRMS-ESI assignment of the key species identified during the formation process of macrocycle **$BiPh_2(NON)_2$**

Entry	assignment	formula	Combined ion	m/z calcd.	m/z found
1	**NON**	$C_4H_{12}N_2O$	$+H^+$	105.1022	105.1028
			$+Na^+$	127.0842	127.0844
2	[**BiPh**+**NON**]-H_2O	$C_{18}H_{20}N_2O_2$	$+H^+$	297.1598	297.1597
			$+Na^+$	319.1417	319.1416
			$+2H^+$	149.0835	N/A
3	[**BiPh**+2**NON**]-2H_2O	$C_{22}H_{30}N_4O_2$	$+H^+$	383.2442	383.2412
			$+Na^+$	405.2261	405.2258
			$+2H^+$	192.1257	192.1256
4	[2**BiPh**+**NON**]-2H_2O	$C_{32}H_{28}N_2O_3$	$+H^+$	489.2173	489.2140
			$+Na^+$	511.1992	511.1960
			$+2H^+$	245.1123	N/A
5	[2**BiPh**+2**NON**]-3H_2O	$C_{36}H_{38}N_4O_3$	$+H^+$	575.3017	575.2980
			$+Na^+$	597.2836	597.2926
			$+2H^+$	288.1545	N/A
6	[2**BiPh**+2**NON**]-4H_2O	$C_{36}H_{36}N_4O_2$	$+H^+$	557.2911	557.2876
			$+Na^+$	579.2730	579.2696
			$+2H^+$	279.1492	279.1473

N/A: Unable to read the mass-to-charge ratio (m/z) abundance as it has an extremely close m/z value to other more abundant ion-combined species.

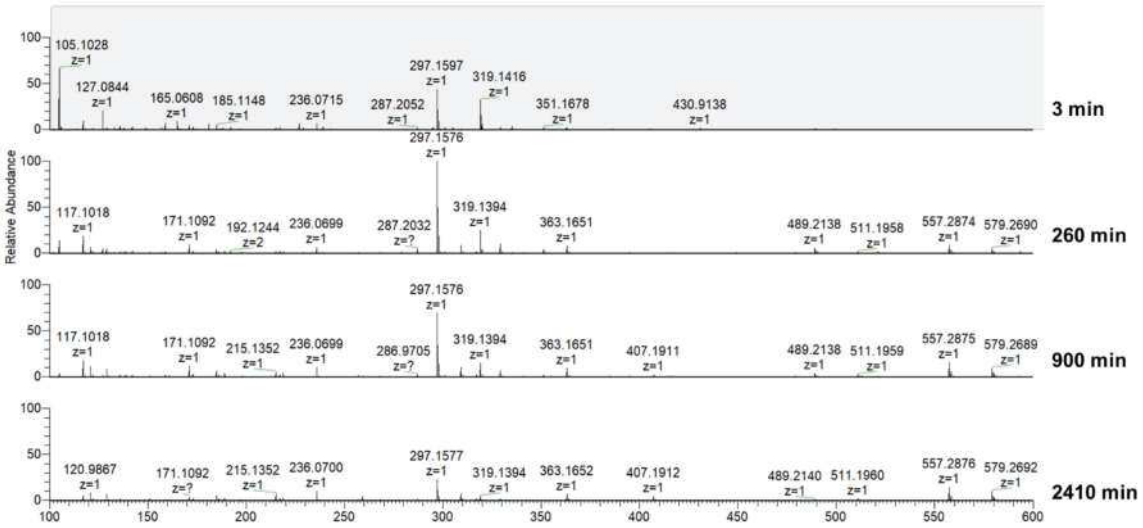

Figure S-II-24. Evolution of the HRMS-ESI spectra of a 1/1 mixture of **BiPh** and **NON** (2 mM each in 50%-50% $CHCl_3$/MeOH) after 3 minutes, 260 minutes, 900 minutes and 2410 minutes.

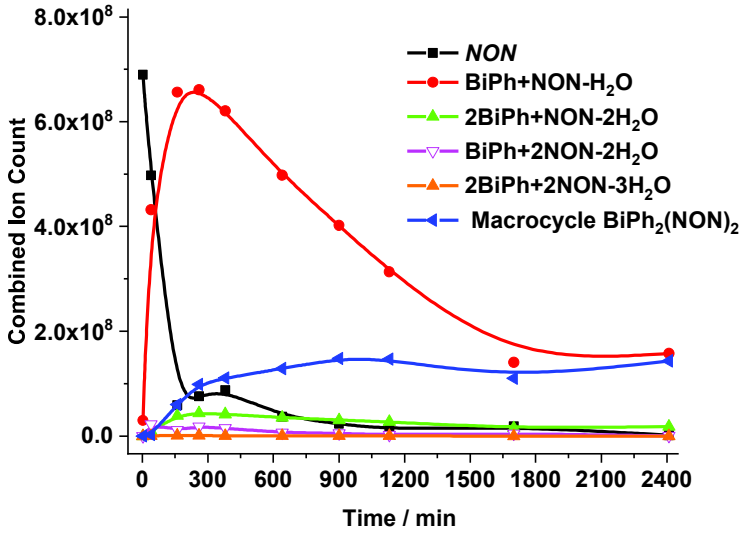

Figure S-II-25. HRMS-ESI monitoring of the evolution of the species generated during the formation of the macrocycle **$BiPh_2(NON)_2$** from **BiPh** and **NON** (2 mM each, 50%-50% $CHCl_3$/MeOH, r.t) as a function of time over 2410 min. NB: These data do not provide quantitative information about the relative amounts of each species identified by its mass, but, taken separately, they display the evolution of a given identified species during the course of the reaction. The curves are added to guide the eye.

5.4. Formation of the separate macrobicyclic cages

5.4.1. Time-dependent ^{1}H NMR of macrobicyclic cage $BiPh_3T_2$

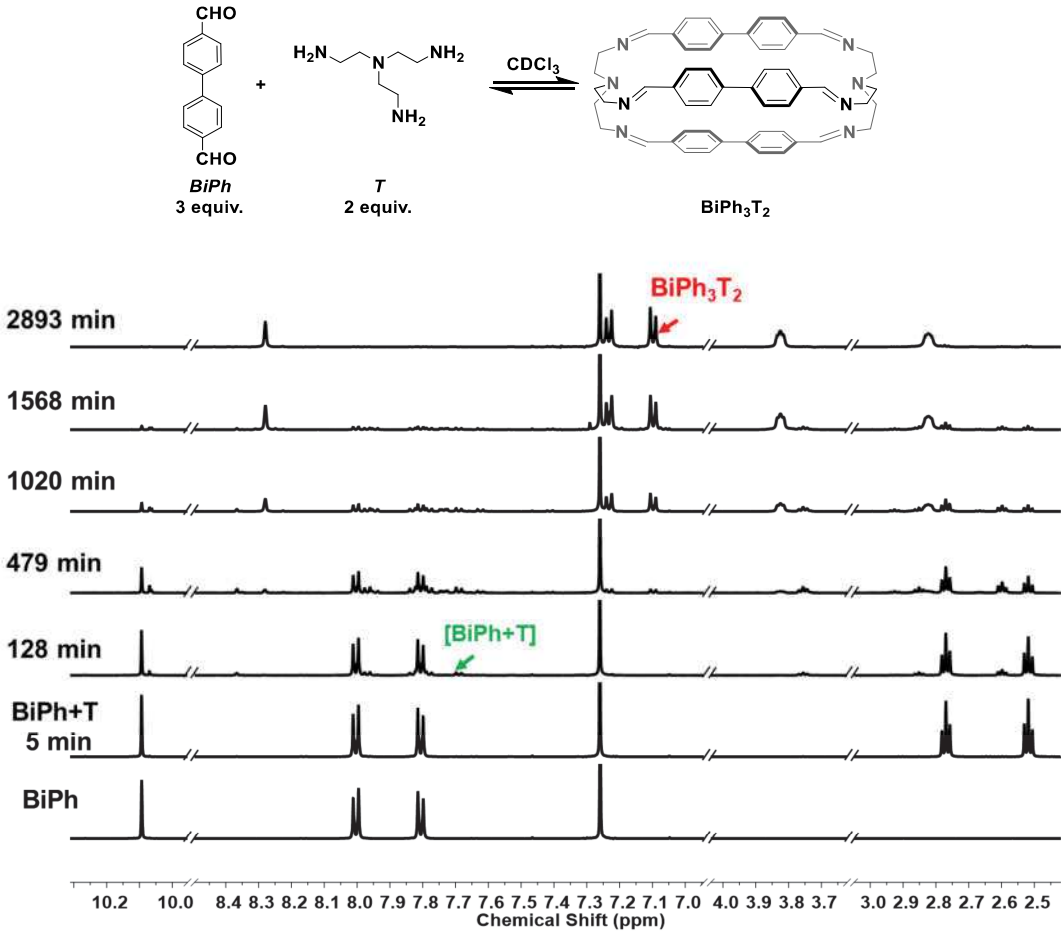

Figure S-II-26. Evolution of the ^{1}H NMR spectra (500 MHz, $CDCl_3$) of a 3/2 mixture of **BiPh** (3.6 mM) and **T** showing the formation of intermediate **[BiPh+T]** and of the final macrobicyclic cage **$BiPh_3T_2$**.

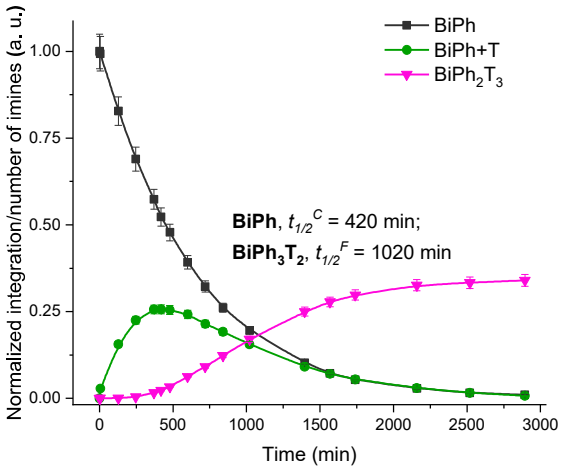

Figure S-II-27. ^{1}H NMR monitoring of the evolution of cage **BiPh$_3$T$_2$** formation as a function of time over 2893 min. Error in ^{1}H-NMR signal integration: ±5%.

5.4.2. Time-dependent HRMS changes in the formation of macrobicyclic cage pPh$_3$T$_2$

Table S-II-3. HRMS-ESI assignment of the key species identified during the formation process of macrocycle **pPh$_3$T$_2$**

Entry	assignment	formula	Combined ion	m/z calcd.	m/z found
1	**T**	$C_6H_{18}N_4$	$+H^+$	147.1604	147.1595
			$+Na^+$	169.1424	169.1413
2	[**pPh**+**T**-H_2O]	$C_{14}H_{22}N_4O$	$+H^+$	263.1866	263.1849
			$+Na^+$	285.1686	285.1666
			$+2H^+$	132.0970	N/A[a.]
4	[2**pPh**+**T**-2H_2O]	$C_{22}H_{26}N_4O_2$	$+H^+$	379.2129	379.2102
			$+Na^+$	401.1948	401.1921
			$+2H^+$	190.1101	N/A
5	[3**pPh**+**T**-3H_2O]	$C_{30}H_{30}N_4O_3$	$+H^+$	495.2391	495.2358
			$+Na^+$	517.2210	517.2171
			$+2H^+$	248.1232	N/A
3	[**pPh**+2**T**-2H_2O]	$C_{20}H_{38}N_8$	$+H^+$	391.3292	391.3265
			$+Na^+$	413.3112	413.3083
			$+2H^+$	196.1682	196.1670
6	[2**pPh**+2**T**-3H_2O]	$C_{28}H_{42}N_8O$	$+H^+$	507.3554	N/A
			$+Na^+$	529.3374	N/A
			$+2H^+$	254.1814	N/A

7	[2**pPh**+2**T**-4H_2O]	$C_{28}H_{40}N_8$	$+H^+$	489.3449	489.3415
			$+Na^+$	511.3268	511.3236
			$+2H^+$	245.1761	245.1744
8	[3**pPh**+2**T**-4H_2O]	$C_{36}H_{46}N_8O_2$	$+H^+$	623.3816	N/A
			$+Na^+$	645.3636	N/A
			$+2H^+$	312.1945	N/A
9	[3**pPh**+2**T**-5H_2O]	$C_{36}H_{44}N_8O$	$+H^+$	605.3711	605.3671
			$+Na^+$	627.3491	627.3530
			$+2H^+$	303.1892	303.1869
10	[3**pPh**+2**T**-6H_2O]	$C_{36}H_{42}N_8$	$+H^+$	587.3605	587.3568
	Cage **pPh_3T_2**		$+Na^+$	609.3425	609.3388
			$+2H^+$	294.1839	294.1820

N/A: Unable to read the mass-to-charge ratio (m/z) abundance as it has an extremely close m/z value to other more abundant ion-combined species.

5.4.3. Time-dependent HRMS changes in the formation of macrobicyclic cage $BiPh_3T_2$

Table S-II-4. HRMS-ESI assignment of the Key Species Identified during the formation process of macrocycle **$BiPh_3T_2$**

Entry	assignment	formula	Combined ion	m/z calcd.	m/z found
1	**T**	$C_6H_{18}N_4$	$+H^+$	147.1604	147.1595
			$+Na^+$	169.1424	169.1413
2	[**BiPh**+**T**-H_2O]	$C_{20}H_{26}N_4O$	$+H^+$	339.2179	339.2156
			$+Na^+$	361.1999	361.1974
			$+2H^+$	170.1126	N/A
4	[2**BiPh**+**T**-2H_2O]	$C_{34}H_{34}N_4O_2$	$+H^+$	531.2755	531.2720
			$+Na^+$	553.2574	553.2539
			$+2H^+$	266.1414	266.1407
5	[3**BiPh**+**T**-3H_2O]	$C_{48}H_{42}N_4O_3$	$+H^+$	723.3330	723.3275
			$+Na^+$	745.3149	745.3104
			$+2H^+$	362.1701	N/A
3	[**BiPh**+2**T**-2H_2O]	$C_{26}H_{42}N_8$	$+H^+$	467.3605	N/A
			$+Na^+$	489.3425	489.3366
			$+2H^+$	234.1839	234.1824
6	[2**BiPh**+2**T**-3H_2O]	$C_{40}H_{50}N_8O$	$+H^+$	659.4180	N/A
			$+Na^+$	681.4000	N/A
			$+2H^+$	330.2127	N/A

7	[2**BiPh**+2**T**-4H_2O]	$C_{40}H_{48}N_8$	$+H^+$	641.4075	641.4027
			$+Na^+$	663.3844	663.3894
			$+2H^+$	321.2052	321.2074
8	[3**BiPh**+2**T**-4H_2O]	$C_{54}H_{58}N_8O_2$	$+H^+$	851.4755	N/A
			$+Na^+$	873.4575	N/A
			$+2H^+$	426.2414	N/A
9	[3**BiPh**+2**T**-5H_2O]	$C_{54}H_{56}N_8O$	$+H^+$	833.4650	833.4509
			$+Na^+$	855.4469	855.4075
			$+2H^+$	417.2361	517.2229
10	[3**BiPh**+2**T**-6H_2O]	$C_{54}H_{54}N_8$	$+H^+$	815.4544	815.4484
	Cage **$BiPh_3T_2$**		$+Na^+$	837.4364	837.4302
			$+2H^+$	408.2308	408.2283

N/A: Unable to read the mass-to-charge ratio (m/z) abundance as it has an extremely close m/z value to other more abundant ion-combined species.

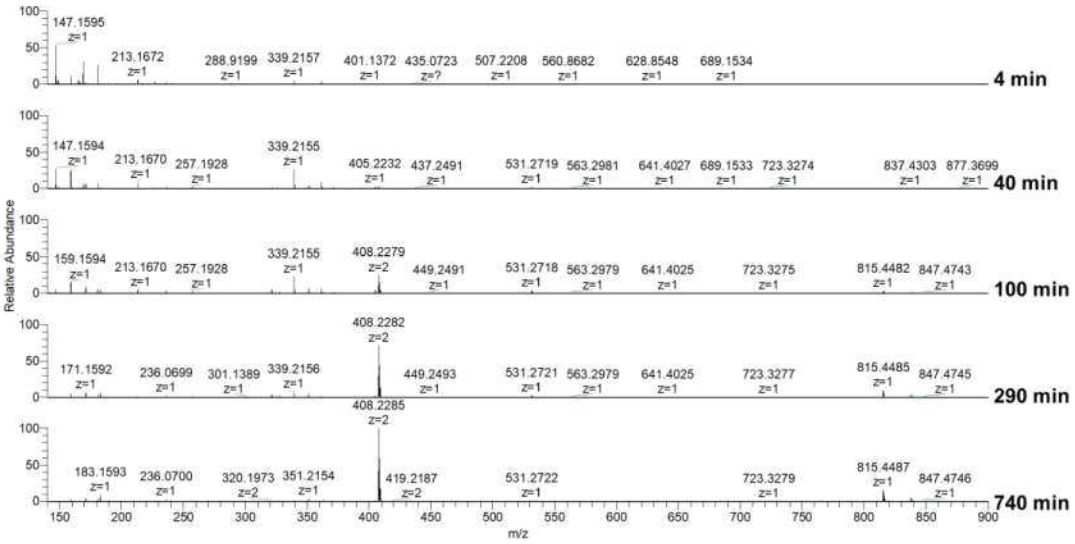

Figure S-II-28. Evolution of the HRMS-ESI spectra of the 3/2 mixture of **BiPh** (2 mM) and **T** in 50%-50% $CHCl_3$/MeOH after 4 minutes, 40 minutes, 100 minutes, 290 minutes and 740 minutes.

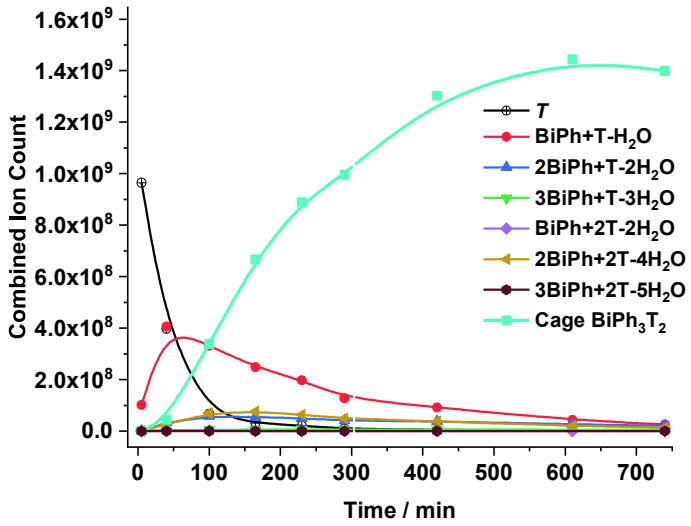

Figure S-II-29. HRMS-ESI kinetic evolution of the species generated during the formation of the macrocycle **$BiPh_3T_2$** from **BiPh** (2 mM) and **T** (50%-50% $CHCl_3$/MeOH, r.t) as a function of time over 740 min. NB: These data do not provide quantitative information about the relative amounts of each species identified by its mass, but, taken separately, they display the evolution of a given identified species during the course of the reaction. The curves are added to guide the eye.

5.5. Self-sorting experiments

5.5.1. Stepwise self-sorting experiment

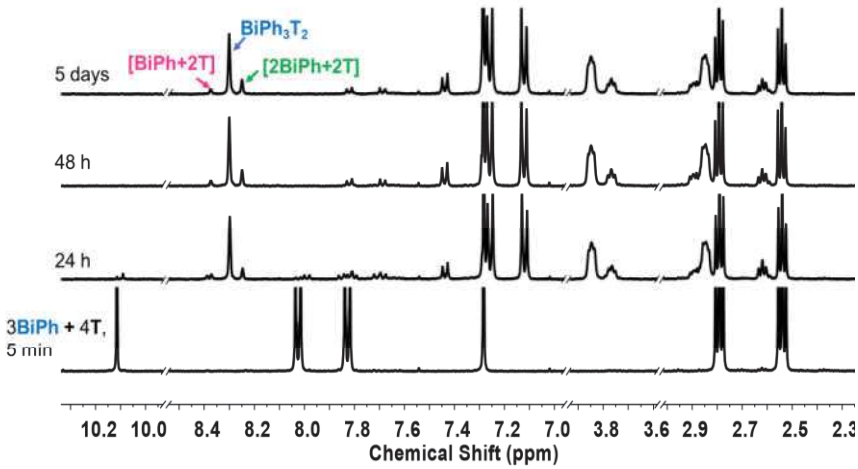

Figure S-II-30. Evolution of the ^{1}H NMR (400 MHz, $CDCl_3$, 23 °C) spectra of 3**BiPh** + 4**T** reaction with dated alumina-treated $CDCl_3$.

5.5.2. Self-sorting experiment 2pPh + 2BiPh + 4NON

Table S-II-5. HRMS-ESI assignments of the key species identified during the self-sorting reaction of 2**pPh** + 2**BiPh** + 4**NON**

Entry	assignment	formula	Combined ion	m/z calcd.	m/z found
1	[**pPh**+**NON**-H_2O]	$C_{12}H_{16}N_2O_2$	$+H^+$	221.1285	221.1283
			$+Na^+$	243.1104	243.1103
2	[**pPh**+2**NON**-$2H_2O$]	$C_{16}H_{26}N_4O_2$	$+H^+$	307.2129	307.2125
			$+Na^+$	329.1948	329.1967
			$+2H^+$	154.1101	154.1100
3	[2**pPh**+**NON**-$2H_2O$]	$C_{20}H_{20}N_2O_3$	$+H^+$	337.1547	337.1542
			$+Na^+$	359.1372	359.1362
			$+2H^+$	169.0810	N/A
4	[2**pPh**+2**NON**-$3H_2O$]	$C_{24}H_{30}N_4O_3$	$+H^+$	423.2391	423.2386
			$+Na^+$	445.2210	445.2118
			$+2H^+$	212.1232	212.1392
5	[2**pPh**+2**NON**-$4H_2O$] **$pPh_2(NON)_2$**	$C_{24}H_{28}N_4O_2$	$+H^+$	405.2285	405.2279
			$+Na^+$	427.2104	427.2099
			$+2H^+$	203.1179	203.1176
6	[**BiPh**+**NON**-H_2O]	$C_{18}H_{20}N_2O_2$	$+H^+$	297.1598	297.1593
			$+Na^+$	319.1417	319.1410
			$+2H^+$	149.0835	149.0834
7	[**BiPh**+2**NON**-$2H_2O$]	$C_{22}H_{30}N_4O_2$	$+H^+$	383.2442	N/A
			$+Na^+$	405.2261	405.2281
			$+2H^+$	192.1257	192.1254
8	[2**BiPh**+**NON**-$2H_2O$]	$C_{32}H_{28}N_2O_3$	$+H^+$	489.2173	489.2166
			$+Na^+$	511.1992	511.2074
			$+2H^+$	245.1123	N/A
9	[2**BiPh**+2**NON**-$3H_2O$]	$C_{36}H_{38}N_4O_3$	$+H^+$	575.3017	N/A
			$+Na^+$	597.2836	N/A
			$+2H^+$	288.1545	N/A
10	[2**BiPh**+2**NON**-$4H_2O$] **$BiPh_2(NON)_2$**	$C_{36}H_{36}N_4O_2$	$+H^+$	557.2911	557.2904
			$+Na^+$	579.2730	579.2722
			$+2H^+$	279.1492	279.1490
11	[**pPh**+**BiPh**+**NON**-$2H_2O$]	$C_{26}H_{24}N_2O_3$	$+H^+$	413.1860	413.1852
			$+Na^+$	435.1679	435.1672
			$+2H^+$	207.0966	N/A

12	[**pPh**+**BiPh**+2**NON**-3H_2O]	$C_{30}H_{34}N_4O_3$	$+H^+$	499.2704	499.2697
			$+Na^+$	521.2523	N/A
			$+2H^+$	250.1388	250.1384
13	[**pPh**+**BiPh**+2**NON**-4H_2O]	$C_{30}H_{32}N_4O_2$	$+H^+$	481.2598	481.2592
	(pPh)(BiPh)(NON)$_2$		$+Na^+$	503.2417	503.2413
			$+2H^+$	241.1335	241.1331

N/A: Unable to read the mass-to-charge ratio (m/z) abundance as it has an extremely close m/z value to other more abundant ion-combined species.

5.5.3. Self-sorting experiment 3pPh + 3BiPh + 4T

Table S-II-6. HRMS-ESI assignments of the key species identified during the self-sorting reaction of 3**pPh** + 3**BiPh** + 4**T**.

Entry	assignment	formula	Combined ion	m/z calcd.	m/z found
1	**T**	$C_6H_{18}N_4$	$+H^+$	147.1604	147.1597
			$+Na^+$	169.1424	169.1415
2	[**pPh**+**T**-H_2O]	$C_{14}H_{22}N_4O$	$+H^+$	263.1866	263.1852
			$+Na^+$	285.1686	285.1671
			$+2H^+$	132.0970	N/A
3	[2**pPh**+**T**-2H_2O]	$C_{22}H_{26}N_4O_2$	$+H^+$	379.2129	379.2100
			$+Na^+$	401.1948	401.1924
			$+2H^+$	190.1101	N/A
4	[3**pPh**+**T**-3H_2O]	$C_{30}H_{30}N_4O_3$	$+H^+$	495.2391	495.2362
			$+Na^+$	517.2210	N/A
			$+2H^+$	248.1232	N/A
5	[**pPh**+2**T**-2H_2O]	$C_{20}H_{38}N_8$	$+H^+$	391.3292	391.3262
			$+Na^+$	413.3112	413.3083
			$+2H^+$	196.1682	196.1671
6	[2**pPh**+2**T**-4H_2O]	$C_{28}H_{40}N_8$	$+H^+$	489.3449	489.3417
			$+Na^+$	511.3268	511.3236
			$+2H^+$	245.1761	245.1745
7	[3**pPh**+2**T**-6H_2O]	$C_{36}H_{42}N_8$	$+H^+$	587.3605	587.3567
	Cage **pPh$_3$T$_2$**		$+Na^+$	609.3425	609.3391
			$+2H^+$	294.1839	294.1820
8	[**BiPh**+**T**-H_2O]	$C_{20}H_{26}N_4O$	$+H^+$	339.2179	339.2156
			$+Na^+$	361.1999	361.1974

			+2H$^+$	170.1126	N/A
9	[2**BiPh**+**T**-2H$_2$O]	$C_{34}H_{34}N_4O_2$	+H$^+$	531.2755	531.2723
			+Na$^+$	553.2574	553.2543
			+2H$^+$	266.1414	N/A
10	[3**BiPh**+**T**-3H$_2$O]	$C_{48}H_{42}N_4O_3$	+H$^+$	723.3330	723.3093
			+Na$^+$	745.3149	N/A
			+2H$^+$	362.1701	362.1998
11	[**BiPh**+2**T**-2H$_2$O]	$C_{26}H_{42}N_8$	+H$^+$	467.3605	467.3576
			+Na$^+$	489.3425	N/A[a]
			+2H$^+$	234.1839	234.1827
12	[2**BiPh**+2**T**-4H$_2$O]	$C_{40}H_{48}N_8$	+H$^+$	641.4075	641.4045
			+Na$^+$	663.3844	663.3864
			+2H$^+$	321.2052	321.2054
13	[3**BiPh**+2**T**-6H$_2$O]	$C_{54}H_{54}N_8$	+H$^+$	815.4544	815.4494
	Cage **BiPh$_3$T$_2$**		+Na$^+$	837.4364	837.4312
			+2H$^+$	408.2308	408.2308
14	[**pPh**+**BiPh**+**T**-2H$_2$O]	$C_{28}H_{30}N_4O_2$	+H$^+$	455.2442	455.2415
			+Na$^+$	477.2261	477.2226
			+2H$^+$	228.1257	N/A
15	[2**pPh**+**BiPh**+**T**-3H$_2$O]	$C_{36}H_{34}N_4O_3$	+H$^+$	571.2704	571.2659
			+Na$^+$	593.2523	N/A
			+2H$^+$	286.1388	N/A
16	[**pPh**+2**BiPh**+**T**-3H$_2$O]	$C_{42}H_{38}N_4O_3$	+H$^+$	647.3017	647.2968
			+Na$^+$	669.2836	N/A
			+2H$^+$	324.1545	N/A
17	[**pPh**+**BiPh**+2**T**-3H$_2$O]	$C_{34}H_{46}N_8O$	+H$^+$	583.3867	583.3823
			+Na$^+$	605.3687	605.3699
			+2H$^+$	292.1970	292.1949
18	[**pPh**+**BiPh**+2**T**-4H$_2$O]	$C_{34}H_{44}N_8$	+H$^+$	565.3762	565.3561
			+Na$^+$	587.3581	N/A
			+2H$^+$	283.1917	283.1897
19	[2**pPh**+**BiPh**+2**T**-5H$_2$O]	$C_{42}H_{48}N_8O$	+H$^+$	681.4024	681.3974
			+Na$^+$	703.3843	7.3.3795
			+2H$^+$	341.2048	341.2025
20	[**pPh**+2**BiPh**+2**T**-4H$_2$O]	$C_{48}H_{54}N_8O_2$	+H$^+$	775.4442	N/A
			+Na$^+$	797.4262	797.4228
			+2H$^+$	388.2258	388.2229
21	[**pPh**+2**BiPh**+2**T**-5H$_2$O]	$C_{48}H_{52}N_8O$	+H$^+$	757.4337	757.4284

			+Na^+	779.4156	779.4086
			+$2H^+$	379.2205	379.2188
22	[**pPh**+2**BiPh**+2**T**-6H_2O]	$C_{48}H_{50}N_8$	+H^+	739.4231	739.4170
	Cage**(pPh)(BiPh)$_2$T$_2$**		+Na^+	761.4051	761.3801
			+$2H^+$	370.2152	370.2128

N/A: Unable to read the mass-to-charge ratio (m/z) abundance as it has an extremely close m/z value to other more abundant ion-combined species.

5.5.4. Self-sorting experiment 2pPh + 2BiPh + 2TriPh + 6NON

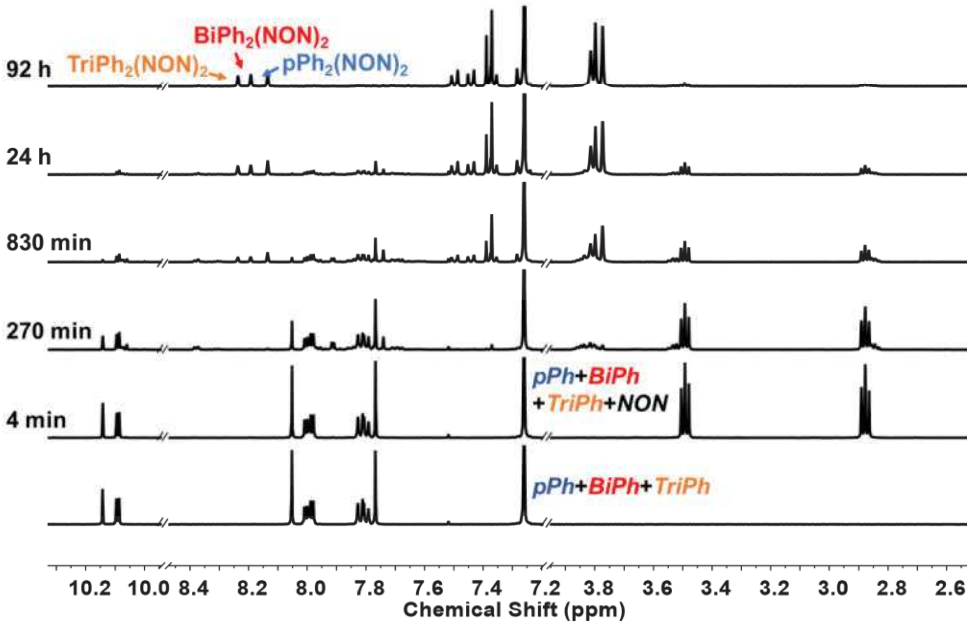

Figure S-II-31. Evolution of the ^{1}H NMR (400 MHz, $CDCl_3$, 40 °C) spectra of 2**pPh** + 2**Biph** + 2**Triph** + 6**NON** ([**pPh**]$_0$ = [**BiPh**]$_0$ = [**TriPh**]$_0$ = 1.0 mM, [**NON**]$_0$ =3.0 mM).

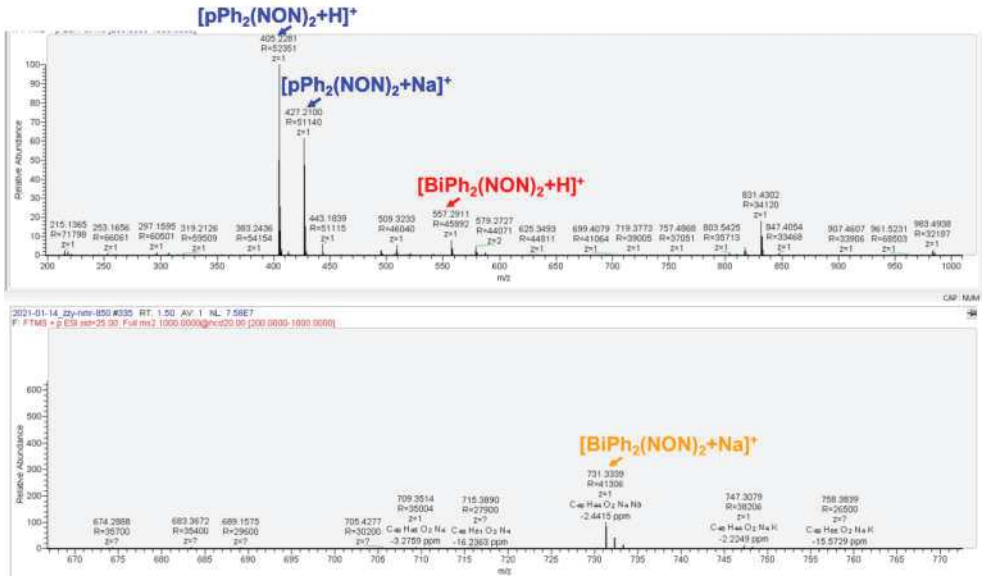

Figure S-II-32. HRMS-ESI spectrum of three macrocycles obtained in situ from 2**pPh** + 2**Biph** + 2**Triph** + 6**NON** reaction in $CDCl_3$ after the equilibration.

5.5.5. Self-sorting experiment 3pPh + 3BiPh + 3TriPh + 6T

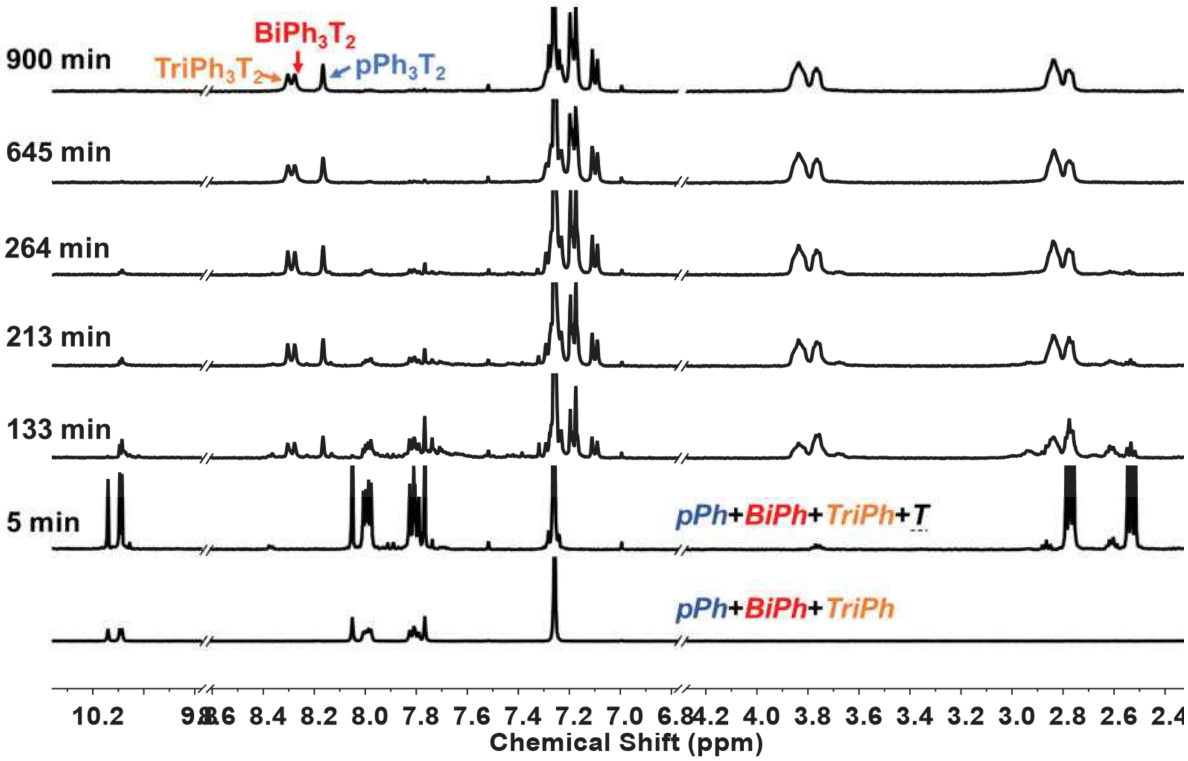

Figure S-II-33. Evolution of the ^{1}H NMR (400MHz, $CDCl_3$, 40 °C) spectra evolution of 3**pPh** + 3**Biph** + 3**Triph** + 6**T** ([**pPh**]$_0$ = [**BiPh**]$_0$ = [**TriPh**]$_0$ = 1.0 mM, [**T**]$_0$ = 2 mM).

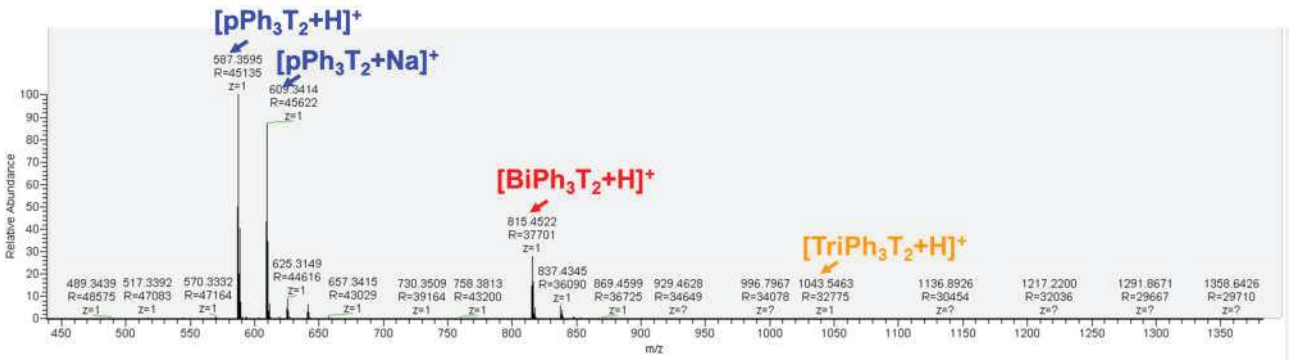

Figure S-II-34. HRMS-ESI spectrum showing peaks for the three macrobicyclic cages obtained in situ from 3**pPh** + 3**Biph** + 3**Triph** + 6**T** reaction in $CDCl_3$ after equilibration.

5.5.6. Effects of the quality of alumina

5.5.6.1. Formation of the macrocycle $pPh_2(NON)_2$

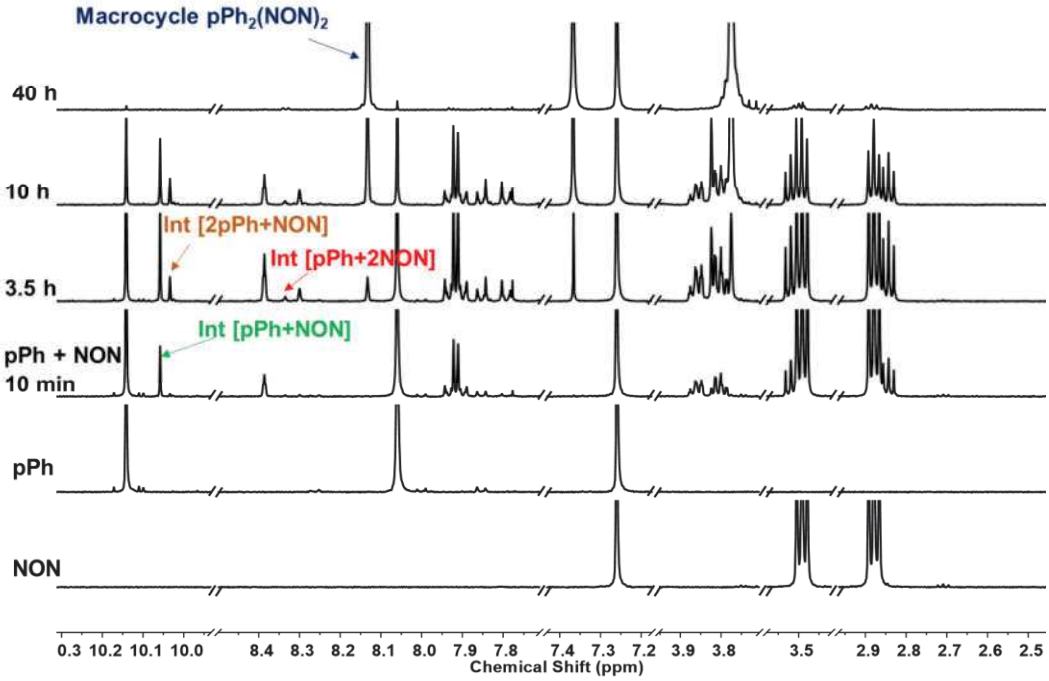

Figure S-II-35. Evolution of the ^1H NMR spectra (500 MHz, $CDCl_3$, 23 °C) during the formation of macrocycle **$pPh_2(NON)_2$** with dated-alumina treated $CDCl_3$.

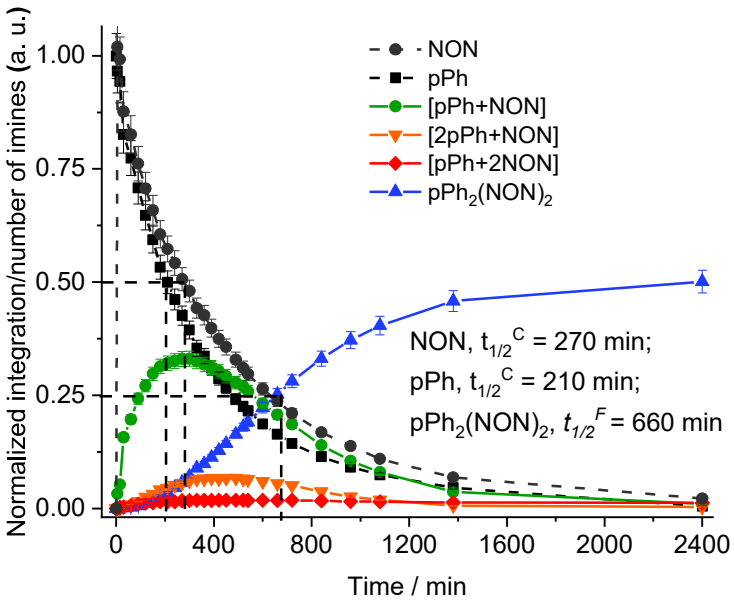

Figure S-II-36. ^{1}H NMR monitoring during the formation of macrocycle **pPh$_2$(NON)$_2$** with dated-alumina treated $CDCl_3$.

5.5.6.2. Formation of macrocycle BiPh$_2$(NON)$_2$

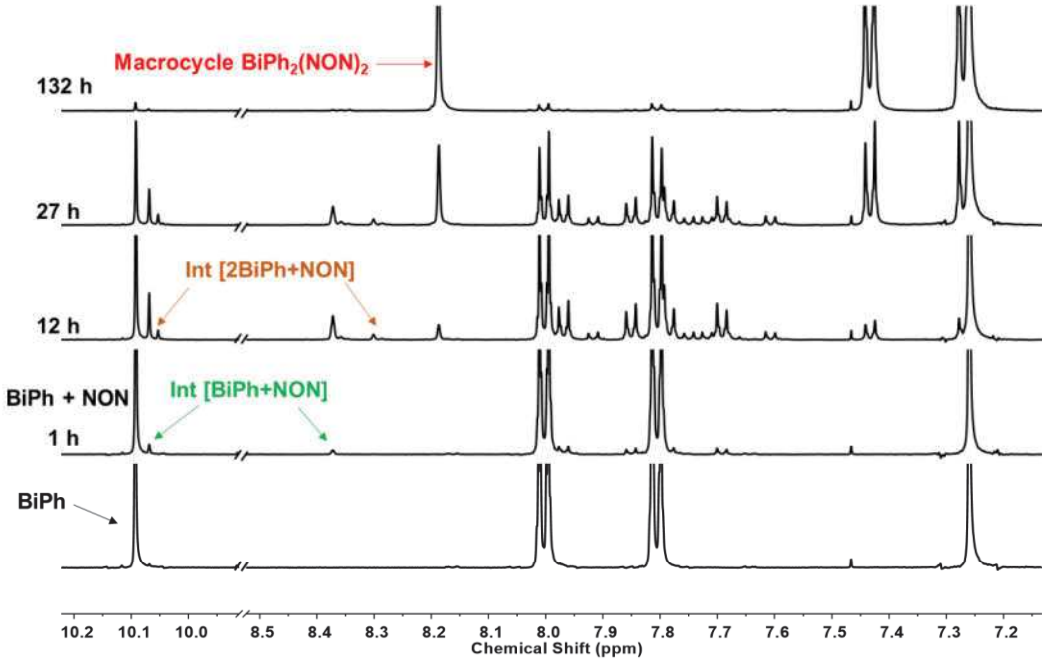

Figure S-II-37. Evolution of the ^{1}H NMR spectra (500 MHz, $CDCl_3$, 23 °C) during the formation of macrocycle **BiPh$_2$(NON)$_2$** with freshly-opened-alumina treated $CDCl_3$.

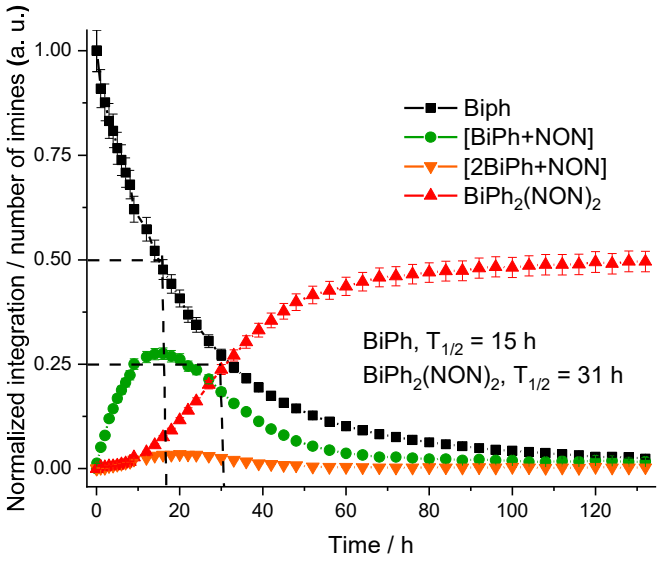

Figure S-II-38. ^{1}H NMR monitoring during the formation of macrocycle **$BiPh_2(NON)_2$** with freshly-opened-alumina treated $CDCl_3$.

5.5.6.3. Self-sorting experiment 2pPh + 2BiPh + 4NON

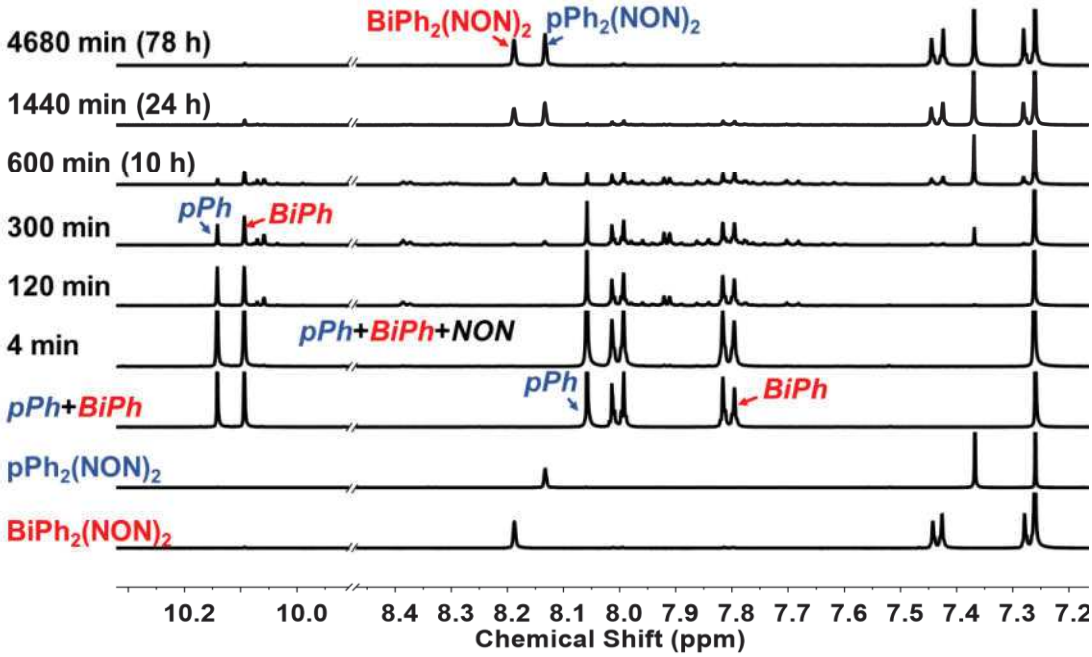

Figure S-II-39. Evolution of the ^{1}H NMR spectra (400 MHz, $CDCl_3$, 23 °C) during the self-sorting of macrocycle **$pPh_2(NON)_2$** and **$BiPh_2(NON)_2$** with dated-alumina treated $CDCl_3$.

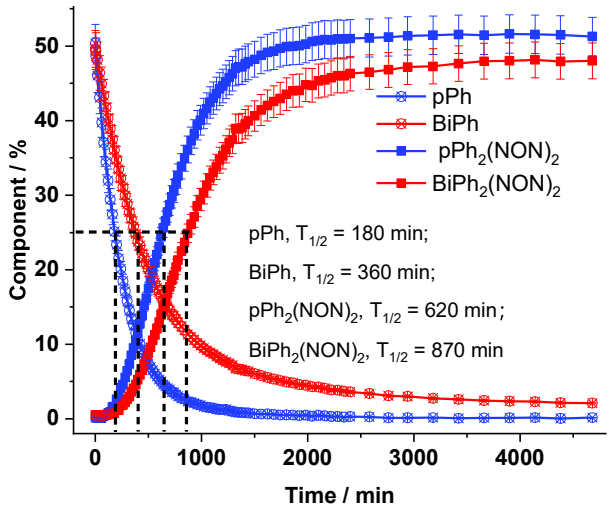

Figure S-II-40. ^{1}H NMR monitoring during the self-sorting of macrocycle **pPh₂(NON)₂** and **BiPh₂(NON)₂** with dated-alumina treated $CDCl_3$.

5.5.6.4. Self-sorting experiment 3pPh + 3BiPh + 4T

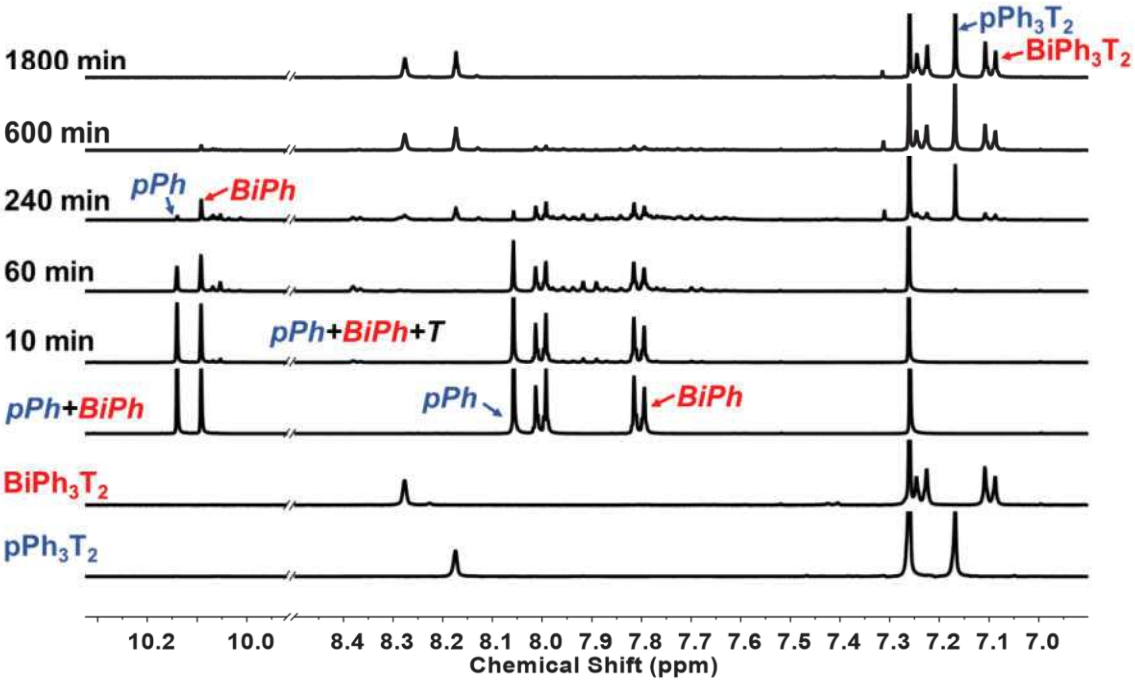

Figure S-II-41. Evolution of the ^{1}H NMR spectra (400 MHz, $CDCl_3$, 23 °C) during the self-sorting of **pPh₃T₂** and **BiPh₃T₂** with dated-alumina treated $CDCl_3$.

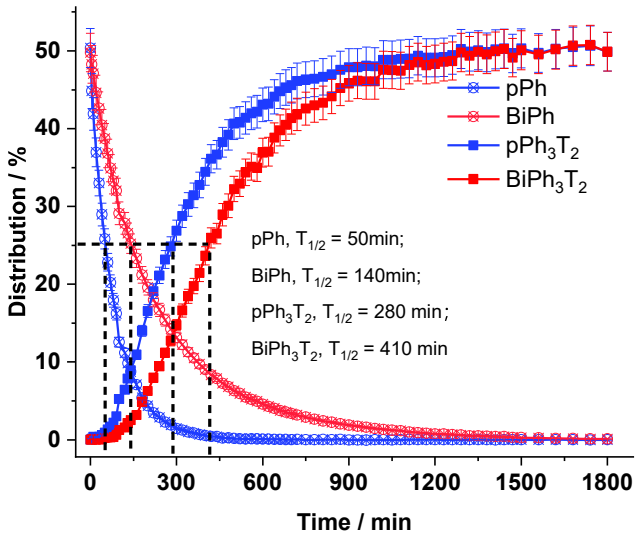

Figure S-II-42. ^{1}H NMR monitoring during the self-sorting of **pPh_3T_2** and **$BiPh_3T_2$** with dated-alumina treated $CDCl_3$

6. Chapter III. Dynamic Covalent Self-Sorting and Kinetic Switching Processes in Two Cyclic Orders: Macrocycles and Macrobicyclic Cages

6.1. Synthesis of intermediate $BiPy_2T_2$

Intermediate **$BiPy_2T_2$** was synthesized in $CDCl_3$ without isolation. For this purpose, 3 equiv. **BiPy** and 4 equiv. **T** were mixed in $CDCl_3$ in an NMR tube. The final concentration of **BiPy** was 3.6 mM.

^{1}H NMR (500 MHz, $CDCl_3$, 25 °C): δ = 7.97 (s, 4H), 7.94 (d, J = 7.7 Hz, 4H), 7.84 (d, J = 7.8 Hz, 4H), 7.69 (t, J = 7.7 Hz, 4H), 3.69 – 3.57 (m, 8H), 2.91 (m, 12H), 2.63 (t, J = 5.4 Hz, 4H).

HRMS (ESI+): m/z calcd for $C_{36}H_{44}N_{12}$ $[M+2H]^{2+}$ 323.1979, found 323.1978; $[M+H]^+$ 645.3885, found 645.3873

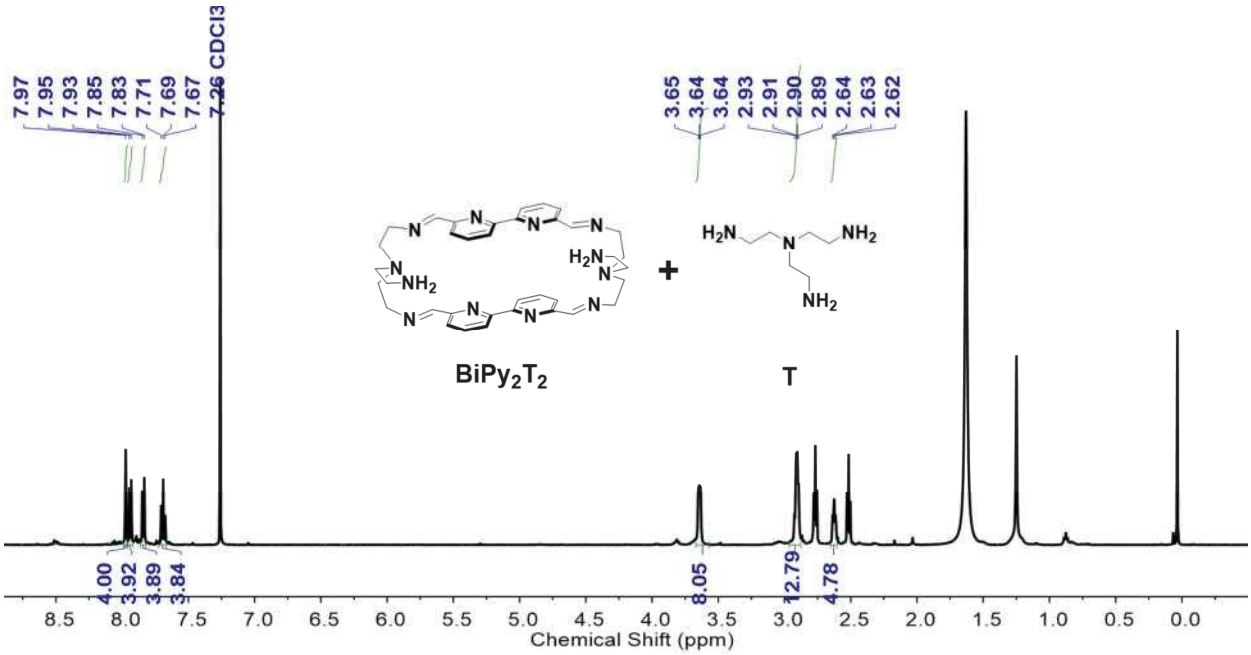

Figure S-III-1. Equilibrium state ^{1}H NMR spectra (500 MHz, $CDCl_3$, 25 °C) of intermediate **$BiPy_2T_2$** obtained in situ from 3 equiv. **BiPy** and 4 equiv. **T**.

Figure S-III-2. HRMS-ESI spectrum of intermediate **$BiPy_2T_2$** obtained in situ from 3 equiv. **BiPy** and 4 equiv. **T**.

6.2. Self-sorting experiment 3Py + 3BiPh + 3TriPh + 2T + 6NON

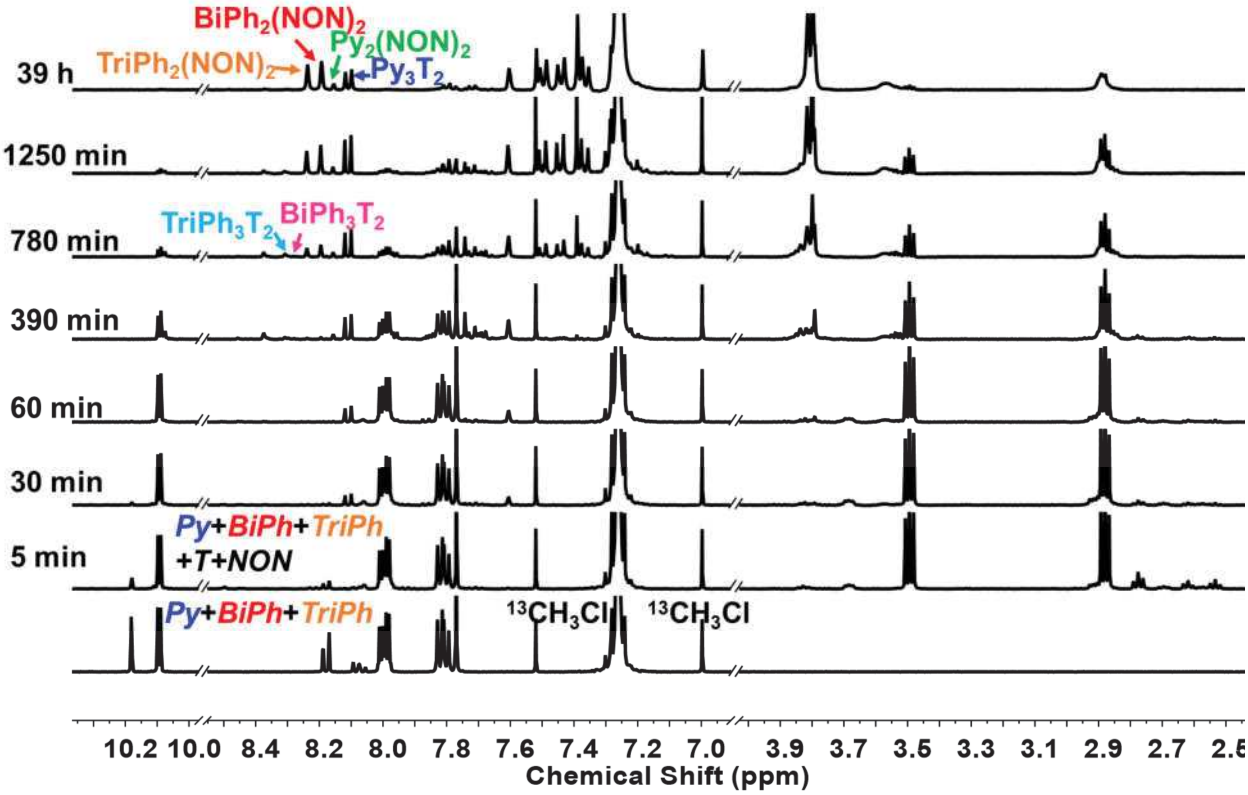

Figure S-III-3. Temporal evolution of the ^{1}H NMR (400MHz, $CDCl_3$, 40 °C) spectra of 3**Py** + 3**Biph** + 3**Triph** + 2**T** + 6**NON** ([**pPh**]$_0$ = [**BiPh**]$_0$ = [**TriPh**]$_0$ = 1.0 mM).

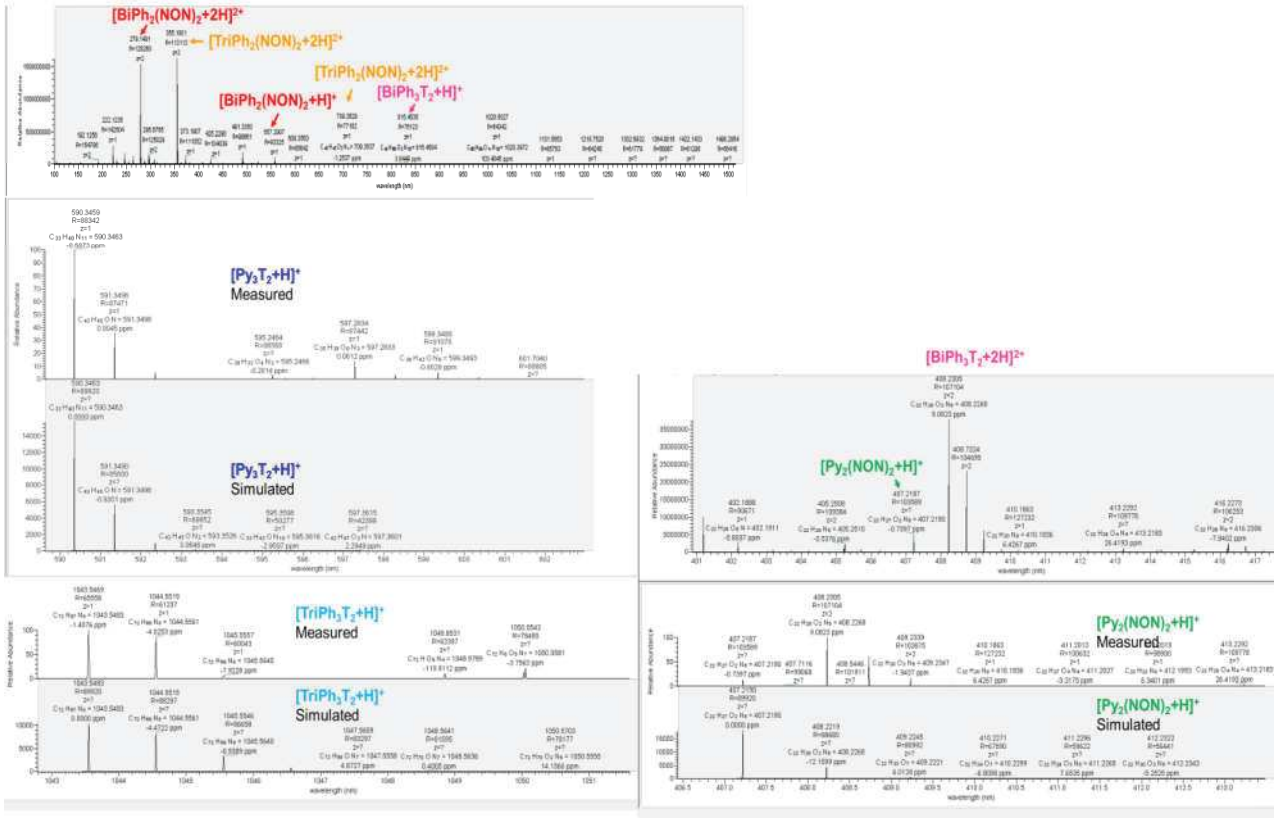

Figure S-III-4. HRMS-ESI spectrum of the final products obtained in situ from 3**Py** + 3**Biph** + 3**Triph** + 2**T** + 6**NON** reaction in $CDCl_3$ after the equilibration.

6.3. Kinetic switching and self-sorting from 5Fur+5BiPy+4T+4NON in the presence of DMA·HCl

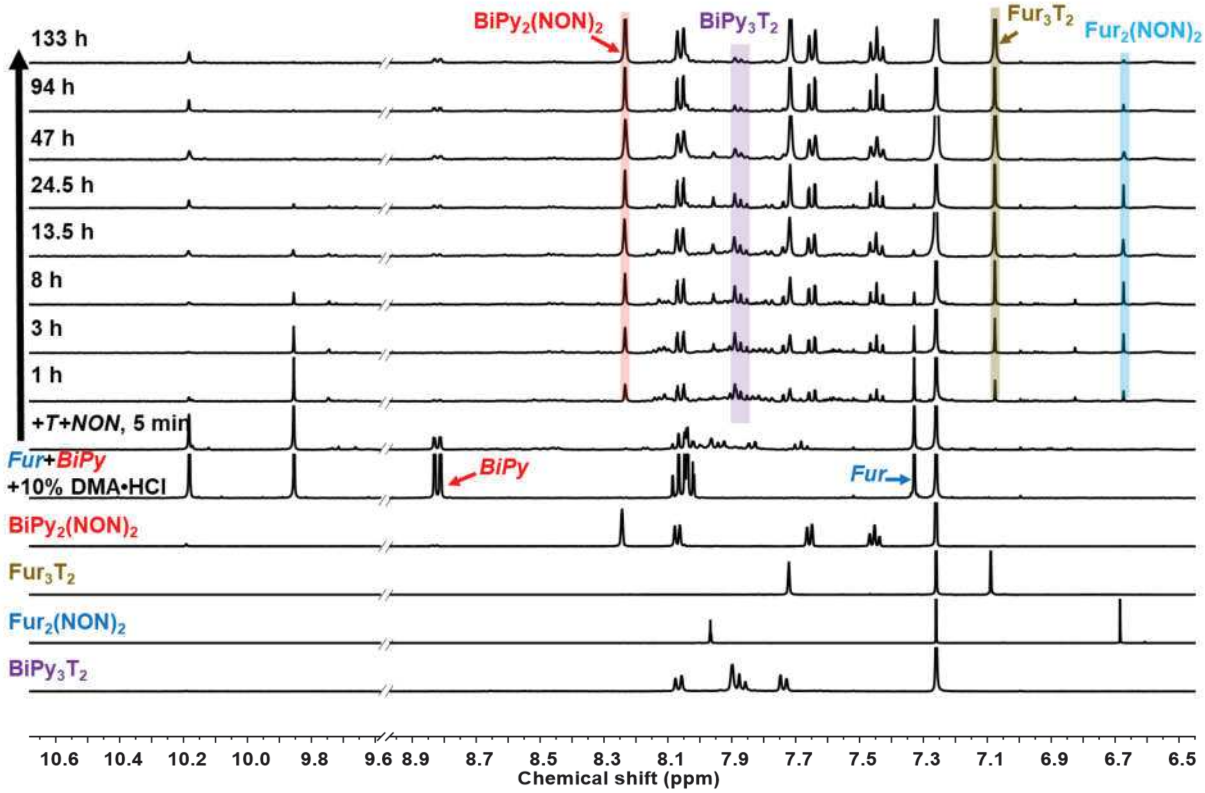

Figure S-III-5. Evolution of the ^{1}H NMR spectra (400MHz, $CDCl_3$, 40 °C) of 5**Fur**+5**BiPy**+4**NON**+4**T** (**[Fur]$_0$** = **[BiPy]$_0$** = 3.6 mM) and 10 molar% (in terms of dialdehyde components) dimethylamine hydrochloride (DMA·HCl) after 5 min, 1 h, 3 h, 8 h, 13.5 h, 24.5h, 47h, 94 h and 133 h. The bottom four traces correspond to the isolated **BiPy$_3$T$_2$**, **Fur2(NON)2**, **Fur$_3$T$_2$**, **BiPy$_2$(NON)$_2$.**

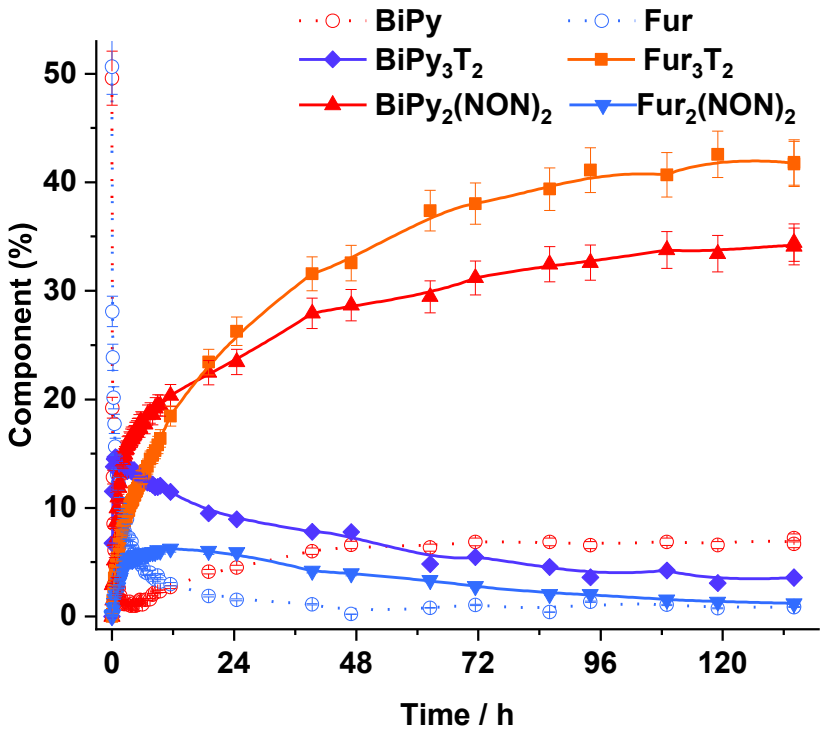

Figure S S-III-6. ^{1}H NMR monitoring of the time-dependent switching evolution of the mixture of components 5**Fur**+5**BiPy**+4**NON**+4**T** and 10 molar% (in terms of dialdehyde components) dimethylamine hydrochloride (DMA·HCl) as a function of time as obtained from the aromatic proton signals in Figure S98. Error in ^{1}H-NMR signal integration: ±5%

6.4. Self-sorting between macrocycles and macrobicyclic cages

Table S-III-1. HRMS-ESI assignments for the macrobicyclic cages **Py$_3$T$_2$**, **BiPh$_3$T$_2$** and macrocycles **Py$_2$(NON)$_2$**, **BiPh$_2$NON$_2$** generated from the self-sorting reaction of 5**Py** + 5**BiPh** + 4**T** + 4**NON (DCL[1])**.

Entry	assignment	formula	Combined ion	m/z calcd.	m/z found
1	**Py$_3$T$_2$**	$C_{33}H_{39}N_{11}$	$+H^+$	590.3463	590.3439
			$+Na^+$	612.3282	612.3256
			$+K^+$	628.3021	628.2987
			$+2H^+$	295.6768	295.6755
2	**Py$_2$(NON)$_2$**	$C_{22}H_{26}N_6O_2$	$+H^+$	407.2190	407.2173
			$+Na^+$	429.2009	429.1992
			$+K^+$	445.1749	445.1746
			$+2H^+$	204.1131	N/A

3	**$BiPh_3T_2$**	$C_{54}H_{54}N_8$	$+H^+$	815.4544	815.4503
			$+Na^+$	837.4364	837.4324
			$+K^+$	853.4103	N/A
			$+2H^+$	408.2308	408.2295
4	**$BiPh_2(NON)_2$**	$C_{36}H_{36}N_4O_2$	$+H^+$	557.2911	557.2891
			$+Na^+$	579.2730	579.2710
			$+K^+$	595.2470	N/A
			$+2H^+$	279.1492	279.1481

N/A: Unable to read the mass-to-charge ratio (m/z) abundance as it has an extremely close m/z value to other more abundant ion-combined species.

Table S-III-2. HRMS-ESI assignments for the macrobicyclic cages **pPh_3T_2**, **$BiPh_3T_2$** and macrocycles **$pPh_2(NON)_2$**, **$BiPh_2NON_2$** generated from the self-sorting reaction of 5**pPh** + 5**BiPh** + 4**T** + 4**NON (DCL[2])**.

Entry	assignment	formula	Combined ion	m/z calcd.	m/z found
1	**pPh_3T_2**	$C_{36}H_{42}N_8$	$+H^+$	587.3605	587.3603
			$+Na^+$	609.3425	609.3423
			$+K^+$	625.3164	625.3165
			$+2H^+$	294.1839	294.1842
2	**$pPh_2(NON)_2$**	$C_{24}H_{28}N_4O_2$	$+H^+$	405.2285	405.2285
			$+Na^+$	427.2104	427.2105
			$+K^+$	443.1844	443.1848
			$+2H^+$	203.1179	N/A
3	**$BiPh_3T_2$**	$C_{54}H_{54}N_8$	$+H^+$	815.4544	815.4538
			$+Na^+$	837.4364	837.4358
			$+K^+$	853.4103	N/A
			$+2H^+$	408.2308	408.2307
4	**$BiPh_2(NON)_2$**	$C_{36}H_{36}N_4O_2$	$+H^+$	557.2911	557.2911
			$+Na^+$	579.2730	579.2736
			$+K^+$	595.2470	N/A
			$+2H^+$	279.1492	279.1491

N/A: Unable to read the mass-to-charge ratio (m/z) abundance as it has an extremely close m/z value to other more abundant ion-combined species.

6.5. Kinetic switching and self-sorting from 5Fur+5BiPy+4T+4NON (DCL[14])

Table S-III-3. HRMS-ESI assignments for the Intermediate **Int[$BiPy_2T_2$]**, cages **$BiPy_3T_2$**, **Fur_3T_2** and macrocycles **$BiPy_2NON_2$**, **$Fur_2(NON)_2$** generated from the self-sorting reaction of 5**Fur** + 5**BiPy** + 4**T** + 4**NON**.

Entry	assignment	formula	Combined ion	m/z calcd.	m/z found
1	**Int[$BiPy_2T_2$]**	$C_{36}H_{44}N_{12}$	$+H^+$	645.3885	645.3860
			$+Na^+$	667.3704	667.3678
			$+K^+$	683.3443	N/A
			$+2H^+$	323.1979	323.1967
2	**$BiPy_3T_2$**	$C_{48}H_{48}N_{14}$	$+H^+$	821.4259	821.4222
			$+Na^+$	851.4347	851.4358
			$+K^+$	859.3818	859.3792
			$+2H^+$	411.2166	411.2150
3	**Fur_3T_2**	$C_{30}H_{36}N_8O_3$	$+H^+$	557.2983	557.2964
			$+Na^+$	579.2803	579.2783
			$+K^+$	595.2542	595.2521
			$+2H^+$	279.1528	279.1526
4	**$BiPy_2NON_2$**	$C_{32}H_{32}N_8O_2$	$+H^+$	561.2721	567.2702
			$+Na^+$	583.2540	583.2519
			$+K^+$	599.2280	599.2260
			$+2H^+$	281.1397	281.1394
5	**$Fur_2(NON)_2$**	$C_{20}H_{24}N_4O_4$	$+H^+$	385.1870	385.1856
			$+Na^+$	407.1690	407.1673
			$+K^+$	423.1429	423.1413
			$+2H^+$	193.0972	N/A

N/A: Unable to read the mass-to-charge ratio (m/z) abundance as it has an extremely close m/z value to other more abundant ion-combined species.

Chapter V. Isomeric Cages with Unsymmetrical Building Blocks

7.1. Synthesis of cage isomers

54.3mg (0.257mol) **Py-Ph** was dissolved in 50mL MeOH. To the solution, 25.0mg (0.171 mmol) of **Tren** in 5 ml MeOH was added over 2 min at room temperature. The reaction mixture was stirred for 24 h. A pale yellow precipitate was collected by centrifugation and washed with small amounts of cold MeOH. The solid was dried at room temperature under vacuum. The resulting pale yellow solid was the desired cage mixture (yield 39.8 mg, 57%) and contained 83% of **cage bbp** and 17% of **cage bbb**.

7.2. Isolation of cage bbp

4.90 mg of cage isomers obtained from MeOH were dispersed on 1/1 MeCN-$CHCl_3$ (4mL). Thereafter, 17 mol% $Zn(OTf)_2$ MeCN solution was added. The suspension was stirred for 10min. The precipitate was collected by centrifugation and washed with MeCN twice. The pale yellow solid was dried at room temperature under vacuum and was confirmed to be the pure cage **bbp** (yield 4.05 mg, 99%).

7.3. Spectroscopic data

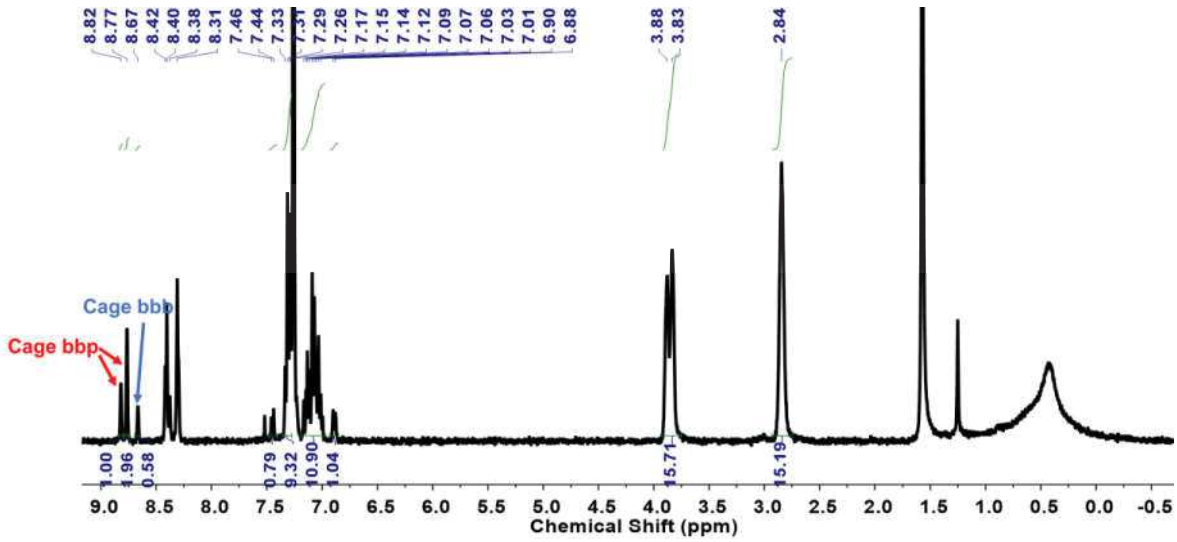

Figure S-V-1. ^1H NMR spectrum (400 MHz, $CDCl_3$, 23 °C) of cage isomers obtained from MeOH

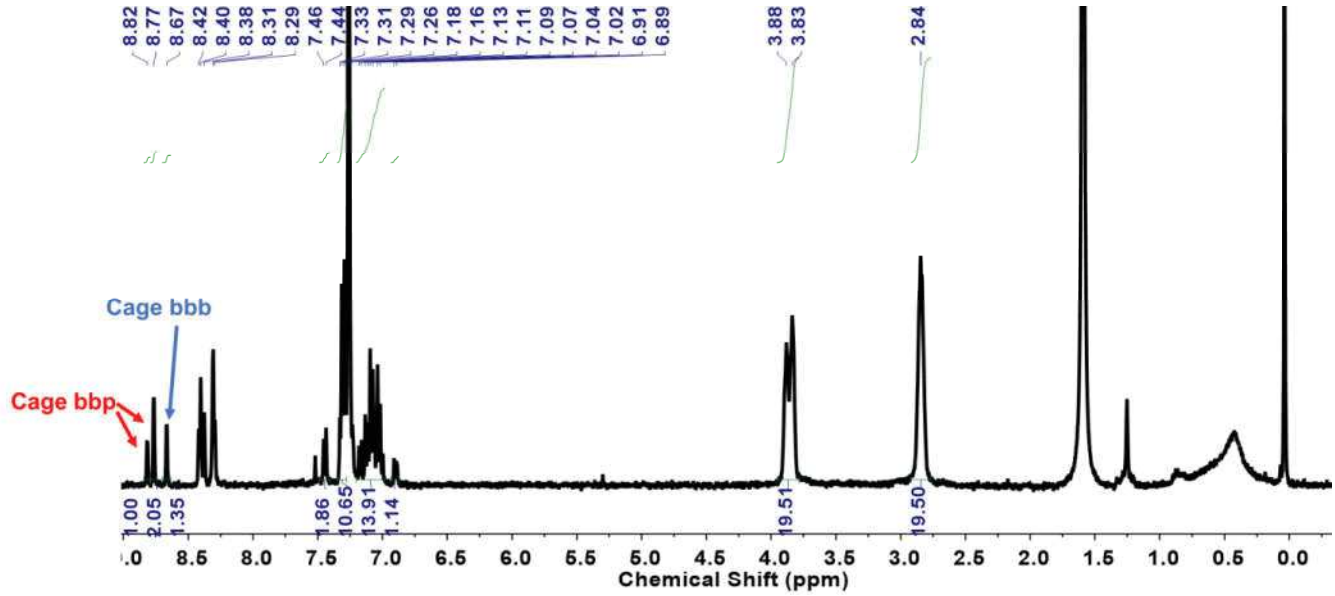

Figure S-V-2. ^{1}H NMR spectrum (400 MHz, $CDCl_3$, 23 °C) of cage isomers obtained *in situ* from $CDCl_3$

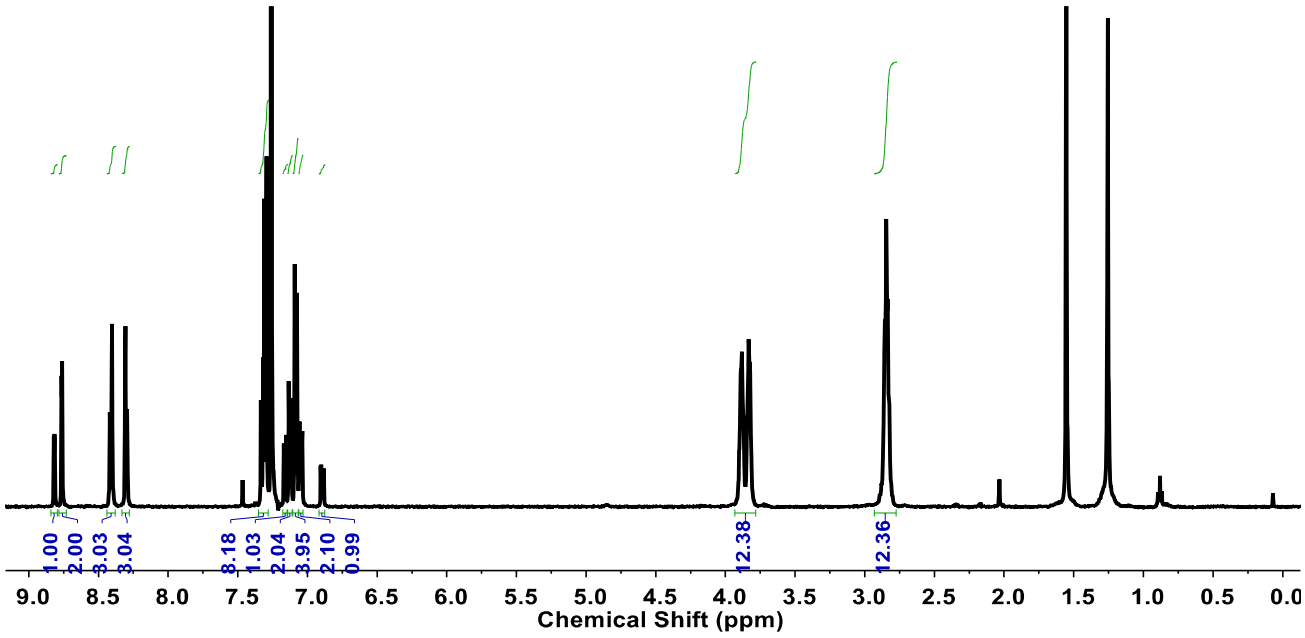

Figure S-V-3. ^{1}H NMR spectrum (500 MHz, $CDCl_3$, 25 °C) of **Cage bbp**

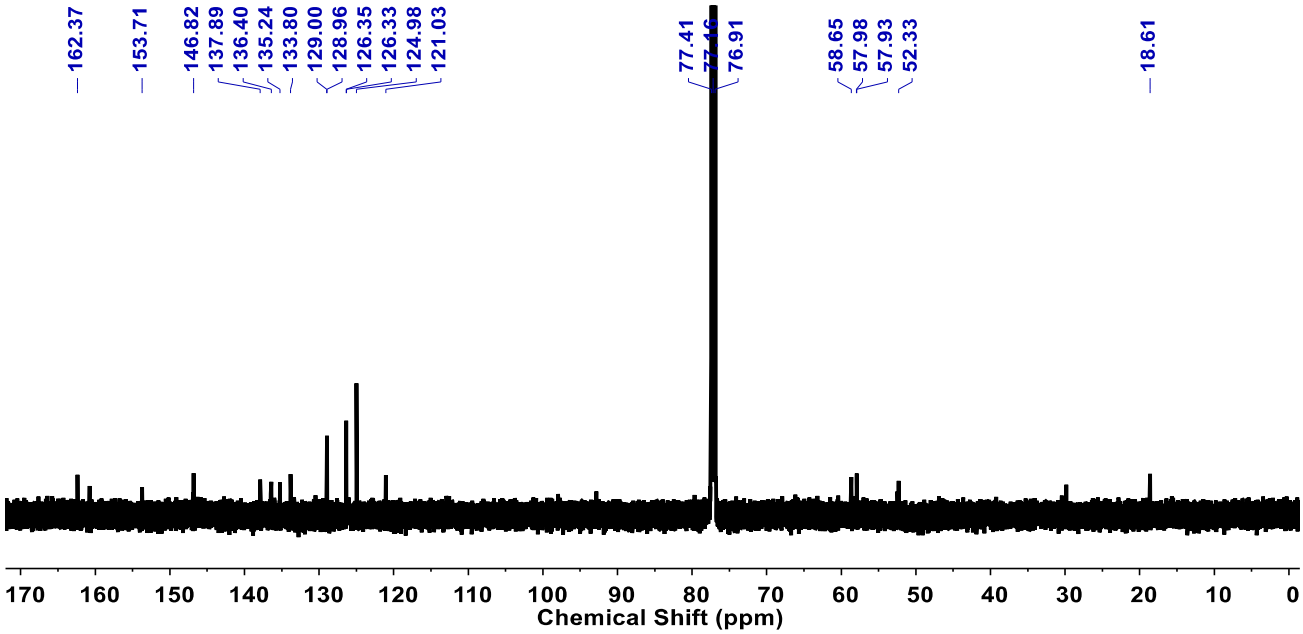

Figure S-V-4. ^{13}C NMR spectrum (500 MHz, $CDCl_3$, 25 °C) of **Cage bbp**

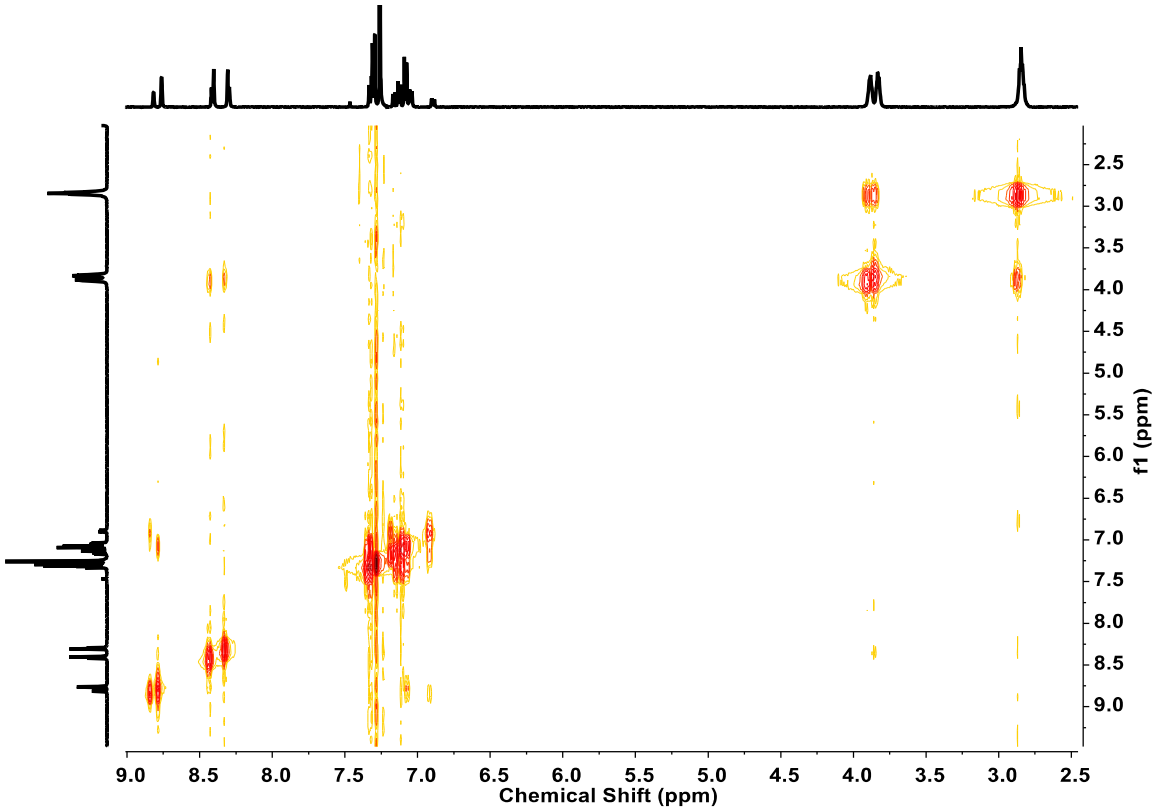

Figure S-V-5. ^{1}H-^{1}H Cosy spectrum (500 MHz, $CDCl_3$, 25 °C) of **Cage bbp**

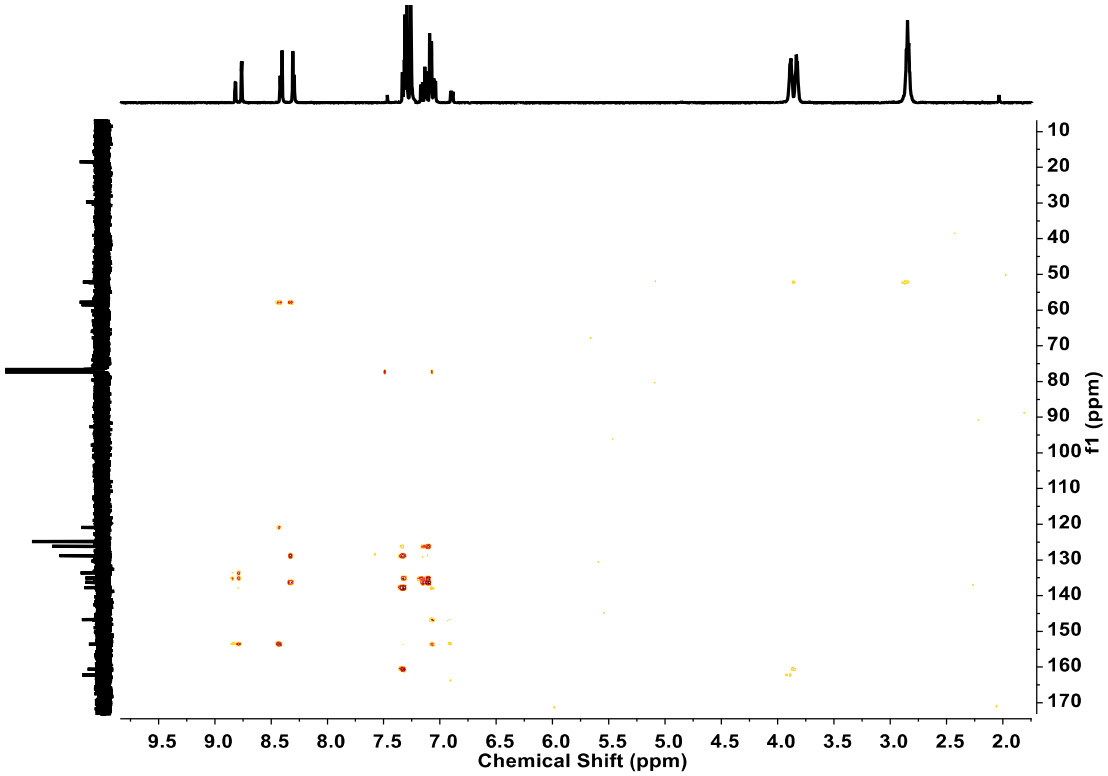

Figure S-V-6. ^{1}H-^{13}C HMBC spectrum (500 MHz of ^{1}H, 125 MHz of ^{13}C, $CDCl_3$, 25 °C) of **Cage bbp**

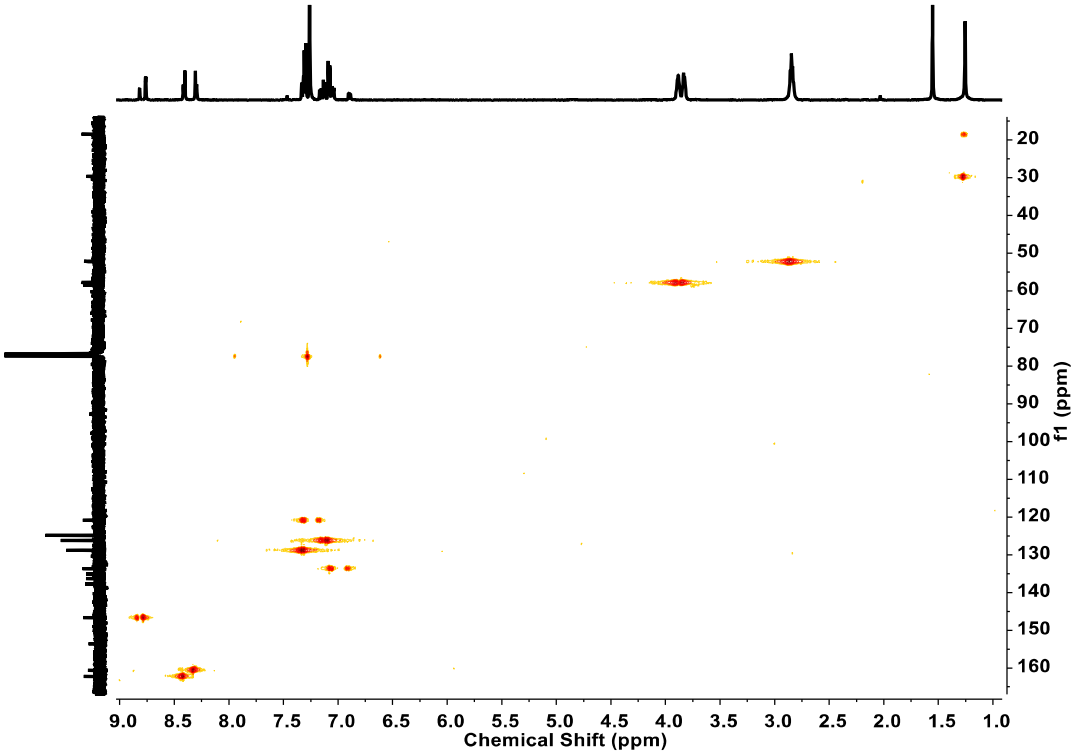

Figure S-V-7. ^{1}H-^{13}C HSQC spectrum (500 MHz of ^{1}H, 125 MHz of ^{13}C,, $CDCl_3$, 25 °C) of **Cage bbp**

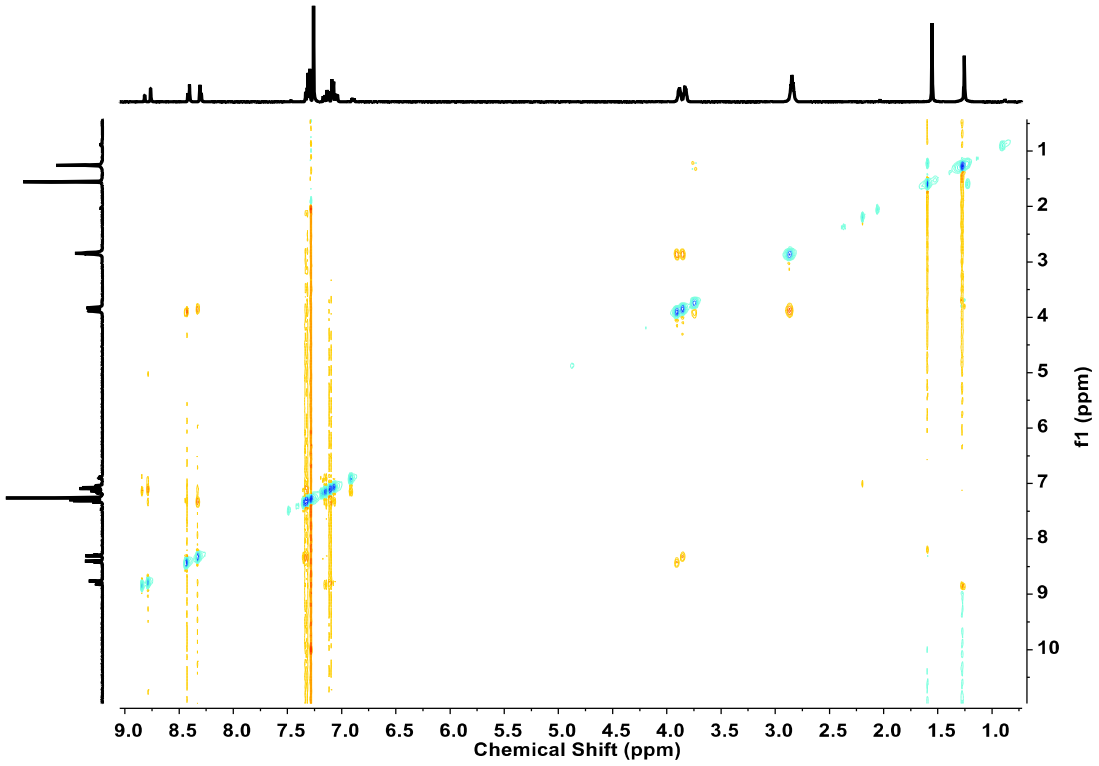

Figure S-V-8. ^{1}H-^{1}H ROESY spectrum (500 MHz of ^{1}H, 125 MHz of ^{13}C,, $CDCl_3$, 25 °C) of **Cage bbp**

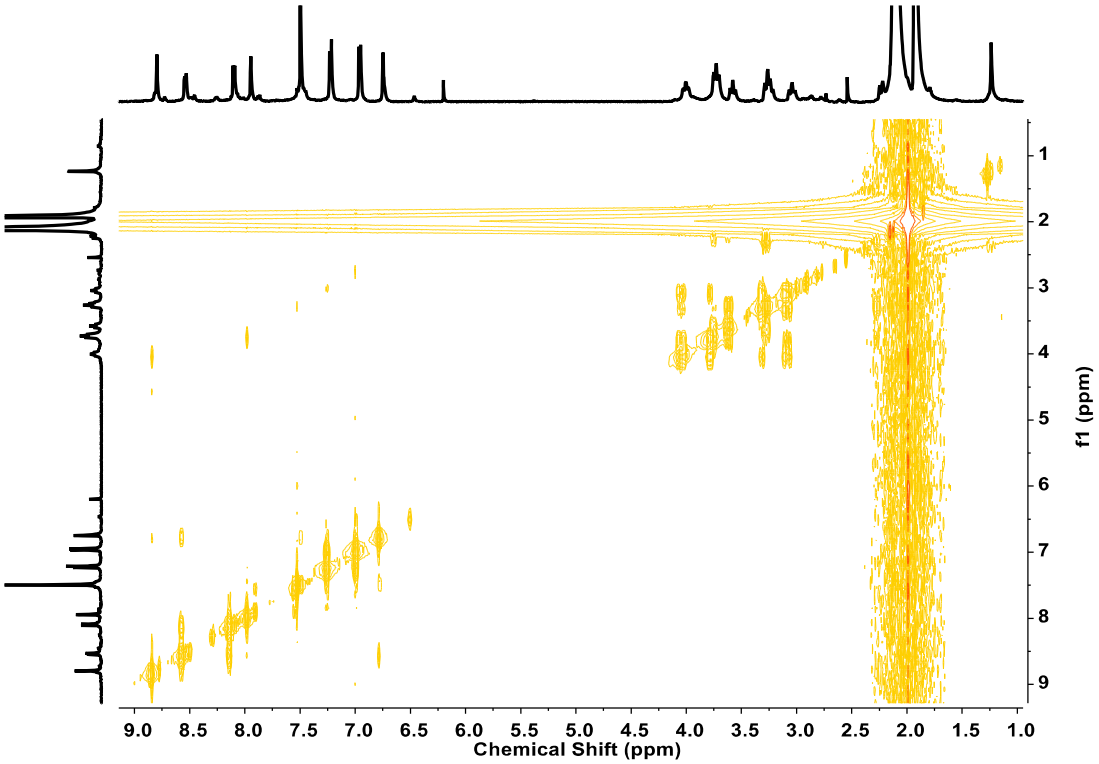

Figure S-V-8. ^{1}H-^{1}H COSY spectrum (500 MHz of ^{1}H, 125 MHz of ^{13}C, $CDCl_3$, 25 °C) of **Cage bbb-Zn(II)**

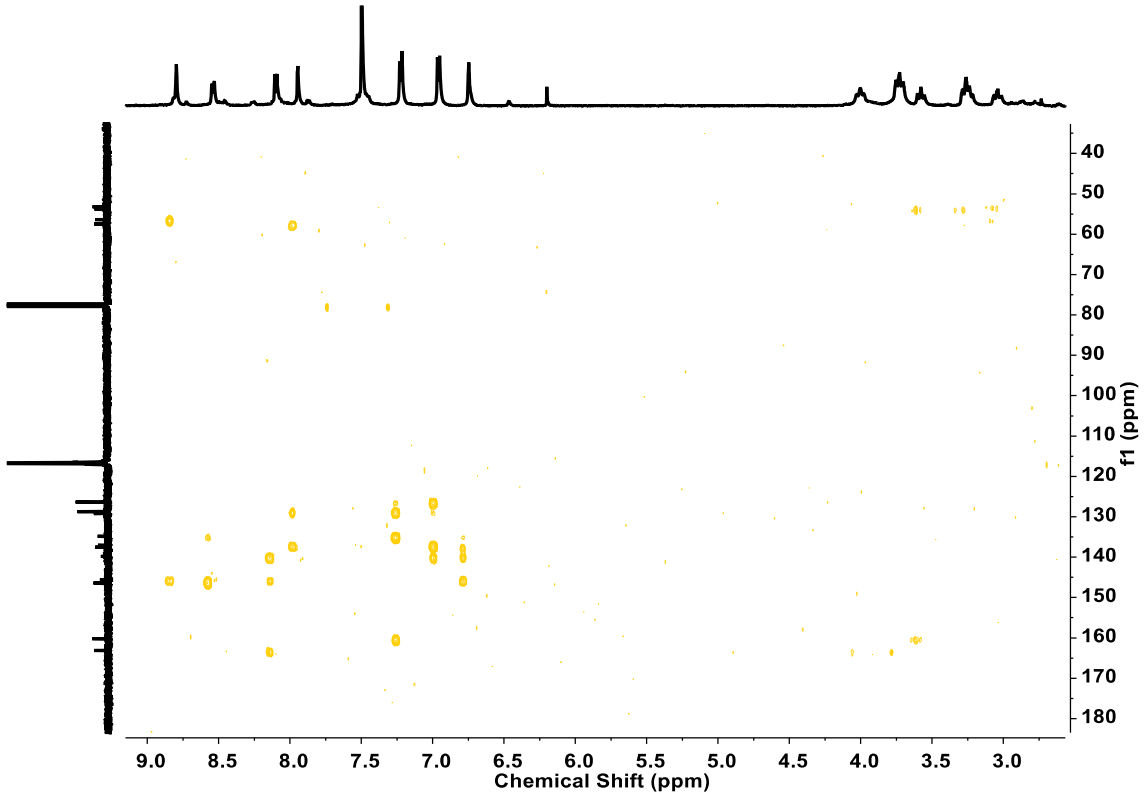

Figure S-V-8. ^{1}H-^{13}C HMBC spectrum (500 MHz of ^{1}H, 125 MHz of ^{13}C, $CDCl_3$, 25 °C) of **Cage bbb-Zn(II)**

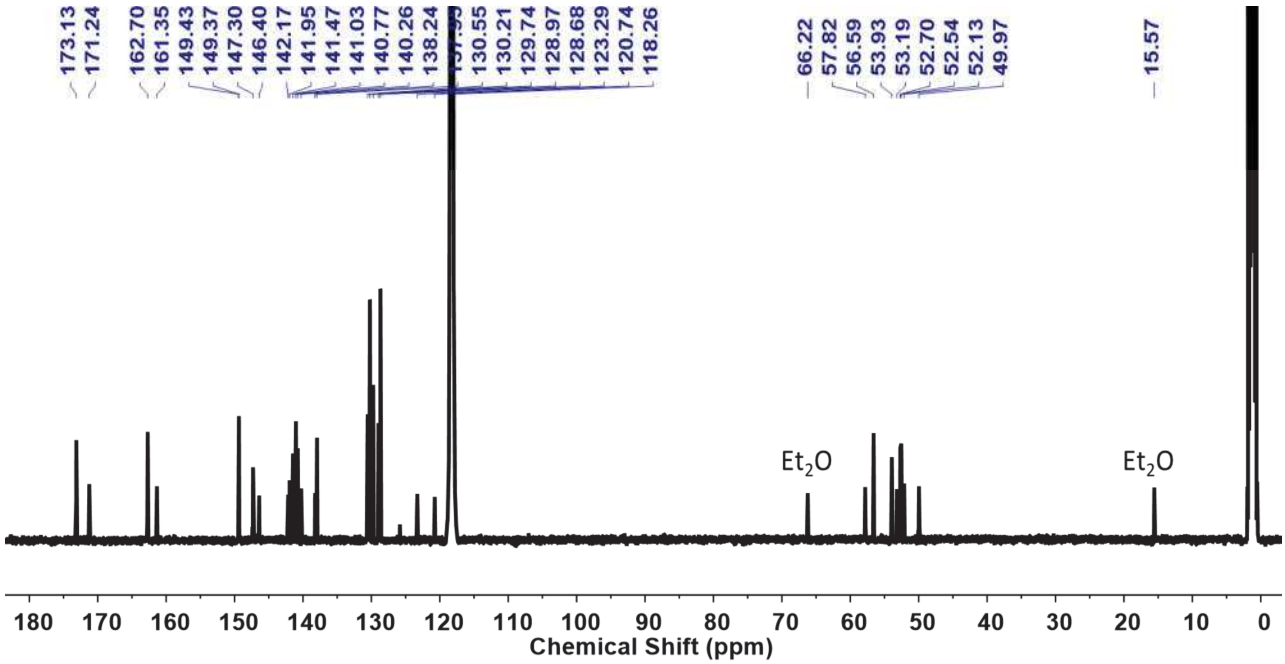

Figure S-V-9. ^{13}C NMR spectrum (500 MHz, CD_3CN, 23 °C) of complex **bbp-2Cd(II)**

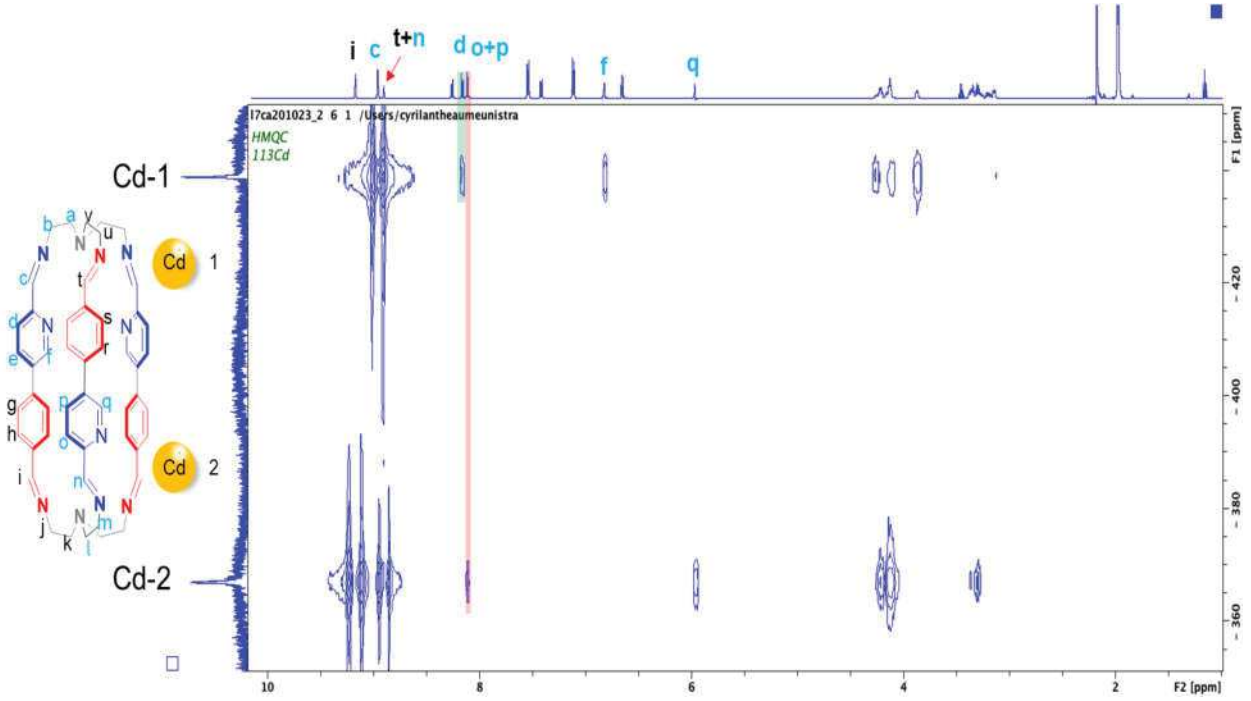

Figure S-V-10. ^{113}Cd-^{1}H HMBC spectrum (CD_3CN, 23 °C) of complex **bbp-2Cd(II)**

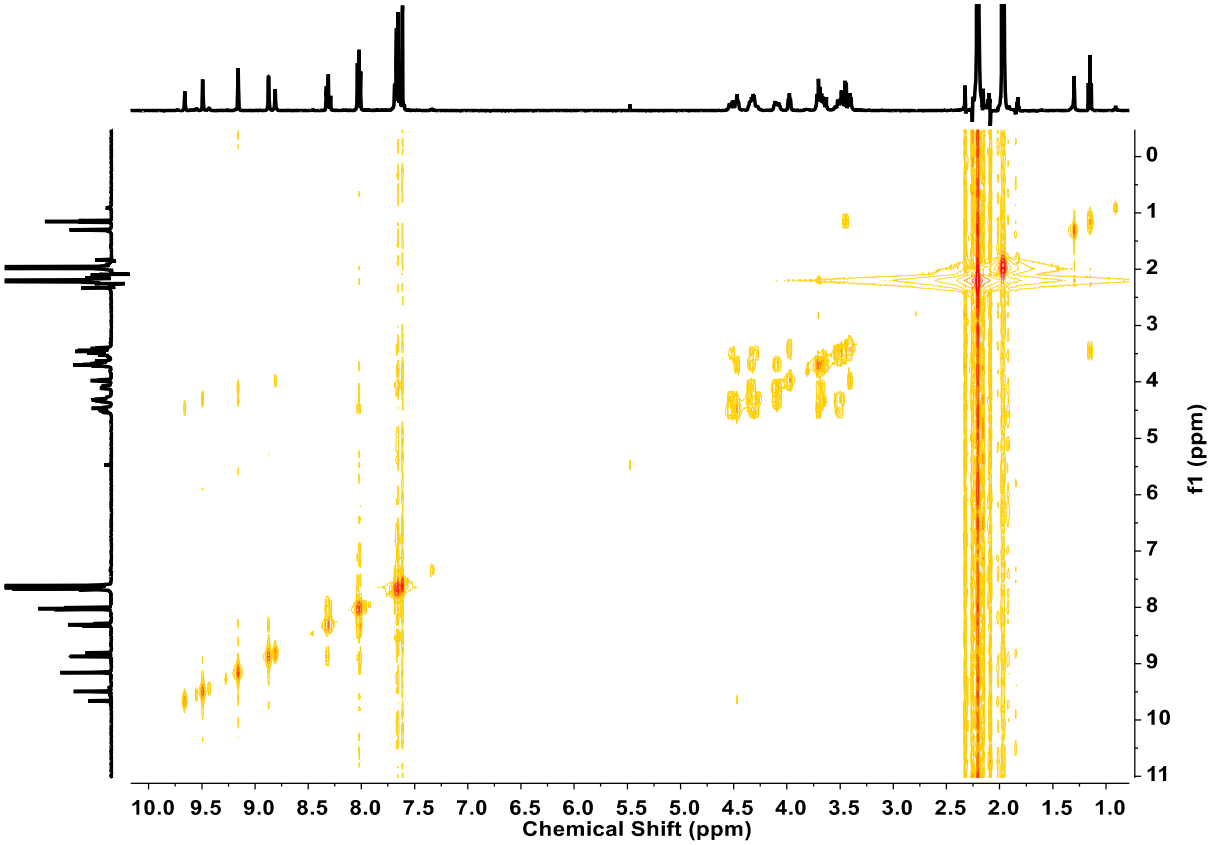

Figure S-V-11. ^{1}H-^{1}H COSY spectrum (500 MHz, $CDCl_3$, 25 °C) of **Cage bbb-2Pb(II)**

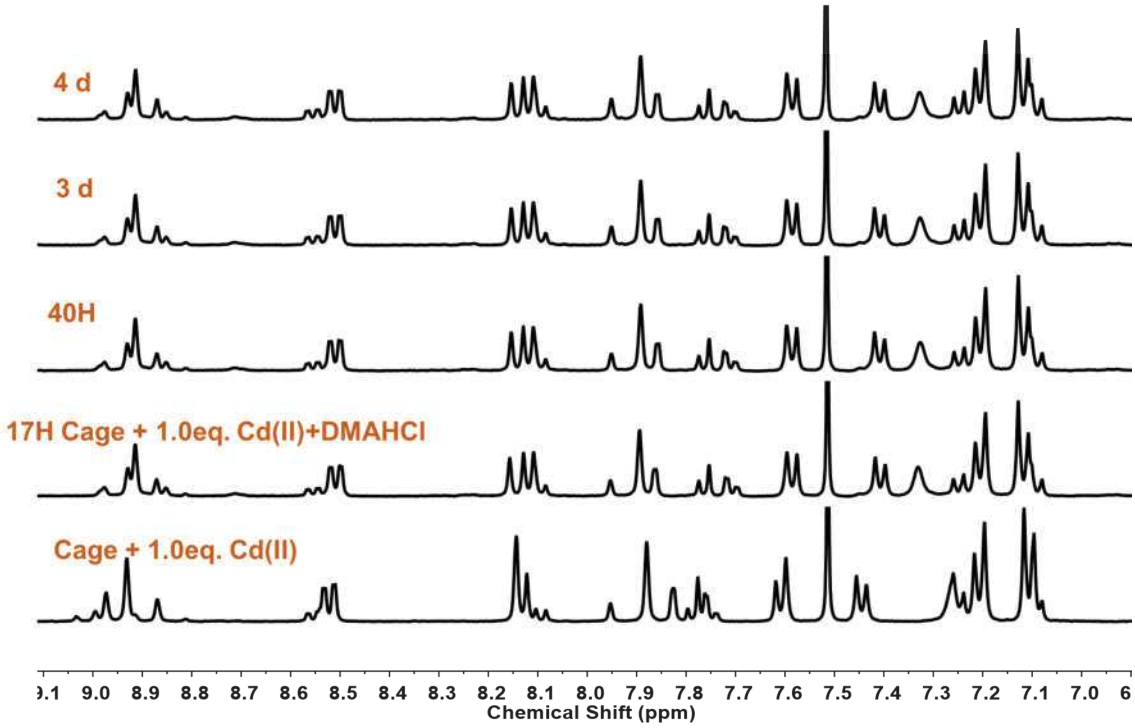

Figure S-V-12. Comparison of ^{1}H NMR spectra (400 MHz, 60%-40% CD_3CN-$CDCl_3$, r.t.) after addition of $Cd(OTf)_2$ to the initial isomeric mixture.

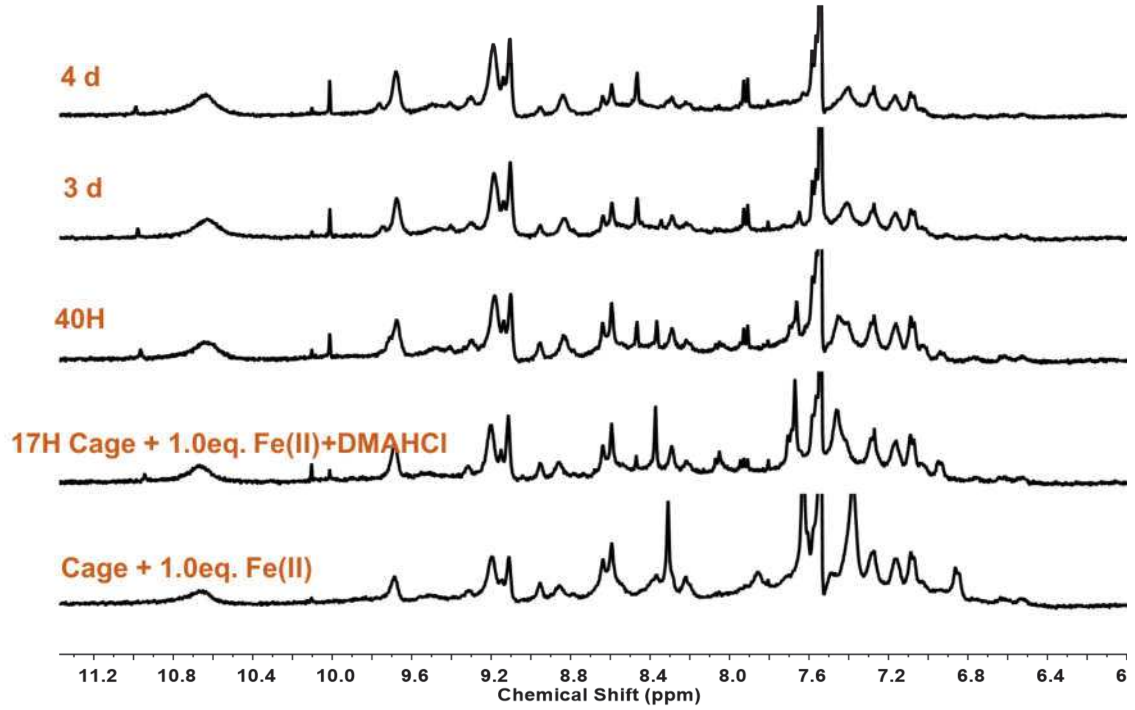

Figure S-V-13. Comparison of ^{1}H NMR spectra (400 MHz, 60%-40% CD_3CN-$CDCl_3$, r.t.) after addition of $Fe(ClO_4)_2$ to the initial isomeric mixture.

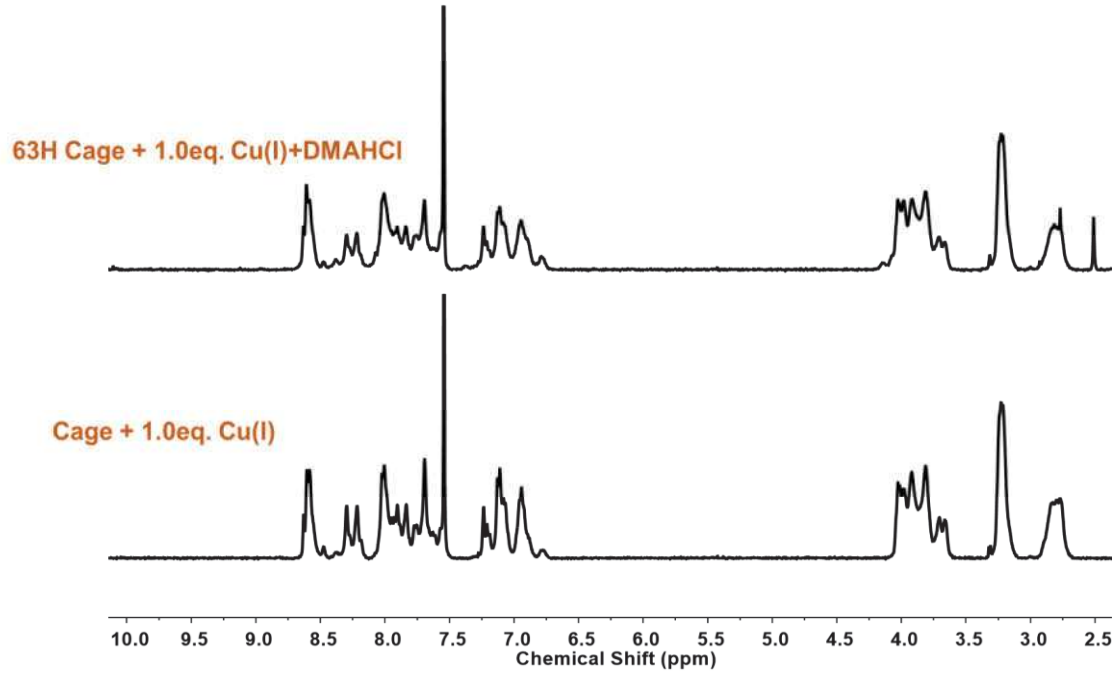

Figure S-V-14. Comparison of ^{1}H NMR spectra (400 MHz, 60%-40% CD_3CN-$CDCl_3$, r.t.) after addition of Cu(OTf) to the initial isomeric mixture.

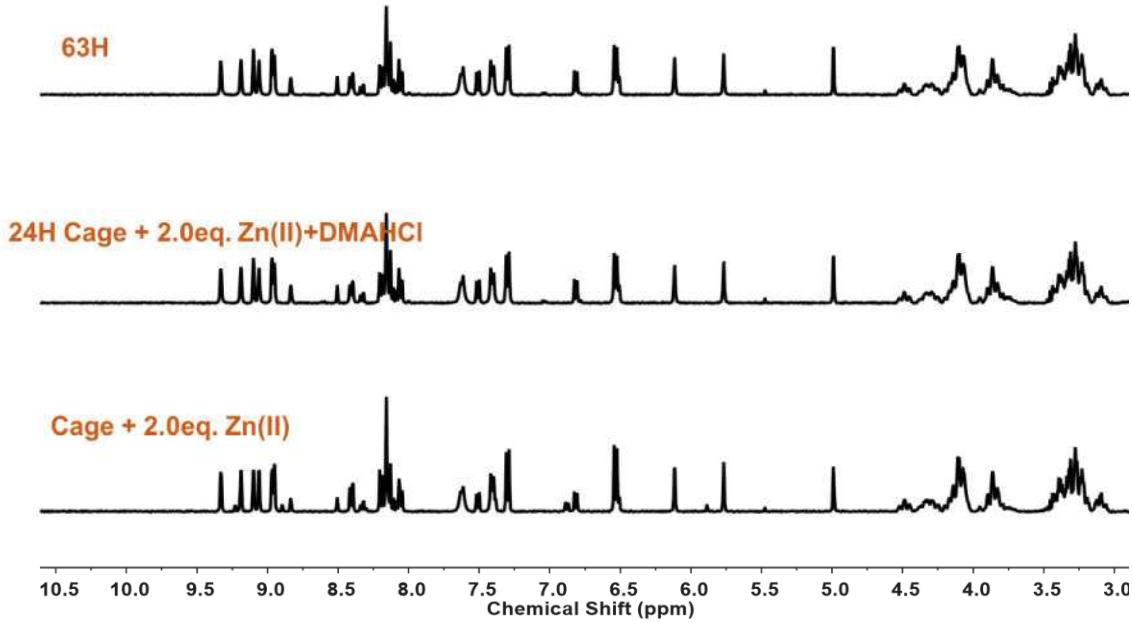

Figure S-V-15 Comparison of ^{1}H NMR spectra (400 MHz, 60%-40% CD_3CN-$CDCl_3$, r.t.) after addition of 2 equiv. of $Zn(OTf)_2$ to the initial isomeric mixture.

8. X-ray crystallography

Colourless, square single crystals of macrocycle **$pPh_2(NON)_2 \cdot H_2O$** and **$BiPh_2(NON)_2$** were respectively obtained by crystallization in MeCN and vapor diffusion of n-Hexane into a $CDCl_3$ solution in a closed vial at room temperature. The crystal of **$2BiPy_2(NON)_2 \cdot CHCl_3$** was obtained by slow evaporation of a chloroform solution at 4 °C. Each **BiPy** unit in the macrocycle showed a planarized structure, rather than a twisted shape and with a distance of 13.39 Å between the O atoms. The colourless crystal of **$TriPh_3T_2 \cdot 3CHCl_3$** was obtained from a reaction solution of 3**TriPh**+2**T** at 4 °C in $CHCl_3$. Crystallographic data for the structure has been deposited with the Cambridge Crystallographic Data Centre (CCDC), 12 Union Road, Cambridge CB21EZ, UK. Copies of the data can be obtained free of charge via www.ccdc.cam.ac.uk on quoting the depository number CCDC 2006765 for **$pPh_2(NON)_2 \cdot H_2O$**, 2006766 for **$BiPh_2(NON)_2$**, 2006767 for **$2BiPy_2(NON)_2 \cdot CHCl_3$**, and 2018494 for **$TriPh_3T_2 \cdot 3CHCl_3$**.

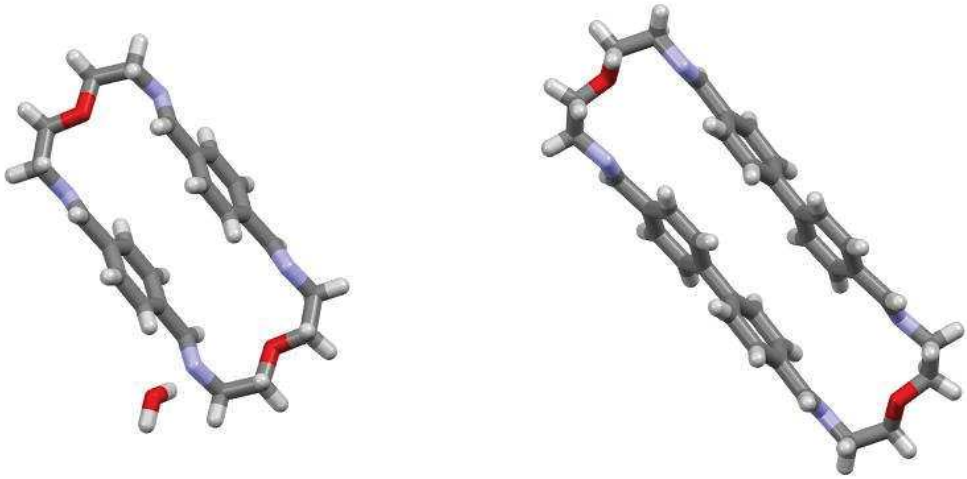

Figure S-Crystal-1. Single-crystal X-ray structure of Macrocycle **$pPh_2(NON)_2 \cdot H_2O$** and **$BiPh_2(NON)_2$**. Color scheme: carbon (grey), hydrogen (white), nitrogen (blue), oxygen (red).

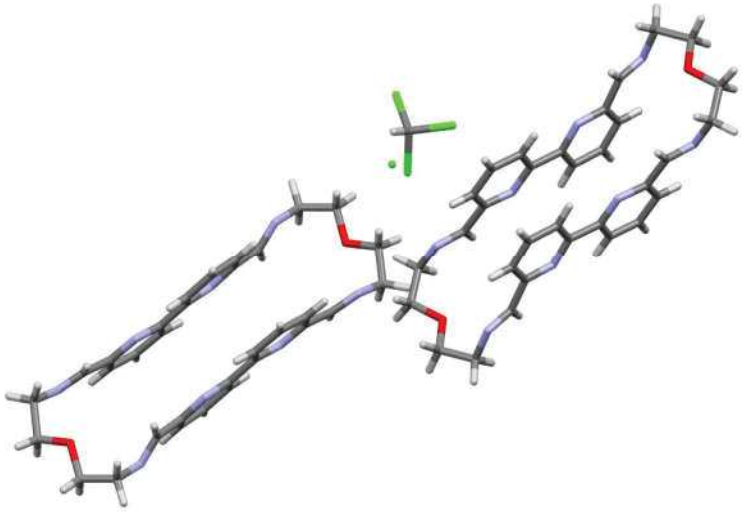

Figure S-Crystal-2. Single-crystal X-ray structure of macrocycle **2BiPy$_2$(NON)$_2$·CHCl$_3$**. Colour scheme: carbon (grey), hydrogen (white), nitrogen (blue), oxygen (red).

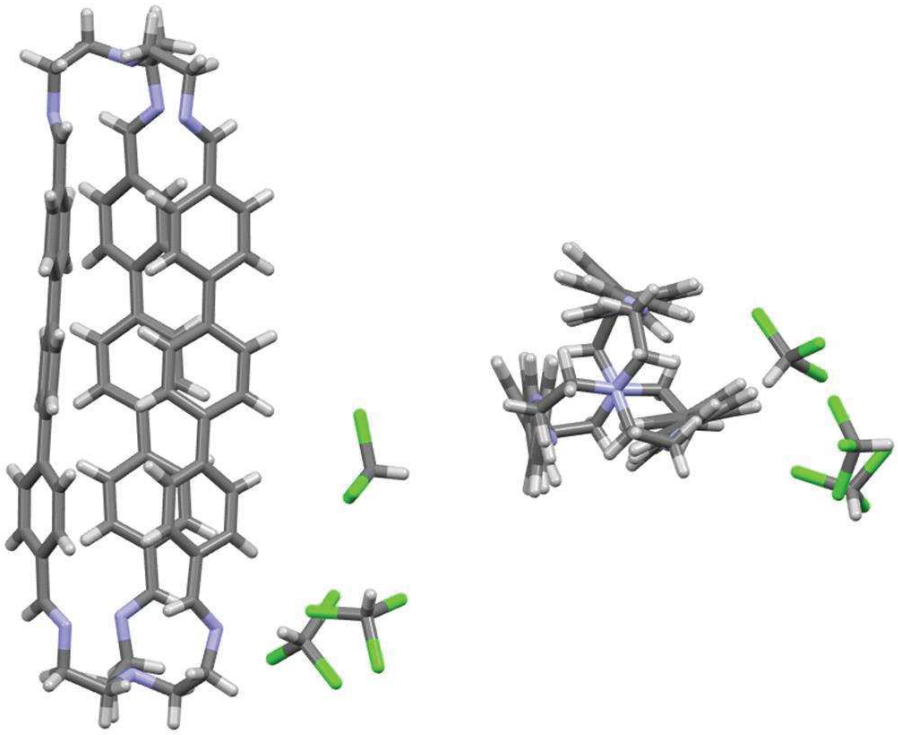

Figure S-Crystal-3. Single-crystal X-ray structure of macrobicyclic cage **TriPh$_3$T$_2$·3CHCl$_3$**. Colour scheme: carbon (grey), hydrogen (white), nitrogen (blue), chlorine (green).

Table S-Crystal-1. Crystal data and structure refinement for Macrocycle **$pPh_2(NON)_2$**, **$BiPh_2(NON)_2$** and **$BiPy_2(NON)_2$**

Identification code	**$pPh_2(NON)_2 \cdot H_2O$**	**$BiPh_2(NON)_2$**	**$2BiPy_2(NON)_2 \cdot CHCl_3$**
Empirical formula	$C_{24}H_{28}N_4O_2 \cdot H_2O$	$C_{36}H_{36}N_4O_2$	$2C_{32}H_{32}N_8O_2 \cdot CHCl_3$
Formula weight	422.52	556.69	680.02
Temperature/K	120(2)	120(2)	173(2)
Crystal system	orthorhombic	triclinic	triclinic
Space group	P c c n	P− 1	P− 1
a/Å	16.0157(5)	8.9175(4)	11.8514(8)
b/Å	16.9055(6)	9.6423(5)	12.1452(8)
c/Å	8.2684(2)	10.4108(5)	12.4329(9)
α/°	90	62.612(2)	92.612(2)
β/°	90	67.462(2)	100.027(2)
γ/°	90	72.983(2)	106.750(2)
Volume/$Å^3$	2238.70(12)	726.71(6)	1678.7(2)
Z	4	1	2
$\rho_{calcd}/g \cdot cm^{-3}$	1.254	1.272	1.345
μ/mm^{-1}	0.084	0.080	0.316
F(000)	904	296	708
Crystal size/mm^3	0.120×0.140×0.160	0.200×0.150×0.080	0.280×0.180×0.140
Radiation	0.71073	0.71073	0.71073
2θ range for data collection/°	2.410-28.012	2.304-30.008	1.760-28.052
Index ranges	-21 ≤ h ≤ 21, -22 ≤ k ≤ 21, -10 ≤ l ≤ 10	-11 ≤ h ≤ 12, -13 ≤ k ≤ 13, -14 ≤ l ≤ 14	-15 ≤ h ≤ 15, -16 ≤ k ≤ 16, -16 ≤ l ≤ 16
Reflections collected	27088	27416	44903
Reflns. unique	2703	4246	8137
Reflns. obsd.	2311	3538	5004
R_{int}	0.0412	0.0341	0.0484
Params. refined	145	190	418
Goodness-of-fit on F^2	1.054	1.025	1.039
Final R indexes [I>=2σ (I)]	R_1=0.0432, wR_2= 0. 1117	R_1= 0.0394, wR_2= 0.1026	R_1=0.0594, wR_2= 0.1437
Final R indexes [all data]	R_1= 0.0513, wR_2= 0.1168	R_1= 0.0498, wR_2= 0.1104	R_1= 0.1077, wR_2= 0.1698

Largest diff. peak/hole / e $Å^{-3}$	0.350/-0.495	0.380/-0.189	1.150/-0.959

Table S-Crystal-2. Crystal data and structure refinement for **$TriPh_3T_2$** and **Cage bbp**

Identification code	**$TriPh_3T_2 \cdot 3CHCl_3$**	**Cage bbp**
Empirical formula	$C_{72}H_{66}N_8$, 3($CHCl_3$)	$C_{51}H_{51}N_{11}$, $CHCl_3$
Formula weight	1401.43	937.39
Temperature/K	120(2)	120(2)
Crystal system	triclinic	triclinic
Space group	P -1	P -1
a/Å	12.9054(10)	9.9355(3)
b/Å	13.4545(11)	15.3115(5)
c/Å	22.5621(18)	16.8456(6)
α/°	76.114(3)	104.1200(10)
β/°	82.526(3)	101.9570(10)
γ/°	62.714(3)	94.1560(10)
Volume/$Å^3$	3379.0(5)	2410.80(14)
Z	2	2
ρ_{calcd}/g·cm^{-3}	1.377	1.291
μ/mm^{-1}	0.424	2.102
F(000)	1456	984
Crystal size/mm^3	0.400×0.200×0.140	0.230×0.210×0.200
Radiation	0.71073	1.54178
2θ range for data collection/°	1.986-27.978	2.781-66.789
Index ranges	-16 ≤ h ≤ 17, -17 ≤ k ≤ 17, -29 ≤ l ≤ 29	-11 ≤ h ≤ 11, -16 ≤ k ≤ 18, -20 ≤ l ≤ 20
Reflections collected	147869	61234
Reflns. unique	16195	8497
Reflns. obsd.	12684	8145
R_{int}	0.0546	0.0312
Params. refined	829	595
Goodness-of-fit on F^2	1.031	1.055
Final R indexes [I>=2σ (I)]	R_1= 0.0659, wR_2= 0.1778	R_1= 0.0894, wR_2= 0.2645
Final R indexes [all data]	R_1= 0.0831, wR_2= 0.1941	R_1= 0.0908, wR_2= 0.2656
Largest diff. peak/hole / e $Å^{-3}$	1.932/-1.456	1.619/-1.598

References

(1) Lehn, J.-M. Supramolecular Chemistry ? Scope and Perspectives: Molecules ? Supermolecules ? Molecular Devices. *Journal of Inclusion Phenomena* **1988**, *6*, 351–396.

(2) Lehn, J.-M. Towards Complex Matter: Supramolecular Chemistry and Self-Organization. *European Review* **2009**, *17*, 263–280.

(3) Lehn, J.-M. Supramolecular Chemistry: Where from? Where To? *Chem. Soc. Rev.* **2017**, *46*, 2378–2379.

(4) Williams, G. T.; Haynes, C. J. E.; Fares, M.; Caltagirone, C.; Hiscock, J. R.; Gale, P. A. Advances in Applied Supramolecular Technologies. *Chem. Soc. Rev.* **2021**, *50*, 2737–2763.

(5) Fischer, E. Einfluss der Configuration auf die Wirkung der Enzyme. *Chem. Ber.* **1894**, *27*, 2985–2993.

(6) Hasenknopf, B.; Lehn, J.-M.; Boumediene, N.; Dupont-Gervais, A.; Van Dorsselaer, A.; Kneisel, B.; Fenske, D. Self-Assembly of Tetra- and Hexanuclear Circular Helicates. *J. Am. Chem. Soc.* **1997**, *119*, 10956–10962.

(7) Hasenknopf, B.; Lehn, J.-M.; Boumediene, N.; Leize, E.; Dorsselaer, A. V. Kinetic and Thermodynamic Control in Self-Assembly: Sequential Formation of Linear and Circular Helicates. *Angew. Chem. Int. Ed.* **1998**, *37*, 3265–3268.

(8) Ruben, M.; Rojo, J.; Romero-Salguero, F. J.; Uppadine, L. H.; Lehn, J.-M. Grid-Type Metal Ion Architectures: Functional Metallosupramolecular Arrays. *Angew. Chem. Int. Ed.* **2004**, *43*, 3644–3662.

(9) Stadler, A.-M.; Kyritsakas, N.; Graff, R.; Lehn, J.-M. Formation of Rack- and Grid-Type Metallosupramolecular Architectures and Generation of Molecular Motion by Reversible Uncoiling of Helical Ligand Strands. *Chem. Eur. J.* **2006**, *12*, 4503–4522.

(10) Ibukuro, F.; Fujita, M.; Yamaguchi, K.; Sauvage, J.-P. Quantitative and Spontaneous Formation of a Doubly Interlocking [2]Catenane Using Copper(I) and Palladium(II) as Templating and Assembling Centers. *J. Am. Chem. Soc.* **1999**, *121*, 11014–11015.

(11) Sauvage, J.-P.; Dietrich-Buchecker, C. Molecular catenanes, rotaxanes and knots : A journey through the world of molecular. Wiley-VCH, Weinheim, **1999**.

(12) Chichak, K. S.; Cantrill, S. J.; Pease, A. R.; Chiu, S.-H.; Cave, G. W. V.; Atwood, J. L.; Stoddart, J. F. Molecular Borromean Rings. *Science* **2004**, *304*, 1308–1312.

(13) Fujita, M.; Fujita, N.; Ogura, K.; Yamaguchi, K. Spontaneous Assembly of Ten Components into Two Interlocked, Identical Coordination Cages. *Nature* **1999**, *400*, 52–55.

(14) Fujita, D.; Ueda, Y.; Sato, S.; Mizuno, N.; Kumasaka, T.; Fujita, M. Self-Assembly of Tetravalent Goldberg Polyhedra from 144 Small Components. *Nature* **2016**, *540*, 563–566.

(15) Bloch, W. M.; Clever, G. H. Integrative Self-Sorting of Coordination Cages Based on 'Naked' Metal Ions. *Chem. Commun.* **2017**, *53*, 8506–8516.
(16) Hu, X.-Y.; Xiao, T.; Lin, C.; Huang, F.; Wang, L. Dynamic Supramolecular Complexes Constructed by Orthogonal Self-Assembly. *Acc. Chem. Res.* **2014**, *47*, 2041–2051.
(17) Barboiu, M.; Stadler, A.-M.; Lehn, J.-M. Controlled Folding, Motional, and Constitutional Dynamic Processes of Polyheterocyclic Molecular Strands. *Angew. Chem. Int. Ed.* **2016**, *55*, 4130–4154.
(18) Rowan, S. J.; Cantrill, S. J.; Cousins, G. R. L.; Sanders, J. K. M.; Stoddart, J. F. Dynamic Covalent Chemistry. *Angew. Chem. Int. Ed.* **2002**, *41*, 898–952.
(19) Belowich, M. E.; Stoddart, J. F. Dynamic Imine Chemistry. *Chem. Soc. Rev.* **2012**, *41*, 2003.
(20) Herrmann, A. Dynamic Combinatorial/Covalent Chemistry: A Tool to Read, Generate and Modulate the Bioactivity of Compounds and Compound Mixtures. *Chem. Soc. Rev.* **2014**, *43*, 1899–1933.
(21) Osypenko, A.; Dhers, S.; Lehn, J.-M. Pattern Generation and Information Transfer through a Liquid/Liquid Interface in 3D Constitutional Dynamic Networks of Imine Ligands in Response to Metal Cation Effectors. *J. Am. Chem. Soc.* **2019**, *141*, 12724–12737.
(22) Corbett, P. T.; Leclaire, J.; Vial, L.; West, K. R.; Wietor, J.-L.; Sanders, J. K. M.; Otto, S. Dynamic Combinatorial Chemistry. *Chem. Rev.* **2006**, *106*, 3652–3711.
(23) Frei, P.; Hevey, R.; Ernst, B. Dynamic Combinatorial Chemistry: A New Methodology Comes of Age. *Chem. Eur. J.* **2019**, *25*, 60–73.
(24) Lehn, J.-M. Constitutional Dynamic Chemistry: Bridge from Supramolecular Chemistry to Adaptive Chemistry. In *Constitutional Dynamic Chemistry*; Barboiu, M., Ed.; Topics in Current Chemistry; Springer Berlin Heidelberg: Berlin, Heidelberg, 2011; Vol. 322, pp 1–32.
(25) *Constitutional Dynamic Chemistry*; Barboiu, M., Aastrup, T., Eds.; Topics in current chemistry; Springer: Heidelberg, **2012**.
(26) Huc, I.; Lehn, J.-M. Virtual Combinatorial Libraries: Dynamic Generation of Molecular and Supramolecular Diversity by Self-Assembly. *Proc. Natl. Acad. Sci. U.S.A.* **1997**, *94*, 2106–2110.
(27) Lehn, J.-M. Dynamic Combinatorial Chemistry and Virtual Combinatorial Libraries. *Chem. Eur. J.* **1999**, *5*, 2455–2463.
(28) Lehn, J.-M. From Supramolecular Chemistry towards Constitutional Dynamic Chemistry and Adaptive Chemistry. *Chem. Soc. Rev.* **2007**, *36*, 151–160.
(29) Ayme, J.-F.; Lehn, J.-M. From Coordination Chemistry to Adaptive Chemistry. In *Advances in Inorganic Chemistry*; Elsevier, **2018**, *71*, 3–78.
(30) He, M.; Lehn, J.-M. Time-Dependent Switching of Constitutional Dynamic Libraries and Networks from Kinetic to Thermodynamic Distributions. *J. Am. Chem. Soc.* **2019**, *141*, 18560–18569.

(31) Ramström, O.; Lehn, J.-M. Drug Discovery by Dynamic Combinatorial Libraries. *Nat Rev Drug Discov* **2002**, *1*, 26–36.
(32) Cheeseman, J. D.; Corbett, A. D.; Gleason, J. L.; Kazlauskas, R. J. Receptor-Assisted Combinatorial Chemistry: Thermodynamics and Kinetics in Drug Discovery. *Chem. Eur. J.* **2005**, *11*, 1708–1716.
(33) Hochgürtel, M.; and Lehn, J.-M. Fragment based Approaches in Drug Discovery. Wiley-VCH, Weinheim, **2006**, ch. 16.
(34) Giuseppone, N.; Lehn, J.-M. Protonic and Temperature Modulation of Constituent Expression by Component Selection in a Dynamic Combinatorial Library of Imines. *Chem. Eur. J.* **2006**, *12*, 1715–1722.
(35) Vantomme, G.; Lehn, J.-M. Reversible Adaptation to Photoinduced Shape Switching by Oligomer-Macrocycle Interconversion with Component Selection in a Three-State Constitutional Dynamic System. *Chem. Eur. J.* **2014**, *20*, 16188–16193.
(36) Vantomme, G.; Hafezi, N.; Lehn, J.-M. A Light-Induced Reversible Phase Separation and Its Coupling to a Dynamic Library of Imines. *Chem. Sci.* **2014**, *5*, 1475–1483.
(37) Herder, M.; Lehn, J.-M. The Photodynamic Covalent Bond: Sensitized Alkoxyamines as a Tool To Shift Reaction Networks Out-of-Equilibrium Using Light Energy. *J. Am. Chem. Soc.* **2018**, *140*, 7647–7657.
(38) Wang, S.; Yue, L.; Li, Z.; Zhang, J.; Tian, H.; Willner, I. Light-Induced Reversible Reconfiguration of DNA-Based Constitutional Dynamic Networks: Application to Switchable Catalysis. *Angew. Chem. Int. Ed.* **2018**, *57*, 8105–8109.
(39) Giuseppone, N.; Lehn, J.-M. Electric-Field Modulation of Component Exchange in Constitutional Dynamic Liquid Crystals. *Angew. Chem. Int. Ed.* **2006**, *45*, 4619–4624.
(40) Herrmann, A.; Giuseppone, N.; Lehn, J.-M. Electric-Field Triggered Controlled Release of Bioactive Volatiles from Imine-Based Liquid Crystalline Phases. *Chem. Eur. J.* **2009**, *15*, 117–124.
(41) Sobczak, S.; Drożdż, W.; Lampronti, G. I.; Belenguer, A. M.; Katrusiak, A.; Stefankiewicz, A. R. Dynamic Covalent Chemistry under High-Pressure:A New Route to Disulfide Metathesis. *Chem. Eur. J.* **2018**, *24*, 8769–8773.
(42) Giuseppone, N.; Schmitt, J.-L.; Lehn, J.-M. Driven Evolution of a Constitutional Dynamic Library of Molecular Helices Toward the Selective Generation of [2 × 2] Gridlike Arrays under the Pressure of Metal Ion Coordination. *J. Am. Chem. Soc.* **2006**, *128*, 16748–16763.
(43) Shyshov, O.; Brachvogel, R.-C.; Bachmann, T.; Srikantharajah, R.; Segets, D.; Hampel, F.; Puchta, R.; von Delius, M. Adaptive Behaviour of Dynamic Orthoester Cryptands. *Angew. Chem. Int. Ed.* **2017**, *56*, 776–781.
(44) Vantomme, G.; Jiang, S.; Lehn, J.-M. Adaptation in Constitutional Dynamic Libraries and Networks, Switching between Orthogonal Metalloselection and Photoselection Processes. *J. Am. Chem. Soc.* **2014**, *136*, 9509–9518.

(45) Nguyen, R.; Buhler, E.; Giuseppone, N. Dynablocks: Structural Modulation of Responsive Combinatorial Self-Assemblies at Mesoscale. *Macromolecules* **2009**, *42*, 5913–5915.

(46) Tauk, L.; Schröder, A. P.; Decher, G.; Giuseppone, N. Hierarchical Functional Gradients of PH-Responsive Self-Assembled Monolayers Using Dynamic Covalent Chemistry on Surfaces. *Nature Chem* **2009**, *1*, 649–656.

(47) Armao, J. J.; Lehn, J.-M. Nonlinear Kinetic Behaviour in Constitutional Dynamic Reaction Networks. *J. Am. Chem. Soc.* **2016**, *138*, 16809–16814.

(48) Lehn, J.-M. Perspectives in Chemistry-Steps towards Complex Matter. *Angew. Chem. Int. Ed.* **2013**, *52*, 2836–2850.

(49) Busch, D. H. First Considerations: Principles, Classification, and History. In *Templates in Chemistry II*; Schalley, C. A., Vögtle, F., Dötz, K. H., Eds.; Topics in Current Chemistry; Springer Berlin Heidelberg: Berlin, Heidelberg, 2005; Vol. 249, pp 1–65.

(50) He, M.; Lehn, J. Metal Cation-Driven Dynamic Covalent Formation of Imine and Hydrazone Ligands Displaying Synergistic Co-catalysis and Auxiliary Amine Effects. *Chem. Eur. J.* **2021**, *27*, 7516–7524.

(51) Holub, J.; Vantomme, G.; Lehn, J.-M. Training a Constitutional Dynamic Network for Effector Recognition: Storage, Recall, and Erasing of Information. *J. Am. Chem. Soc.* **2016**, *138*, 11783–11791.

(52) Men, G.; Lehn, J.-M. Higher Order Constitutional Dynamic Networks: [2×3] and [3×3] Networks Displaying Multiple, Synergistic and Competitive Hierarchical Adaptation. *J. Am. Chem. Soc.* **2017**, *139*, 2474–2483.

(53) Fischer, E.; Frei, Y. Photoisomerization Equilibria Involving the C=N Double Bond. *The Journal of Chemical Physics* **1957**, *27*, 808–809.

(54) Ulrich, S.; Lehn, J.-M. Reversible Switching between Macrocyclic and Polymeric States by Morphological Control in a Constitutional Dynamic System. *Angew. Chem. Int. Ed.* **2008**, *47*, 2240–2243.

(55) Bai, B.; Zhang, M.; Ji, N.; Wei, J.; Wang, H.; Li, M. E–Z Isomerization of the –C N– Bond in Anthracene-Based Acylhydrazone Derivatives under Visible Light. *Chem. Commun.* **2017**, *53*, 2693–2696.

(56) Men, G.; Lehn, J.-M. Multiple Adaptation of Constitutional Dynamic Networks and Information Storage in Constitutional Distributions of Acylhydrazones. *Chem. Sci.* **2019**, *10*, 90–98.

(57) Ulrich, S.; Lehn, J.-M. Adaptation to Shape Switching by Component Selection in a Constitutional Dynamic System. *J. Am. Chem. Soc.* **2009**, *131*, 5546–5559.

(58) Kulchat, S.; Meguellati, K.; Lehn, J.-M. Organocatalyzed and Uncatalyzed C═C/C═C and C═C/C═N Exchange Processes between *Knoevenagel* and Imine Compounds in Dynamic Covalent Chemistry. *HCA* **2014**, *97*, 1219–1236.

(59) Gu, R.; Flidrova, K.; Lehn, J.-M. Dynamic Covalent Metathesis in the C═C/C═N Exchange between Knoevenagel Compounds and Imines. *J. Am. Chem. Soc.* **2018**, *140*, 5560–5568.

(60) Gu, R.; Lehn, J.-M. Constitutional Dynamic Selection at Low Reynolds Number in a Triple Dynamic System: Covalent Dynamic Adaptation Driven by Double Supramolecular Self-Assembly. *J. Am. Chem. Soc.* **2021**, *143*, 14136–14146.

(61) Supuran, C. T.; Scozzafava, A. Carbonic Anhydrases as Targets for Medicinal Chemistry. *Bioorganic & Medicinal Chemistry* **2007**, *15*, 4336–4350.

(62) Zhang, Y.; Feng, W.-X.; Legrand, Y.-M.; Supuran, C. T.; Su, C.-Y.; Barboiu, M. Dynameric Host Frameworks for the Activation of Lipase through H-Bond and Interfacial Encapsulation. *Chem. Commun.* **2016**, *52*, 13768–13770.

(63) Su, D.; Zhang, Y.; Ulrich, S.; Barboiu, M. Constitutional Dynamic Inhibition/Activation of Carbonic Anhydrases. *ChemPlusChem* **2021**, *86*, 1500–1510.

(64) Casciuc, I.; Osypenko, A.; Kozibroda, B.; Horvath, D.; Marcou, G.; Bonachera, F.; Varnek, A.; Lehn, J.-M. Toward in Silico Modeling of Dynamic Combinatorial Libraries. *ACS Cent. Sci.* **2022**, *8*, 804–813.

(65) Charles, C. D.; Bloch, E. D. High-Pressure Methane Storage and Selective Gas Adsorption in a Cyclohexane-Functionalised Porous Organic Cage. *Supramolecular Chemistry* **2019**, *31*, 508–513.

(66) Zhang, F.; He, Y.; Huang, J.; Sumpter, B. G.; Qiao, R. Multicomponent Gas Storage in Organic Cage Molecules. *J. Phys. Chem. C* **2017**, *121*, 12426–12433.

(67) Marchetti, L.; Levine, M. Biomimetic Catalysis. *ACS Catal.* **2011**, *1*, 1090–1118.

(68) Shang, J.; Liu, Y.; Pan, T. Macrocycles in Bioinspired Catalysis: From Molecules to Materials. *Front. Chem.* **2021**, *9*, 635315.

(69) He, Q.; Vargas-Zúñiga, G. I.; Kim, S. H.; Kim, S. K.; Sessler, J. L. Macrocycles as Ion Pair Receptors. *Chem. Rev.* **2019**, *119*, 9753–9835.

(70) Wu, J.; Kwon, B.; Liu, W.; Anslyn, E. V.; Wang, P.; Kim, J. S. Chromogenic/Fluorogenic Ensemble Chemosensing Systems. *Chem. Rev.* **2015**, *115*, 7893–7943.

(71) Dondoni, A.; Marra, A. Calixarene and Calixresorcarene Glycosides: Their Synthesis and Biological Applications. *Chem. Rev.* **2010**, *110*, 4949–4977.

(72) Pedersen, C J. Cyclic Polyethers and Their Complexes with Metal Salts. *J. Am. Chem. Soc.* **1967**, *89*, 7017–7036.

(73) Pedersen, C. J. The Discovery of Crown Ethers (Noble Lecture). *Angew. Chem. Int. Ed. Engl.* **1988**, *27*, 1021–1027.

(74) Cram, D. J. The Design of Molecular Hosts, Guests, and Their Complexes (Nobel Lecture). *Angew. Chem. Int. Ed. Engl.* **1988**, *27*, 1009–1020.

(75) Dietrich, B.; Lehn, J.-M.; Sauvage, J. P. Diaza-polyoxa-macrocycles et macrobicycles. *Tetrahedron Letters* **1969**, *10*, 2885–2888.

(76) Jazwinski, J.; Lehn, J.-M.; Meric, R.; Vigneron, J. P.; Cesario, M.; Guilhem, J.; Pascard, C. Polyaza-macrocycles of cyclophane type: Synthesis, struc-ture of a chloroform inclusion complex and anion binding. *Tetrahedron Lett.* **1987**, *28*, 3489–3492.

(77) Vigato, P. A.; Tamburini, S. The Challenge of Cyclic and Acyclic Schiff Bases and Related Derivatives. *Coordination Chemistry Reviews* **2004**, *248*, 1717–2128.
(78) Akine, S.; Nabeshima, T. Cyclic and Acyclic Oligo(N2O2) Ligands for Cooperative Multi-Metal Complexation. *Dalton Trans.* **2009**, No. 47, 10395.
(79) Frydrych, R.; Ślepokura, K.; Bil, A.; Gregoliński, J. Mixed Macrocycles Derived from 2,6-Diformylpyridine and Opposite Enantiomers of *Trans* -1,2-Diaminocyclopentane and *Trans* -1,2-Diaminocyclohexane. *J. Org. Chem.* **2019**, *84*, 5695–5711.
(80) Curtis, N. F. Macrocyclic Coordination Compounds Formed by Condensation of Metal-Amine Complexes with Aliphatic Carbonyl Compounds. *Coordination Chemistry Reviews* **1968**, *3*, 3–47.
(81) Sarnicka, A.; Starynowicz, P.; Lisowski, J. Controlling the Macrocycle Size by the Stoichiometry of the Applied Template Ion. *Chem. Commun.* **2012**, *48*, 2237.
(82) He, Z.; Ye, G.; Jiang, W. Imine Macrocycle with a Deep Cavity: Guest-Selected Formation of *Syn/Anti* Configuration and Guest-Controlled Reconfiguration. *Chem. Eur. J.* **2015**, *21*, 3005–3012.
(83) Jazwinski, J.; Lehn, J.-M.; Lilienbaum, D.; Ziessel, R.; Guilhem, J.; Pascard, C. Polyaza Macrobicyclic Cryptands: Synthesis, Crystal Structures of a Cyclophane Type Macrobicyclic Cryptand and of Its Dinuclear Copper(I) Cryptate, and Anion Binding Features. *J. Chem. Soc., Chem. Commun.* **1987**, 22, 1691.
(84) MacDowell, D.; Nelson, J. Facile Synthesis of a New Family of Cage Molecules. *Tetrahedron Letters* **1988**, *29*, 385–386.
(85) Zhang, G.; Mastalerz, M. Organic Cage Compounds – from Shape-Persistency to Function. *Chem. Soc. Rev.* **2014**, *43*, 1934–1947.
(86) Mastalerz, M. Porous Shape-Persistent Organic Cage Compounds of Different Size, Geometry, and Function. *Acc. Chem. Res.* **2018**, *51*, 2411–2422.
(87) Berardo, E.; Turcani, L.; Miklitz, M.; Jelfs, K. E. An Evolutionary Algorithm for the Discovery of Porous Organic Cages. *Chem. Sci.* **2018**, *9*, 8513–8527.
(88) Li, P.; Xu, S.; Yu, C.; Li, Z.; Xu, J.; Li, Z.; Zou, L.; Leng, X.; Gao, S.; Liu, Z.; Liu, X.; Zhang, S. De Novo Construction of Catenanes with Dissymmetric Cages by Space-Discriminative Post-Assembly Modification. *Angew. Chem. Int. Ed.* **2020**, *59*, 7113–7121.
(89) Ono, K.; Iwasawa, N. Dynamic Behaviour of Covalent Organic Cages. *Chem. Eur. J.* **2018**, *24*, 17856–17868.
(90) Liu, X.; Warmuth, R. Solvent Effects in Thermodynamically Controlled Multicomponent Nanocage Syntheses. *J. Am. Chem. Soc.* **2006**, *128*, 14120–14127.
(91) Hasell, T.; Wu, X.; Jones, J. T. A.; Bacsa, J.; Steiner, A.; Mitra, T.; Trewin, A.; Adams, D. J.; Cooper, A. I. Triply Interlocked Covalent Organic Cages. *Nature Chem* **2010**, *2*, 750–755.
(92) Greenaway, R. L.; Santolini, V.; Bennison, M. J.; Alston, B. M.; Pugh, C. J.; Little, M. A.; Miklitz, M.; Eden-Rump, E. G. B.; Clowes, R.; Shakil, A.; Cuthbertson, H. J.; Armstrong, H.; Briggs, M. E.; Jelfs, K. E.; Cooper, A. I. High-Throughput Discovery

of Organic Cages and Catenanes Using Computational Screening Fused with Robotic Synthesis. *Nat Commun* **2018**, *9*, 2849.

(93) Bravin, C.; Badetti, E.; Scaramuzzo, F. A.; Licini, G.; Zonta, C. Triggering Assembly and Disassembly of a Supramolecular Cage. *J. Am. Chem. Soc.* **2017**, *139*, 6456–6460.

(94) Bravin, C.; Guidetti, A.; Licini, G.; Zonta, C. Supramolecular Cages as Differential Sensors for Dicarboxylate Anions: Guest Length Sensing Using Principal Component Analysis of ESI-MS and ^{1}H-NMR Raw Data. *Chem. Sci.* **2019**, *10*, 3523–3528.

(95) Hristova, Y. R.; Smulders, M. M. J.; Clegg, J. K.; Breiner, B.; Nitschke, J. R. Selective Anion Binding by a "Chameleon" Capsule with a Dynamically Reconfigurable Exterior. *Chem. Sci.* **2011**, *2*, 638–641.

(96) Weißenfels, M.; Gemen, J.; Klajn, R. Dissipative Self-Assembly: Fueling with Chemicals versus Light. *Chem* **2021**, *7*, 23–37.

(97) Singh, N.; Formon, G. J. M.; De Piccoli, S.; Hermans, T. M. Devising Synthetic Reaction Cycles for Dissipative Nonequilibrium Self-Assembly. *Adv. Mater.* **2020**, *32* (20), 1906834.

(98) Liyana Gunawardana, V. W.; Finnegan, T. J.; Ward, C. E.; Moore, C. E.; Badjić, J. D. Dissipative Formation of Covalent Basket Cages. *Angew Chem Int Ed* **2022**, *61*.

(99) Pasteur, L. Recherches sur les relations qui peuvent exister entre la forme cristalline, la composition chimique et le sens de la polarisation rotatoire. *Annales de chimie et de physique*, **1848**, *24*, 442–459.

(100) Kramer, R.; Lehn, J.-M.; Marquis-Rigault, A. Self-Recognition in Helicate Self-Assembly: Spontaneous Formation of Helical Metal Complexes from Mixtures of Ligands and Metal Ions. *Proceedings of the National Academy of Sciences* **1993**, *90*, 5394–5398.

(101) Jolliffe, K. A.; Timmerman, P.; Reinhoudt, D. N. Noncovalent Assembly of a Fifteen-Component Hydrogen-Bonded Nanostructure. *Angew. Chem.,Int. Ed.* **1999**, *38*, 933–937.

(102) Singh, A. S.; Sun, S.-S. Narcissistic Self-Sorting of Hydrogen-Bonded Dimeric Capsules Formed through Self-Assembly of Flexible Tripodal Receptors in Polar Solvents. *Chem. Commun.* **2012**, *48*, 7392.

(103) Aratsu, K.; Takeya, R.; Pauw, B. R.; Hollamby, M. J.; Kitamoto, Y.; Shimizu, N.; Takagi, H.; Haruki, R.; Adachi, S.; Yagai, S. Supramolecular Copolymerization Driven by Integrative Self-Sorting of Hydrogen-Bonded Rosettes. *Nat Commun* **2020**, *11*, 1623.

(104) Mahata, K.; Saha, M. L.; Schmittel, M. From an Eight-Component Self-Sorting Algorithm to a Trisheterometallic Scalene Triangle. *J. Am. Chem. Soc.* **2010**, *132*, 15933–15935.

(105) Zheng, Y.-R.; Yang, H.-B.; Northrop, B. H.; Ghosh, K.; Stang, P. J. Size Selective Self-Sorting in Coordination-Driven Self-Assembly of Finite Ensembles. *Inorg. Chem.* **2008**, *47*, 4706–4711.

(106) Wang, W.; Zhou, Z.; Zhou, J.; Shi, B.; Song, B.; Li, X.; Huang, F.; Stang, P. J. Self-Assembled Amphiphilic Janus Double Metallacycle. *Inorg. Chem.* **2019**, *58*, 7141–7145.

(107) Ogoshi, T.; Takashima, S.; Inada, N.; Asakawa, H.; Fukuma, T.; Shoji, Y.; Kajitani, T.; Fukushima, T.; Tada, T.; Dotera, T.; Kakuta, T.; Yamagishi, T. Ring Shape-Dependent Self-Sorting of Pillar[n]Arenes Assembled on a Surface. *Commun Chem* **2018**, *1*, 92.

(108) Rowan, S. J.; Hamilton, D. G.; Brady, P. A.; Sanders, J. K. M. Automated Recognition, Sorting, and Covalent Self-Assembly by Predisposed Building Blocks in a Mixture. *J. Am. Chem. Soc.* **1997**, *119*, 2578–2579.

(109) Wu, A.; Isaacs, L. Self-Sorting: The Exception or the Rule? *J. Am. Chem. Soc.* **2003**, *125*, 4831–4835.

(110) Jiang, W.; Winkler, H. D. F.; Schalley, C. A. Integrative Self-Sorting: Construction of a Cascade-Stoppered Hetero[3]Rotaxane. *J. Am. Chem. Soc.* **2008**, *130*, 13852–13853.

(111) Jiang, W.; Schalley, C. A. Integrative Self-Sorting Is a Programming Language for High Level Self-Assembly. *Proc. Natl. Acad. Sci. U.S.A.* **2009**, *106*, 10425–10429.

(112) Hsu, C.-W.; Miljanić, O. Š. Self-Sorting through Dynamic Covalent Chemistry. In *Dynamic Covalent Chemistry*; Zhang, W., Jin, Y., Eds.; John Wiley & Sons, Ltd: Chichester, UK, **2017**; 253–286.

(113) Mittal, N.; Saha, M. L.; Schmittel, M. Fully Reversible Three-State Interconversion of Metallosupramolecular Architectures. *Chem. Commun.* **2016**, *52*, 8749–8752.

(114) Timmerman, P.; Vreekamp, R. H.; Hulst, R.; Verboom, W.; Reinhoudt, D. N.; Rissanen, K.; Udachin, K. A.; Ripmeester, J. Noncovalent Assembly of Functional Groups on Calix[4]Arene Molecular Boxes. *Chem. Eur. J.* **1997**, *3*, 1823–1832.

(115) Schmittel, M.; Saha, M. L.; Fan, J. Scaffolding a Cage-Like 3D Framework by Coordination and Constitutional Dynamic Chemistry. *Org. Lett.* **2011**, *13*, 3916–3919.

(116) Ayme, J.-F.; Beves, J. E.; Campbell, C. J.; Leigh, D. A. The Self-Sorting Behaviour of Circular Helicates and Molecular Knots and Links. *Angew. Chem., Int. Ed.* **2014**, *53*, 7823–7827.

(117) Wiley, C. A.; Holloway, L. R.; Miller, T. F.; Lyon, Y.; Julian, Ryan. R.; Hooley, R. J. Electronic Effects on Narcissistic Self-Sorting in Multicomponent Self-Assembly of Fe-Iminopyridine *Meso* -Helicates. *Inorg. Chem.* **2016**, *55*, 9805–9815.

(118) Schultz, D.; Nitschke, J. R. Choices of Iron and Copper: Cooperative Selection during Self-Assembly. *Angew. Chem., Int. Ed.* **2006**, *45*, 2453–2456.

(119) Acharyya, K.; Mukherjee, S.; Mukherjee, P. S. Molecular Marriage through Partner Preferences in Covalent Cage Formation and Cage-to-Cage Transformation. *J. Am. Chem. Soc.* **2013**, *135*, 554–557.

(120) Acharyya, K.; Mukherjee, P. S. Hydrogen-Bond-Driven Controlled Molecular Marriage in Covalent Cages. *Chem. Eur. J.* **2014**, *20*, 1646–1657.

(121) Acharyya, K.; Mukherjee, P. S. Organic Imine Cages: Molecular Marriage and Applications. *Angew. Chem. Int. Ed.* **2019**, *58*, 8640–8653.

(122) Kołodziejski, M.; Stefankiewicz, A. R.; Lehn, J.-M. Dynamic Polyimine Macrobicyclic Cryptands – Self-Sorting with Component Selection. *Chem. Sci.* **2019**, *10*, 1836–1843.
(123) Ayme, J.-F.; Lehn, J.-M.; Bailly, C.; Karmazin, L. Simultaneous Generation of a [2 × 2] Grid-Like Complex and a Linear Double Helicate: A Three-Level Self-Sorting Process. *J. Am. Chem. Soc.* **2020**, *142*, 5819–5824.
(124) Liu, B.; Beatty, M. A.; Pappas, C. G.; Liu, K.; Ottelé, J.; Otto, S. Self-Sorting in Dynamic Combinatorial Libraries Leads to the Co-Existence of Foldamers and Self-Replicators. *Angew. Chem.* **2021**, *133*, 13681–13685.
(125) Ji, Q.; Lirag, R. C.; Miljanić, O. Š. Kinetically Controlled Phenomena in Dynamic Combinatorial Libraries. *Chem. Soc. Rev.* **2014**, *43*, 1873–1884.
(126) Ayme, J.-F.; Lehn, J.-M. Self-Sorting of Two Imine-Based Metal Complexes: Balancing Kinetics and Thermodynamics in Constitutional Dynamic Networks. *Chem. Sci.* **2020**, *11*, 1114–1121.
(127) Osowska, K.; Miljanić, O. Š. Oxidative Kinetic Self-Sorting of a Dynamic Imine Library. *J. Am. Chem. Soc.* **2011**, *133*, 724–727.
(128) Lirag, R. C.; Osowska, K.; Miljanić, O. Š. Precipitation-Driven Self-Sorting of Imines. *Org. Biomol. Chem.* **2012**, *10*, 4847.
(129) Ji, Q.; Miljanić, O. Š. Distillative Self-Sorting of Dynamic Ester Libraries. *J. Org. Chem.* **2013**, *78* (24), 12710–12716.
(130) Hsu, C. W.; Miljanić, O. Š. Adsorption-Driven Self-Sorting of Dynamic Imine Libraries. *Angew. Chem., Int. Ed.* **2015**, *54*, 2219–2222.
(131) Hsu, C.-W.; Miljanić, O. Š. Kinetically Controlled Simplification of a Multiresponsive [10 × 10] Dynamic Imine Library. *Chem. Commun.* **2016**, *52*, 12357–12359.
(132) He, Z.; Jiang, W.; Schalley, C. A. Integrative Self-Sorting: A Versatile Strategy for the Construction of Complex Supramolecular Architecture. *Chem. Soc. Rev.* **2015**, *44*, 779–789.
(133) Abet, V.; Szczypiński, F. T.; Little, M. A.; Santolini, V.; Jones, C. D.; Evans, R.; Wilson, C.; Wu, X.; Thorne, M. F.; Bennison, M. J.; Cui, P.; Cooper, A. I.; Jelfs, K. E.; Slater, A. G. Inducing Social Self-Sorting in Organic Cages To Tune The Shape of The Internal Cavity. *Angew. Chem. Int. Ed.* **2020**, *59*, 16755–16763.
(134) Jiang, W.; Schäfer, A.; Mohr, P. C.; Schalley, C. A. Monitoring Self-Sorting by Electrospray Ionization Mass Spectrometry: Formation Intermediates and Error-Correction during the Self-Assembly of Multiply Threaded Pseudorotaxanes. *J. Am. Chem. Soc.* **2010**, *132*, 2309–2320.
(135) Kulchat, S.; Chaur, M. N.; Lehn, J.-M. Kinetic Selectivity and Thermodynamic Features of Competitive Imine Formation in Dynamic Covalent Chemistry. *Chem. Eur. J.* **2017**, *23*, 11108–11118.
(136) Osowska, K.; Miljanić, O. Kinetic and Thermodynamic Self-Sorting in Synthetic Systems. *Synlett* **2011**, *2011*, 1643–1648.

(137) Safont-Sempere, M. M.; Fernández, G.; Würthner, F. Self-Sorting Phenomena in Complex Supramolecular Systems. *Chem. Rev.* **2011**, *111*, 5784–5814.
(138) Jędrzejewska, H.; Szumna, A. Making a Right or Left Choice: Chiral Self-Sorting as a Tool for the Formation of Discrete Complex Structures. *Chem. Rev.* **2017**, *117*, 4863–4899.
(139) Li, C.; Zuo, Y.; Zhao, Y.-Q.; Zhang, S. Chiral Self-Sorting in Cage-like Compounds. *Chem. Lett.* **2020**, *49*, 1356–1366.
(140) Zhan, Y.-Y. Kojima, T.; Ishii, K.; Takahashi, S.; Haketa, Y.; Maeda, H.; Uchiyama, S.; Hiraoka, S. Temperature-Controlled Repeatable Scrambling and Induced-Sorting of Building Blocks between Cubic Assemblies. *Nat Commun* **2019**, *10*, 1440
K.; Ishii, S.; Takahashi, Y.; Haketa, H.; Maeda, S.; Uchiyama & S.; Hiraoka 8.
(141) Kieffer, M.; Bilbeisi, R. A.; Thoburn, J. D.; Clegg, J. K.; Nitschke, J. R. Guest Binding Drives Host Redistribution in Libraries of $Co^{II}_4L_4$ Cages. *Angew. Chem.* **2020**, *132*, 11465–11469.
(142) Ulrich, S.; Buhler, E.; Lehn, J.-M. Reversible Constitutional Switching between Macrocycles and Polymers Induced by Shape Change in a Dynamic Covalent System. *New J. Chem.* **2009**, *33*, 271.
(143) Shi, Q.; Bergquist, K.-E.; Huo, R.; Li, J.; Lund, M.; Vácha, R.; Sundin, A.; Butkus, E.; Orentas, E.; Wärnmark, K. Composition- and Size-Controlled Cyclic Self-Assembly by Solvent- and C_{60} -Responsive Self-Sorting. *J. Am. Chem. Soc.* **2013**, *135*, 15263–15268.
(144) Esteve, F.; Altava, B.; García-Verdugo, E.; Luis, S. V.; Lehn, J.-M. Doubly Chiral Pseudopeptidic Macrobicyclic Molecular Cages: Water-Assisted Dynamic Covalent Self-Assembly and Chiral Self-Sorting. *Chem* **2022**, *8*, 2023–2042.
(145) Acharyya, K.; Mukherjee, P. S. Shape and Size Directed Self-Selection in Organic Cage Formation. *Chem. Commun.* **2015**, *51*, 4241–4244.
(146) Gu, R.; Lehn, J. Metal Ion-Driven Constitutional Adaptation in Dynamic Covalent C=C/C=N Organo-Metathesis. *Chem. Asian J.* **2021**, *16*, 44–48.
(147) Melson, G. A.; Busch, D. H. Reactions of Coordinated Ligands. X. The Formation and Properties of a Tetradentate Macrocyclic Ligand by the Self-Condensation of o-Aminobenzaldehyde in the Presence of Metal Ions. *J. Am. Chem. Soc.* **1964**, *86*, 4834–4837.
(148) Rucareanu, S.; Schuwey, A.; Gossauer, A. One-Step Template-Directed Synthesis of a Macrocyclic Tetraarylporphyrin Hexamer Based on Supramolecular Interactions with a C_3 -Symmetric Tetraarylporphyrin Trimer. *J. Am. Chem. Soc.* **2006**, *128*, 3396–3413.
(149) Han, M.; Engelhard, D. M.; Clever, G. H. Self-Assembled Coordination Cages Based on Banana-Shaped Ligands. *Chem. Soc. Rev.* **2014**, *43*, 1848–1860.
(150) Ahmad, N.; Younus, H. A.; Chughtai, A. H.; Verpoort, F. Metal–Organic Molecular Cages: Applications of Biochemical Implications. *Chem. Soc. Rev.* **2015**, *44*, 9–25.

(151) Pan, M.; Wu, K.; Zhang, J.-H.; Su, C.-Y. Chiral Metal–Organic Cages/Containers (MOCs): From Structural and Stereochemical Design to Applications. *Coordination Chemistry Reviews* **2019**, *378*, 333–349.

(152) Percástegui, E. G.; Ronson, T. K.; Nitschke, J. R. Design and Applications of Water-Soluble Coordination Cages. *Chem. Rev.* **2020**, *120*, 13480–13544.

(153) Fujita, D.; Suzuki, R.; Fujii, Y.; Yamada, M.; Nakama, T.; Matsugami, A.; Hayashi, F.; Weng, J.-K.; Yagi-Utsumi, M.; Fujita, M. Protein Stabilization and Refolding in a Gigantic Self-Assembled Cage. *Chem* **2021**, *7*, 2672–2683.

(154) Martín Díaz, A. E.; Lewis, J. E. M. Structural Flexibility in Metal-Organic Cages. *Front. Chem.* **2021**, *9*, 706462.

(155) Tateishi, T.; Yoshimura, M.; Tokuda, S.; Matsuda, F.; Fujita, D.; Furukawa, S. Coordination/Metal–Organic Cages inside Out. *Coordination Chemistry Reviews* **2022**,

(156) Tarzia, A.; Jelfs, K. E. Unlocking the Computational Design of Metal–Organic Cages. *Chem. Commun.* **2022**, *58*, 3717–3730.

(157) Ratjen, L.; Vantomme, G.; Lehn, J.-M. Strain-Induced Reactivity in the Dynamic Covalent Chemistry of Macrocyclic Imines. *Chem. Eur. J.* **2015**, *21* (28), 10070–10081.

(158) Liu, G.; Zeller, M.; Su, K.; Pang, J.; Ju, Z.; Yuan, D.; Hong, M. Controlled Orthogonal Self-Assembly of Heterometal-Decorated Coordination Cages. *Chem. Eur. J.* **2016**, *22*, 17345–17350.

(159) Alzakhem, N.; Bischof, C.; Seitz, M. Dependence of the Photophysical Properties on the Number of 2,2′-Bipyridine Units in a Series of Luminescent Europium and Terbium Cryptates. *Inorg. Chem.* **2012**, *51*, 9343–9349.

(160) Gholami, G.; Zhu, K.; Baggi, G.; Schott, E.; Zarate, X.; Loeb, S. J. Influence of Axle Length on the Rate and Mechanism of Shuttling in Rigid H-Shaped [2]Rotaxanes. *Chem. Sci.* **2017**, *8*, 7718–7723.

(161) Granzhan, A.; Largy, E.; Saettel, N.; Teulade-Fichou, M.-P. Macrocyclic DNA-Mismatch-Binding Ligands: Structural Determinants of Selectivity. *Chemistry - A European Journal* **2010**, *16*, 878–889.

Publications and Conferences

Conferences:

(1) Zhaozheng Yang, Jean-Marie Lehn. Kinetic Complexity of the Self-Sorting Process in Dynamic Covalent Libraries of Imine Cages, 47th International Union of Pure and Applied Chemistry (IUPAC) World Chemistry Congress, Paris, France, 7-12 July 2019.

(2) Zhaozheng Yang, Jean-Marie Lehn. Time-dependent switching in self-sorted macrocycles & cages: kinetics vs thermodynamics, 2021 Systems Chemistry Virtual Symposium, Strasbourg, France, 07-09 July 2021.

(3) Zhaozheng Yang, Jean-Marie Lehn. Constitutional Dynamic Networks of Covalent Organic Macrocycles and Cages: Self-Sorting and Orthogonal Switching, 8th The European Chemical Society (EuChemS) Chemistry Congress, Lisbon, Portugal, 28 August-01 September 2022.

Publications

(1) Zhaozheng Yang, Jean-Marie. Lehn*. Dynamic Covalent Self-Sorting and Kinetic Switching Processes in Two Cyclic Orders: Macrocycles and Macrobicyclic Cages. *J. Am. Chem. Soc.* **2020**, 142, 35, 15137–15145.

Zhaozheng YANG

Dynamic Covalent Macrocycles and Macrobicyclic Cages: Self-Sorting, Kinetics and Thermodynamics

Résumé

L'étude des systèmes d'auto-triage, notamment leur comportement sous contrôle cinétique, pourrait ouvrir la voie à une meilleure compréhension des propriétés intrinsèques et de l'intrication de la matière. Cette thèse est centrée autour de l'étude des caractéristiques cinétiques et thermodynamiques dans les systèmes d'auto-triage de macrocycles de polyimines et de cages macrobicycliques. Les forces motrices de chaque distribution, obtenues à la fois à des temps de réaction courts et après avoir atteint l'équilibre, ont été étudiées dans un premier temps. Ces résultats mettent en évidence le rôle essentiel du choix judicieux des composants initiaux, qui permet l'évolution des DCLs (initialement composées des produits cinétiques hors équilibre) vers des états thermodynamiquement favorisés. Dans le dernier chapitre, les interconnexions isomériques entre les constituants ont été évaluées afin d'explorer une nouvelle approche pour le développement de DCLs d'une plus grande complexité.

Mots cles : chimie covalente dynamique, bibliothèque covalente dynamique, triage automatique dynamique, macrocycles, cages moléculaires, systèmes hors équilibre, commutation cinétique

Abstract

The study of self-sorting systems, especially their behaviour under kinetic control, may pave the way to understand the intrinsic properties and intricacy of matter. This thesis focuses on the study of kinetic and thermodynamic features in self-sorting systems of polyimine macrocycles and macrobicyclic cages. The driving forces for each distribution obtained at both short reaction times and after reaching the equilibrium were firstly investigated. The results highlight the essential role of an appropriate design of initial components, which allows the evolution of DCLs from out-of-equilibrium kinetic products to thermodynamically favoured states. In the last chapter, isomeric interconnections between constituents were evaluated in order to provide a new aspect for developing DCLs of higher complexity.

Key words: dynamic covalent chemistry, dynamic covalent library, dynamic self-sorting, macrocycles, molecular cages, out-of-equilibrium systems, kinetic switching